Electroweak quantum chemistry: Parity violation in spectra of chiral molecules containing heavy atoms

Dissertation
zur Erlangung der Doktorgrades
der Naturwissenschaften

vorgelegt beim Fachbereich Physik
der Johann Wolfgang Goethe–Universität
in Frankfurt am Main

von
Sophie Louise Nahrwold
aus Bückeburg

Frankfurt am Main 2010
(D-30)

vom Fachbereich Physik der Johann Wolfgang Goethe–Universität
als Dissertation angenommen.

Dekan: Prof. Dr. Michael Huth

Gutachter: Prof. Dr. Robert Berger

Gutachter: Apl. Prof. Dr. Dieter Schuch

Datum der Disputation: 29.08.2011

Abstract

The intriguing effects of electroweak induced parity violation (PV) in molecules have yet to be observed, but experiments on molecular PV promise to provide fascinating insights. They potentially offer a novel testing ground for the low energy sector of the standard model and, in addition, a successful measurement of PV differences between the two enantiomers of a chiral molecule could promote a deeper understanding of molecular chirality, by essentially establishing a new link between particle physics and biochemistry. A key challenge in the design of such experiments is the identification of suitable molecules, which in turn requires widely applicable computational schemes for the prediction of PV experimental signals. To this end, a quasirelativistic density functional theory approach to the calculation of PV effects in nuclear magnetic resonance (NMR) spectra of chiral molecules has been developed and implemented during the course of this thesis. It includes relativistic as well as electron–correlation effects and has been used extensively in the screening of molecules possibly suited for a first observation of molecular PV. Some relevant compound classes have been identified, but none of their selected representatives are predicted to exhibit PV NMR frequency shifts that can be detected under current experimental restrictions. In order to advance the design of molecules which exhibit particularly large PV signals in experiments, systematic effects on PV NMR frequency splittings such as scaling with nuclear charge, conformational dependence and the impact of atomic substitution around the NMR active nucleus have been studied. Previously predicted scaling laws were confirmed and it was determined that the environment of the NMR active nucleus, both in terms of conformation and atomic composition, can be tuned to increase PV frequency shifts by several orders of magnitude. In addition to molecules suited for NMR experiments, a fascinating chiral actinide compound was studied with regard to PV frequency shifts in vibrational spectra. This compound displays the largest such shift ever predicted for an existing molecule, which lies well within the attainable experimental resolution. The challenge now lies in making it compatible with current experimental setups.

Kurzbeschreibung

Die Berücksichtigung der schwachen Wechselwirkung bei der Berechnung molekularer Eigenschaften führt, insbesondere für chirale Moleküle, zu faszinierenden Vorhersagen: Die Enantiomere (links- und rechtshändige Formen eines chiralen Moleküls) können sich energetisch leicht unterscheiden, weisen unterschiedliche Resonanzfrequenzen in einer Anzahl spektroskopischer Experimente auf, oder verhalten sich in chemischen Reaktionen mit achiralen Edukten nicht mehr genau gleich. Eine erfolgreiche Messung solcher Phänomene könnte entscheidend zum Verständnis molekularer Chiralität beitragen und in gewisser Weise eine neue Verbindung zwischen Teilchenphysik und Biochemie herstellen. Des Weiteren würde die Molekülspektroskopie zusätzliche Möglichkeiten eröffnen, den Niedrigenergiesektor des Standardmodells zu untersuchen. Bis jetzt ist es jedoch noch nicht gelungen, derartige Effekte im Experiment zu beobachten. Eine zentrale Herausforderung bei der Vorbereitung solcher Experimente ist die Identifikation geeigneter Moleküle, für die breit einsetzbare Computerprogramme benötigt werden, um paritätsverletzende Signale in molekularen Spektren zu berechnen. Im Rahmen dieser Arbeit wurde ein solches Programm basierend auf einem quasirelativistischen dichtefunktionaltheoretischen Ansatz entwickelt, mit dem paritätsverletzende Effekte in Kernspinresonanzspektren (NMR–Spektren) chiraler Moleküle berechnet werden können. Der verwendete Ansatz berücksichtigt sowohl relativistische als auch Elektronenkorrelationseffekte, und das Programm wurde intensiv eingesetzt, um potentiell für eine erste Messung molekularer Paritätsverletzung geeignete Moleküle zu untersuchen. Es konnten einige relevante Klassen von Verbindungen identifiziert werden, aber bei allen betrachteten Vertretern dieser Klassen liegen die paritätsverletzenden NMR–Frequenzverschiebungen unterhalb der derzeitigen experimentellen Auflösung. Dieses Problem kann theoretisch gelöst werden, indem man dazu übergeht, eine Verbindung mit für die Messung paritätsverletzender Signale optimalen Eigenschaften zu suchen, wobei systematische Effekte wie z. B. das Skalierungsverhalten mit der Kernladung, konformationelle Abhängigkeit und die Abhängigkeit der paritätsverletzenden NMR–Frequenzverschiebung von der Auswahl der Kerne, die den untersuchten Kern umgeben,

ausgenutzt werden können. Solche systematischen Effekte wurden im Rahmen dieser Arbeit an Modellverbindungen analysiert. Zuvor abgeschätzte Skalierungsverhalten konnten numerisch bestätigt werden, und es wurde gezeigt, dass die Umgebung des NMR-aktiven Kerns sowohl im Hinblick auf Konformation als auch chemische Zusammensetzung die paritätsverletzende Frequenzverschiebung um mehrere Größenordnungen beeinflussen kann. Zusätzlich zu den Untersuchungen über paritätsverletzende Signale in NMR–Spektren chiraler Moleküle wurde ein neu synthetisierter, chiraler Actinoidkomplex im Hinblick auf paritätsverletzende Verschiebungen in Schwingungsspektren behandelt. Diese ungewöhnliche Verbindung weist die größten paritätsverletzenden Schwingungsfrequenzverschiebungen auf, die je für ein existierendes Molekül berechnet wurden und die mit gegenwärtigen experimentellen Methoden nachzuweisen sein müssten. Es bleibt die praktische Herausforderung, den Einsatz dieser Verbindung in bestehenden Experimenten zu ermöglichen.

Zusammenfassung

Wird die intramolekulare schwache Wechselwirkung bei quantenchemischen Rechnungen an molekularen Systemen berücksichtigt, gelangt man zu der Vorhersage einer elektronischen Struktur, die die Symmetrie unter Inversion der Raumkoordinaten verletzt. Dieses Phänomen wird gemeinhin mit dem Ausdruck „molekulare Paritätsverletzung" bezeichnet, und kann sich auf unterschiedlichste Art und Weise manifestieren. In chiralen Molekülen („händige" Moleküle, deren Gleichgewichtsgeometrie keine Drehspiegelachse besitzt) kommt es zu der Vorhersage von leicht unterschiedlichen elektronischen Energien und kleinen Unterschieden in spektroskopischen Eigenschaften zwischen den Enantiomeren (den beiden nicht–superpositionierbaren spiegelbildlichen Formen eines chiralen Moleküls.) [1–8] In achiralen Molekülen (Moleküle mit einer uneigentlichen Rotationssymmetrie S_n) führt die schwache Wechselwirkung zur Bildung sogenannter Spin–Helices und dadurch zu chiralen Charakteristiken der Elektronendichte.[9–11]

Die Berücksichtigung elektroschwacher Effekte in Molekülen korreliert mit Fragestellungen, die eine überraschende Verbindung zwischen Teilchenphysik und Chemie erzeugen: Ist es möglich, chemische Systeme zu benutzen, um das Standardmodell der Teilchenphysik zu untersuchen und eventuell sogar niederenergetische Signaturen von neuen Phänomenen außerhalb des Standardmodells zu entdecken? Könnte es sein, dass Moleküle dafür in mancher Hinsicht sogar besser geeignet sind als Atome? [6, 11–21] Aus der Perspektive der Chemie besteht eine faszinierende Verbindung zwischen der Untersuchung molekularer Chiralität und fundamentaler Symmetrien: Gibt es einen Zusammenhang zwischen elektroschwacher Paritätsverletzung und der Tatsache, dass viele Moleküle nur in chiralen Konfigurationen beobachtet werden und niemals in Eigenzuständen des Paritätsoperators? [2–4, 22–30] Und ist der Effekt vielleicht sogar stark genug, um das überwiegende Auftreten von L–Aminosäuren (oft linkshändige Aminosäuren genannt) in der Natur zu erklären? [1, 3, 31–36]

Um solche Fragen beantworten zu können, ist es notwendig, Paritätsverletzung in Molekülen überhaupt erst einmal zu beobachten. Aufgrund der Schwäche des Effekts ist

dies aber bis heute nicht gelungen, obwohl der erste Versuch, Paritätsverletzung in molekularem Sauerstoff zu messen, bereits 1962 unternommen wurde.[11].

Es werden zwei komplementäre Richtungen verfolgt, um eine Messung zu erreichen, die in Kapitel 2 dieser Arbeit näher beschrieben werden. Bei der ersten werden achirale Moleküle (meist zwei– oder höchstens dreiatomig) im Hinblick darauf untersucht, dass ihre Elektronenstruktur durch Mischung von Zuständen unterschiedlicher Parität einen leicht chiralen Charakter annimmt.[37, 38] Diese elektroschwach induzierte Chiralität ist bekannt aus der Atomphysik (einige Beispiele für paritätsverletzende Eigenschaften, die in Atomen gemessen wurden sind in Lit. [39–45] zu finden), und kann z.B. dazu führen, dass achirale Moleküle die Polarisationsebene von linear polarisiertem Licht rotieren.[11, 14, 46, 47] Paritätsverletzende Effekte sind in manchen polaren Molekülen, die schwere Kerne enthalten, im Verhältnis zu Atomen deutlich verstärkt, was auf die Existenz dicht beieinander liegender Energieniveaus unterschiedlicher Parität zurückzuführen ist (siehe z.B. Lit. [14, 37, 38]). Aus diesem Grund wird insbesondere gehofft, dass es mit Hilfe der Molekülspektroskopie gelingen kann, Kernanapolmomente von unterschiedlichen Kernen zu messen (einige neuere Beispiele für diese Diskussion bieten Lit. [16, 48, 49]), was bisher nur an Cäsiumatomen gelungen ist. [39]

Die zweite Forschungsrichtung zielt auf chirale Moleküle, für deren links- und rechtshändige Enantiomere leicht unterschiedliche Elektronenenergien und weitere elektronische Eigenschaften vorhergesagt werden, wenn die schwache Wechselwirkung bei der Berechnung berücksichtigt wird. [2, 3, 6] Hierdurch bietet sich die Möglichkeit, paritätsverletzende Frequenzunterschiede zwischen zwei Molekülen direkt zu messen, ohne externe Felder anlegen zu müssen, um „dressed states" zu präparieren (unterschiedliche experimentelle Ansätze wurden zu diesem Zweck vorgeschlagen, einige Beispiele sind in Lit. [8, 50] und Kapitel 2.2 zu finden). In Zukunft mag es möglich sein, Parameter des Standardmodells auf diese Weise zu messen oder sogar Physik zu untersuchen, die nicht im Standardmodell enthalten ist. Momentan liegt bei dieser Art von Experiment das Hauptinteresse allerdings darin, das Phänomen paritätsverletzender Unterschiede zwischen zwei Enantiomeren erst einmal nachzuweisen, woraus sich ein tieferes Verständnis molekularer Chiralität ergeben könnte. Hierbei geht es unter anderem um die Frage nach der Möglichkeit, Superpositionen von links– und rechtshändigen Enantiomeren eines chiralen Moleküls herzustellen. Diese Superpositionen sind Eigenzustände des elektromagnetischen Hamiltonoperators und des Paritätsoperators, die durch Wechselwirkung mit der Umgebung in einen der (meist sehr stabilen) chiralen Zustände übergehen. Fraglich ist, ob es überhaupt möglich ist, solche achiralen Superpositionen zu beobachten und damit, ob die Existenz chiraler Moleküle in der Natur auf Superauswahlregeln zurückgeht oder auf fundamentalere Weise zu begründen ist.[51, 52]

Die Messung von Kernspinresonanzfrequenzverschiebungen (Kernspinresonanz wird im Folgenden durch „NMR" abgekürzt, was für „nuclear magnetic resonance" steht) gilt als eine realisierbare Möglichkeit, Paritätsverletzung in chiralen Molekülen zu beobachten.[6, 53–56] Darüber hinaus wäre eine erfolgreiche Messung auch aufschlussreich für die Kern– und Teilchenphysik, da der kernspinabhängige Teil des effektiven Operators für die schwache Wechselwirkung zwischen Elektronen und Kernen den wichtigsten Beitrag zu paritätsverletzenden NMR–Effekten liefert.[6] Diese kernspinabhängige Wechselwirkung ihrerseits wird dominiert von der elektromagnetischen Kopplung der molekularen Elektronen an die Kernanapolmomente [9] im Molekül. Da nun, wie schon erwähnt, bis heute nur das Anapolmoment von Cäsium gemessen werden konnte,[39] würde eine Messung von Paritätsverletzung in NMR–Spektren nicht nur neue Informationen über die intramolekulare schwache Wechselwirkung sondern auch über die schwachen Prozesse im Innern des Kerns liefern, die die Ursache des Kernanapolmoments sind.

Die Erforschung dieses und anderer Aspekte der molekularen Paritätsverletzung ist stark auf computerbasierte Methoden angewiesen, die es ermöglichen, verschiedene experimentelle Herangehensweisen theoretisch zu evaluieren und Moleküle zu identifizieren, die besonders gut für geplante Experimente geeignet sind. Darüber hinaus werden zuverlässige theoretische Berechnungen benötigt, um experimentelle Daten zu interpretieren und eventuell Standardmodellparameter aus ihnen zu bestimmen.

Der Schwerpunkt dieser Arbeit liegt auf der Erweiterung einer quasirelativistischen, quantenchemischen Methode um die Berechnung kernspinabhängiger paritätsverletzender Effekte in Molekülspektren, insbesondere NMR–Frequenzverschiebungen in Spektren von geschlossenschaligen, chiralen Molekülen.[57] Eine relativistische Methode wird deswegen benötigt, weil davon auszugehen ist, dass der Betrag der Frequenzverschiebungen etwa mit der Ladung Z des NMR–aktiven Kerns zur vierten Potenz skaliert [6] und daher chirale Moleküle, die schwere Kerne enthalten, experimentell von besonderem Interesse sind.

Um Effekte wie diese besser zu verstehen, wurde eine Methode gewählt, die sowohl relativistische Phänomene (über den „zeroth order regular approximation" (ZORA) Ansatz, zu Deutsch „regularisierte Näherung nullter Ordnung") als auch Elektronenkorrelationseffekte (im Rahmen der Dichtefunktionaltheorie (DFT)) beschreiben kann. Es war die erste Methode, die diese beiden Aspekte der Elektronenstrukturtheorie zusammen bei der *ab initio* Berechnung paritätsverletzender NMR–Eigenschaften berücksichtigte. Sie basiert auf einem zuvor entwickelten quasirelativistischen Ansatz zur Berechnung paritätsverletzender Energieunterschiede zwischen Enantiomeren. [58, 59]

Die quasirelativistische ZORA Methode [60, 61] wird in Kapitel 4 dieser Arbeit eingeführt und der molekulare ZORA Hamiltonian inklusive elektromagnetischer Störungen und

Beiträgen der schwachen Wechselwirkung hergeleitet. Zudem werden die Eigenschaften und die Anwendbarkeit dieser speziellen quasirelativistischen Näherung diskutiert.

Der in Kapitel 4 diskutierte Hamiltonian ist der Ausgangspunkt für einen Formalismus zur Berechnung molekularer Eigenschaften innerhalb des ZORA Ansatzes, der im Rahmen dieser Arbeit entwickelt wurde. Dieser Formalismus stellt eine Verallgemeinerung und Erweiterung älterer ZORA Ansätze zur Berechnung von paritätsverletzenden Energieverschiebungen [58, 59] und NMR–Abschirmungstensoren [62] dar und wird in Kapitel 5 ausführlich beschrieben. Die Berechnung einer Vielzahl von spektroskopischen Eigenschaften als Energieableitungen höchstens dritten Grades wird dort für allgemeine Vielelektronensysteme erklärt. Der Spezialfall paritätsverletzender NMR–Abschirmungstensoren für geschlossenschalige Systeme innerhalb eines dichtefunktionaltheoretischen (DFT) Ansatzes wird besonders detailliert beschrieben; vor allem im Hinblick auf rechnerische Vereinfachungen, die durch Ausnutzen der Zeitumkehrsymmetrie verdeutlicht werden können, und im Hinblick auf die Implementierung der hergeleiteten Ausdrücke in eine modifizierte Version [58, 63] des TURBOMOLE Programms.[64, 65]

Die hier vorgestellte Methode ermöglicht es, systematische Effekte wie das Skalieren paritätsverletzender NMR–Frequenzverschiebungen mit der Ladung des betrachteten Kerns oder konformationelle Abhängigkeiten zu untersuchen. In Kapitel 6 sind derartige Ergebnisse aus Referenz [57] für die Reihe der Dihydrogen–Dichalkogenide (H_2X_2 mit X=^{17}O, ^{33}S, ^{77}Se, ^{125}Te oder ^{209}Po) zusammengestellt, wobei die präsentierten Ergebnisse auch dazu dienten, die entwickelte ZORA Methode zu testen und mit anderen zu vergleichen. Im nichtrelativistischen Grenzfall der ZORA Näherung wurden die paritätsverletzenden NMR–Frequenzverschiebungen aus Referenz [66] reproduziert, und das beobachtete Skalierungsverhalten mit der Ladung Z des Chalkogenkerns (Z^3 Skalierung für den paramagnetischen und Z^5 Skalierung für den Spin–Bahn–Kopplungs Beitrag) stimmt gut mit früheren Größenordnungsabschätzungen [6] überein, wenn relativistische Verstärkungsfaktoren [67] berücksichtigt werden. Die übliche konformationelle $\sin(2\alpha)$–Abhängigkeit paritätsverletzender Eigenschaften vom Diederwinkel α in diesen Molekülen wurde für isotrope NMR–Abschirmungskonstanten aller Dihydrogen–Dichalkogenide beobachtet. Aufgrund von Diskrepanzen zwischen diesen Ergebnissen und den Resultaten einer Dirac–Hartree–Fock–Coulomb (DHFC) Studie paritätsverletzender NMR–Eigenschaften [68] konnte eine Instabilität in den DHFC Rechnungen an H_2Po_2 identifiziert werden.[69]

In Kapitel 7 wird die entwickelte Methode weiter angewendet, wobei es um die Möglichkeit geht, paritätsverletzende Frequenzverschiebungen in NMR–Spektren chiraler Moleküle tatsächlich zu messen. Die experimentellen Anforderungen werden diskutiert und unterschiedliche Klassen von Verbindungen, die für eine Messung geeignet erscheinen, mit

Hilfe der ZORA Methode analysiert. Die experimentelle Auflösung ist schätzungsweise hoch genug, um paritätsverletzende Frequenzaufspaltungen von etwa 10 mHz zwischen zwei Enantiomeren zu messen,[56] doch ein derartig großer paritätsverletzender Effekt wurden bisher nur für das hypothetische H_2Po_2 Molekül in einer speziellen Konformation vorhergesagt,[57] wodurch die aus dem schon erwähnten Skalierungsverhalten von bis zu Z^5 abgeleitete experimentelle Präferenz für Verbindungen mit schweren Kernen für den Bereich der konventionellen NMR Spektroskopie bestätigt wurde.

Einer der interessantesten Kernen, die man in diesem Zusammenhang untersuchen kann, ist wegen seines großen Gewichts und gyromagnetischen Verhältnisses ^{195}Pt. Die konformationelle Abhängigkeit der paritätsverletzenden NMR–Frequenzaufspaltungen wurde für einen $C_{2\nu}$–symmetrischen Pt–Testkomplex untersucht, und ist ähnlich der in den C_2–symmetrischen Dihydrogen–Dichalkogeniden ein Phänomen, das bei der Entwicklung speziell für die Messung von paritätsverletzenden NMR–Effekten optimierter Moleküle helfen könnte. Drei Platinverbindungen wurden im Hinblick auf ihre experimentelle Eignung untersucht, von denen eine besonders große paritätsverletzende NMR–Frequenzaufspaltungen von etwa 400 μHz in der Gleichgewichtsgeometrie aufweist. Diese Verbindung könnte für einen ersten Messversuch geeignet sein,[70] und ein vergleichbarer Ligand wurde bereits mit Blick auf ein mögliches Experiment synthetisiert.

Ein weiterer Kern, der für die Messung von paritätsverletzenden NMR–Eigenschaften interessant ist, ist ^{183}W. Für eine Reihe von Wolfram–Testkomplexen NWXYZ (mit $X, Y, Z = $ H, F, Cl, Br oder I) wurde die Auswirkung atomarer Substitution in unmittelbarer Umgebung des NMR–aktiven Kerns untersucht. Der Effekt ist für paritätsverletzende NMR–Frequenzaufspaltungen besonders groß, und zwischen der kleinsten und der größten ^{183}W Frequenzaufspaltung in der untersuchten Reihe von Molekülen liegen drei Größenordnungen.[71] Es deutet dabei vieles darauf hin, dass bei der Optimierung von Molekülen für die Maximierung paritätsverletzender NMR–Effekte der Fokus darauf liegen sollte, den NMR–aktiven Kern mit möglichst heterogenen Liganden zu umgeben, sowohl im Hinblick auf Gewicht als auch Elektronegativität. Allein die Anwesenheit weiterer schwerer Kerne ist nicht ausschlaggebend. Der Effekt der atomaren Substitution könnte bei einer Klasse von Wolfram–Verbindungen sehr vorteilhaft ausgenutzt werden, vier derer Vertreter als mögliche Kandidaten für ein Experiment untersucht wurden. Es handelt sich dabei um Trimetall–Cluster, die in der Zusammensetzung des zentralen „Metallkäfigs" äußerst flexibel sind und damit viel Spielraum für die Optimierung paritätsverletzender Effekte bieten. Bei den bisher betrachteten Exemplaren weisen vorläufige Rechnungen nicht auf besonders große ^{183}W NMR–Frequenzaufspaltungen hin, jedoch steht diese Untersuchung aufgrund der Komplexität der Moleküle noch ganz am Anfang.

Während das Interesse an NMR–Spektroskopie als Methode, molekulare Paritätsverletzung zu messen, erst relativ kürzlich wiedererstarkt ist, wird Vibrationsspektroskopie seit langem als eine der besten Optionen für ein solches Experiment betrachtet.[51, 72] Die beiden Ansätze sind komplementär in dem Sinne, dass nicht derselbe Effekt gemessen wird. Paritätsverletzende NMR–Frequenzverschiebungen werden höchstwahrscheinlich von der kernspinabhängigen paritätsverletzenden Wechselwirkung dominiert, während Abweichungen in Vibrationsspektren dem kernspinunabhängigen Beitrag zugeschrieben würden. Im Rahmen dieser Arbeit wurden paritätsverletzende Frequenzverschiebungen im Vibrationsspektrum einer neu synthetisierten Actinoidverbindung berechnet. Die Verbindung weist die größten solcher Frequenzverschiebungen auf, die je für ein existierendes Molekül vorhergesagt wurden und die mit bestehenden experimentellen Methoden gemessen werden könnten.[72, 73] Die Barriere für Stereomutation ist in dieser Verbindung allerdings relativ niedrig, so dass die chirale Dynamik vermutlich eher durch Tunneln als Paritätsverletzung bestimmt ist.[74] Dies ist möglicherweise durch isotopische Substitution änderbar, so dass diese oder ähnliche Verbindungen bei der Planung neuer Experimente berücksichtigt werden sollten.

Für die Zukunft ist eine Erweiterung der in dieser Arbeit vorgestellten Methode auf eine größere Auswahl von unterschiedlichen Methoden zur Berechnung der Elektronenstruktur, z.B. Hybridfunktionale im Rahmen der Dichtefunktionaltheorie und Hartree–Fock–Theorie vorgesehen, was besonders für die untersuchten Übergangsmetallkomplexe von Bedeutung sein wird. Die Anwendung einer Methode zur Verringerung der Abhängigkeit vom Eichursprung des Magnetfeldes ist ebenso geplant, da dadurch der numerische Aufwand stark vermindert würde. Des Weiteren soll die Methode auf zusätzliche molekulare Eigenschaften ausgedehnt werden. Ein vor kurzem vorgestelltes Experiment zur Messung von Kernspin–Kernspin–Kopplungen bei verschwindendem äußerem Magnetfeld [75] scheint für eine Messung von paritätsverletzenden Effekten sehr interessant zu sein und eine Erweiterung der ZORA Methode um die Möglichkeit, derartige Eigenschaften zu berechnen, ist in Arbeit.

Phänomenologisch ist nach wie vor nicht vollständig geklärt, welche Faktoren entscheidend dafür sind, dass ein bestimmtes Molekül große oder kleine paritätsverletzende Eigenschaften aufweist. Dies zu verstehen ist essentiell dafür, experimentell geeignete Verbindungen effizient auszusondern oder zu optimieren. Skalierung mit der Ladung des NMR–aktiven Kerns wird zwar bereits ausgenutzt, aber es gibt definit weitere wichtige Faktoren, die bis jetzt nicht berücksichtigt werden. Die Untersuchungen, die in dieser Arbeit besprochen wurden, weisen darauf hin, dass die Größe paritätsverletzender NMR–Frequenzaufspaltungen mit der Asymmetrie der elektronischen Umgebung des betrachteten Kerns korreliert. Dies macht deutlich, dass Chiralität als eine inkrementelle Eigenschaft verstanden werden muss, wenn man sich mit Phänomenen wie diesen

beschäftigen möchte. Ein weiterer Faktor, der die Größe paritätsverletzender Effekte beeinflussen könnte, ist die Stärke der Spin–Bahn–Kopplung in einem Molekül. Diese unterschiedlichen Aspekte müssen besser verstanden werden, um qualitative Modelle zu entwickeln, mit deren Hilfe die Größenordnung paritätsverletzender Phänomene schnell und ohne großen numerischen Aufwand abgeschätzt werden könnte.

Acknowledgements

"Nichts sagen ist eine Blume. Viel sagen ist ein Blumenstrauß."

– Tse–Tang, der Ältere

First and foremost I wish to acknowledge the contribution of my principal advisor Robert Berger to this thesis. I doubt that there can be any scientist more diligent and conscientious than he and his never wavering conviction that, in science, one should strive to achieve perfect clarity of understanding and expression has been truly inspiring for me.

Dieter Schuch has been very kind in accepting the role of my secondary supervisor and I have learned much from him about the classical and quantum mechanics of dissipative systems.

My colleagues have greatly contributed to making my time pleasant and productive. Jason L. Stuber was most helpful and encouraging in our conversations about my work and broadened my horizon significantly as to the universality of the many–body problem in all areas of theoretical physics. In addition, I think I might not have prevailed in my first close encounters with the Turbomole program package, if it hadn't been for his assistance. Discussions with Yunlong Xiao about many aspects of relativistic electronic structure theory and magnetic properties and with Timur Isaev about parity violation in atomic systems were always insightful for me. Guido Laubender provided me with much help in computational matters and Hans-Christian Jankowiak and Christian Krekeler offered their chemical expertise in dealing with some of the more complicated molecules in this thesis.

I am happy to have been a member of the Frankfurt Institute for Advanced Studies during these last years, where I met intriguing people working in different areas of science than myself. I particularly enjoyed the many interesting conversations with Hasnaa Fatehi, Michael Hauer, Khin Nyan Linn, Jorge Noronha, Basil Sa'd and Giorgio Torrieri on a vast variety of subjects from elementary particle physics to theoretical biology.

Outside of Frankfurt, I wish to thank Peter Schwerdtfeger and Wenjian Liu for their interest in my work and fruitful discussions. Christina Thiele has been very helpful in sharing her expertise on NMR spectroscopy. Trygve Helgaker, Pøul Jørgensen and Jeppe Olsen allowed me to work as a tutor at the 10th Sostrop summer school on quantum chemistry, which I thoroughly enjoyed. From Walter A. Siebel I learned many things, among them much about the history and philosophy of science, which enabled me to see my work in a wider context.

Contents

Bibliography   **165**

List of Figures

List of Tables

Abbreviations

CCSD   **C**oupled **C**luster **S**ingles and **D**oubles

DFT   **D**ensity **F**unctional **T**heory

DHF   **D**irac–**H**artree–**F**ock

DHFC   **D**irac–**H**artree–**F**ock–**C**oulomb

DKS   **D**irac–**K**ohn–**S**ham

GIAO   **G**auge **I**ncluding **A**tomic **O**rbitals

HF   **H**artree–**F**ock

LCAO   **L**inear **C**ombination of **A**tomic **O**rbitals

MO   **M**olecular **O**rbital

NMR   **N**uclear **M**agnetic **R**esonance

P   **P**arity

PV   **P**arity **V**iolation or **V**iolating

SCF   **S**elf **C**onsistent **F**ield

ZORA   **Z**eroth **O**rder **R**egular **A**pproximation

فقل لمن يدّعي في العلم فلسفة

حفظت شيئًا ، وغابت عنك اشياء !

ابو نواس

Say too him who claims great knowledge in science:
You learned one thing and missed many others!

Abu Nuwas

Chapter 1

Introduction

The term "molecular parity violation" (PV) usually refers to the phenomenon that, upon the addition of weak interaction corrections to the electromagnetic interaction in molecular systems, their electronic structure is slightly altered in a way that violates symmetry with respect to space inversion. There are many different signatures of this effect. In achiral molecules (molecules with improper rotation (S_n) symmetry) for example, the electron density distribution is predicted to exhibit minute chiral characteristics through the formation of so–called spin helices.[9–11, 76] In chiral molecules, on the other hand, two enantiomers (the non–superimposable mirror forms of a chiral molecule) have slightly different electronic energies and display small variations in spectroscopic properties, when weak interaction corrections are included in calculations.[1–8]

The investigation of electroweak effects in molecules bridges the gap between particle physics and chemistry in a surprising way, because it is related to questions such as (see also the review Ref. [77]): Is it possible to use chemical systems to discover more about the standard model of particle physics and perhaps uncover the footprints of new phenomena which are apparent at very high energies only? And do molecules even have certain advantages over atoms in this respect?[6, 11–21] Is the effect big enough to explain why many molecules apparently do not adopt stable forms that are eigenstates of the parity operator but chiral configurations instead?[2–4, 22–30, 78] And could the predominant appearance of L–amino acids (commonly referred to as left–handed) in nature have anything to do with an asymmetry in the fundamental interactions?[1, 3, 31–36, 79]

In order to answer any of these questions, one must, first of all, observe the effect itself. However, due to its smallness, there hasn't been an experimental observation of molecular PV to this day, even though the first attempt to measure a PV property in molecular oxygen was made as early as 1962.[11]

Two complementary directions are being pursued in order to obtain a measurement: The first is the study of achiral molecules (usually di– or at most triatomic molecules) which are expected to be slightly chiral in their electronic structure due to mixing of states of different parity.[37, 38] This electroweak induced chirality is well known from atomic physics (Refs. [39–45] are some examples of PV properties measured in atoms) and can lead achiral molecules to, for example, rotate the polarization plane of linearly polarized light.[11, 14, 46, 47, 80] With respect to atoms, PV effects are predicted to be dramatically enhanced in some polar, heavy–atom molecules due to the existence of close lying energy levels of opposite parity (see e.g. Refs. [14, 37, 38]). It is particularly hoped, that the use of molecules will allow for measurements of nuclear anapole moments other than that of atomic cesium, which is the only nuclear anapole moment that could be measured so far [39] (some recent examples of this discussion are Refs. [16, 48, 49]).

The second direction of research is concerned with chiral molecules, whose left– and right–handed enantiomers are predicted to have slightly different electronic energies and other properties, when the weak interaction is included in calculations.[2, 3, 6] This offers the possibility of measuring PV as a frequency difference without having to apply external fields in order to prepare "dressed" states (different experimental schemes have been proposed for this purpose, some examples can be found in Refs. [8, 50]). While it may eventually be possible to determine standard model parameters from such measurements and even use them to investigate phenomena beyond the standard model, the focus, at present, lies on a first detection of the effect itself, which could promote a deeper understanding of molecular chirality. The question here points to the possibility of preparing superpositions of the left– and right–handed enantiomers of a chiral molecule. These superpositions would be eigenstates of the electromagnetic Hamiltonian and would also share its symmetry with respect to parity. Through interaction with the environment such states would quickly collapse into one of the (usually very stable) chiral forms, but it is currently unclear if it is possible to observe them at all. This is linked to the question of whether the appearance of chiral molecules in nature should be solely attributed to environmental superselection rules or has a more fundamental underlying cause.[51, 52]

Both directions of research into molecular parity violation rely heavily on computational approaches for a primary, theoretical exploration of different experimental routes and the identification of molecules particularly suited for experiments. The analysis of experimental data and possibly the extraction of standard model parameters from results will eventually also depend on an accurate theoretical description.

The focus of this thesis lies on the extension of a quasirelativistic quantum chemical approach [58–62] to the calculation of nuclear spin–dependent PV effects in molecular spectra, with emphasis on nuclear magnetic resonance (NMR) frequency shifts in the

NMR spectra of closed–shell chiral molecules.[57] A relativistic approach is required, because the absolute value of the frequency shifts is expected to scale with nuclear charge Z of the NMR active nucleus up to the fifth power [6] and therefore chiral molecules containing heavy nuclei are of considerable interest in the search for experimentally suited compounds.

The experimental detection of these NMR resonance frequency shifts is considered to be a feasible route towards a first observation of PV in chiral molecules.[6, 53–56] In addition, a successful measurement promises to be insightful from a particle and nuclear physics perspective. The reason for this is that one expects the dominant contribution to PV NMR properties to stem from the nuclear spin–dependent part of the effective operator for the weak interaction between electrons and nuclei.[6] To this spin–dependent part the nuclear anapole moment,[9, 76] which, as mentioned earlier, has only been measured once before in cesium atoms [39], contributes significantly, and thus an observation of parity violation in NMR spectra would present valuable information not only on the intra–molecular weak interaction but also on weak processes within the atomic nucleus, which are the cause of the nuclear anapole moment.

This thesis is organized as follows: the upcoming Chapter 2 gives an overview of theoretical and experimental studies of the weak interaction in atomic and molecular systems. Chapter 3 reviews the development of relativistic many–body methods in the field of quantum chemistry. In chapter 4 the derivation of the quasirelativistic zeroth order regular approximation (ZORA) Hamiltonian [60, 61] is reviewed with the inclusion electromagnetic perturbations and weak interaction effects. The properties and limits of this particular quasirelativistic approximation are discussed.

The Hamiltonian derived in chapter 4 forms the basis of the formalism for the calculation of molecular properties within the ZORA method developed during the course of this thesis. The formalism constitutes a generalization and extension of previously reported ZORA approaches to the calculation of PV energy shifts [58, 59] and NMR shielding tensors [62] and is described in detail in Chapter 5. The calculation of a range of spectroscopic properties up to third order is elucidated for general many–electron systems. Particular attention is payed to the calculation of PV NMR shielding tensors for closed shell systems within a density functional theory (DFT) framework, especially with respect to computational simplifications that can appear due to time–reversal symmetry and with respect to the implementation of derived expressions in a modified version [58, 63] of the TURBOMOLE [64, 65] program package.

The approach presented here allows for the investigation of systematic effects like scaling with nuclear charge or the impact of conformational changes on PV NMR parameters. Corresponding results for the series of dihydrogen dichalcogens of Ref. [57] are presented

in Chapter 6. In Chapter 7 the possibility of an experimental observation of PV NMR splittings is addressed and the developed method is used to analyze the potential of some possible experimental candidate compounds. Chapter 8 contains calculations of PV splittings in the vibrational spectrum of a recently discovered chiral actinide complex which are larger than any previously reported for this experimental approach.

Chapter 2

Molecular parity violation

"Physicists must find physics very difficult."

– Hermann Weyl

This chapter provides a background for the study of molecular parity violation. The history of the investigation of parity violation in atomic systems, starting from its discovery in the intra–nuclear weak interaction is reviewed. Atomic experiments were among the first to produce evidence for the weak neutral current interaction and are being used today for precision measurements of electroweak parameters of the standard model of particle physics and even in the search for new physics beyond the standard model, which is addressed in section 2.1 of this chapter. Molecular parity violation, on the other hand, has so far not been observed. In section 2.2, the principles of parity violation in chiral molecules are discussed and the theoretical study of related effects is inspected. Emphasis is put on parity violating effects in nuclear magnetic resonance spectra, which is a focal point of some of the subsequent chapters.

2.1 Discovery of parity violation and consequences for atomic systems

The possibility that the fundamental weak interaction could change under an inversion of the coordinate system (e.g. $(x, y, z) \to (-x, -y, -z)$), which constitutes a violation of parity, was first considered in 1956 in an attempt to solve the so–called "$\theta - \tau$–puzzle" (the decay of the K–meson into states of different parity, three pions or two pions) of
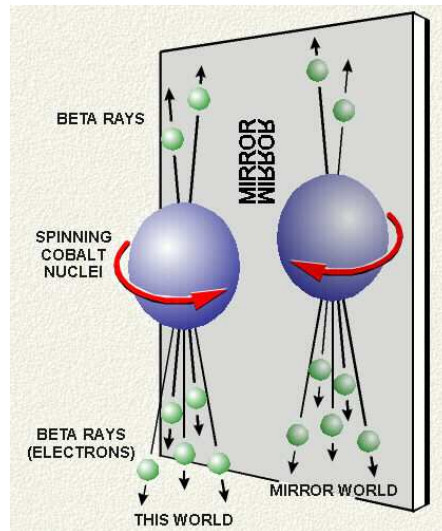
Figure 2.1: Illustration of parity violation in ^{60}Co β–decay from Ref. [90].

particle physics [81].[1] Experimental verifications of this hypothesis followed shortly in 1957, when it was shown, for instance, that parity (P) is indeed violated in the β–decay of ^{60}Co[88] and of ^{58}Co [89] isotopes. The parity violating (PV) aspect of ^{60}Co β–decay is illustrated in Figure 2.1.

In β–decay the weak interaction is mediated by the charge–carrying exchange bosons W^+ and W^-. It was already recognized then, that electromagnetic interactions with parity violation could create a new kind of property, called the anapole moment.[9] The PV anapole moment can be illustrated as an electromagnetic field caused by a toroidal current as shown in Figure 2.2. This current is caused by the mixing of states of even and odd parity through the PV interaction. The mixing of S and P states, for example, leads to the formation of a so–called spin helix, in which the spin of the particle is rotated by a small angle which depends on the distance from the center of symmetry. Such a spin helix and the resulting PV magnetic moment are illustrated in Figure 2.3. This phenomenon is of particular interest in nuclear physics, where it results in a PV contribution to the nuclear magnetic moment. Inside an atom or molecule, electrons can couple to the nuclear anapole moment electromagnetically, leading to a PV shift in energy and PV transitions in spectra.[91]

---

[1]One of the earlier confrontations with parity violation was made in 1929 by H. Weyl when he developed a two–component theory of particles with zero mass and spin 1/2.[82] Because of its parity violating character the theory was rejected (as a description of neutrinos) by Pauli in 1933 [83] but eventually revised after parity violation was discovered.[84–86] The joke at the beginning of this chapter is rumored to have been made by Weyl to A. Salam in connection with the discussion about parity violation and the "$\theta - \tau$–puzzle".[87]
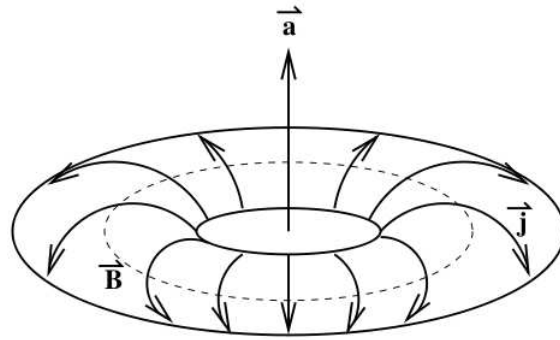
Figure 2.2: The toroidal current induced by the weak interaction inside the nucleus causes a ring field which corresponds to the anapole moment. Image taken from Ref. [92].
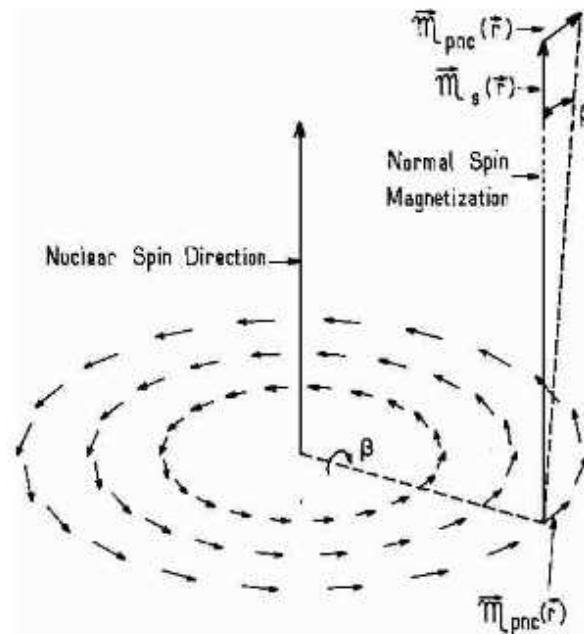
Figure 2.3: Rotation of nuclear spin due to the PV weak interaction, with the rotation angle depending on the distance from the center of the nucleus. The magnetic moment of the nucleus and the induced PV moment are also depicted. Image taken from Ref. [93].

The existence of a neutral exchange particle of the weak interaction, which would allow for processes without charge transfer, such as the elastic scattering of an electron off a nucleon, could never be excluded on the basis of known conservation laws and was first discussed in 1958.[94] The relevance of such neutral currents for parity non–conservation in atomic systems was quickly realized, and it was already noted then that such an interaction would lead to an optical activity of the hydrogen atom.[10] The interest in neutral currents and their effects increased after it became clear that their existence was required by renormalizable models of a unified electromagnetic and weak interaction,[37] such as the neutral Z^0 boson of the prevailing theory of the unified electroweak interaction of

Glashow,[95] Salam [96] and Weinberg [97].

Z^0–exchange between electrons and nuclei is usually expected to account for the dominant PV effect in atoms and molecules containing stable nuclei only [2, 3, 23, 77]. The exchange of the charged $W^{\pm}$ bosons of the weak interaction, however, plays an important role for PV effects in atomic systems containing β–decaying nuclei and in PV interactions inside the nuclei giving rise to the anapole moment, which can presumably dominate PV effects in nuclear–spin dependent atomic and molecular properties.

It should be noted, that the P–even weak interaction potential usually has a quantitatively bigger effect on electronic structure than the tiny P–odd contribution. For example, the hyperfine splitting of the hydrogen ground state is changed on the order of 10^{-4} MHz by the P–even weak interaction.[37] This effect lies well within the experimental resolution of 10^{-9} MHz [98] but a high precision measurement is, at present, of no use in detecting weak interaction effects here. The reason for this is that theoretical uncertainties in the calculation of the hydrogen ground state hyperfine structure are of the order of 10^{-3} MHz [98] since they rely on proton structure calculations, and even the electron and proton magnetic moment values limit the attainable precision to 10^{-3} MHz.[37]

This is a general phenomenon where P–even weak interactions in atomic systems are concerned: even though the experimental resolution is high enough to detect them, the results can not be interpreted without ambiguities.[37] Parity violation, on the other hand, is a unique characteristic of the weak interaction and measurements of P–odd effects, such as circular polarization of radiation by an atom or energy differences between the two enantiomers of a chiral molecule, can therefore be interpreted more easily. The problem here lies in actually obtaining a measurement due to the smallness of effects. The optical activity of hydrogen atoms due to neutral current interactions for instance was estimated to be so small, that any possibility of detecting it was dismissed out of hand.[10] Things changed, however, with the 1974 prediction, that P–odd effects in atoms scale with nuclear charge Z as Z^3,[67, 99] which can be considered as the starting signal for investigations of the fundamental weak interaction by means of atomic spectroscopy.[37]

Experimental observations of neutral current induced effects have been difficult to achieve and spectroscopic experiments have contributed greatly to the investigation of electroweak phenomena. The first indications for the existence of a neutral weak current came from neutrino–nucleon scattering data in 1973,[100] but Z^0–exchange between electrons and nucleons was first observed during the late 1970s in terms of the optical activity of bismuth vapor,[101, 102] the $6^2P_{1/2} - 7^2P_{1/2}$ transition in thallium,[103] and inelastic scattering of high–energy electrons from protons and deuterons.[104] A few

Z^0 particles were finally observed directly in proton–antiproton collisions at CERN in 1983,[105] more than twenty years after their existence had first been predicted.

At this time there was also a great increase in the number of successful atomic measurements. One class of experiments focussed on highly forbidden magnetic dipole transitions in cesium [106, 107] or thallium [103, 108–110]. These measurements were aimed at detecting a PV electric dipole (E1) transition against the background of highly suppressed magnetic dipole (M1) transitions, i.e. transitions with large asymmetry (signal to noise ratio between the parity violating electric dipole transition and the suppressed magnetic dipole transition). An advantage of the Cs experiments is the relatively simple electronic structure which allows for higher accuracy in theoretical calculations thereby facilitating the interpretation of experimental data and extraction of standard model parameters. Another class of experiments was aimed at the detection of PV optical rotation of atoms by studying allowed magnetic dipole transitions with a smaller suppression factor and asymmetry in thallium, lead or bismuth [41, 42, 111, 112] (see also, for example, the review articles [113–115]).

A measurement of the nuclear anapole moment has so far only been accomplished once, in 1997 in an experiment with Cs [39] with more data presented in 1999 [40]. The result for the anapole is in agreement with calculated values but does not compare too well to other measurements of electroweak effects in nuclei.[92, 114] In any case, the debate about the analysis of the experimental data has shown, that the quality of electronic structure calculations is the limiting factor for the interpretability of results.[116] The most accurate experiments on Tl [43, 44] have so far only yielded an upper bound for the anapole moment.

Today, atomic parity violation experiments as tests of the standard model of particle physics are still of great interest. Measurements of the weak nuclear charge, which have been achieved by the Cs and Tl experiments [39, 43, 44], can determine the electroweak mixing angle θ_{W} at low momentum transfer and thereby test the energy dependence of the electroweak interaction.[17, 18] These measurements are also predicted to be suitable for tests of theories beyond the standard model.[18–21] Measurements of anapole moments, on the other hand, can offer insight into purely hadronic weak interactions mediated by Z^0, which are even more elusive than the leptonic kind.[92] (Charged current contributions to the anapole moment also exist, but the corresponding interactions can be studied using a variety of different experimental schemes.) The anapole measurements are also sensitive to long–range PV interactions mediated through pion exchange.[92]

New experimental schemes are also being pursued: Single–atom spectroscopy on alkali–like ions has been suggested [117] and such experiments on Ba$^+$ [118] and Ra$^+$ [119] are being prepared. An alternative way of measuring PV in the forbidden Cs M1 transition

has been tested,[120, 121] but has yet to reached the precision of previous experiments. Recently, a measurement of a PV transition amplitude in ytterbium has been performed [45] and predictions of a large enhancement of PV effects in Yb have been confirmed. With improved apparatus this experiment can potentially be used to compare PV amplitudes of different isotopes, which would reveal information on the neutron distribution in the relevant nuclei, and measure Yb anapole moments.

It is interesting to note, that in 1962 one of the very first attempts to detect parity violation in semi–leptonic interactions was performed on molecular oxygen and not on atoms (Ref. [11] as cited in Refs. [37, 38]). The experiment could only provide an upper bound for the mixing of states of opposite parity that would cause circular dichroism in the M1 transition in O_2, but since the first definitive measurements of parity violation in atoms have been achieved, interest in molecular systems has been on the increase again.

When it comes to the measurement of nuclear spin–dependent PV effects, usually dominated by the anapole moment for nuclei with atomic mass number A greater than 20, heteronuclear diatomic molecules are in some sense preferable to atoms because of the existence of near–degenerate levels of opposite parity which enhances the mixing of such states by the nuclear spin–dependent PV weak interaction (see e.g. Ref. [37], Chapter 9.3 or Refs. [14, 38] and references cited therein).

The mechanism for this is qualitatively as follows (as described in Refs. [37, 38]): When considering the projection Ω of the total electron angular momentum onto the molecular axis, it changes sign upon reflection at a plane through the axis, whereas the energy of the system is unchanged. The two states $|\Omega\rangle$ and $-|\Omega\rangle$ are therefore degenerate and degenerate states of definite parity can be constructed as linear combinations of the two. The degeneracy is lifted by the interaction of electron angular momentum with the rotation of the molecule, which is typically extremely weak compared to most atomic energy intervals. The nuclear spin–independent PV interaction does not lead to a mixing of these states, but the nuclear spin–dependent operator can have non vanishing matrix elements between the states of different angular momentum and thus leads to a mixing of the states of opposite parity.

There are several schemes for measurements of such effects, depending on the relative coupling strength of angular momenta.[38] The most ardently pursued direction seems to be using molecules in a $^2\Sigma_{1/2}$ ground state with one valence electron over closed shells. In such molecules, spin–spin coupling between electron and nucleus dominates the coupling of the electron spin to the molecular rotation, but is still so small, that quasidegeneracy of the two rotational/hyperfine levels of opposite parity can be achieved using external magnetic fields, leading to an even greater mixing of the two states and further enhancing the PV signature. It could be measured in terms of a rotation of

(a)   (b)
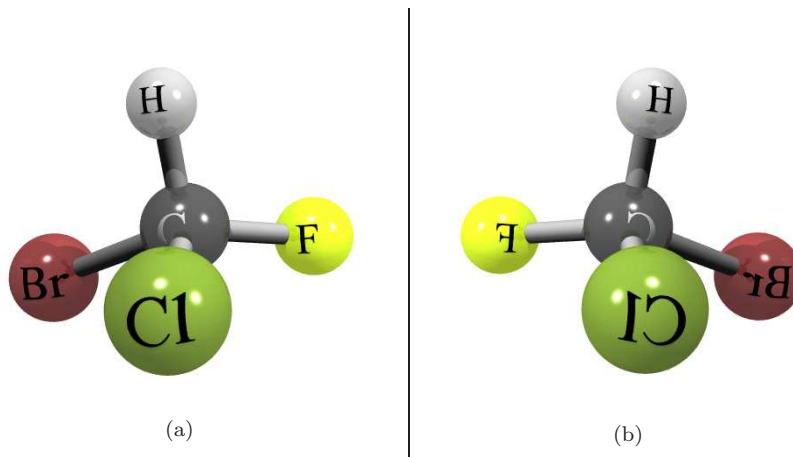
Figure 2.4: The two enantiomers $|S\rangle$ and $|R\rangle$ of CHFClBr, Subfigures (a) and (b), respectively.

the polarization plane of polarized light (as suggested for example in Ref. [14]), by means of electron paramagnetic resonance spectroscopy,[122] or a Stark–interference method described in Refs. [14, 16, 38] (and Refs. [46, 47, 80] cited therein), in which the interference between the PNC mixing of states with the mixing induced by a time–dependent electric field would be measured. This particular experimental approach, which was suggested only recently, seems to be widely applicable and is currently being implemented using BaF [16, 123].

In this context, it should be noted also, that diatomic molecules play an important part in the search for weak interaction properties that violate both parity and time–reversal invariance. Such properties could be manifested, for example, in the existence of a permanent electric dipole moment of the electron or proton.[48]

2.2   Parity violation in chiral molecules

The discovery, that the weak interaction violates mirror symmetry also had immediate consequences for the study of chiral molecules in chemistry and biochemistry, and a few years after the discovery of parity violation in nuclear β–decay the impact of polarized bremsstrahlung stemming from polarized electrons emitted during this process on chemical reactions was already considered as a possible explanation for the appearance of chiral molecules in nature.[124]

Later, it was hypothesized, that a PV component of the electromagnetic force in molecules could be the origin of the predominant appearance of L–amino acids in nature [1] (all naturally occurring amino acids except glycine are chiral, L–amino acids are those that

can theoretically be synthesized from the glyceraldehyde isomers that rotate the polarization plane of polarized light counterclockwise, i.e. are levorotary), using roughly the following argument: A PV weak interaction correction to the electromagnetic interaction in chiral molecules, however small, should lead to a slight deviation between the electronic wavefunction of a right–handed molecule and the mirror image of the electronic wavefunction of the corresponding left–handed molecule. Consequently, it would also lead to slightly different electronic energies and rate constants for chemical reactions, which could over the very long time–span in question (and with the help of some enantioselective enhancement mechanism) have an impact on biochemical evolution.[1]

The hypothesis that electroweak interaction and biomolecular homochirality have a causal connection (i.e. that fundamental parity non–conservation is the source of parity violation apparent in the biochemical selection of one enantiomer over the other) has been discussed intensively over many years (see, for example, Refs.[7, 33–35, 79, 125–129]), including different non–linear amplification methods, such as autocatalytic chemical reactions [130, 131] or a phase transition to an enantiopure state [132]. It is quite possible that such a causal connection may never be refuted entirely, but recent computations of PV energy differences between L– and D–amino acids have shown, that in some significant cases the L–form is not stabilized by the weak interaction.[35, 79] There are also numerous competing theories on *de facto* violations of parity (PV through initial conditions) in the evolution of biomolecules, such as asymmetric photoreactions [133–135] or the influence of magnetic fields [136]. For critical reviews of the ongoing research into a connection between molecular PV and homochirality Refs. [33, 34, 36] should be consulted.

Another intriguing aspect of PV effects in chiral molecules is that they could have far reaching consequences for the understanding of molecular chirality itself: As mentioned earlier, a chiral molecule has two non–superimposable stereoisomers called enantiomers, often referred to as L/D– or R/S–enantiomers.[2] Two enantiomers $|S\rangle$ and $|R\rangle$ of a chiral molecule are not eigenstates of the parity operator $\hat{P}$ but linear combinations of the two eigenstates $|+\rangle$ and $|-\rangle$:

$$\hat{P}\,|+\rangle = |+\rangle\,, \quad \hat{P}\,|-\rangle = -\,|+\rangle\,. \tag{2.1}$$

---

[2]In the R/S nomenclature a label is assigned to a chiral center based on a bond hierarchy established according to the Cahn–Ingold–Prelog priority rules.[137] A clockwise (R for *rectus*) or counterclockwise (S for *sinister*) sense of rotation is then defined. In the L/D–nomenclature mentioned earlier, the enantiomers are named according to the enantiomer of glyceraldehyde from which they can be derived. It is used mostly for amino–acids.
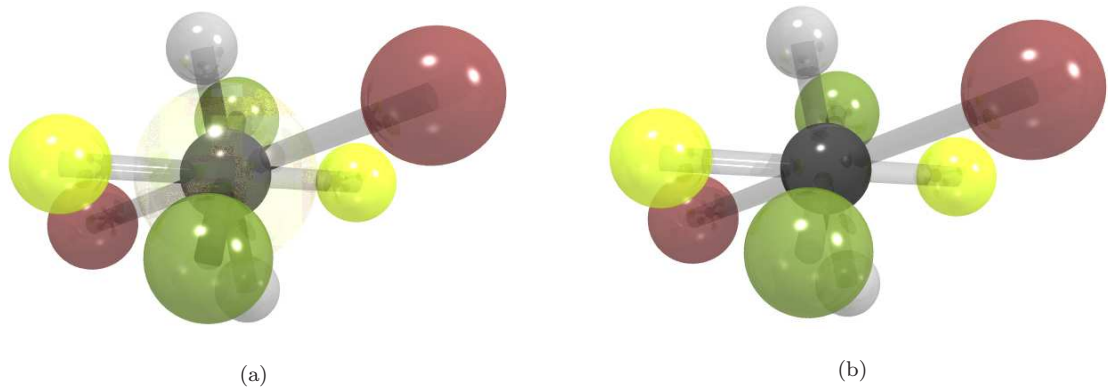
Figure 2.5: Visualization of the two achiral superpositions $|+\rangle$ (Subfigure (a)) and $|-\rangle$ (Subfigure (b)) of $S-$ and $R-$CHFClBr according to Eq. 2.4.

The superpositions can be formed as

$$|S\rangle = \left(|+\rangle + |-\rangle\right)/\sqrt{2}, \quad |R\rangle = \left(|+\rangle - |-\rangle\right)/\sqrt{2}, \tag{2.2}$$

with

$$\hat{P}\,|S\rangle = |R\rangle\,, \quad \hat{P}\,|R\rangle = |S\rangle\,. \tag{2.3}$$

A Hamiltonian that conserves parity should have simultaneous eigenstates with the parity operator and therefore one might expect to be able to find a molecule such as CHBrClF not only in the chiral forms depicted in Figure 2.4 but also the achiral eigenstates of the parity operator, which correspond to superpositions of the chiral forms:

$$|+\rangle = \left(|S\rangle + |R\rangle\right)/\sqrt{2}, \quad |-\rangle = \left(|S\rangle - |R\rangle\right)/\sqrt{2}, \tag{2.4}$$

and are illustrated in Figure 2.5.

The fact that these superpositions are not found in nature and have never been successfully created in the laboratory indicates that parity symmetry is broken on some level but it remains unclear whether this parity violation is related to the fundamental symmetry breaking of the electroweak interaction or an effect of superselection rules which result from coupling of the molecule to its environment, e.g. radiation fields or other molecules.[51, 52, 138, 139]

Over the past thirty years or so there have been a number of different experiments aiming at a measurement of parity violation in chiral molecules. Starting with very early attempts to detect molecular PV in infrared spectra of bromochlorofluoromethane

(CHFClBr) and camphor [22, 78], there have been reports for example of an experiment involving Mössbauer spectroscopy on an iron complex [140] and of measurements of the circular dichroism in recrystallized transition metal complexes [141].

The tightest upper bound on molecular PV established so far was achieved through a highly refined version of CHFClBr infrared spectroscopy, where a resolution $\Delta\nu_{\mathrm{PV}}/\nu \approx 10^{-13}$ was reached for the relative PV difference of the C–F stretching frequency between the $S-$ and $R-$enantiomers.[72] The theoretical predictions for this relative frequency splitting are several orders of magnitude lower, of the order of 10^{-17}.[142–144] The experimental technique has since been improved, a measurement of the same compound with a resolution of 5×10^{-14} has been reported in 2002,[73] and with a new setup it is hoped that a precision of 10^{-16} can be reached.[145] In addition to the optimization of the experimental resolution the search for compounds suitable for experiments has attracted a lot of attention in recent years. It was realized that, since the effect scales approximately with nuclear charge Z to the power five, compounds containing heavy metal centers could be of greater experimental value than the originally used organic molecules with regard to a maximization of PV frequency splittings. Calculations on molecules containing e.g. bismuth, rhenium, mercury, astatine or tungsten have been reported.[146–150]

The interpretability of experimental results and the potential to extract standard model parameters from such experiments rely on the possibility of performing highly accurate electronic structure calculations. This consideration can suggest a preference for rather lighter molecules in the long run while those molecules containing heavy nuclei could offer a better chance at a first detection of PV effects in chiral molecules.[34, 77, 151–153] In any case, the delicate balance between maximizing the effect and optimizing computational accuracy and experimental precision has to be struck.[36, 154]

Another way to observe molecular PV is in line splittings between nuclear magnetic resonance (NMR) spectra of enantiomers, since the weak interaction, in theory, gives rise to slightly different shielding tensors for the two mirror image molecules. Surprisingly, there have been no reports of attempted PV NMR measurements, despite the fact that even the very first order of magnitude estimates of PV NMR frequency splittings suggested that these effects could be close to the experimental resolution at the time: In 1982, it was estimated that PV NMR frequency splittings scale linearly with the magnetic field strength B and, for $B \approx 0.1$T, are of the characteristic order of magnitude of 10^{-3} Hz for chiral molecules containing heavy nuclei with $Z \approx 100$.[6] It was also noted however, that significant cancellation could take place in actual molecular systems.[4, 6] The effect was predicted to scale with Z^2 to Z^4, [6] so that chiral compounds containing

heavy nuclei were considered to be promising candidates for experiments aiming at a measurement of PV effects in NMR.

Since those first order of magnitude estimates, there has been an increasing effort in improving techniques for computation of these effects. Results of quantitative numerical calculations on PV NMR frequency splittings between enantiomers were published in Refs. [53, 155]. In these studies, relativistically parameterized extended Hückel theory was employed and it was predicted that some chiral conformations of compounds containing e.g. thallium, platinum or lead could show parity violating frequency splittings of some milli–Hertz, close to the maximum resolution of NMR experiments at the time. If one wishes to make accurate theoretical predictions as to the size of PV effects, the semi–empirical extended Hückel theory is not the tool of choice, and an *ab initio* approach to PV NMR shielding tensors was presented in Ref. [156]. The Hartree–Fock framework employed in this work neglected electron correlation and relativistic effects beyond leading order, as did the study of Ref. [157] which also utilized Hartree–Fock theory. Calculations of PV NMR shielding tensors and spin–spin coupling constants including correlation effects at the density functional theory (DFT) level were presented in Ref. [158]. A systematically improvable treatment of electron correlation effects on PV NMR shielding tensors, including static correlation effects via the complete active space self–consistent field (CASSCF) method or dynamic correlation effects using the second–order approximate coupled–cluster (CC2) and coupled–cluster singles–and–doubles (CCSD) approaches was introduced in Ref. [66], where the impact of correlation effects was found to be on the order of 10% to 20% for hydrogen peroxide (H_2O_2) and its heavier homologues disulfane and diselane (H_2S_2 and H_2Se_2, respectively).

A relativistic *ab initio* treatment of PV contributions to NMR shielding constants within four–component Dirac–Hartree–Fock–Coulomb (DHFC) theory was presented in Ref. [68]. While the previously reported, nonrelativistic Hartree–Fock results for the dihydrogen dichalcogenides (H_2X_2),[156] scaling with nuclear charge Z to the power of about 2.5 were confirmed, the authors observed a Z^5 scaling for the scalar–relativistic contribution and a strong, but less regular scaling for the spin–orbit contribution with up to Z^7 in H_2Po_2. These results were quite unexpected because earlier estimates of the scaling behavior predicted Z^2 scaling of the electron spin–independent and Z^4 scaling of the electron spin–dependent contribution to the shielding tensor,[6] with a possible relativistic correction factor of up to perhaps $Z^{1.5}$.[37, 67, 159] The quasirelativistic zeroth order regular approximation (ZORA) approach to the calculation of PV corrections to NMR parameters within a DFT framework, which was developed during the course of this thesis (see Ref. [57] and Chapters 5.5 and 6), confirmed the originally predicted scaling behavior, and the unusual scaling observed within the DHFC study

has since been attributed to an instability of the four–component wavefunction under time–reversal anti–symmetric perturbations.

Relativistic approaches are particularly important with respect to the preparation of experiments because, due to the scaling of PV NMR effects with nuclear charge Z, chiral compounds containing heavy NMR active nuclei are the most likely experimental candidates. In order to make accurate theoretical predictions for such compounds, a relativistic treatment is necessary, and it was the goal of this work to develop such an approach to be used in the screening of molecules potentially suited for an experimental observation of PV NMR signals.

In the following chapter general aspects of relativistic electronic structure theory are introduced. In this context, an effective potential for the PV weak interaction of electrons and nucleons inside an atom or molecule is also derived. Chapters 4 and 5 then provide details on the ZORA approach [60, 61] and a formalism for the calculation of molecular properties within this framework, which was extended with emphasis on PV NMR shielding tensors as part of this thesis.

Chapter 3

Relativistic electronic structure theory

In this chapter a brief overview of relativistic electronic structure theory is presented. Starting from a discussion of the single–particle Dirac equation and the energy spectrum of the hydrogen–like atom in Section 3.1, properties of relativistic many–electron Hamiltonians are reviewed in Section 3.2. The most prevalent of these is the Dirac–Coulomb Hamiltonian, and atomic mean field calculations based on it were performed as early as the 1930s [160]. Nevertheless, many misconceptions and uncertainties about the validity of this approach persisted for a long time, some of which are addressed in the present chapter. In part as a result of perceived difficulties with the many–electron Dirac–Coulomb Hamiltonian, much effort was put in the development of quasi–relativistic methods in which the four–component Dirac bispinors are reduced to two–component form. Such an approach, the zeroth order regular approximation (ZORA) will be used in the remainder of this thesis (specifically Chapters 4 and 5), and some more general issues related to two–component methods are introduced already in Section 3.3 of this chapter. The possibility of including parity violating weak interaction effects in electronic structure calculations is discussed in Section 3.4, and the derivation of an effective operator for the lowest order electron–nucleon neutral current interaction is outlined.

3.1   The Dirac equation

Within the theory of special relativity the Hamiltonian $\mathcal{H}$ of a particle of mass m moving with momentum $\vec{p}$ is given by (see e.g. Ref. [161]):

$$\mathcal{H} = \sqrt{\vec{p}^2 c^2 + m^2 c^4},\tag{3.1}$$

where c is the speed of light in vacuum and m^2c^4 is the square of the rest energy of the particle. For the derivation of a quantum mechanical operator related to the energy by replacing $\vec{p}$ with the operator $\hat{\vec{p}} = -i\hbar\nabla$ in position space ($i = \sqrt{-1}$, $\hbar = h/2\pi$ is the reduced Planck constant and $\nabla^{\mathrm{T}} = (\partial/\partial x\,,\,\partial/\partial y\,,\,\partial/\partial z)$) this expression poses some problems, because the square root is ill defined.

One way to circumvent this problem is to employ the equation for the square of the energy (kinetic energy and rest mass):

$$E^2 = \vec{p}^2 c^2 + m^2 c^4. \tag{3.2}$$

Using the substitution rules $\vec{p} \to \hat{\vec{p}} = -i\hbar\nabla$ and $E \to i\hbar\frac{\partial}{\partial t}$ for operators in position space, one obtains the Klein-Gordon equation [162, 163] for a free particle:

$$\left(-\frac{1}{c^2}\frac{\partial^2}{\partial t^2} + \nabla^2\right)\phi = \frac{m^2 c^2}{\hbar^2}\phi. \tag{3.3}$$

The Klein-Gordon equation was the first quantum-mechanical wave-equation derived by Schrödinger who initially discarded it because it could not describe the fine structure of the hydrogen atom (see e.g. the historical introduction of Ref. [164] and references cited therein). The reason for this is that the Klein-Gordon equation does not account for the electron's spin which, coupled to the electron orbital angular momentum, is the source of the fine structure of atomic spectra.

A relativistic quantum equation that naturally accounted for the spin of the electron was finally derived by Dirac [165]. He was dissatisfied with the Klein-Gordon equation because the probability density associated with this equation could be negative and realized that the reason for this was that the Klein-Gordon equation is a second order differential equation in time. His original goal was thus the derivation of a relativistic quantum mechanical equation linear in time differentiation, which is now commonly written as:

$$\left(c\vec{\alpha}\cdot\hat{\vec{p}} + \beta mc^2\right)\psi = i\hbar\frac{\partial}{\partial t}\psi, \tag{3.4}$$

with the matrices

$$\beta = \begin{pmatrix} \mathbf{1} & \mathbf{0} \\ \mathbf{0} & -\mathbf{1} \end{pmatrix}; \quad \vec{\alpha} = \begin{pmatrix} \mathbf{0} & \vec{\sigma} \\ \vec{\sigma} & \mathbf{0} \end{pmatrix}, \tag{3.5}$$

where $\vec{\sigma}$ is the vector of Pauli matrices:

$$\sigma_x = \begin{pmatrix} 0 & 1 \\ 1 & 0 \end{pmatrix}; \quad \sigma_y = \begin{pmatrix} 0 & -i \\ i & 0 \end{pmatrix}; \quad \sigma_z = \begin{pmatrix} 1 & 0 \\ 0 & -1 \end{pmatrix}. \tag{3.6}$$

The four–component Dirac bispinor $\psi^{\mathrm{T}} = \left(\phi^{\mathrm{T}}, \chi^{\mathrm{T}}\right)$ is commonly expressed in terms of its upper and lower components, ϕ and χ, respectively, so that Eq. 3.4 takes the form:

$$\begin{pmatrix} \mathbf{1}mc^2 & c\vec{\sigma} \cdot \hat{\vec{p}} \\ c\vec{\sigma} \cdot \hat{\vec{p}} & -\mathbf{1}mc^2 \end{pmatrix} \begin{pmatrix} \phi \\ \chi \end{pmatrix} = i\hbar \frac{\partial}{\partial t} \begin{pmatrix} \phi \\ \chi \end{pmatrix}. \tag{3.7}$$

In order to study the behavior of an electron inside an external electromagnetic field, one can follow the usual minimal coupling prescription $\hat{\vec{p}} \to \vec{\pi} = \hat{\vec{p}} - q\vec{A}$ for a particle with charge q moving inside a magnetic field $\vec{B} = \nabla \times \vec{A}$ with vector potential $\vec{A}$, and add an electrostatic potential $\mathbf{1}_{4 \times 4} q\varphi$. Dirac found that within his formalism the angular momentum conserved inside a central potential is equal to $-i\hbar \vec{r} \times \nabla + \hbar \vec{\Sigma}/2$, where $\vec{\Sigma}$ is a 4×4 realization of the Pauli spin matrices with eigenvalues ± 1:

$$\vec{\Sigma} = \begin{pmatrix} \vec{\sigma} & 0 \\ 0 & \vec{\sigma} \end{pmatrix}. \tag{3.8}$$

Accordingly, Dirac's theory correctly describes the electron as having an intrinsic angular momentum equal to $\pm \hbar/2$ and at least qualitatively includes fine structure splitting (see e.g. Ref. [166]). There is also a positive probability density $\rho = |\psi|^2$ associated with the equation with constant total probability, so that Dirac's primary goal was achieved.

For a free particle moving with momentum $\vec{p}$, the Dirac equation has four plane wave solutions, two corresponding to the two spin states of the electron with energy $E = +\sqrt{\vec{p}^2 c^2 + m^2 c^4}$ and two other solutions with $E = -\sqrt{\vec{p}^2 c^2 + m^2 c^4}$. This appearance of negative energy states was already known from the Klein-Gordon equation, and solutions of negative energy also appear in classical relativistic mechanics, of course, but pose no problem there because they are separated from the solutions of positive energy by an energy gap that can not be crossed. Within a quantum mechanical framework, however, there is the possibility of discontinuous energy transitions and the negative energy solutions have to be considered. In that case, questions as to the stability of matter have to be addressed. Dirac proposed that matter is stable, because most of the negative energy states are occupied and Pauli's exclusion principle prevents other particles from transitions to these low energy states. This explanation eventually lead to the prediction of the existence of the positron, a particle with positive elementary charge e and the same mass as the electron [167–169].
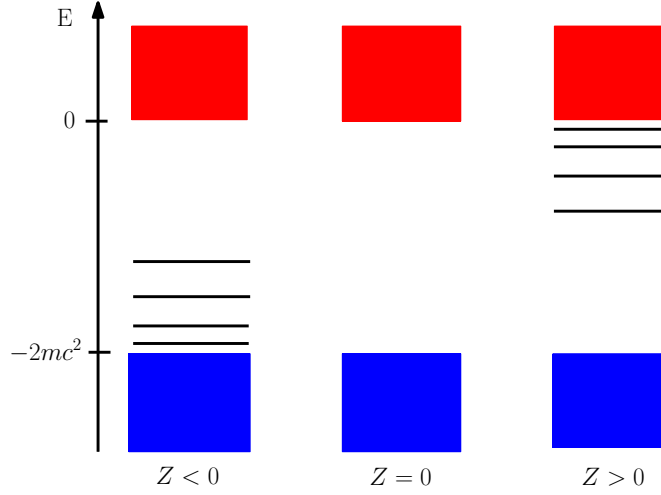
Figure 3.1: Schematic drawing of the eigenvalue spectrum of the Dirac operator for the hydrogen-like atom with nuclear charge Z. Electronic and positronic bound states have been assigned to positively and negatively charged nuclei, respectively. Continuum states of positive and negative energy are indicated by red and blue boxes.

For the hydrogen–like atom with electrons moving inside the Coulomb potential $V(\vec{r}) = -e\varphi(\vec{r}) = -e^2 Z / (4\pi\varepsilon_0 r)$ generated by a nucleus of charge number Z (here e is the charge of the proton, ε_0 is the vacuum dielectric constant and r is the distance between the electron and nucleus), the time–independent Dirac equation is given by:

$$\left(c\vec{\alpha} \cdot \hat{\vec{p}} + \beta m_{\mathrm{e}} c^2 + \mathbf{1}_{4\times4} V(\vec{r}) \right) \psi = \epsilon\psi, \tag{3.9}$$

with m_{e} being the mass of the electron. It can be solved analytically and the corresponding energy levels are given by:[170–172]

$$\epsilon_{nj} = \pm m_{\mathrm{e}} c^2 \left(1 + \frac{(Z\alpha)^2}{\left(n - j - \frac{1}{2} + \sqrt{\left(j + \frac{1}{2} \right)^2 - (Z\alpha)^2} \right)^2} \right)^{-\frac{1}{2}}, \tag{3.10}$$

with the fine structure constant $\alpha = e^2 / 4\pi\varepsilon_0 \hbar c$. The principal quantum number of the energy levels is n, j is the total angular momentum. The two sets of solutions are separated by an energy gap of $\approx 2 m_{\mathrm{e}} c^2$. Shifted by the negative rest–mass $-m_{\mathrm{e}} c^2$, the spectrum is depicted schematically in Figure 3.1, where electronic and positronic bound states have been assigned to positively and negatively charged nuclei, respectively.

In the present discussion of the hydrogen atom, the classical Coulomb interaction between electron and nucleus was used, which poses an inconsistency. As a result, some of the phenomenology of the hydrogen atom can not be described in this framework. States with the same n and j values but different orbital angular momentum (e.g. $2s_{1/2}$ and

$2\mathrm{p}_{-1/2}$) are predicted to have the same energy, whereas a lift of the degeneracy (the Lamb shift) is observed experimentally.[173] This discrepancy can be removed by quantization of the electromagnetic field. The dominant correction then stems from the interaction of the electron with its own electromagnetic field, the so–called self–interaction. Another important contribution, called vacuum polarization, is due to interaction with virtual electron–positron pairs. The source of these corrections will be touched on briefly in Section 3.2.1.

3.2   Relativistic Hamiltonian for many–electron systems

The basis for most relativistic molecular electronic structure calculations, including the ZORA framework discussed in Chapters 4 and 5 of this thesis, is the Dirac–Coulomb Hamiltonian. It is written as the sum of n one–electron free particle Dirac operators of Eq. 3.4, the (external) electrostatic potential caused by the N_{nuc} nuclei and the Coulomb repulsion between the electrons:

$$\hat{H}^{\mathrm{DC}} = \sum_i^n \left[\left(c\vec{\alpha}_i \cdot \vec{\pi}_i + \beta_i m_{\mathrm{e}} c^2 \right) - \frac{e^2}{4\pi\varepsilon_0} \mathbf{1}_{4\times 4} \sum_A^{N_{\mathrm{nuc}}} \frac{Z_A}{r_{Ai}} + \frac{e^2}{4\pi\varepsilon_0} \sum_{j<i} \frac{\mathbf{1}_i \mathbf{1}_j}{r_{ij}} \right]. \qquad (3.11)$$

This Hamiltonian has been used with great success in relativistic mean field calculations since 1935,[160] but there are two issues that need to be addressed. The first is related to the fact that there is no closed form expression for a Lorentz–invariant electron–electron interaction, and the Coulomb interaction of Eq. 3.11 is not even approximately Lorentz–invariant. The second issue concerns the fact that the Hamiltonian of Eq. 3.11 does not conserve particle number but charge, which means that for every n–electron bound state of a specific energy, there is an infinite number of states of equal energy with $(n+1)$ electrons and 1 positron, $(n+2)$ electrons and 2 positrons and so forth (see for example the review Ref. [174]). It was first observed in Ref. [175] that such a Hamiltonian cannot have a stable bound state spectrum, as discrete states embedded in a continuum must autoionize. This phenomenon is called "continuum dissolution" or "Brown Ravenhall disease" after the authors of Ref. [175]. Another, somewhat related issue called "variational collapse" or "finite basis set disease" is the observation that application of matrix–based variational methods known from nonrelativistic theory can sometimes lead to a spectrum that is qualitatively very different from that of the Hamiltonian of Eq. 3.11. This stems from the fact that the Dirac operator for the kinetic energy is not bounded from below and that therefore the variational principle is not, strictly speaking, applicable to the Dirac–Coulomb equation without taking special care, as discussed for example in Refs. [176, 177].

The formally correct way of deriving a relativistic many–electron Hamiltonian and (at least in principle) solving the above mentioned problems is to start with quantum electrodynamics (QED) where matter and radiation fields are described relativistically on equal footing. In order to derive an effective Schrödinger–type equation (the eigenvalues of which correspond to electronic energy levels), it is then necessary to consider the bound state problem within a QED framework, decouple photons from electrons and positrons by means of a unitary transformation and subsequently decouple electrons and positrons through another unitary transformation. Both of these transformations can not be given in closed form, however, and divergences appear.[176] Any relativistic many–electron Hamiltonian can thus only be given correct up to a certain order in the fine structure constant α, usually α or α^2, and renormalization techniques have to be employed.

Examples for such efforts can be found in Refs. [175, 178–186]. In the upcoming Section 3.2.1, basic steps required for such a procedure will be indicated with emphasis on the relativistic electron–electron interaction. Reviews of the formalism can be found e.g. in Refs. [185, 187, 188], and an example of a textbook that is quite detailed on bound state QED is Ref. [189]. Section 3.2.2 contains a brief discussion of the handling of negative energy states in electronic structure calculations.

3.2.1   Relativistic electron–electron interaction

The QED Hamiltonian for electrons (and positrons) inside an external field A_μ^{ext} is given by (see for example Refs. [183, 187, 188]):

$$\hat{H} = \hat{H}^{\text{rad}} + \hat{H}^{\text{mat}} + \frac{1}{c} \int \mathrm{d}^3x \; \hat{j}^\mu \left(A_\mu^{\text{ext}} + \hat{A}_\mu \right). \tag{3.12}$$

$\hat{H}^{\text{rad}}$ is the Hamiltonian describing the free radiation field (with $\vec{E}$ being the electric field vector):

$$\hat{H}^{\text{rad}} = \frac{\varepsilon_0}{2} \int \mathrm{d}^3x \; \left(\vec{E}^2 + c^2 \vec{B}^2 \right), \tag{3.13}$$

and $\hat{H}^{\text{mat}}$ is related to the free particle Dirac Hamiltonian of Eq. 3.4. The four–potential of the external field A_μ^{ext} is generated by the atomic nuclei in the system and considered to be constant, implying use of the Born–Oppenheimer approximation. It can be expressed in terms of the scalar electric potential φ and the vector potential $\vec{A}$: $A^\mu = \left(\varphi, c\vec{A} \right)$, with Greek indices running over $0, 1, 2, 3$ or ct, x, y, z. Covariant and contravariant vectors

are connected by the metric tensor $g_{\mu\nu}$:

$$v_\mu = g_{\mu\nu} v^\nu, \quad g_{\mu\nu} = 0 \quad \text{for} \quad \mu \neq \nu \quad \text{and} \quad g_{00} = -g_{11} = -g_{22} = -g_{33} = -1. \quad (3.14)$$

The Einstein summation convention for scalar products of the type $v^\mu w_\mu = \sum_{\mu=0}^{4} v^\mu w_\mu$ is being used in this entire chapter, where repeated covariant and contravariant indices are implicitly summed over.

The $\hat{A}_\mu$ term in Eq. 3.12 constitutes a coupling between the photon field and the current operator $\hat{j}^\mu$ related to the matter fields:

$$\hat{j}^\mu = -\frac{ec}{2} \left[\hat{\bar{\psi}} \gamma^\mu, \hat{\psi} \right]. \quad (3.15)$$

The electron–positron field operator is commonly expanded in a complete orthonormal set of solutions of the Dirac equation $\{\psi_m\}$:

$$\hat{\psi} = \sum_{\epsilon_m > 0} \hat{a}_m \psi_m + \sum_{\epsilon_m < 0} \hat{b}_m^\dagger \psi_m, \quad (3.16)$$

with the electron and positron creation and annihilation operators $\left\{ \left(\hat{a}_m^\dagger, \hat{a}_m \right) \right\}$ and $\left\{ \left(\hat{b}_m^\dagger, \hat{b}_m \right) \right\}$, respectively that fulfill the usual anticommutation rules and the conditions $\hat{a}_m \ket{0} = \hat{b}_m \ket{0}$, where $\ket{0}$ is the vacuum state vector (see for instance Refs. [189, 190]). $\hat{\bar{\psi}}$ is the adjoint of the field operator $\hat{\psi}$:

$$\hat{\bar{\psi}} = \hat{\psi}^\dagger \gamma^0, \quad (3.17)$$

and the Dirac gamma matrices in their standard representation are given by:

$$\gamma^0 = \beta, \qquad \gamma^i = \beta \alpha^i. \quad (3.18)$$

In Eq. 3.15 $[\cdot, \cdot]$ is the commutator: $[a, b] = ab - ba$.

In order to treat electronic bound states in atoms or molecules within the framework of QED, the field generated by the nuclei can not be treated as weak and must be included in the zero order approximation of a perturbative approach to the problem. This leads to the so–called Furry representation,[191] somewhat of an intermediate between the Heisenberg and interaction representations. The Hamiltonian 3.12 is partitioned accordingly into a zero order Hamiltonian including the external electromagnetic field:

$$\hat{H}^0 = \hat{H}^{\text{rad}} + \hat{H}^{\text{mat}} + \frac{1}{c} \int \mathrm{d}^3 x \, \hat{j}^\mu A_\mu^{\text{ext}} \quad (3.19)$$

and the coupling part between the radiation and matter fields:

$$\hat{V} = \frac{1}{c} \int d^3x \, \hat{j}^{\mu} \hat{A}_{\mu}. \tag{3.20}$$

This particular partitioning is similar to the independent particle model used in nonrelativistic electronic structure theory, as the fermion field operators $\hat{\psi}$ and $\hat{\bar{\psi}}$ of Eq. 3.16 are expanded in terms of the (complete) set of solutions of the Dirac equation inside the external potential, i.e. one–particle states are used as a starting point for the calculation of a many–particle bound state. It is customary to add a mass renormalization counter term $\frac{1}{2}\delta m \left[\hat{\bar{\psi}}, \hat{\psi}\right]$ to the integrand of Eq. 3.20 in order to cancel an infinite self–energy term of first order in α (see e.g. Refs. [185, 189]). For the present purpose, which is mainly to identify effective electron–electron interaction operators as a starting point for relativistic many–body calculations, it can be omitted.

In order to use perturbative approaches developed for scattering problems, adiabatic dampening of the interaction Hamiltonian is convenient:[192]

$$\hat{V}_{\gamma}^{F}(t) = e^{-\gamma|t|}\hat{V}^{F}(t), \tag{3.21}$$

with $\gamma > 0$. The interaction is now switched off at times $t = \pm\infty$ but the fact that the interaction between bound electrons in an atom or molecule is present at all times can be accounted for by taking the limit $\gamma \to 0$ and restoring the interaction during the entire time–interval.

With these modifications it is now possible to use the machinery originally developed for free–electron QED. The shift in energy of a level associated with the state vector $\left|\Phi^0\right\rangle$ of noninteracting matter and electromagnetic fields is given by (Refs. [192, 193] as cited in Refs. [185, 187])

$$\Delta E = \lim_{\substack{\gamma \to 0 \\ \lambda \to 1}} \frac{i\hbar\gamma\lambda}{2} \frac{\frac{\partial}{\partial\lambda} \left\langle \Phi^0 \left| \hat{S}_{\gamma,\lambda}^{F} \right| \Phi^0 \right\rangle}{\left\langle \Phi^0 \left| \hat{S}_{\gamma,\lambda}^{F} \right| \Phi^0 \right\rangle}, \tag{3.22}$$

which is expanded in powers of λ for practical purposes.[187] The S–matrix $\hat{S}_{\gamma,\lambda}^{F}$ is defined using the time–evolution operator in the Furry picture:

$$\hat{S}_{\gamma,\lambda}^{F} = \hat{U}_{\gamma,\lambda}^{F}(\infty, -\infty), \tag{3.23}$$

and expanded perturbatively:

$$\hat{S}_{\gamma,\lambda}^{F} = 1 + \sum_{n=1}^{\infty} \hat{S}_{\gamma,\lambda}^{F(n)}, \tag{3.24}$$

with

$$
\hat{S}^{\mathrm{F}(n)}_{\gamma,\lambda} = \left(\frac{-\mathrm{i}\lambda}{\hbar c}\right)^n \frac{1}{n!} \int \mathrm{d}^4 x_1 \ldots \int \mathrm{d}^4 x_n \; e^{-\gamma|t_1|} \ldots e^{-\gamma|t_n|} \times
$$
$$
\mathrm{T}\left[\hat{j}^\mu (x_1)\, \hat{A}_\mu (x_1) \ldots \hat{j}^\nu (x_n)\, \hat{A}_\nu (x_n)\right]. \tag{3.25}
$$

Here, $\mathrm{T}\left[\ldots\right]$ designates a time–ordered product of operators:

$$
\mathrm{T}\left[\hat{\bar{\psi}}(t_1)\,\hat{\psi}(t_2)\right] = \hat{\bar{\psi}}(t_1)\,\hat{\psi}(t_2)\,\theta(t_1 - t_2) - \hat{\psi}(t_2)\,\hat{\bar{\psi}}(t_1)\,\theta(t_2 - t_1), \tag{3.26}
$$

for fermion operators, using the θ–function ($\theta(x) = 1$ for $x > 0$ and $\theta(x) = 0$ for $x < 0$) and without the sign change for photon operators $\hat{A}_\mu$.

For free atoms and molecules this approach eventually leads to an expansion of the electronic energy in even powers of the coupling constant e:[185, 187, 188]

$$
E = E^{(0)} + E^{(2)} + E^{(4)} + \ldots, \tag{3.27}
$$

where the zero order term is equal to the energy of noninteracting electrons (and positrons) inside the nuclear Coulomb potential. The first correction is related to the second–order S–matrix $\hat{S}^{\mathrm{F}(2)}_{\gamma,\lambda}$:

$$
\lim_{\lambda \to 1} \hat{S}^{\mathrm{F}(2)}_{\gamma,\lambda} = -\frac{e^2}{\hbar^2} \int \mathrm{d}^4 x_1 \, \mathrm{d}^4 x_2 \; e^{-\gamma|t_1|} e^{-\gamma|t_2|} \mathcal{D}_{\mu\nu}(x_2 - x_1) \times
$$
$$
\left\{ \sum_{mn} \left[\bar{\psi}_n(x_2)\,\gamma^\mu \mathcal{S}(x_2, x_1)\,\gamma^\nu \psi_m(x_1) \right.\right.
$$
$$
\left. - \mathrm{Tr}\left[\gamma^\mu \mathcal{S}(x_2, x_2)\right] \bar{\psi}_n(x_1)\,\gamma^\nu \psi_m(x_1)\right] \hat{a}^\dagger_n \hat{a}_m
$$
$$
\left. + \sum_{\substack{mn \\ op}} \frac{1}{2}\bar{\psi}_n(x_2)\,\gamma^\mu \psi_m(x_2)\,\bar{\psi}_p(x_1)\,\gamma^\nu \psi_o(x_1)\,\hat{a}^\dagger_n \hat{a}^\dagger_p \hat{a}_o \hat{a}_m \right\}, \tag{3.28}
$$

with the three terms corresponding to the Feynman diagrams depicted in Fig. 3.2 (it can be shown that disconnected diagrams lead to the same energy shift for every level and can therefore be eliminated from the discussion, see e.g. Ref. [185]).

The electron propagator $\mathcal{S}$ is defined as:

$$
\mathcal{S}(x_2, x_1) = \left\langle 0 \left| \mathrm{T}\left[\hat{\psi}(x_2)\,\hat{\bar{\psi}}(x_1)\right] \right| 0 \right\rangle, \tag{3.29}
$$

where $|0\rangle$ is the vacuum state vector. The photon propagator $\mathcal{D}$ is defined along the same lines, its form depending on the chosen gauge. In Feynman gauge it is given by

(a)   (b)   (c)
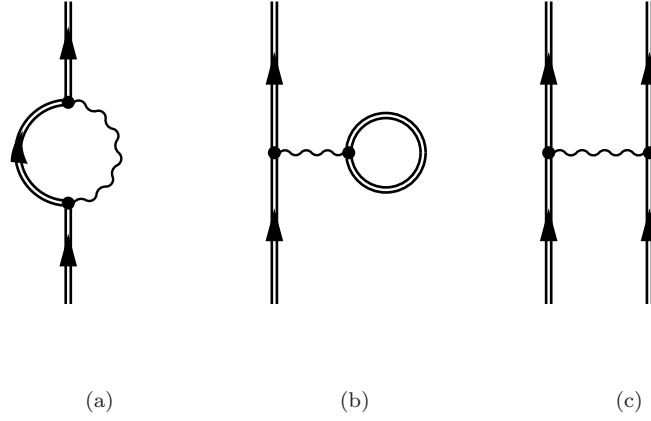
Figure 3.2: Feynman diagrams of order α for bound electrons indicated by double lines. Graphs (a) and (b) describe radiative corrections, namely electron self–energy and vacuum polarization, respectively. Graph (c) corresponds to the lowest order electron–electron interaction.

(see e.g. Refs. [185, 187, 188]):

$$\mathcal{D}_{\mu\nu}^{\mathrm{F}}\left(x_2 - x_1\right) = \frac{-\mathrm{i}}{2\pi\varepsilon_0}\frac{g_{\mu\nu}}{r_{21}}\int\mathrm{d}\omega\; e^{\mathrm{i}|\omega|r_{21}-\mathrm{i}\omega(t_2-t_1)}, \tag{3.30}$$

and in Coulomb gauge by:

$$\mathcal{D}_{\mu\nu}^{\mathrm{C}}\left(x_2 - x_1\right) = \frac{\mathrm{i}}{4\pi\varepsilon_0}\frac{1}{r_{21}}\delta\left(t_2 - t_1\right)\delta_{\mu 0}\delta_{\nu 0} \tag{3.31}$$

$$\mathcal{D}_{\mu\nu}^{\mathrm{t}}\left(x_2 - x_1\right) = \frac{-\mathrm{i}}{2\pi\varepsilon_0}\left\{\frac{g_{\mu\nu}}{r_{21}}\int\mathrm{d}\omega\; e^{\mathrm{i}|\omega|r_{21}-\mathrm{i}\omega(t_2-t_1)} - \nabla_{2\mu}\nabla_{1\nu}\frac{1}{r_{21}}\times\right.$$
$$\left. \int\mathrm{d}\omega\; e^{\mathrm{i}\omega(t_2-t_1)}\frac{e^{\mathrm{i}|\omega|r_{21}}-1}{\omega^2}\right\}\left(1 - \delta_{\mu 0}\right)\left(1 - \delta_{\nu 0}\right), \tag{3.32}$$

where the 00–component of $\mathcal{D}$, which gives the instantaneous Coulomb interaction, has been isolated in $\mathcal{D}^{\mathrm{C}}$, whereas the remaining space–like components of $\mathcal{D}^{\mathrm{t}}$ describe transversely polarized photons.[187, 188]

Figures 3.2(a) and 3.2(b) describe radiative corrections of order $\alpha \propto e^2$ called self–energy and vacuum polarization, respectively, and correspond to the first two terms in Eq. 3.28. The third digram, Fig. 3.2(c), corresponds to the first order electron–electron interaction inside an atom or molecule (given by the third term in Eq. 3.28, $\hat{S}_x^{\mathrm{F}(2)}$). It involves matrix elements of $\hat{S}_x^{\mathrm{F}(2)}$ with at least two–electron initial and final states, $|i\rangle$ and $|f\rangle$, respectively. After performing the time integrations in Eq. 3.28 and taking the

limit $\gamma \to 0$ one arrives at the expression:[184, 185]

$$
\begin{aligned}
\left\langle f \left| \hat{S}_x^{\mathrm{F}(2)} \right| i \right\rangle_{\mathrm{x}} = & - 2\pi\delta \left(\omega_{1_i} + \omega_{2_i} - \omega_{1_f} - \omega_{2_f}\right) \frac{e^2}{\hbar^2} \int \mathrm{d}^3 x_1 \, \mathrm{d}^3 x_2 \, \mathcal{D}_{\mu\nu} \left(\vec{x}_2 - \vec{x}_1, \omega\right) \\
& \times \left[\bar{\psi}_{2_f} \left(\vec{x}_2\right) \gamma^\mu \psi_{2_i} \left(\vec{x}_2\right) \bar{\psi}_{1_f} \left(\vec{x}_1\right) \gamma^\nu \psi_{1_i} \left(\vec{x}_1\right) \right. \\
& \left. - \bar{\psi}_{1_f} \left(\vec{x}_2\right) \gamma^\mu \psi_{2_i} \left(\vec{x}_2\right) \bar{\psi}_{2_f} \left(\vec{x}_1\right) \gamma^\nu \psi_{1_i} \left(\vec{x}_1\right)\right],
\end{aligned}
\tag{3.33}
$$

where $\mathcal{D}_{\mu\nu} \left(\vec{x}_2 - \vec{x}_1, \omega\right)$ is the Fourier transform of the photon propagator:

$$
\mathcal{D}_{\mu\nu} \left(x_2 - x_1\right) = \int \frac{\mathrm{d}z}{2\pi} e^{-iz(t_2 - t_1)} \mathcal{D}_{\mu\nu} \left(\vec{x}_2 - \vec{x}_1, z\right).
\tag{3.34}
$$

The delta function involving frequencies ω is related to energy conservation at the vertices of Fig.3.2(c), and the minus sign in front of the exchange term in Eq. 3.33 reflects the antisymmetric character of many–fermion wavefunctions.

Now S–matrix elements can be identified formally with those for scattering with an effective potential $V_{12}^{(1)}$:[184, 185, 187]

$$
\hat{V}_{12}^{(1)} \left(x_{21}, \omega\right) = e^2 \gamma_2^\mu \gamma_1^\nu \mathcal{D}_{\mu\nu} \left(\vec{x}_2 - \vec{x}_1, \omega\right),
\tag{3.35}
$$

where $\hat{V}_{12}^{(1)} \left(x_{21}, \omega\right)$ depends on the gauge via the photon propagators of Eqs. 3.30 and 3.32. In Feynman gauge it becomes:[184, 185]

$$
\hat{V}_{12}^{\mathrm{F}} \left(x_{21}, \omega\right) = \frac{e^2}{4\pi\varepsilon_0} \frac{1}{x_{21}} \left(1 - \vec{\alpha}_2 \cdot \vec{\alpha}_1\right) e^{-\mathrm{i}|\omega|x_{21}}.
\tag{3.36}
$$

For calculations of atomic or molecular energy levels, the Coulomb gauge is often preferred because it leads to a closed form expression for the Coulomb interaction. In this gauge, the 00–component of $\mathcal{D}$ yields the instantaneous Coulomb interaction, whereas the space–like components describe transversely polarized photons,[187, 188] leading to the effective potential

$$
\hat{V}_{12}^{\mathrm{C}} \left(x_{21}, \omega\right) = \frac{e^2}{4\pi\varepsilon_0} \left(\frac{1}{x_{21}} - \vec{\alpha}_2 \cdot \vec{\alpha}_1 \frac{e^{-\mathrm{i}|\omega|x_{21}}}{x_{21}} + \left[\vec{\alpha}_2 \cdot \nabla_2, \left[\vec{\alpha}_1 \cdot \nabla_1, \frac{e^{-\mathrm{i}|\omega|x_{21}} - 1}{\omega^2 x_{21}}\right]\right]\right).
\tag{3.37}
$$

QED is gauge invariant in every order of the coupling constant. Within this framework, the same results are therefore obtained using the Feynman or Coulomb propagators. When used iteratively in many–body calculations, however, the potentials of Eqs. 3.36 and 3.37 lead to different results, because they are strictly valid only for first–order shifts in the energy.[184, 185] The Coulomb gauge is usually preferred in these calculations because the Coulomb interaction is recovered to leading order in the nonrelativistic

limit and both the magnetic interaction (the $\vec{\alpha_2} \cdot \vec{\alpha_1}$ term) and the "gauge term" or "retardation term" (the third term in Eq. 3.37) are suppressed by an additional order of α as the operators mix upper and lower components of the Dirac spinors. The nonrelativistic limit of the effective potential in Feynman gauge is not as easily taken because here the pure Coulomb interaction includes the effect of retardation and higher order terms would have to be taken into account for consistency.[185]

In many practical applications, the frequency dependence of the effective potentials of Eqs. 3.36 and 3.37 is neglected, and in the limit $\omega \to 0$ one obtains the more familiar, instantaneous Coulomb–Gaunt[194] and Coulomb–Breit[195] interactions:

$$\hat{V}_{12}^{\text{CG}}(x_{21}) = \frac{e^2}{4\pi\varepsilon_0} \frac{1}{x_{21}} \left(1 - \vec{\alpha}_2 \cdot \vec{\alpha}_1\right) \tag{3.38}$$

$$\hat{V}_{12}^{\text{CB}}(x_{21}) = \frac{e^2}{4\pi\varepsilon_0} \frac{1}{x_{21}} \left(1 - \frac{1}{2}\vec{\alpha}_2 \cdot \vec{\alpha}_1 - \frac{(\vec{\alpha}_2 \cdot \vec{x}_{21})(\vec{\alpha}_1 \cdot \vec{x}_{21})}{2x_{21}^2}\right). \tag{3.39}$$

The Coulomb–Breit potential is the one that is conventionally used, but the retardation term (the last term in Eq. 3.39) is sometimes neglected.

The different operators in Eq. 3.39 can be analyzed by reducing them to two–component form involving only the large components of the Dirac spinors. One finds, that the pure Coulomb potential accounts for the spin–own–orbit interaction and the Gaunt term ($\propto \vec{\alpha}_2 \cdot \vec{\alpha}_1$) for the spin–other–orbit, spin–spin and orbit–orbit contributions. The retardation part of the Coulomb–Breit interaction leads to corrections of spin–independent potential only (see e.g. Ref. [196] and references cited therein). The consideration of the Gaunt or Breit interaction in addition to the Coulomb potential is particularly important when dealing with relativistic effects in light elements, whereas other relativistic effects dominate around heavy nuclei (see e.g. Ref. [197]). When spin–dependent properties of light molecules or atoms are concerned, it is crucial to include both the spin–own–orbit and spin–other–orbit interactions in the calculation. This has been analyzed, for example, in Ref. [159] concerning parity violating potentials (discussed in Chapters 5.4 and 8 of this thesis) in chiral molecules containing light atoms.

3.2.2 Electrons, positrons and projection operators

The second of the unitary transformations needed to derive a Schrödinger–type operator from Eq. 3.12 decouples electronic and positronic degrees of freedom. It requires charge renormalization,[176] but is often omitted entirely. The reason for this is that terms of the same order in α as corrections derived from the decoupling of electrons and positrons are usually already neglected after decoupling the matter and radiation fields.[176] Instead of the full transformation it is possible to simply restrict the Hamiltonian to

positive energy states. In Fock space this can be achieved by restricting the basis of one–particle states to include only electrons, in configuration space, positive energy projectors appear.[176] This approach is often called the no–(virtual)–pair approximation, as intermediate states involving virtual electron–positron pairs can no longer appear, and a number of such Hamiltonians have been derived from QED (examples can be found in Refs. [175, 179, 180, 182]).

In the special case of mean field calculations, it is sufficient to restrict the basis in which the single–determinantal many–electron wavefunction is expanded to electronic states in order to consistently retain terms of up to $\mathcal{O}\left(\alpha^2\right)$. As a result, unprojected Hamiltonians of Dirac–Coulomb type, which describe both electrons and positrons are used as the basis of such calculations.

These developments were subject to a persistent debate on whether or not unprojected Hamiltonians of Dirac–Coulomb type could be used in many–body calculations, and even a closer look at current publications still has the potential to confuse: In a recent monograph on relativistic electronic structure theory, for example, the authors of chapter eight (Ref. [187]) point out, that the Dirac–Coulomb (or Dirac–Coulomb–Breit) Hamiltonian has no stable bound state spectrum due to the presence of negative energy states and as a solution to this problem refer to publications such as Refs. [180, 182], which suggest the use of projection operators onto positive energy states (around the two–body interaction potentials). The authors of chapter three (Ref. [188]), however, stress "...many authors still believe that it is necessary to enclose electron–electron interaction operators with positive energy projection operators which are not only ill–defined but also totally unnecessary."

The point made in Ref. [187] about the non existing bound state spectrum of Dirac–Coulomb type Hamiltonians can be misleading in the context of mean field calculations, as it was shown in Ref. [182] that the commonly used Dirac–Hartree–Fock (DHF) approach based on the unprojected Dirac–Coulomb Hamiltonian 3.11 (the same argument is valid for the Dirac–Coulomb–Breit Hamiltonian) implicitly includes projection operators onto the positive–energy DHF solutions, which are by construction N–particle Slater determinants and only positive–energy single–particle states are retained. The explicit use of projection operators is thus unnecessary in DHF calculations, but one has to be aware of the fact that the results of such calculations can to some extend be viewed as approximations not to, for example, the eigenstates of the Dirac–Coulomb

Hamiltonian 3.11 but the projected no–pair Hamiltonian:

$$H = \sum_i^n \Lambda_+(i) \left[\left(c\vec{\alpha}_i \cdot \vec{\pi}_i + \beta_i m_\text{e} c^2 \right) - \frac{e^2}{4\pi\varepsilon_0} \mathbf{1}_{4\times4} \sum_A^{N_\text{nuc}} \frac{Z_A}{r_{Ai}} \right] \Lambda_+(i)$$
$$+ \frac{e^2}{4\pi\varepsilon_0} \sum_i^n \sum_{j<i} \Lambda_+(j) \Lambda_+(i) \frac{\mathbf{1}_i \mathbf{1}_j}{r_{ij}} \Lambda_+(i) \Lambda_+(j), \tag{3.40}$$

where the $\Lambda_+(i)$ are projection operators onto the positive–energy one–particle DHF solutions.

In addition, some projection operators suggested for practical calculations were problematic: For the originally recommended Hamiltonian of Ref. [175] projection operators onto the positive energy solutions of the free particle Dirac Eq. 3.4 were used. Another suggestion was to use projectors onto positive energy eigenstates of the Dirac Hamiltonian including the nuclear Coulomb potential.[180] However, both of these approaches, instead of removing negative energy states actually introduce them, because the negative energy states of the Hamiltonian under consideration are in general not orthogonal to the positive energy eigenstates of some other Hamiltonian which are used in the projection operators.[198]

When electron correlation is to be dealt with in a systematic fashion, it becomes necessary to use projection operators explicitly and usually a no–pair Hamiltonian such as the projected Dirac–Coulomb Hamiltonian of Eq. 3.40 is employed, where projection is on to positive energy solutions of the zero order problem, usually a self consistent field calculation (see e.g. the review article [199] and references cited therein).

The problem of the "variational collapse" mentioned in the beginning of Section 3.2 should also be addressed. The Dirac kinetic energy operator is not bounded from below (as discussed in Section 3.1) and the basis of many nonrelativistic many–body methods, the variational principle, is not necessarily applicable to a relativistic extension of these methods based on the Dirac equation. This problem can be dealt with in practice by assuring that the nonrelativistic limit of the theory is reproduced correctly.[176] The most frequently used way of doing this is to use kinetically balanced basis sets, see e.g. Refs. [200–202]. This or other procedures to ensure the correct nonrelativistic limit do not guarantee the validity of the variational principle but yield good results in practice.[176]

3.3 Two–component approaches

The perceived conceptual problems with Hamiltonians of Dirac–Coulomb type mentioned in Section 3.2, such as uncertainties about the treatment of negative energy states and doubts regarding the applicability of the variational principle were perhaps one reason for an increasing interest in approximate relativistic schemes involving two–component wavefunctions during the 1980s. In addition, two–component approaches offered the possibility of reducing computational costs — a reasonable incentive. One such approach, the two–component zeroth order regular approximation (ZORA) [60, 61, 203, 204] forms the basis of this thesis and is discussed in Chapter 4. The present section is meant to lay the ground work for that discussion and a few issues related to two–component methods in general, such as assessment of relativistic content, variational stability and picture change effects will be touched on.

There are essentially two ways of transforming the four–component Dirac equation to a two–component form. The first is to block–diagonalize the Dirac Hamiltonian $\hat{H}^{\mathrm{D}}$ by means of a unitary transformation:

$$\hat{H}^{\mathrm{FW}} = \hat{U}\hat{H}^{\mathrm{D}}\hat{U}^{\dagger} = \left(\begin{array}{cc} \hat{H}^{+} & 0 \\ 0 & \hat{H}^{-} \end{array} \right), \tag{3.41}$$

with $\hat{U}\hat{U}^{\dagger} = 1$. The eigenstates of $\hat{H}^{\mathrm{FW}}$, $\psi^{\mathrm{FW}} = \hat{U}\psi$ fall into two classes, one with vanishing lower component $\chi^{\mathrm{FW}} = 0$ and another with vanishing upper component $\phi^{\mathrm{FW}} = 0$, so that the calculation of the spectrum of the four–component Dirac operator is reduced to two independent two–component problems. This type of transformation is called a Foldy–Wouthuysen transformation after the authors of Ref. [205]. For free electrons, the operator $\hat{U}_{\mathrm{fFW}}$ is known in closed form,[205] but difficulties arise in the presence of an external potential V if one follows the original approach which involved a highly singular expansion of the Dirac Hamiltonian in orders of $1/c^2$ (see e. g. the review article Ref. [206] and references cited therein).

The well–known Douglas–Kroll–Hess method [207, 208] is based on a Foldy–Wouthuysen transformation, but $\hat{U}$ is decomposed into a series of transformations $\hat{U}_1 \ldots \hat{U}_n$ which remove off-diagonal parts of increasing order in the external potential from a Hamiltonian $\hat{H}^{\mathrm{fFW}}$, which is obtained after an initial free–particle transformation $\hat{U}_{\mathrm{fFW}}$:

$$\hat{H}^{\mathrm{fFW}} = \hat{U}_{\mathrm{fFW}}\hat{H}^{\mathrm{D}}\hat{U}_{\mathrm{fFW}}^{\dagger}. \tag{3.42}$$

The expansion in powers of V does not share the problems of the original $1/c^2$ expansion and leads to well–defined regular expressions that can be used within a variational approach.[206]

The second possibility of reducing the Dirac equation to two components is the so–called elimination of the small component. It involves an approximate expression of the lower or "small" component χ of a Dirac spinor in terms of the upper or "large" component ϕ.[1] Expanding a one–electron Hamiltonian of the type given in Eq. 3.9 (with the energy spectrum now shifted by $-m_e c^2$) one obtains coupled equations for the upper and lower components of the bispinor ψ:

$$(V - \epsilon)\phi + c\vec{\sigma} \cdot \hat{\vec{p}}\chi = 0 \tag{3.43}$$

$$c\vec{\sigma} \cdot \hat{\vec{p}}\phi + (V - 2m_e c^2 - \epsilon)\chi = 0. \tag{3.44}$$

Using Eq. 3.44, χ can be expressed in terms of ϕ:

$$\chi = \frac{1}{(\epsilon - V + 2m_e c^2)} c\vec{\sigma} \cdot \hat{\vec{p}}\phi, \tag{3.45}$$

and this expression, inserted into Eq. 3.43, yields an equation for the upper component ϕ alone:

$$c\vec{\sigma} \cdot \hat{\vec{p}} \frac{1}{(\epsilon - V + 2m_e c^2)} c\vec{\sigma} \cdot \hat{\vec{p}}\phi + (V - \epsilon)\phi = 0. \tag{3.46}$$

In order to solve Eq. 3.46, the $(\epsilon - V + 2m_e c^2)^{-1}$ term can be expanded in a power series. One of the earliest of such approaches involved an expansion for $(V - \epsilon) < 2m_e c^2$:

$$\frac{1}{(\epsilon - V + 2m_e c^2)} = \frac{1}{2m_e c^2} \left[1 - \frac{V - \epsilon}{2m_e c^2} \right]^{-1} = \frac{1}{2m_e c^2} \sum_{k=0}^{\infty} \left(\frac{V - \epsilon}{2m_e c^2} \right)^k, \tag{3.47}$$

which, truncated at first order, leads to the Pauli Hamiltonian if the dependence on ϵ eliminated by another expansion in c^{-2} (see e.g. Ref. [206]):

$$\hat{H}^P = \frac{\hat{\vec{p}}^2}{2m_e} + V - \frac{\hat{\vec{p}}^4}{8m_e^3 c4} + \frac{\hbar^2}{8m_e^2 c^2}(\Delta V) + \frac{\hbar}{4m_e^2 c^2}\sigma \cdot \left[(\nabla V) \times \hat{\vec{p}} \right]. \tag{3.48}$$

The first two terms are the same as in nonrelativistic theory, and the subsequent mass–velocity, Darwin and spin–orbit coupling terms, proportional to $-\hat{\vec{p}}^4$, (ΔV) and $\sigma \cdot \left[(\nabla V) \times \hat{\vec{p}} \right]$, respectively, describe all relativistic corrections up to $\mathcal{O}\left(c^{-2}\right)$ contained in the Dirac–Coulomb Hamiltonian.

As was the case for the general Foldy–Wouthuysen transformation (Eq. 3.41), the expansion in orders of c^{-2} is problematic: Near the atomic nucleus the Coulomb potential becomes very large with respect to $2m_e c^2$ and the criterion $(V - \epsilon) < 2m_e c^2$ is no longer

---

[1]The small–large–nomenclature, even though it is traditionally used, is somewhat misleading, since even for electrons the lower component can become the larger one if fields are strong enough

fulfilled. In any case, the three relativistic correction operators are not suited for inclusion in a variational scheme.[206, 209] When used perturbatively in lowest order, however, the operators yield good results for first and second row transition elements,[206] and the Pauli Hamiltonian is often used as a reference for $\mathcal{O}\left(c^{-2}\right)$ relativistic corrections (see e.g. Ref. [210] or Section 4.2.2 of this thesis).

Another approach to the elimination of the small component is called the regular approximation.[60, 61, 198] It is also based on Eq. 3.46, but the expansion of the $(\epsilon - V + 2m_\mathrm{e}c^2)^{-1}$ term is regularized by using the expansion parameter $\epsilon/(2m_\mathrm{e}c^2 - V)$:

$$\frac{1}{(\epsilon - V + 2m_\mathrm{e}c^2)} = \frac{1}{2m_\mathrm{e}c^2 - V}\left[1 + \frac{\epsilon}{2m_\mathrm{e}c^2 - v}\right]^{-1} = \frac{1}{2m_\mathrm{e}c^2 - V}\sum_{k=0}^{\infty}\left(\frac{-\epsilon}{2m_\mathrm{e}c^2 - V}\right)^k.$$

(3.49)

Truncation of this expansion at zeroth and first order defines the ZORA and FORA Hamiltonians, respectively,[61] and the related infinite order regular approximation (IORA) can also be derived from it.[211] Out of these variants, the zeroth order regular approximation seems to be the most widely used. It is reviewed in detail in Chapter 4, where particularly in Section 4.2 its strengths and weaknesses are discussed.

In recent years, matrix–based two–component formalisms have been developed that include (nonradiative) relativistic effects to the level of numerical exactness.[212–214] With the existence of such schemes and increasingly efficient programs for the solution of the relativistic many–body problem based directly on the Dirac–Coulomb Hamiltonian, two– and four–component approaches have, for many practical considerations, become equivalent: Four–component calculations are no longer much more costly than their two–component counterparts and all relativistic effects encountered in standard four–component calculations can now be included in a two–component framework to numerical precision.[215]

Concerning the applicability of the variational principle, it has been discussed in Ref. [216] (see also references cited therein, particularly Ref. [198]), that for an electronic eigenstate of the Dirac equation inside a potential V, described by the bispinor $\psi^\mathrm{T} = \left(\phi^\mathrm{T}, \chi^\mathrm{T}\right)$, the kinetic balance relation

$$\chi = \hat{X}\phi \tag{3.50}$$

with

$$\hat{X} = \frac{1}{2m_\mathrm{e}c^2}\left(c\vec{\sigma}\cdot\hat{\vec{p}} + \left[V, \hat{X}\right] - c\hat{X}\vec{\sigma}\cdot\hat{\vec{p}}\hat{X}\right) \tag{3.51}$$

has to be fulfilled. For such spinors the variational principle holds, and the expectation value of the Dirac Hamiltonian with respect to ψ is bounded from below by the true energy of the electronic ground state. However, the operator $\hat{X}$ can only be given in closed form for a restricted class of potentials, and two–component approaches to relativistic electronic structure theory usually only satisfy an approximate kinetic balance condition established between χ and ϕ.[206] For this case, it has been shown that the approximate relation can be chosen in such a way as to make the problem variationally stable, i.e. a lower bound for the energy exists, but it is shifted below the actual ground state energy.[216] The variational stability of the ZORA approach is briefly addressed in Section 4.2.1 and was proven rigorously in Ref. [204].

Another issue that needs to be addressed in connection with two–component methods is the effect of picture change. In order to be consistent, all operators need to be transformed from a four– to a two–component framework together with the wavefunction and Hamiltonian, otherwise so–called picture change errors are introduced. In approaches based on the elimination of the small component, renormalization of the approximate large component is another source of deviations from four–component results. With regard to the ZORA approach this has been discussed e.g. in Refs. [217–219] and it is also addressed in Chapter 4 in so far as it concerns calculations performed within the scope of this thesis.

3.4 Electroweak effects

A relativistic theory of atoms and molecules not only sheds light on otherwise incomprehensible aspects of electromagnetic interactions in these systems, it also opens the door to the investigation of phenomena beyond electromagnetism. One could exaggeratingly say that a complete theoretical description of electronic structure should take into account the whole spectrum of interactions of the standard model of physics, such as effects of the strong and weak interactions on the nucleon density distribution, or the weak interaction of electrons and nucleons, perhaps even aspects of a grand unified theory or quantum gravity. All of these effects are very small, however, and prior to worrying about most them one would have to go through a very long list of approximations made within the current theory whose impact on computational results is much bigger. The exception here are interactions with unique symmetry characteristics, such as the parity violating (PV) weak interaction. As discussed in Chapter 2 PV properties, such as optical activity of atoms or a difference in energy between the two enantiomers of a chiral molecule can be linked directly to the weak interaction, making their interpretation much easier than that of larger but parity conserving weak interaction effects.

The calculation of PV properties of atoms and molecules is based on effective operators that can be derived in a similar fashion to the electron–electron interaction operators which were the focus of Section 3.2.1, with the modification that the neutral current interaction of free fermions is considered. The formalism was reviewed in detail in Ref. [77]. Here only a short synopsis will be given.

When dealing with parity violating phenomena in stable atoms and molecules, the neutral current interaction (mediated by Z^0 bosons) is the weak process of primary interest. The interaction potential related to the symmetry broken electroweak Lagrangian, which describes the neutral current interaction between free electrons, up and down quarks, and their antiparticles is given by:[77]

$$\hat{V}^{Z^0} = \int \mathrm{d}^3x\, \hat{j}^{0,\mu} \hat{Z}^0_\mu, \tag{3.52}$$

where $\hat{Z}^0_\mu$ corresponds to the neutral Z^0 field and the current operator that couples to it is given by:

$$\hat{j}^{0,\mu} = \hat{j}^{0e,\mu} + \hat{j}^{0u,\mu} + \hat{j}^{0d,\mu}, \tag{3.53}$$

with the neutral electron, up and down quark currents defined as:[2]

$$\hat{j}^{0e,\mu} = \frac{-e}{2\sin\theta_{\mathrm{W}}\cos\theta_{\mathrm{W}}} : \hat{\bar{\psi}}_e \gamma^\mu \left(g_{\mathrm{V}}^e - g_{\mathrm{A}}^e \gamma^5 \right) \hat{\psi}_e : \tag{3.54}$$

$$\hat{j}^{0u,\mu} = \frac{-e}{2\sin\theta_{\mathrm{W}}\cos\theta_{\mathrm{W}}} : \hat{\bar{\psi}}_u \gamma^\mu \left(g_{\mathrm{V}}^u - g_{\mathrm{A}}^u \gamma^5 \right) \hat{\psi}_u : \tag{3.55}$$

$$\hat{j}^{0d,\mu} = \frac{-e}{2\sin\theta_{\mathrm{W}}\cos\theta_{\mathrm{W}}} : \hat{\bar{\psi}}_d \gamma^\mu \left(g_{\mathrm{V}}^d - g_{\mathrm{A}}^d \gamma^5 \right) \hat{\psi}_d : . \tag{3.56}$$

$\hat{\psi}_e$, $\hat{\psi}_u$ and $\hat{\psi}_d$ are the electron, and up and down quark field operators, respectively, which are defined along the lines of the electron field operator $\hat{\psi}$ in Eq. 3.16. Colons around an operator product, $: \cdots :$ indicate normal ordering, where all annihilation operators are to the right of all creation operators. θ_{W} is the Weinberg or weak mixing angle, and γ^5 is given by:

$$\gamma^5 = \mathrm{i}\gamma^0\gamma^1\gamma^2\gamma^3. \tag{3.57}$$

It is used to project a fermion field $\hat{\psi}$ onto it's left– or right–handed components $\hat{\psi}_{\mathrm{L}}$ and $\hat{\psi}_{\mathrm{R}}$, respectively:

$$\hat{\psi}_{\mathrm{L}} = \frac{1-\gamma^5}{2}\hat{\psi}, \qquad \hat{\psi}_{\mathrm{R}} = \frac{1+\gamma^5}{2}\hat{\psi}. \tag{3.58}$$

---

[2]In this section, natural units with $\hbar = c = 1$ are employed.

The vector and axial coupling coefficients g_V^f and g_A^f of Eq. 3.53 depend on weak isospin $t_{3,f}$ and charge number q_f of the fermion f:

$$g_V^f = t_{3,f} - 2q_f \sin^2 \theta_W, \qquad g_A^f = t_{3,f}, \tag{3.59}$$

with values given in Table 3.1.

Table 3.1: Weak isospin $t_{3,f}$, charge number q_f and vector and axial coupling coefficients g_V^f and g_A^f of fermions f.

f	$t_{3,f}$	q_f	g_V^f	g_A^f
e	$-\frac{1}{2}$	-1	$-\frac{1}{2} + 2\sin^2\theta_W$	$-\frac{1}{2}$
u	$\frac{1}{2}$	$\frac{2}{3}$	$\frac{1}{2} - \frac{4}{3}\sin^2\theta_W$	$\frac{1}{2}$
d	$-\frac{1}{2}$	$-\frac{1}{3}$	$-\frac{1}{2} + \frac{2}{3}\sin^2\theta_W$	$-\frac{1}{2}$

Following the procedure indicated in Section 3.2.1 for the electromagnetic interaction between bound electrons, one can once again use the S–matrix expanded in orders of the perturbation, the free–particle analogue of Eq. 3.25, where the perturbation, in this case, is given by Eq. 3.52. As before, the second–order S–matrix (see Eqs. 3.25 and 3.28 for comparison) contains the lowest order contribution to the interaction of two fermions:[77]

$$
\begin{aligned}
\hat{S}^{(2)} =& \frac{-e^2}{8\sin^2\theta_W \cos^2\theta_W} \int d^4x_1 \int d^4x_2 \\
& T\left[\sum_i : \hat{\bar{\psi}}_i(x_2)\gamma^\mu \left(g_V^i - g_A^i\gamma^5\right)\hat{\psi}_i(x_2) : \hat{Z}_\mu^0(x_2) \right. \\
& \left. \times \sum_j : \hat{\bar{\psi}}_j(x_1)\gamma^\nu \left(g_V^j - g_A^j\gamma^5\right)\hat{\psi}_j(x_1) : \hat{Z}_\nu^0(x_1) \right].
\end{aligned}
\tag{3.60}
$$

Focussing only on the contribution of the diagram depicted in Fig. 3.3, i.e. the lowest order contribution to the Z^0–mediated interaction between an electron and an up or down quark, one arrives at the operator:

$$
\begin{aligned}
\hat{S}_x^{(2)} =& \frac{-e^2}{8\sin^2\theta_W \cos^2\theta_W} \frac{1}{2} \int d^4x_1 \, d^4x_2 \, \mathcal{P}_{\mu\nu}(x_2 - x_1) \\
& \times \bar{\psi}_{q'}(x_2)\gamma^\mu \left(g_V^q - g_A^q\gamma^5\right)\psi_q(x_2) \bar{\psi}_{e'}(x_1)\gamma^\nu \left(g_V^e - g_A^e\gamma^5\right)\psi_e(x_1) \, \hat{a}_{q'}^\dagger \hat{a}_{e'}^\dagger \hat{a}_e \hat{a}_q,
\end{aligned}
\tag{3.61}
$$
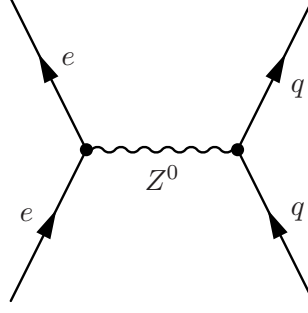
Figure 3.3: Lowest order Feynman diagram for electron–quark Z^0 exchange.

where the Z^0 propagator $\mathcal{P}$ is defined as:

$$
\begin{aligned}
\mathcal{P}_{\mu\nu}\left(x_2 - x_1\right) &= \left\langle 0 \left| \mathrm{T}\left[\hat{Z}_\mu^0\left(x_2\right) \hat{Z}_\nu^0\left(x_1\right)\right]\right| 0 \right\rangle \\
&= \frac{-\mathrm{i}}{(2\pi)^4} \int \mathrm{d}^4 q\, \frac{g_{\mu\nu} - q_\mu q_\nu / m_Z^2}{q^2 - m_Z^2}\, e^{\mathrm{i}(x2-x1)q}.
\end{aligned}
\tag{3.62}
$$

Here, m_Z is the mass of the Z^0 boson which, with $m_Z = 91.1876 \pm 0.0021$ GeV,[220] is extremely heavy, making the interaction very short ranged. For electrons and nuclear valence quarks interacting inside a stable molecule or atom, momentum transfer q is very small compared to m_Z, so that the Fourier transformed Z^0 propagator can be significantly simplified (see e.g. Refs. [77, 221]

$$
\frac{g_{\mu\nu} - q_\mu q_\nu / m_Z^2}{q^2 - m_Z^2} \approx -\frac{g_{\mu\nu}}{m_Z^2}.
\tag{3.63}
$$

The interaction potential, in this case, takes the form of an effective Fermi–type current–current interaction:[77, 221]

$$
\hat{V}_{\mathrm{eff}}^{Z^0} = \frac{G_{\mathrm{F}}}{\sqrt{2}} \int \mathrm{d}^3 x \sum_{ij} : \hat{\bar{\psi}}_i\left(x\right) \gamma_\mu \left(g_{\mathrm{V}}^i - g_{\mathrm{A}}^i \gamma^5\right) \hat{\psi}_i\left(x\right) :: \hat{\bar{\psi}}_j\left(x\right) \gamma^\mu \left(g_{\mathrm{V}}^j - g_{\mathrm{A}}^j \gamma^5\right) \hat{\psi}_j\left(x\right) :,
\tag{3.64}
$$

which would give the same contribution to the energy in first order as the second order S–matrix of Eq. 3.60. G_{F} is Fermi's constant:

$$
\frac{G_{\mathrm{F}}}{\sqrt{2}} = \frac{e^2}{8 \sin^2 \theta_{\mathrm{W}} \cos^2 \theta_{\mathrm{W}} m_Z^2}.
\tag{3.65}
$$

In order to evaluate matrix elements of the second order S–matrix Eq. 3.60 or of the effective potential Eq. 3.64 for an electron interacting with a valence quark inside the atomic nucleus, one would in principle have to use the wavefunction of the quark inside

a nucleon.[221] What is usually done, however, is that the quark currents are replaced by nucleon currents with vector and axial coupling coefficients given by the sum over those of the valence quarks:[221]

$$\hat{j}^{0p,\mu} = \frac{-e}{2\sin\theta_{\mathrm{W}}\cos\theta_{\mathrm{W}}} : \hat{\bar{\psi}}_p \gamma^\mu \left(g_{\mathrm{V}}^p - g_{\mathrm{A}}^p \gamma^5\right)\hat{\psi}_p : \tag{3.66}$$

$$\hat{j}^{0n,\mu} = \frac{-e}{2\sin\theta_{\mathrm{W}}\cos\theta_{\mathrm{W}}} : \hat{\bar{\psi}}_n \gamma^\mu \left(g_{\mathrm{V}}^n - g_{\mathrm{A}}^n \gamma^5\right)\hat{\psi}_n : \tag{3.67}$$

with

$$g_{\mathrm{V}}^p = 2g_{\mathrm{V}}^u + g_{\mathrm{V}}^d = \frac{1}{2} - 2\sin^2\theta_{\mathrm{W}}, \quad g_{\mathrm{A}}^p = 2g_{\mathrm{A}}^u + g_{\mathrm{A}}^d = \frac{1}{2} \tag{3.68}$$

$$g_{\mathrm{V}}^n = g_{\mathrm{V}}^u + 2g_{\mathrm{V}}^d = -\frac{1}{2}, \qquad\qquad g_{\mathrm{A}}^n = g_{\mathrm{A}}^u + 2g_{\mathrm{A}}^d = -\frac{1}{2}. \tag{3.69}$$

The interaction energy for an electron and a proton (the expression for neutrons is completely equivalent) can then be calculated from Eqs. 3.64 or 3.60 as:[221]

$$E_{ep}^{Z^0} = \frac{G_{\mathrm{F}}}{\sqrt{2}} \int \mathrm{d}^3x\, \bar{\psi}_e\left(\vec{x}\right)\gamma_\mu \left(g_{\mathrm{V}}^e - g_{\mathrm{A}}^e \gamma^5\right)\psi_e\left(\vec{x}\right)\, \bar{\psi}_p\left(\vec{x}\right)\gamma^\mu \left(g_{\mathrm{V}}^p - g_{\mathrm{A}}^p \gamma^5\right)\psi_p\left(\vec{x}\right). \tag{3.70}$$

The parity odd terms in Eq. 3.70 can be identified as those linear in γ^5:

$$\begin{aligned} E_{ep}^{Z^0,\mathrm{PV}} = -\frac{G_{\mathrm{F}}}{\sqrt{2}} \int \mathrm{d}^3x\, \Big[&\bar{\psi}_e\left(\vec{x}\right)\gamma_\mu g_{\mathrm{V}}^e \psi_e\left(\vec{x}\right)\, \bar{\psi}_p\left(\vec{x}\right)\gamma^\mu g_{\mathrm{A}}^p \gamma^5 \psi_p\left(\vec{x}\right) \\ &+ \bar{\psi}_e\left(\vec{x}\right)\gamma_\mu g_{\mathrm{A}}^e \gamma^5 \psi_e\left(\vec{x}\right)\, \bar{\psi}_p\left(\vec{x}\right)\gamma^\mu g_{\mathrm{V}}^p \psi_p\left(\vec{x}\right) \Big]. \end{aligned} \tag{3.71}$$

If the nucleons are assumed to be infinitely heavy point–like particles with only spin degrees of freedom, the following relations hold:[37, 221]

$$\bar{\psi}_{n/p}\left(\vec{x}\right)\gamma^0 \psi_{n/p}\left(\vec{x}\right) = -\delta_{n/p}\left(\vec{x}\right) \qquad \bar{\psi}_{n/p}\left(\vec{x}\right)\gamma^i \psi_{n/p}\left(\vec{x}\right) = 0 \tag{3.72}$$

$$\bar{\psi}_{n/p}\left(\vec{x}\right)\gamma^0 \gamma^5 \psi_{n/p}\left(\vec{x}\right) = 0 \qquad \bar{\psi}_{n/p}\left(\vec{x}\right)\gamma^i \gamma^5 \psi_{n/p}\left(\vec{x}\right) = -\sigma_i^{n/p}\delta_{n/p}\left(\vec{x}\right), \tag{3.73}$$

where $\delta_{n/p}\left(\vec{x}\right)$ gives the position of a nucleon and $\vec{\sigma}^{n/p}$ are the nucleon Pauli matrices. Equation 3.71 for the energy is then reduced to:

$$\begin{aligned} E_{ep}^{Z^0,\mathrm{PV}} = -\frac{G_{\mathrm{F}}}{\sqrt{2}} \int \mathrm{d}^3x\, \Big[&\bar{\psi}_e\left(\vec{x}\right)\beta\alpha_i g_{\mathrm{V}}^e \psi_e\left(\vec{x}\right) g_{\mathrm{A}}^p \sigma_i^p \delta_p\left(\vec{x}\right) \\ &+ \bar{\psi}_e\left(\vec{x}\right)\beta g_{\mathrm{A}}^e \gamma^5 \psi_e\left(\vec{x}\right) g_{\mathrm{V}}^p \delta_p\left(\vec{x}\right) \Big]. \end{aligned} \tag{3.74}$$

Summing over all nucleons leads to an effective Hamiltonian for the parity violating interaction between an electron and nucleus:

$$\hat{h}^{\mathrm{PV}} = \frac{G_{\mathrm{F}}}{2\sqrt{2}} \left(Q_{\mathrm{W}}\left(A\right)\gamma^5 \varrho_A\left(\vec{x}\right) + \left(1 - 4\sin^2\theta_{\mathrm{W}}\right)\left(N_A - Z_A\right)\varrho_A\left(\vec{x}\right)\vec{\alpha}\cdot\vec{I}_A \right). \tag{3.75}$$
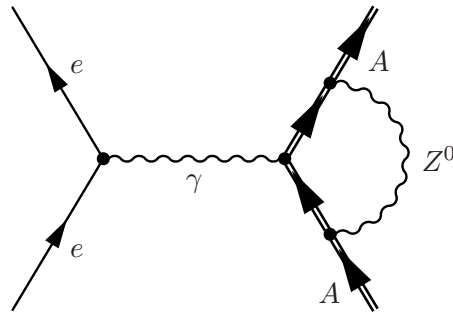
Figure 3.4: Anapole moment contribution to fourth order radiative corrections for the electroweak interaction of electrons e and nucleons inside nucleus A (indicated schematically by double lines).

Here, $Q_{\mathrm{W}}(A) = \left(1 - 4\sin^2\theta_{\mathrm{W}}\right) Z_A - N_A$ is the weak charge of nucleus A with proton number Z_A and neutron number N_A. $\varrho_A(\vec{x})$ is the nucleon density distribution of nucleus A, and $\vec{I}_A$ its spin.

The appearance of the nucleon density distribution ϱ_A in the effective Hamiltonian Eq. 3.75 is an important characteristic of the weak interaction between electrons and nucleons inside an atom or molecule, signifying its extremely short range: The only non vanishing contributions stem from electrons inside the atomic nucleus. Another important feature of the Hamiltonian is Fermi's constant $G_{\mathrm{F}} = 1.166364(5) \times 10^{-5}$ GeV^{-2} which is indicative of the weakness of the interaction. There are two different operators, as can be seen from Eq. 3.75. The first is proportional to γ^5 and yields the dominant contribution to the energy, unless nucleon spins are aligned inside the nucleus.[221] This operator is therefore often used on its own when nuclear spin–independent PV properties such as energy differences between enantiomers of a chiral molecule are calculated. The second term depends on the nuclear spin $\vec{I}_A$ and is usually neglected, unless explicitly nuclear spin–dependent properties such as corrections to hyperfine splittings or nuclear magnetic resonance frequencies are calculated.

The second term in the Hamiltonian of Eq. 3.75 is physically very interesting also because there is a specific type of radiative correction depicted in Fig. 3.4 which leads to an effective interaction with the same basic $\vec{\alpha}\cdot\vec{I}_A$–structure (see e.g. Refs. [37, 92]). This particular contribution is part of the so–called nuclear anapole moment interaction, the phenomenology of which was already mentioned in Chapter 2 with a qualitative illustration in Fig. 2.2. It is this contribution which dominates the nuclear spin–dependent PV interaction between electrons and nucleons and therefore the Hamiltonian of Eq. 3.75

will be used in a recast form:

$$\hat{h}^{\mathrm{PV},a} = \frac{G_{\mathrm{F}}}{2\sqrt{2}} \left(Q_{\mathrm{W}}\left(A\right)\gamma^5 \varrho_A\left(\vec{x}\right) - 2\left(1 - 4\sin^2\theta_{\mathrm{W}}\right)\lambda_A \varrho_A\left(\vec{x}\right)\vec{\alpha}\cdot\vec{I}_A \right), \qquad (3.76)$$

where λ_A is a nuclear state dependent parameter that incorporates the effect of the intra–nuclear weak interaction. As its determination requires detailed knowledge of the structure of the nucleus in question, it is a challenging quantity to calculate. However, its absolute value was estimated to lie between 1 and 10 for heavy nuclei,[91] and an approximate analytical expression for λ_A which depends only on the proton and neutron numbers of a nucleus has been derived.[13] As the focus of this thesis with regard to nuclear spin–dependent PV observables in chiral molecules is not so much the prediction of absolute values but rather a systematic study and comparison of different compounds, λ_A has been set to minus one in all calculations presented in Chapters 6 and 7.

It has been discussed e.g. in Ref. [37], that strictly speaking the anapole moment (of a general system) as it is introduced here is not a physically well–defined observable, as only the sum of all radiative corrections of a given order defines a gauge–invariant quantity. In the present case of electrons coupling to the anapole moment of an atomic nucleus, however, other fourth–order contributions can be neglected and the interaction can be considered a physical process.

3.5   Summary

In the first section of this chapter, the Dirac equation was introduced and some of the basic phenomenology of relativistic electronic structure theory such as the appearance of physical states of negative energy was reviewed. Subsequently, the problem of relativistic many–electron calculations was introduced. The Dirac–Coulomb Hamiltonian (Eq. 3.11), which forms the basis for most of these calculations, does not conserve particle number and hence has no stable bound state spectrum. For many practical purposes this does not pose a problem, however, since a restriction to N–electron states is achieved in terms of the wavefunction, as discussed in Section 3.2.2.

This property of the Dirac–Coulomb Hamiltonian has however served to encourage the development of quasirelativistic two–component methods, which decouple electronic and positronic degrees of freedom. General characteristics of such approaches, such as applicability of variational methods and picture change errors were reviewed in Section 3.3.

A formally correct way of treating the relativistic many–electron problem would have to start from quantum electrodynamics. Such a procedure was outlined in Section 3.2 with

specific focus on the electron–electron interaction in Section 3.2.1. If only the instantaneous Coulomb repulsion between electrons is considered, some important contributions such as the spin–other–orbit, spin–spin and orbit–orbit interactions are neglected, which are particularly important in relatively light elements or for the calculation of explicitly spin–dependent properties. It can thus be somewhat misleading to speak of calculations based on the Dirac–Coulomb Hamiltonian as fully relativistic as opposed to quasirelativistic calculations based on two–component Hamiltonians.

In addition to electromagnetic interactions, the weak neutral current interaction between electrons and nucleons was considered in Section 3.4. The derivation of an effective operator for the lowest order contribution to this interaction was outlined and its properties, such as contact character and the existence of parity odd as well as parity even components were described.

In the upcoming Chapter 4, the ZORA approach to molecular parity violation will be reviewed in detail. Starting from the Dirac–Coulomb Hamiltonian Eq. 3.11 with the inclusion of external electric and magnetic fields and the parity odd contribution to the effective neutral current interaction between electrons and nuclei, Eq. 3.74, the ZORA equation including these perturbations is derived and properties of the approximation are reviewed.

Chapter 4

The ZORA approach

> *"These are my principles. And if you don't like them,*
> *I have others."*

> **– Groucho Marx**

In this chapter the zeroth order regular approximation (ZORA) [60, 61, 203, 204] formalism is reviewed. Starting from the Dirac–Hartree–Fock–Coulomb or Dirac–Kohn–Sham equation including possible electric, magnetic and parity violating (PV) perturbations, the derivation of the ZORA Hamiltonian is elucidated and the validity of the ZORA expansion as well as the relativistic content of the Hamiltonian are analyzed. As discussed in Section 3.3, modern two– and four–component methods can be considered equivalent in terms of physical content and computational efficiency for many applications in electronic structure theory. The ZORA approach is lacking in some respects to be discussed further in this chapter, but it does yield very good numerical results for the kind of molecular properties considered in Chapters 6, 8 and 7 of this thesis. A reliable implementation of ZORA mean field calculations [63] and PV potentials [58, 59] was available as a basis of this work, but the formalism for the calculation of molecular properties described in Chapter 5 can relatively easily be adapted also to more accurate, matrix–based two–component approaches.

4.1 ZORA Hamiltonian with PV and electromagnetic perturbations

According to the discussion in Section 3.4, the parity violating (PV) effective operator corresponding to the lowest order electron–nucleus Z^0–exchange between the n electrons

and N_{nuc} nuclei inside a molecule is given in a four–component framework by (see e.g. Ref. [77] and Eq. 3.76)

$$\hat{H}_{\mathrm{PV}} = \hat{H}_{\mathrm{PV}}^{(1)} + \hat{H}_{\mathrm{PV}}^{(2)} = \sum_{i=1}^{n} \left(\hat{h}_{\mathrm{PV},i}^{(1)} + \hat{h}_{\mathrm{PV},i}^{(2)} \right)$$

$$= \frac{G_{\mathrm{F}}}{2\sqrt{2}} \sum_{i=1}^{n} \left(\sum_{A=1}^{N_{\mathrm{nuc}}} Q_{\mathrm{W}}\left(A\right) \gamma_i^5 \varrho_A\left(\vec{r_i}\right) + \sum_{A=1}^{N_{\mathrm{nuc}}} \frac{\kappa_A}{\hbar\gamma_A} \varrho_A\left(\vec{r_i}\right) \vec{\alpha_i} \cdot \vec{\mu}_A \right). \qquad (4.1)$$

Fermi's constant, given by Eq. 3.65 is $G_{\mathrm{F}} = (2.22254 \times 10^{-14})E_{\mathrm{h}}a_0^3$, and for the Weinberg angle θ_{W} the value $\sin^2\theta_{\mathrm{W}} = 0.2319$ is used[1]. γ_A and $\vec{\mu}_A = \hbar\gamma_A \vec{I}_A$ are the gyromagnetic ratio and magnetic moment of nucleus A, respectively. $\kappa_A = -2\left(1 - 4\sin^2\theta_{\mathrm{W}}\right)\lambda_A$, where λ_A is a nuclear state dependent parameter related to the anapole moment of the nucleus, which is set equal to minus one in all calculations presented in this thesis, as discussed in connection with Eq. 3.76. Accordingly, values reported herein for shielding constants and frequency splittings are effective in the sense that they have to be scaled by the negative of the actual value of λ_A, in order to obtain the estimate of the measurable physical values. $\vec{r_i}$ is the position vector of electron i, and γ_i^5 and $\vec{\alpha_i}$ are given by Eqs. 3.57 and 3.5, respectively.

The pseudo–eigenvalue problem arising from the Dirac–Coulomb–Hamiltonian (Eq. 3.11 with the spectrum shifted by $-m_{\mathrm{e}}c^2$) in a mean field approximation including additional electromagnetic fields the PV potential of Eq. 4.1 is:

$$\begin{pmatrix} (V + q\varphi - \epsilon_i) & c\vec{\sigma} \cdot \vec{\pi} + \hat{f}_{\mathrm{PV}} \\ c\vec{\sigma} \cdot \vec{\pi} + \hat{f}_{\mathrm{PV}} & (V + q\varphi - 2m_{\mathrm{e}}c^2 - \epsilon_i) \end{pmatrix} \begin{pmatrix} \phi_i \\ \chi_i \end{pmatrix} = 0, \qquad (4.2)$$

with

$$\hat{f}_{\mathrm{PV}} = \hat{f}_{\mathrm{PV}}^{(1)} + \hat{f}_{\mathrm{PV}}^{(2)}$$

$$= \lambda^{\mathrm{PV}} \frac{G_{\mathrm{F}}}{2\sqrt{2}} \left(\sum_{A=1}^{N_{\mathrm{nuc}}} Q_{\mathrm{W}}\left(A\right) \varrho_A\left(\vec{r}\right) + \sum_{A=1}^{N_{\mathrm{nuc}}} \frac{\kappa_A}{\hbar\gamma_A} \varrho_A\left(\vec{r}\right) \vec{\sigma} \cdot \vec{\mu}_A \right), \qquad (4.3)$$

corresponding to the PV operator of Eq. 4.1 multiplied by a formal perturbation parameter λ^{PV} (not to be confused with λ_A above).

Within a density functional theory (DFT) approach, the potential V is given by $V = J + V_{\mathrm{XC}} + V_{\mathrm{N}}$, with the electron–nucleus attraction potential V_{N} and the Hartree potential

---

[1] This value was chosen in order to be able to compare numerical results to earlier studies. The most recent value measured at comparable energies is $\sin^2\theta_{\mathrm{W}} = 0.2397\,(18)$[222]

$J = J_{\phi\phi} + J_{\chi\chi}$, matrix elements of which are defined as:

$$\langle \psi_i \left| J \right| \psi_j \rangle = \sum_k (\psi_i \psi_j | \psi_k \psi_k) = \sum_k \left[(\psi_i \psi_j | \phi_k \phi_k) + (\psi_i \psi_j | \chi_k \chi_k) \right], \qquad (4.4)$$

using Mulliken's notation for two–electron integrals:

$$(\psi_i \psi_j | \psi_k \psi_l) = \int \mathrm{d}\vec{r}_1 \, \mathrm{d}\vec{r}_2 \, \psi_i^\dagger (\vec{r}_1) \, \psi_j (\vec{r}_1) \frac{1}{r_{12}} \psi_k^\dagger (\vec{r}_2) \, \psi_l (\vec{r}_2) , \qquad (4.5)$$

in this case for Dirac bispinors $\psi_i^{\mathrm{T}} = \left(\phi_i^{\mathrm{T}}, \chi_i^{\mathrm{T}} \right)$.

Within a relativistic framework, the exchange–correlation potential V_{XC} is an exceedingly complicated object, with the development of relativistic density functionals usually being based on a QED description of the homogeneous electron gas (see e.g. Refs. [223, 224] or part II of Ref. [225]). In this work, only nonrelativistic albeit spin–dependent density functionals will be employed, which is consistent with regard to the nonrelativistic Coulomb potential of the electron–electron interaction used in the Dirac–Coulomb Hamiltonian, Eq. 3.11. Further details on the density functionals used are given in Chapter 5.

In Hartree–Fock theory, $V = J - K + V_{\mathrm{N}}$, where the exchange–correlation potential V_{XC} has been replaced by the exchange operator $K = K_{\phi\phi} + K_{\chi\chi}$, whose matrix elements are given by:

$$\langle \psi_i \left| K \right| \psi_j \rangle = \sum_k (\psi_i \psi_k | \psi_k \psi_j) . \qquad (4.6)$$

In principle, the Dirac–Hartree–Fock–Coulomb (DHFC) Hamiltonian also contains non-local, off–diagonal contributions stemming from the coupling of large and small component through the exchange operators $K_{\phi\chi}$ and $K_{\chi\phi}$, so that Eq. 4.2 becomes:

$$\begin{pmatrix} (V + q\varphi - \epsilon_i) & c\vec{\sigma} \cdot \vec{\pi} - K_{\phi\chi} + \hat{f}_{\mathrm{PV}} \\ c\vec{\sigma} \cdot \vec{\pi} - K_{\chi\phi} + \hat{f}_{\mathrm{PV}} & (V + q\varphi - 2m_{\mathrm{e}}c^2 - \epsilon_i) \end{pmatrix} \begin{pmatrix} \phi_i \\ \chi_i \end{pmatrix} = 0. \qquad (4.7)$$

This contribution, however, is suppressed by a factor c^{-2} compared to $c\vec{\sigma} \cdot \vec{p}$ and is therefore usually neglected for the purpose of developing an approximate two–component treatment, see Ref. [226] for details.

The four–component, PV Dirac equation (Eq. 4.2) involves two coupled equations for the two–component spinors ϕ_i and χ_i:

$$(V + q\varphi - \epsilon_i)\phi_i + \left(c\vec{\sigma} \cdot \vec{\pi} + \hat{f}_{\mathrm{PV}} \right) \chi_i = 0 \qquad (4.8)$$

$$\left(c\vec{\sigma} \cdot \vec{\pi} + \hat{f}_{\mathrm{PV}} \right) \phi_i + (V + q\varphi - 2m_{\mathrm{e}}c^2 - \epsilon_i)\chi_i = 0. \qquad (4.9)$$

Following the procedure already outlined in Chapter 3.3, the lower component χ_i can be expressed in terms of ϕ_i with the help of Eq. 4.9:[60, 61, 198]

$$\chi_i = \left(2m_e c^2 + \epsilon_i - V - q\varphi\right)^{-1} \left(c\vec{\sigma} \cdot \vec{\pi} + \hat{f}_{PV}\right) \phi_i \tag{4.10}$$

$$= \left(2m_e c^2 - V - q\varphi\right)^{-1} \sum_k \left(\frac{-\epsilon_i}{2m_e c^2 - V - q\varphi}\right)^k \left(c\vec{\sigma} \cdot \vec{\pi} + \hat{f}_{PV}\right) \phi_i. \tag{4.11}$$

To zeroth order in the orbital energies ϵ_i this expression is reduced to

$$\chi_i \approx \left(2m_e c^2 - V - q\varphi\right)^{-1} \left(c\vec{\sigma} \cdot \vec{\pi} + \hat{f}_{PV}\right) \phi_i. \tag{4.12}$$

Utilizing Eq. 4.12 to eliminate χ_i from Eq. 4.8 and renormalizing yields the ZORA equation for the two–spinor ϕ_i,

$$\left(c\vec{\sigma} \cdot \vec{\pi} + \hat{f}_{PV}\right) \left(2m_e c^2 - V - q\varphi\right)^{-1} \left(c\vec{\sigma} \cdot \vec{\pi} + \hat{f}_{PV}\right) \phi_i + (V + q\varphi - \epsilon_i)\phi_i = 0. \tag{4.13}$$

ϕ_i now no longer represents the large component of a Dirac eigenfunction but a quasi relativistic two–component wavefunction approximating the electronic degrees of freedom of the four–spinor. The potential V in Eq. 4.13 depends on the one–electron density ρ, calculated in the ZORA framework as:[61]

$$\rho\left(\vec{r}\right) = \sum_{i=1}^{n} \left\langle \phi_i\left(\vec{r}'\right) | \delta\left(\vec{r} - \vec{r}'\right) | \phi_i\left(\vec{r}'\right) \right\rangle \tag{4.14}$$

with the approximate, renormalized large component ϕ_i of the Dirac spinor ψ_i. This is not the same as the original Dirac density:

$$\rho^D\left(\vec{r}\right) = \sum_{i=1}^{n} \left\langle \psi_i\left(\vec{r}'\right) | \delta\left(\vec{r} - \vec{r}'\right) | \psi_i\left(\vec{r}'\right) \right\rangle$$

$$= \sum_{i=1}^{n} \left(\left\langle \phi_i^D\left(\vec{r}'\right) | \delta\left(\vec{r} - \vec{r}'\right) | \phi_i^D\left(\vec{r}'\right) \right\rangle + \left\langle \chi_i^D\left(\vec{r}'\right) | \delta\left(\vec{r} - \vec{r}'\right) | \chi_i^D\left(\vec{r}'\right) \right\rangle \right), \tag{4.15}$$

where the superscript ^{D} is used to clarify the distinction between the large component ϕ_i^D of ψ_i and the renormalized approximation thereof. The difference in densities leads to a so–called picture change error if the ZORA density is used in calculations. This can be circumvented by adequately transforming the operator probing for the existence of an electron at position $\vec{r}$, thereby transforming both the wavefunction and the observable and avoiding any picture change errors, which means however, that any gain compared to solving the four–component equation directly is lost. Another way to deal with the problem is by calculating an approximate small component χ_i from ϕ_i using Eq. 4.12. This reduces the error but does not eliminate it completely, see Ref. [61, 217]. In

practice, the error introduced by neglecting picture change is expected to be small for valence states.

In order to be able to treat the external electrical potential perturbatively, it is necessary to eliminate it from the denominator in the ZORA expression for the kinetic energy. Using the relation

$$(a+b)^{-1} = a^{-1} - (a+b)^{-1}\,ba^{-1}, \tag{4.16}$$

as suggested in Ref. [226] one arrives at

$$\left(c\vec{\sigma}\cdot\vec{\pi} + \hat{f}_{\mathrm{PV}}\right)\left(2m_{\mathrm{e}}c^2 - V\right)^{-1}\left(c\vec{\sigma}\cdot\vec{\pi} + \hat{f}_{\mathrm{PV}}\right)\phi_i + (V - \epsilon_i)\phi_i$$
$$+ q\varphi\phi_i + \left(c\vec{\sigma}\cdot\vec{\pi} + \hat{f}_{\mathrm{PV}}\right)\frac{q\varphi}{\left(2m_{\mathrm{e}}c^2 - V - q\varphi\right)}\left(2m_{\mathrm{e}}c^2 - V\right)^{-1}\left(c\vec{\sigma}\cdot\vec{\pi} + \hat{f}_{\mathrm{PV}}\right)\phi_i = 0. \tag{4.17}$$

Introducing the ZORA factor $\tilde{\omega}$

$$\tilde{\omega} = c^2\omega = \frac{c^2}{2m_{\mathrm{e}}c^2 - V} = \frac{1}{2m_{\mathrm{e}} - V/c^2}, \tag{4.18}$$

the (one–electron) ZORA Hamiltonian up to first order in λ^{PV} is given by:

$$\hat{h}^{\mathrm{zora}} = \vec{\sigma}\cdot\vec{\pi}\,\tilde{\omega}\,\vec{\sigma}\cdot\vec{\pi} + \left\{\vec{\sigma}\cdot\vec{\pi}, \frac{\tilde{\omega}}{c}\,\hat{f}_{\mathrm{PV}}\right\} + V$$
$$+ \vec{\sigma}\cdot\vec{\pi}\,\frac{q\varphi\tilde{\omega}}{2m_{\mathrm{e}}c^2 - V - q\varphi}\,\vec{\sigma}\cdot\vec{\pi} + \left\{\vec{\sigma}\cdot\vec{\pi}, \frac{q\varphi\tilde{\omega}}{c\left(2m_{\mathrm{e}}c^2 - V - q\varphi\right)}\,\hat{f}_{\mathrm{PV}}\right\} + q\varphi$$
$$= \vec{\sigma}\cdot\vec{p}\,\tilde{\omega}\,\vec{\sigma}\cdot\vec{p} + V - q\left\{\vec{\sigma}\cdot\vec{p}, \tilde{\omega}\vec{\sigma}\cdot\vec{A}\right\} + q^2\left\{\vec{\sigma}\cdot\vec{A}, \tilde{\omega}\vec{\sigma}\cdot\vec{A}\right\} + \left\{\vec{\sigma}\cdot\vec{\pi}, \frac{\tilde{\omega}}{c}\hat{f}_{\mathrm{PV}}\right\}$$
$$+ \vec{\sigma}\cdot\vec{\pi}\,\frac{q\varphi\tilde{\omega}}{2m_{\mathrm{e}}c^2 - V - q\varphi}\,\vec{\sigma}\cdot\vec{\pi} + \left\{\vec{\sigma}\cdot\vec{\pi}, \frac{q\varphi\tilde{\omega}}{c\left(2m_{\mathrm{e}}c^2 - V - q\varphi\right)}\,\hat{f}_{\mathrm{PV}}\right\} + q\varphi, \tag{4.19}$$

with $\{x, y\} = xy + yx$ being the anticommutator.

For the computation of $\tilde{\omega}$ a model potential $\widetilde{V}$ instead of V is used in order to circumvent a direct dependence of $\tilde{\omega}$ on the molecular orbitals and to alleviate the gauge dependence of the ZORA approach. The model potential comprises the nuclear attraction potential, the electronic Coulomb repulsion and an exchange–correlation potential, the calculation of which is based on superpositions of model densities for every atom in the system. This choice ensures that $\widetilde{V}$ has the right behavior near the nuclei and that $\tilde{\omega}$ has to be computed only once, at the beginning of the calculation, because it no longer depends on molecular orbitals. The procedure is described in detail in Ref. [63].

Assuming a constant and homogeneous external magnetic field $\vec{B}$ and taking into account the internal magnetic field caused by the nuclei's magnetization density $\vec{\mu}_A(\vec{r})$, we employ a vector potential

$$\vec{A}(\vec{r}) = \vec{A}_B(\vec{r}) + \vec{A}_\mu(\vec{r}), \tag{4.20}$$

with

$$\vec{A}_B(\vec{r}) = \frac{1}{2}\left(\vec{B} \times \left(\vec{r} - \vec{R}_\mathrm{O}\right)\right) \tag{4.21}$$

and

$$\vec{A}_\mu(\vec{r}) = \frac{\mu_0}{4\pi} \sum_{A=1}^{N_\mathrm{nuc}} \int \frac{\vec{\nabla}' \times \vec{\mu}_A(\vec{r}')}{|\vec{r} - \vec{r}'|}\mathrm{d}\vec{r}', \tag{4.22}$$

where μ_0 is the vacuum permeability, $\vec{R}_\mathrm{O}$ is the gauge origin of the external field and $\vec{r}_A = \vec{r} - \vec{R}_A$ with the position vector $\vec{R}_A$ of nucleus A. For a point–like nucleus Eq. 4.22 takes the more common form: $\vec{A}_\mu(\vec{r}) = \frac{\mu_0}{4\pi} \sum_{A=1}^{N_\mathrm{nuc}} (\vec{\mu}_A \times \vec{r}_A)/r_A^3$.

For an externally applied electric field $\vec{E}$ that is constant and homogeneous, the scalar potential can be expressed as

$$\varphi(\vec{r}) = -\vec{r} \cdot \vec{E}. \tag{4.23}$$

4.2   Analysis of the ZORA Hamiltonian

4.2.1   Validity of the expansion

The regular approximation derives its name from the treatment of the denominator in the expression for the small component of the Dirac spinor in terms of the large component, Eq. 4.10. As mentioned in Chapter 3.3, the denominator is expanded for $\frac{-\epsilon_i}{(2m_\mathrm{e}c^2 - V)} \ll 1$ instead of $\frac{(V - \epsilon_i)}{2m_\mathrm{e}c^2} \ll 1$, which regularizes the expansion at the site or center of the nucleus, where the attractive Coulomb potential becomes singular. Broadly speaking it is possible to say that for a given orbital with energy ϵ_i, close to the nucleus the expansion is in inverse powers of the Coulomb potential and thus remains valid even as the nucleus is approached and the potential diverges. In the valence region, where the Coulomb potential is small, it is essentially an expansion of $1/c^2$. The applicability of the expansion thus depends on the orbital energies rather than the potential. For electron bound states and especially valence orbitals the assumption that $|\epsilon_i| \ll |2m_\mathrm{e}c^2 - V|$ is

clearly justified. In the core region, however, the absolute values of the orbital energies become increasingly large and the regular expansion may no longer converge.

In order to understand the connection between the ZORA and Dirac eigenvalues, an exact relationship between the them was established in Ref. [204] for the hydrogen–like atom and some classes of two–electron atoms. Since, for the lowest bound states in a molecule containing heavy centers, the electron–electron interaction is small and the Coulomb attraction is dominant, the argument is insightful for a discussion of the validity of the ZORA approximation for core orbitals.

The Dirac equation corresponding to an electron moving in a Coulomb potential with exact elimination of the small component is given by:

$$\left(\vec{\sigma} \cdot \vec{p} \, \frac{c^2}{2m_{\mathrm{e}}c^2 + \epsilon_i^{\mathrm{D}} + Z/r} \, \vec{\sigma} \cdot \vec{p} - \frac{Z}{r} \right) \phi_i^{\mathrm{D}} \left(\vec{r} \right) = \epsilon_i^{\mathrm{D}} \phi_i^{\mathrm{D}} \left(\vec{r} \right) . \tag{4.24}$$

Defining a scaled coordinate $\vec{r}' = \zeta \vec{r}$ with a constant ζ so that $\vec{p}' = \vec{p}/\zeta$ this equation can be written as:

$$\left(\vec{\sigma} \cdot \vec{p}' \, \frac{c^2}{\left(2m_{\mathrm{e}}c^2 + \epsilon_i^{\mathrm{D}} \right)/\zeta + Z/r'} \, \vec{\sigma} \cdot \vec{p}' - \frac{Z}{r'} \right) \phi_i^{\mathrm{D}} \left(\frac{\vec{r}'}{\zeta} \right) = \frac{\epsilon_i^{\mathrm{D}}}{\zeta} \phi_i^{\mathrm{D}} \left(\frac{\vec{r}'}{\zeta} \right) , \tag{4.25}$$

and if ζ is chosen as the norm of the upper component of the Dirac four–spinor:

$$\zeta = \langle \phi_i^{\mathrm{D}} | \phi_i^{\mathrm{D}} \rangle = \left(2m_{\mathrm{e}}c^2 + \epsilon_i^{\mathrm{D}} \right)/2m_{\mathrm{e}}c^2 \tag{4.26}$$

one obtains the ZORA equation for a scaled coordinate system:

$$\left(\vec{\sigma} \cdot \vec{p}' \, \frac{c^2}{2m_{\mathrm{e}}c^2 + Z/r'} \, \vec{\sigma} \cdot \vec{p}' - \frac{Z}{r'} \right) \phi_i^{\mathrm{D}} \left(\frac{\vec{r}'}{\zeta} \right) = \frac{2m_{\mathrm{e}}c^2 \epsilon_i^{\mathrm{D}}}{2m_{\mathrm{e}}c^2 + \epsilon_i^{\mathrm{D}}} \phi_i^{\mathrm{D}} \left(\frac{\vec{r}'}{\zeta} \right) . \tag{4.27}$$

Thus, a relation between ZORA and Dirac eigenvalues can be established:

$$\epsilon_i = \frac{2m_{\mathrm{e}}c^2 \epsilon_i^{\mathrm{D}}}{2m_{\mathrm{e}}c^2 + \epsilon_i^{\mathrm{D}}} = \epsilon_i^{\mathrm{D}} \left(1 + \frac{\epsilon_i^{\mathrm{D}}}{2m_{\mathrm{e}}c^2} \right)^{-1} = 2m_{\mathrm{e}}c^2 \left(1 + \frac{2m_{\mathrm{e}}c^2}{\epsilon_i^{\mathrm{D}}} \right)^{-1} . \tag{4.28}$$

For the lowest bound states of a Dirac spectrum $\epsilon^{\mathrm{D}} \approx -m_{\mathrm{e}}c^2$ the ZORA orbital energies are $\epsilon \approx -2m_{\mathrm{e}}c^2$. The estimate that the energy error for the innermost orbitals is proportional to $\epsilon/2m_{\mathrm{e}}c^2$ is supported by numerical calculations, see e.g. Ref. [61].

The relationship between the spectra is illustrated in Fig. 4.1, it is shown that the positive energy spectrum of the Dirac equation is mapped from the interval $(0, \infty)$ to $(0, 2m_{\mathrm{e}}c^2)$ of the ZORA spectrum. The Dirac bound states, which, for the Coulomb potential of a positively charged nucleus and shifted by the electron rest mass $2m_{\mathrm{e}}c^2$, lie in the interval $(0, -m_{\mathrm{e}}c^2)$ are mapped to $(0, -2m_{\mathrm{e}}c^2)$, and the negative energy continuum
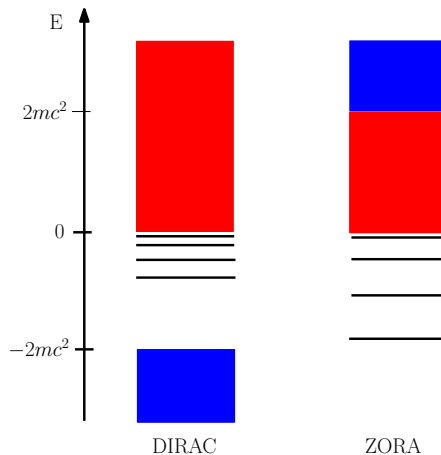
Figure 4.1: Comparison of the eigenvalue spectra of the Dirac (left) and ZORA (right) equations.

states are mapped from $\left(-\infty, -m_{\mathrm{e}}c^2\right)$ to $\left(2m_{\mathrm{e}}c^2, \infty\right)$ (see also the discussion in chapter 18 of Ref. [226]). From this one can suspect that the ZORA Hamiltonian is bounded from below which has been shown rigorously in Ref.[204].

From Eq. 4.27 it is evident, that the ZORA eigenfunctions are scaled versions of the large component of the Dirac four–spinors, with the same number of nodes and the same behavior at the nucleus. For valence orbitals the scaling factor ζ is close to one and the ZORA eigenfunctions reproduce the large components of the Dirac eigenfunctions well. For the core orbitals, ζ can be significantly smaller than one, leading to a stretching of the ZORA eigenfunctions in the vicinity of the nucleus, compared to the Dirac large components. An illustration of this effect for the orbital densities of uranium can be found in Ref. [61].

One could suspect that these shortcomings of ZORA in the description of core orbitals around heavy nuclei would make the approach unsuitable for the prediction of PV properties, as these depend strongly on the overlap of the wavefunction with the nucleon density. However, the parity violating effects considered here can essentially be classified as valence properties. In closed shell chiral molecules, properties such as the PV energy difference or the PV NMR frequency shifts between two enantiomers depend on the mixing of the valence orbitals of different parity and their overlap with the nucleon density. The core orbitals themselves are almost spherical so that they do not contribute to PV properties such as PV energy or NMR frequency differences. Thus, an excellent agreement between ZORA and DHFC or Dirac–Kohn–Sham (DKS) PV energy differences and NMR frequency splittings is observed, see e.g. Ref. [159] for a discussion of the PV energy differences and Chapter 6 of this thesis for the PV NMR frequency splittings. In open shell systems of interest such as atoms or diatomic molecules, the

PV properties are usually also determined by the valence structure, especially that of the open shell, and ZORA is expected to predict them well.[227]

For the standard NMR shielding tensors computed within ZORA it was shown in Ref. [228] that while the absolute ZORA NMR shieldings of a heavy nucleus differ greatly from improved scaled ZORA values, which are generally considered to be comparable to four–component calculations with respect to orbital energies,[203] the chemical shift is largely unaffected by the scaling. Again, the reason for this is that the valence orbitals are well described within the ZORA approximation and the core orbitals, where ZORA is deficient, are basically independent of the molecular environment so that their contribution to the relative chemical shifts is cancelled out.

4.2.2 Inclusion of relativistic effects

The ZORA Hamiltonian contains a number of relativistic corrections, which singles out the series of regular approximations with respect to other quasirelativistic treatments that reproduce the nonrelativistic Hamiltonian in zeroth order.

The relativistic content of the ZORA Hamiltonian can be analyzed by expanding the ZORA factor $\tilde{\omega}$ around the point $V/2m_{\mathrm{e}}c^2 = 0$ (this analysis follows the discussions in Refs. [204] and [226]):

$$\tilde{\omega} = \frac{1}{2m_{\mathrm{e}}} \frac{1}{(1 - V/2m_{\mathrm{e}}c^2)} = \frac{1}{2m_{\mathrm{e}}} \sum_k \left(\frac{V}{2m_{\mathrm{e}}c^2} \right)^k . \tag{4.29}$$

Reinserting this into the kinetic energy term of the ZORA Hamiltonian, $\vec{\sigma} \cdot \vec{p}\,\tilde{\omega}\,\vec{\sigma}\vec{p}$, and using the Dirac identity

$$(\vec{\sigma} \cdot \vec{a})(\vec{\sigma} \cdot \vec{b}) = \vec{a} \cdot \vec{b} + \mathrm{i}\vec{\sigma} \cdot (\vec{a} \times \vec{b}) \tag{4.30}$$

one obtains:

$$\vec{\sigma} \cdot \vec{p}\,\tilde{\omega}\,\vec{\sigma}\vec{p} = \frac{\vec{p}^2}{2m_{\mathrm{e}}} + \frac{1}{4m_{\mathrm{e}}^2 c^2} V \vec{p}^2 + \frac{1}{4m_{\mathrm{e}}^2 c^2} (\vec{p}V) \cdot \vec{p} + \frac{\hbar}{4m_{\mathrm{e}}^2 c^2} \vec{\sigma} \cdot (\nabla V) \times \vec{p} + \mathcal{O}\left(c^{-4}\right) . \tag{4.31}$$

Comparing this to the kinetic energy term of the Pauli Hamiltonian for $(\epsilon_i - V)/2m_{\mathrm{e}}c^2 \ll 1$ (see Eq. 3.48):

$$\vec{\sigma} \cdot \vec{p} \frac{c^2}{2m_{\mathrm{e}}c^2 + \epsilon_i - V} \vec{\sigma} \cdot \vec{p} = \frac{1}{2m_{\mathrm{e}}} \vec{\sigma} \cdot \vec{p} \frac{1}{1 + (\epsilon_i - V)/2m_{\mathrm{e}}c^2} \vec{\sigma} \cdot \vec{p}$$

$$= \frac{1}{2m_{\mathrm{e}}} \vec{\sigma} \cdot \vec{p} \sum_k \left(\frac{-(\epsilon_i - V)}{2m_{\mathrm{e}}c^2} \right)^k \vec{\sigma} \cdot \vec{p}$$

$$= \frac{\vec{p}^2}{2m_{\mathrm{e}}} - \frac{1}{4m_{\mathrm{e}}^2 c^2} (\epsilon_i - V) \vec{p}^2 + \frac{1}{4m_{\mathrm{e}}^2 c^2} (\vec{p}V) \cdot \vec{p}$$

$$+ \frac{\hbar}{4m_{\mathrm{e}}^2 c^2} \vec{\sigma} \cdot (\nabla V) \times \vec{p} + \mathcal{O}(c^{-4}) , \qquad (4.32)$$

it is seen that both terms contain the nonrelativistic kinetic energy and a scalar relativistic and a spin–orbit coupling correction of order $\mathcal{O}(c^{-2})$ plus higher order relativistic corrections. The spin–orbit coupling corrections of order $\mathcal{O}(c^{-2})$ are identical in both expansions, the only term missing from the ZORA expression compared to the Pauli Hamiltonian at that order is the energy dependent scalar relativistic correction. It can thus be expected, that the spin–orbit interaction is well described by the ZORA Hamiltonian, whereas it will have shortcomings in the prediction of spin–free relativistic effects. Because of the strong impact of spin–orbit coupling on PV properties, the full inclusion of spin–orbit coupling up to $\mathcal{O}(c^{-2})$ in the ZORA kinetic energy operator is another argument for the applicability of the ZORA approach to questions of molecular parity violation.

In the following chapter the calculation of PV potentials and NMR shielding tensors within the ZORA framework is elucidated as part of a general approach to the calculation of molecular properties of up to third order.

Chapter 5

Molecular properties within the ZORA approach

A general formalism for the calculation of molecular properties of up to third order within the ZORA framework is introduced in terms of derivatives of the total energy. Special attention is paid to possible simplifications that can be achieved through exploitation of symmetries of perturbing operators. For the parity violating (PV) energy difference between two enantiomers and the PV contribution to the nuclear magnetic resonance (NMR) shielding tensor explicit expressions are derived. In the case of PV NMR shieldings, the corresponding equations are decoupled for certain choices of density functionals due to time–reversal symmetry. Further details on the electronic Hessian of Section 5.3 and property derivatives of Section 5.2 are given in Appendix A.

5.1 ZORA total energy

Molecular properties are commonly defined as energy derivatives with respect to certain perturbation parameters, which correspond either to internal processes leading to an observable property, such as the parity violating (PV) weak interaction and energy differences between enantiomers, or to a perturbation that is introduced in order to measure the molecular property in question, e.g. a laser pulse applied to a molecule in order to measure ionization energies. The underlying assumption of this definition is, that the total energy can be expanded in a Taylor series of the perturbation parameters. In terms of the full ZORA Hamiltonian of Eq. 4.19 and using a general vector (denoted here by an underline in order to distinguish it from Euclidean vectors $\vec{v}$) of perturbation

parameters $\underline{T}^{\mathrm{T}} = (\vec{B}^{\mathrm{T}}, \vec{\mu}_1^{\mathrm{T}}, \dots, \vec{\mu}_{N_{\mathrm{nuc}}}^{\mathrm{T}}, \vec{E}^{\mathrm{T}}, \lambda^{\mathrm{PV}})$ this would be (see e.g. Ref. [218]):

$$
\begin{aligned}
E &= \sum_{n=0}^{\infty} \frac{1}{n!} \sum_{\underline{x} \in \{\underline{T}\}^n} E_{\underline{x}}^{[n]} x_1 x_2 \dots x_n \\
&= E^{[0]} + \vec{B} \cdot \left[\nabla_{\vec{B}} E\right]_{\underline{T}=\vec{0}} + \sum_{A=1}^{N_{\mathrm{nuc}}} \vec{\mu}_A \cdot \left[\nabla_{\vec{\mu}_A} E\right]_{\underline{T}=\vec{0}} + \vec{E} \cdot \left[\nabla_{\vec{E}} E\right]_{\underline{T}=\vec{0}} + \lambda^{\mathrm{PV}} \left.\frac{\mathrm{d}E}{\mathrm{d}\lambda^{\mathrm{PV}}}\right|_{\underline{T}=\vec{0}} \\
&\quad + \frac{1}{2} \sum_{A,B=1}^{N_{\mathrm{nuc}}} \sum_{i,j=1}^{3} \mu_{Ai} \left.\frac{\mathrm{d}^2 E}{\mathrm{d}\mu_{Ai}\mathrm{d}\mu_{Bj}}\right|_{\underline{T}=\vec{0}} \mu_{Bj} + \frac{1}{2} \sum_{A=1}^{N_{\mathrm{nuc}}} \sum_{i,j=1}^{3} B_i \left.\frac{\mathrm{d}^2 E}{\mathrm{d}B_i\mathrm{d}\mu_{Aj}}\right|_{\underline{T}=\vec{0}} \mu_{Aj} + \dots \\
&\quad + \frac{1}{6} B_i \left.\frac{\mathrm{d}^3 E}{\mathrm{d}B_i\mathrm{d}\mu_{Aj}\mathrm{d}\lambda^{\mathrm{PV}}}\right|_{\underline{T}=\vec{0}} \mu_{Aj}\lambda^{\mathrm{PV}} + \dots .
\end{aligned}
\tag{5.1}
$$

The sum over all $\underline{x} \in \{\underline{T}\}^n$ at each order n is a summation over all n–tuples of perturbation parameters, i.e. components of $\underline{T}$. The superscript $[n]$ of E indicates the derivative status of E (evaluated for vanishing perturbations, $\underline{T} = \vec{0}$), the subscript $\underline{x}$ indicates the perturbation parameters with respect to which the derivatives are taken. In the second part of the equation examples of possible contributions are listed.

The energy of the unperturbed system $E^{[0]}$ corresponds to the Hamiltonian:

$$
\hat{H}^{\mathrm{zora},0} = \sum_{i=1}^{n} \vec{\sigma}_i \cdot \vec{p}_i \tilde{\omega} \, \vec{\sigma}_i \cdot \vec{p}_i + V_{\mathrm{N}} + J - \eta K + V_{\mathrm{XC}} + V_{\mathrm{NN}},
\tag{5.2}
$$

with the newly introduced parameter η. In the Hartree-Fock case $\eta = 1$ and $V_{\mathrm{XC}} = 0$, for DFT calculations, V_{XC} corresponds to the density functional of choice, for pure density functionals $\eta = 0$ and in the case of hybrid functionals, η takes a value between zero and one corresponding to the fraction of Fock exchange used in the calculation. V_{NN} is the nuclear repulsion energy.

In the case of a time–independent Hamiltonian the energy of the system can be calculated using the variational principle by minimizing the mean energy functional:

$$
E\left[\tilde{0}\right] = \frac{\left\langle \tilde{0}|\hat{H}^{\mathrm{zora}}|\tilde{0}\right\rangle}{\left\langle \tilde{0}|\tilde{0}\right\rangle},
\tag{5.3}
$$

where $|\tilde{0}\rangle$ is the one–determinantal many–electron wavefunction describing the system.

The many–electron Hamiltonian Eq. 4.19 can be recast in a second quantized form, which has the advantage that formal developments can be given in a very compact manner. The fashion in which it is developed here is based largely on Refs. [218, 229, 230]. The

Hamiltonian is then expressed as:

$$\hat{H}^{\mathrm{zora}} = \sum_{pq} \left[z_{pq}^{\mathrm{zora}} + l_{pq}^{\eta} [\rho] + v_{pq}^{\mathrm{xc}} [\rho_{\uparrow}, \rho_{\downarrow}] + v'_{pq}(\underline{T}) \right] \hat{a}_p^{\dagger} \hat{a}_q + V_{NN}, \tag{5.4}$$

acting on the reparameterized wavefunction

$$\left| \tilde{0} \right\rangle = \exp\left(-\hat{\kappa} \right) \left| 0 \right\rangle \tag{5.5}$$

with

$$\hat{\kappa} = \sum_{pq} \kappa_{pq} \hat{a}_p^{\dagger} a_q. \tag{5.6}$$

This reparameterization is based on Thouless theorem (Ref. [231] as cited in Refs. [232, 233]), which states that two single–determinantal wavefunctions can be related using the type of transformation given by Eq. 5.5, unless they are mutually orthogonal.

In Eq. 5.5, $|0\rangle$ is a reference determinant created from an intermediate basis set of orthonormal, two–component molecular orbitals $\{\phi_p\}$, usually constructed as a linear combination of atomic orbital (LCAO) basis functions χ_μ:

$$\phi_p = \sum_{\mu} c_{\mu p} \chi_\mu, \tag{5.7}$$

with complex, two-component LCAO coefficients

$$c_{\mu p} = \begin{pmatrix} c_{\mu p}^{\alpha} \\ c_{\mu p}^{\beta} \end{pmatrix},$$

and satisfying the orthonormality condition:

$$\langle \phi_p | \phi_q \rangle = \delta_{pq}. \tag{5.8}$$

Reparameterization in terms of an anti–Hermitian orbital rotation operator (Eq. 5.6) ensures the conservation of the orthonormality of the wavefunction, so that the condition $\langle \tilde{0} | \tilde{0} \rangle = 1$ is fulfilled automatically. It is thus possible to circumvent an optimization taking into account constraints of the wavefunction and one can easily restrict the optimization procedure to non–redundant parameters (i.e. rotations between occupied and unoccupied orbitals only). The operator $\hat{\kappa}$ has to be anti–Hermitian in order for $\exp(-\hat{\kappa})$ to be unitary, thus the elements of the matrix κ obey the relation

$$\kappa_{pq} = -\kappa_{qp}^*. \tag{5.9}$$

The individual contributions to the Hamiltonian of Eq. 5.4 are given by:

$$z_{pq}^{\text{zora}} = \left\langle \phi_p \left| \vec{\sigma} \cdot \vec{p}\,\tilde{\omega}\,\vec{\sigma} \cdot \vec{p} + \sum_{A=1}^{N_{\text{nuc}}} qZ_A/r_A \right| \phi_q \right\rangle \tag{5.10}$$

$$l_{pq}^{\eta}[\rho] = \sum_{rs} \left[(\phi_p\phi_q|\phi_r\phi_s) - \eta\,(\phi_p\phi_s|\phi_r\phi_q) \right] \tilde{D}_{rs}(\kappa), \tag{5.11}$$

with $(\phi_p\phi_q|\phi_r\phi_s)$ denoting the two–electron integrals in Mulliken's notation (see Eq. 4.5) and

$$\tilde{D}_{rs}(\kappa) = \left\langle \tilde{0} \left| \hat{a}_r^\dagger \hat{a}_s \right| \tilde{0} \right\rangle = \left\langle 0 \left| \exp(\hat{\kappa})\,\hat{a}_r^\dagger \hat{a}_s \exp(-\hat{\kappa}) \right| 0 \right\rangle \tag{5.12}$$

$$= \sum_{n=0}^{\infty} \frac{1}{n!} \left\langle 0 \left| \left[\hat{\kappa}, \hat{a}_r^\dagger \hat{a}_s \right]^{(n)} \right| 0 \right\rangle, \tag{5.13}$$

where the Baker–Campbell–Hausdorff expansion has been used on the last line (see e.g. Ref. [229]). The multi-commutator $\left[\hat{A}, \hat{B} \right]^{(n)}$ is defined here according to Ref. [232] as:

$$\left[\hat{A}, \hat{B} \right]^{(0)} = \hat{B} \tag{5.14}$$

$$\left[\hat{A}, \hat{B} \right]^{(1)} = \left[\hat{A}, \hat{B} \right] \tag{5.15}$$

$$\left[\hat{A}, \hat{B} \right]^{(n)} = \left[\hat{A}, \left[\ldots, \left[\hat{A}, \hat{B} \right] \ldots \right] \right]. \tag{5.16}$$

The ZORA kinetic energy term $\vec{\sigma} \cdot \vec{p}\,\tilde{\omega}\,\vec{\sigma} \cdot \vec{p}$ is treated as a one–electron operator, because of the model density and potential used in the calculation of the ZORA factor $\tilde{\omega}$ Eq. 4.18.

The matrix elements of the exchange–correlation potential are given by

$$v_{pq}^{\text{xc}}[\rho_\uparrow, \rho_\downarrow] = \int \mathrm{d}^3r \left(\frac{\delta\varepsilon^{\text{xc}}}{\delta\rho_\uparrow} \Omega_{pq}^\uparrow + \frac{\delta\varepsilon^{\text{xc}}}{\delta\rho_\downarrow} \Omega_{pq}^\downarrow \right), \tag{5.17}$$

where the exchange–correlation functional ε^{xc} depends on the local spin densities $\rho_\uparrow$ and $\rho_\downarrow$ (see e.g. Ref. [234]):

$$\rho_\uparrow = \frac{1}{2}(\rho + s) \tag{5.18}$$

$$\rho_\downarrow = \frac{1}{2}(\rho - s), \tag{5.19}$$

with the density ρ and the absolute value $s = |\vec{m}|$ of the magnetization $\vec{m}$:

$$\rho = \sum_{pq} \tilde{D}_{pq}(\kappa)\,\Omega_{pq} \tag{5.20}$$

$$\vec{m} = \sum_{pq} \tilde{D}_{pq}(\kappa)\,\vec{\Sigma}_{pq}, \tag{5.21}$$

corresponding to the operators

$$\hat{\rho} = \sum_{pq} \Omega_{pq} \hat{a}_p^\dagger \hat{a}_q \tag{5.22}$$

$$\hat{\vec{m}} = \sum_{pq} \vec{\Sigma}_{pq} \hat{a}_p^\dagger \hat{a}_q. \tag{5.23}$$

Here, Ω_{pq} and $\vec{\Sigma}_{pq}$ are the electron spin–independent and –dependent orbital overlap densities, respectively, and given by:

$$\Omega_{pq} = \phi_p^\dagger \phi_q \tag{5.24}$$

$$\vec{\Sigma}_{pq} = \phi_p^\dagger \vec{\sigma} \phi_q. \tag{5.25}$$

A possible dependence of the functional on gradients of the spin densities is neglected for simplicity, as it does not change the structure of any of the expressions derived in the following.

In Eq. 5.4 the matrix elements of all the perturbing operators have been collected in $v'(\underline{T})$:

$$v'_{pq}(\underline{T}) = \left\langle \phi_p \left| e \left\{ \vec{\sigma} \cdot \vec{p}, \tilde{\omega} \vec{\sigma} \cdot \vec{A} \right\} + e^2 \left\{ \vec{\sigma} \cdot \vec{A}, \tilde{\omega} \vec{\sigma} \cdot \vec{A} \right\} + \left\{ \vec{\sigma} \cdot \vec{\pi}, \frac{\tilde{\omega}}{c} \hat{f}_{PV} \right\} \right. $$
$$\left. + \vec{\sigma} \cdot \vec{\pi} \frac{\varphi \tilde{\omega}}{2m_e c^2 - V - \varphi} \vec{\sigma} \cdot \vec{\pi} + \left\{ \vec{\sigma} \cdot \vec{\pi}, \frac{\varphi \tilde{\omega}}{c(2m_e c^2 - V - \varphi)} \hat{f}_{PV} \right\} + \varphi \right| \phi_q \right\rangle. \tag{5.26}$$

As with the kinetic energy term, the perturbing operators are treated as one–electron operators despite the appearance of the potential V in the denominator of $\tilde{\omega}$ because, for all practical purposes in this thesis, V is replaced there by a model potential $\tilde{V}$ depending on atomic model densities $\tilde{\rho}$, as discussed in connection with Eq. 4.19.

The total ZORA energy can now be expressed as the minimum of a function $E(\kappa)$ with respect to variations of the parameters:

$$E(\kappa) = \sum_{pq} \left[z_{pq}^{\text{zora}} + l_{pq}^\eta(\kappa) + v_{pq}^{\text{xc}}(\kappa) + v'(\underline{T}) \right] \tilde{D}_{pq}(\kappa) + V_{NN}, \tag{5.27}$$

5.2   Analytical derivatives

Of the properties considered in this thesis, the PV energy shift of a chiral molecule is defined as the first total derivative of the energy with respect to the perturbation parameter λ^{PV} evaluated for vanishing perturbations. The NMR shielding tensor is

related to the second total derivative of the energy with respect to the external magnetic field and the nuclear magnetic moment of the nucleus in question. The lowest order contribution to the PV NMR shielding tensor of a nucleus Q is then related to the third derivative of the total energy E with respect to the external magnetic field $\vec{B}$, the magnetic moment of the nucleus $\vec{\mu}_Q$ and the PV perturbation parameter λ^{PV}, evaluated at zero external field, magnetic moments $\vec{\mu}_A$ (for $A = 1 \dots N_{\mathrm{nuc}}$) and λ^{PV}.

In terms of the parameters κ of the wavefunction, the first derivative of the energy with respect to one of the perturbation parameters is given by (for analytical derivatives in general see for example Refs. [235, 236]):

$$E_l^{[1]}(\kappa) := \left.\frac{\mathrm{d}E(\kappa)}{\mathrm{d}T_l}\right|_{\underline{T}=\vec{0}} = \left.\frac{\partial E(\kappa)}{\partial T_l}\right|_{\underline{T}=\underline{0}}, \tag{5.28}$$

using the Hellman–Feynman theorem for variational wavefunctions (Ref. [237] and references cited therein), satisfying $\partial E/\partial \kappa_{pq} = 0$ for all κ_{pq}. The second derivative of the energy is

$$\begin{aligned} E_{lm}^{[2]}(\kappa) &:= \left.\frac{\mathrm{d}^2 E(\kappa)}{\mathrm{d}T_m \mathrm{d}T_l}\right|_{\underline{T}=\underline{0}} \\ &= \left(\frac{\partial^2 E(\kappa)}{\partial T_m \partial T_l}\right) + \sum_{pq}\left(\frac{\partial^2 E(\kappa)}{\partial \kappa_{pq} \partial T_l}\frac{\partial \kappa_{pq}}{\partial T_m}\right). \end{aligned} \tag{5.29}$$

Here and in the following, explicit reference to variables held constant under partial differentiation is omitted but indicated by round brackets and derivatives are taken at $\underline{T} = \underline{0}$, unless otherwise specified.

The third derivative of the energy with respect to the perturbation parameters is then given by (see e.g. Refs. [235, 236]):

$$\begin{aligned} E_{lmn}^{[3]}(\kappa) &:= \left.\frac{\mathrm{d}^3 E(\kappa)}{\mathrm{d}T_n \mathrm{d}T_m \mathrm{d}T_l}\right|_{\underline{T}=\underline{0}} \\ &= \left(\frac{\partial^3 E}{\partial T_n \partial T_m \partial T_l}\right) + \sum_{pq}\left[\left(\frac{\partial^3 E}{\partial T_n \partial T_m \partial \kappa_{pq}}\right)\left(\frac{\partial \kappa_{pq}}{\partial T_l}\right) + \left(\frac{\partial^3 E}{\partial T_n \partial \kappa_{pq} \partial T_l}\right)\left(\frac{\partial \kappa_{pq}}{\partial T_m}\right)\right. \\ &\quad \left. + \left(\frac{\partial^3 E}{\partial \kappa_{pq} \partial T_m \partial T_l}\right)\left(\frac{\partial \kappa_{pq}}{\partial T_n}\right)\right] + \sum_{pq,rs}\left[\left(\frac{\partial^3 E}{\partial T_n \partial \kappa_{rs} \partial \kappa_{pq}}\right)\left(\frac{\partial \kappa_{rs}}{\partial T_m}\right)\left(\frac{\partial \kappa_{pq}}{\partial T_l}\right)\right. \\ &\quad \left. + \left(\frac{\partial^3 E}{\partial \kappa_{rs} \partial T_m \partial \kappa_{pq}}\right)\left(\frac{\partial \kappa_{rs}}{\partial T_n}\right)\left(\frac{\partial \kappa_{pq}}{\partial T_l}\right) + \left(\frac{\partial^3 E}{\partial \kappa_{rs} \partial \kappa_{pq} \partial T_l}\right)\left(\frac{\partial \kappa_{rs}}{\partial T_n}\right)\left(\frac{\partial \kappa_{pq}}{\partial T_m}\right)\right] \\ &\quad + \sum_{pq,rs,tu}\left(\frac{\partial^3 E}{\partial \kappa_{tu} \partial \kappa_{rs} \partial \kappa_{pq}}\right)\left(\frac{\partial \kappa_{tu}}{\partial T_n}\right)\left(\frac{\partial \kappa_{rs}}{\partial T_m}\right)\left(\frac{\partial \kappa_{pq}}{\partial T_l}\right). \end{aligned} \tag{5.30}$$

In accordance with Wigner's $2n + 1$ rule, the third total derivative can be determined using linear response of the parameters to the perturbations only.

A partial derivative of the energy with respect to one or more perturbation parameters is simply the expectation value of the corresponding perturbing operator, i.e. of the partial derivative of the full Hamiltonian with respect to the parameters in question. A partial derivative of the energy with respect to perturbation parameters and the parameters of the wavefunction then gives a matrix element of the perturbing operator and so forth. A detailed discussion of the calculation of partial energy derivatives is presented in Appendix A. The calculation of the response of the wavefunction parameters κ_{pq} to perturbations will be addressed in the next section.

5.3   Structure and symmetries of the linear response equations

Using the variational energy condition once more, the response of the parameters κ_{pq} to a perturbation T_i can be calculated in the standard way:

$$
\begin{aligned}
0 &= \frac{d}{dT_i}\left(\frac{\partial E}{\partial \kappa_{pq}}\right)\Bigg|_{\underline{T=0}} \\
&= \left(\frac{\partial^2 E}{\partial T_i \partial \kappa_{pq}}\right) + \sum_{rs}\left(\frac{\partial^2 E}{\partial \kappa_{pq}\partial \kappa_{rs}}\right)\left(\frac{\partial \kappa_{rs}}{\partial T_i}\right).
\end{aligned}
\tag{5.31}
$$

In general, these equations are coupled and an iterative method can be applied in order to solve them.[238, 239] It will be shown later, however, that for magnetic perturbations and a limited range of density functionals these equations can be uncoupled.

Since the matrix κ is anti–Hermitian, it can be recast in vector form of the type:

$$
\vec{a} = \begin{pmatrix} \vec{\kappa} \\ \vec{\kappa}^* \end{pmatrix}
\tag{5.32}
$$

with a column vector $\vec{\kappa}$ containing elements κ_{pq} where from now on $p > q$. This then allows for Eq. 5.31 to be expressed in matrix form (see e.g. Ref. [230]):

$$
0 = \mathbf{M}\vec{Y} + \vec{G}.
\tag{5.33}
$$

The Hessian or stability matrix $\mathbf{M}$ of the system has the structure:

$$
\mathbf{M} = \begin{pmatrix} \mathbf{A} & \mathbf{B} \\ \mathbf{B}^* & \mathbf{A}^* \end{pmatrix}
\tag{5.34}
$$

with

$$A_{pq,rs} = - \left(n_p + n_r - 2n_q\right) \delta_{qs} F_{pr} - \left(n_q + n_s - 2n_r\right) \delta_{pr} F_{sq}$$
$$+ \left(n_p - n_q\right) \left(n_r - n_s\right) \left(2\Lambda^\eta_{pqsr} + W^{\mathrm{XC}}_{pqsr}\right) \tag{5.35}$$

$$B_{pq,rs} = \left(n_p + n_s - 2n_q\right) \delta_{qr} F_{ps} + \left(n_q + n_r - 2n_s\right) \delta_{ps} F_{rq}$$
$$+ \left(n_p - n_q\right) \left(n_r - n_s\right) \left(2\Lambda^\eta_{pqrs} + W^{\mathrm{XC}}_{pqrs}\right) . \tag{5.36}$$

Details on the calculation of $\mathbf{M}$ are given in Appendix A.1. $n_{p/q/r/s}$ are occupation numbers, equal to one if the corresponding orbital is occupied in $|0\rangle$ and zero otherwise. The Fock matrix elements F_{pq} in Eqs. 5.35 and 5.36 are given by

$$F_{pq} = z^{\mathrm{zora}}_{pq} + \sum_{i=1}^{N^{\mathrm{occ}}} \Lambda^\eta_{iipq} + V^{\mathrm{XC}}_{pq}. \tag{5.37}$$

The two–electron Coulomb and exchange integrals have been collected in

$$\Lambda^\eta_{pqrs} = \left(\phi_p \phi_q | \phi_r \phi_s\right) - \eta \left(\phi_p \phi_s | \phi_r \phi_q\right), \tag{5.38}$$

and the integrals involving the exchange–correlation functional are denoted as

$$V^{\mathrm{XC}}_{lm} = \frac{1}{2} \int \mathrm{d}^3 r \left(\frac{\delta \varepsilon^{\mathrm{XC}}}{\delta \rho_\uparrow} \Omega^\uparrow_{lm} + \frac{\delta \varepsilon^{\mathrm{XC}}}{\delta \rho_\downarrow} \Omega^\downarrow_{lm}\right) \tag{5.39}$$

$$W^{\mathrm{XC}}_{lm,no} = \int \mathrm{d}^3 r \left(\frac{\delta^2 \varepsilon^{\mathrm{XC}}}{\delta \rho_\uparrow^2} \Omega^\uparrow_{lm} \Omega^\uparrow_{no} + \frac{\delta^2 \varepsilon^{\mathrm{XC}}}{\delta \rho_\downarrow^2} \Omega^\downarrow_{lm} \Omega^\downarrow_{no} + \frac{\delta^2 \varepsilon^{\mathrm{XC}}}{\delta \rho_\uparrow \delta \rho_\downarrow} \left[\Omega^\uparrow_{lm} \Omega^\downarrow_{no} + \Omega^\downarrow_{lm} \Omega^\uparrow_{no}\right]\right), \tag{5.40}$$

which are generalized forms of expressions derived in Ref. [230] for spin density–independent functionals.

$\Omega^\uparrow_{pq}$ and $\Omega^\downarrow_{pq}$ are linear combinations of elements of the density matrix and projections of $\vec{\Sigma}_{pq}$ on the direction of the magnetization of the unperturbed system:

$$\Omega^\uparrow_{pq} = \frac{1}{2} \left(\Omega_{pq} + \Sigma^{\mathrm{p}0}_{pq}\right) \tag{5.41}$$

$$\Omega^\downarrow_{pq} = \frac{1}{2} \left(\Omega_{pq} - \Sigma^{\mathrm{p}0}_{pq}\right), \tag{5.42}$$

with

$$\Sigma^{\mathrm{p}}_{pq} = \frac{\vec{m}_0}{|\vec{m}_0|} \cdot \vec{\Sigma}_{pq}, \tag{5.43}$$

which goes to zero in the limit $|\vec{m}_0| \to 0$. Details on the derivation of these expressions are given in Appendix A.

$\vec{G}$ is the so–called property-gradient and $\vec{Y}$ is the response vector of interest, i.e. the vector containing the first derivative of the parameters κ_{pq} and κ^*_{pq} with respect to a perturbation parameter. Both of them retain the dual structure of $\vec{a}$, in which the property gradient retains the Hermiticity and time–reversal symmetry of the perturbing operator and is given by:

$$\vec{G} = \begin{pmatrix} \vec{i} \\ h\vec{i}^* \end{pmatrix}, \tag{5.44}$$

where $h = -1$ for a Hermitian perturbing operator and $h = 1$ if the perturbing operator is anti–Hermitian (the signs have been chosen in order to match the structure of $\vec{a}$ of Eq. 5.32). The blocks of $\vec{G}$ are given by:

$$i_{pq} = \left(\frac{\partial^2 E}{\partial T_i \partial \kappa_{pq}} \right) \qquad i^*_{pq} = \left(\frac{\partial^2 E}{\partial T_i \partial \kappa^*_{pq}} \right). \tag{5.45}$$

Since multiplication with the Hessian conserves Hermiticity (see e.g. Ref. [230]):

$$\begin{pmatrix} \mathbf{A} & \mathbf{B} \\ \mathbf{B}^* & \mathbf{A}^* \end{pmatrix} \begin{pmatrix} \vec{x} \\ h\vec{x}^* \end{pmatrix} = \begin{pmatrix} \mathbf{A}\vec{x} + h\mathbf{B}\vec{x}^* \\ \mathbf{B}^*\vec{x} + h\mathbf{A}^*\vec{x}^* \end{pmatrix} = \begin{pmatrix} \vec{y} \\ h\vec{y}^* \end{pmatrix}, \tag{5.46}$$

the solution vector also is of well-defined Hermiticity if the perturbing operator is:

$$\vec{Y} = \begin{pmatrix} \vec{y} \\ h\vec{y}^* \end{pmatrix}, \tag{5.47}$$

with elements

$$y_{pq} = \left(\frac{\partial \kappa_{pq}}{\partial T_i} \right) \qquad y^*_{pq} = \left(\frac{\partial \kappa^*_{pq}}{\partial T_i} \right). \tag{5.48}$$

Anti–Hermitian contributions to the solution vector vanish unless time–dependent perturbations are considered.[230] The matrix problem of Eq. 5.33 can thus be reduced by half as only the upper block of $\vec{Y}$ needs to be determined in order to fully solve the equation (see e.g. the discussion in Ref. [218]).

5.3.1 Time–reversal symmetry

Electric or magnetic perturbations are usually described by time–reversal symmetric or antisymmetric operators, respectively, and the response problem (Eq. 5.33) can be further reduced by if time–reversal symmetry is taken into account. In numerical calculations presented in this thesis, time–reversal symmetry is not used explicitly. It is

introduced here, however, to elucidate certain simplifications of the formalism that appear for time–reversal–odd (e.g. magnetic) perturbations. Such simplifications will be discussed also in Section 5.5.1.

The anti–unitary time–reversal operator can be expressed as:

$$\Theta = \exp\left(-\mathrm{i}\pi\hat{S}_y\right)\mathcal{K}, \tag{5.49}$$

where $\hat{S}_y$ is the y-component of the general spin operator and $\mathcal{K}$ is the complex conjugation operator. When the molecular orbital basis for a single–determinantal wavefunction is chosen to consist of Kramer's pairs

$$\left\{\phi_{P\tau}, \phi_{P\overline{\tau}} = \Theta\phi_{P\tau}\right\}, \tag{5.50}$$

Θ reduces to the usual form

$$\Theta = -\mathrm{i}\sigma_y\mathcal{K}, \tag{5.51}$$

when acting on the one–electron two-spinors. The representation of the time–reversal operator in a Kramer's adapted basis is thus particularly simple, but, since the symmetry is a local invariant and independent of the choice of basis,[233] choosing such a basis does not limit the validity of conclusions drawn for problems with well-defined behavior under time–reversal.

The additional index τ introduced for the basis functions above is analogous to spin indices σ and $\overline{\sigma}$ denoting α or β spin-orbitals in a non-relativistic framework. τ takes the value $1/2$ for a reference orbital $\phi_{P\tau}$ and $\overline{\tau} = -1/2$ for it's Kramer's conjugated counterpart $\Theta\phi_{P\tau}$. In the following derivation we will also use indices τ_p and $\tau_{\overline{p}}$ which can each take the values $\pm 1/2$ depending on the reference orbital: For a reference orbital $\phi_p = \phi_{P\tau}$, $\tau_p = 1/2$ and $\tau_{\overline{p}} = -1/2$ but for the orbital $\phi_p = \phi_{P\overline{\tau}}$, $\tau_p = -1/2$ and $\tau_{\overline{p}} = 1/2$.

An arbitrary operator $\hat{A}$ is said to be time–reversal symmetric or antisymmetric if it fulfills the conditions:

$$\Theta\hat{A}\Theta^{-1} = \hat{A} \tag{5.52}$$

$$\Theta\hat{A}\Theta^{-1} = -\hat{A}, \tag{5.53}$$

respectively, where $\Theta^{-1} = -\Theta$. The action of Θ on the basic creation and annihilation operators is given by:[232]

$$\Theta d\hat{a}_p^\dagger \Theta^{-1} = (-1)^{\tau_p - 1/2} \, d^* \hat{a}_{\overline{p}}^\dagger \tag{5.54}$$

$$\Theta d\hat{a}_p \Theta^{-1} = (-1)^{\tau_p - 1/2} \, d^* \hat{a}_{\overline{p}}, \tag{5.55}$$

so that on an arbitrary one–electron operator given by

$$\hat{A} = \sum_{pq} A_{pq} \hat{a}_p^\dagger \hat{a}_q \tag{5.56}$$

Θ acts as:

$$\begin{aligned}
\Theta \hat{A} \Theta^{-1} &= \sum_{pq} A_{pq}^* \Theta \hat{a}_p^\dagger \hat{a}_q \Theta^{-1} \\
&= \sum_{pq} A_{pq}^* (-1)^{\tau_p + \tau_q - 1} \hat{a}_{\overline{p}}^\dagger \hat{a}_{\overline{q}} \\
&= \sum_{pq} A_{\overline{pq}}^* (-1)^{\tau_{\overline{p}} + \tau_{\overline{q}} - 1} \hat{a}_p^\dagger \hat{a}_q.
\end{aligned} \tag{5.57}$$

Accordingly, for an operator with well defined behavior under time–reversal, matrix elements are related by

$$A_{\overline{pq}} = t(-1)^{\tau_p + \tau_q - 1} A_{pq}^*, \tag{5.58}$$

where $t = 1$ for time–reversal symmetric and $t = -1$ for time–reversal antisymmetric operators.

An arbitrary operator $\hat{A}$ can be split into a time–reversal symmetric and a time–reversal antisymmetric contribution, $\hat{A}^P$ and $\hat{A}^Q$, respectively:

$$\hat{A} = \hat{A}^P + \hat{A}^Q. \tag{5.59}$$

In order to show that multiplication with the Hessian of Eq. 5.34 conserves time–reversal symmetry as long as the Hamiltonian describing the system is time–reversal symmetric, one can repartition the orbital rotation operator $\hat{\kappa}$ as:

$$\hat{\kappa}_\Theta = \begin{pmatrix} \hat{\kappa}^P \\ \hat{\kappa}^Q \end{pmatrix}. \tag{5.60}$$

In this basis the stability matrix 5.34 has the structure:

$$\mathbf{M}_\Theta = \begin{pmatrix} \mathbf{M}^{PP} & \mathbf{M}^{PQ} \\ \mathbf{M}^{QP} & \mathbf{M}^{QQ} \end{pmatrix} \tag{5.61}$$

with

$$\mathbf{M}^{PP}_{pq,rs} = \frac{\partial^2 E}{\partial \kappa^{P*}_{pq} \partial \kappa^{P}_{rs}} \tag{5.62}$$

$$\mathbf{M}^{PQ}_{pq,rs} = \frac{\partial^2 E}{\partial \kappa^{P*}_{pq} \partial \kappa^{Q}_{rs}} \tag{5.63}$$

$$\mathbf{M}^{QP}_{pq,rs} = \mathbf{M}^{PQ*}_{rs,pq} \tag{5.64}$$

$$\mathbf{M}^{QQ}_{pq,rs} = \frac{\partial^2 E}{\partial \kappa^{Q*}_{pq} \partial \kappa^{Q}_{rs}}. \tag{5.65}$$

Whenever $\mathbf{M}^{PQ}$ is equal to zero, which is the case for a time–reversal symmetric Hamiltonian of a closed–shell, Kramer's paired system, multiplication with the Hessian conserves time–reversal symmetry and the number of elements of the response vector $\vec{Y}$ unrelated by symmetry is further reduced.[218]

Using Eqs. 5.54 and 5.55 one finds:

$$\hat{\kappa}^P = \frac{1}{2} \sum_{pq} \left(\kappa_{pq} \hat{a}^\dagger_p \hat{a}_q + (-1)^{\tau_p + \tau_q - 1} \kappa^*_{pq} \hat{a}^\dagger_{\overline{p}} \hat{a}_{\overline{q}} \right) = \sum_{pq} \kappa^P_{pq} \hat{a}^\dagger_p \hat{a}_q \tag{5.66}$$

$$\hat{\kappa}^Q = \frac{1}{2} \sum_{pq} \left(\kappa_{pq} \hat{a}^\dagger_p \hat{a}_q - (-1)^{\tau_p + \tau_q - 1} \kappa^*_{pq} \hat{a}^\dagger_{\overline{p}} \hat{a}_{\overline{q}} \right) = \sum_{pq} \kappa^Q_{pq} \hat{a}^\dagger_p \hat{a}_q, \tag{5.67}$$

where

$$\kappa^P_{pq} = \frac{1}{2} \left(\kappa_{pq} + (-1)^{\tau_{\overline{p}} + \tau_{\overline{q}} - 1} \kappa^*_{\overline{pq}} \right) \tag{5.68}$$

$$\kappa^Q_{pq} = \frac{1}{2} \left(\kappa_{pq} - (-1)^{\tau_{\overline{p}} + \tau_{\overline{q}} - 1} \kappa^*_{\overline{pq}} \right) \tag{5.69}$$

have been introduced. In terms of these parameters, κ_{pq} and κ^*_{pq} are given by:

$$\kappa_{pq} = \kappa^P_{pq} + \kappa^Q_{pq} \tag{5.70}$$

$$\kappa^*_{pq} = (-1)^{1 - \tau_p - \tau_q} \left(\kappa^P_{\overline{pq}} - \kappa^Q_{\overline{pq}} \right), \tag{5.71}$$

and the matrix elements of $\mathbf{M}_{pq,rs}^{PQ}$ can be expressed in terms of the original blocks $\mathbf{A}$ and $\mathbf{B}$ of the stability matrix Eq. 5.34 as:

$$
\begin{aligned}
\mathbf{M}_{pq,rs}^{PQ} &= \sum_{lmno} \left(\frac{\partial^2 E}{\partial \kappa_{no}^* \partial \kappa_{lm}^*} \frac{\partial \kappa_{no}^*}{\partial \kappa_{pq}^P} \frac{\partial \kappa_{lm}^*}{\partial \kappa_{rs}^Q} + \frac{\partial^2 E}{\partial \kappa_{no} \partial \kappa_{lm}} \frac{\partial \kappa_{no}}{\partial \kappa_{pq}^P} \frac{\partial \kappa_{lm}}{\partial \kappa_{rs}^Q} \right. \\
&\quad \left. + \frac{\partial^2 E}{\partial \kappa_{no}^* \partial \kappa_{lm}} \frac{\partial \kappa_{no}^*}{\partial \kappa_{pq}^P} \frac{\partial \kappa_{lm}}{\partial \kappa_{rs}^Q} + \frac{\partial^2 E}{\partial \kappa_{no} \partial \kappa_{lm}^*} \frac{\partial \kappa_{no}}{\partial \kappa_{pq}^P} \frac{\partial \kappa_{lm}^*}{\partial \kappa_{rs}^Q} \right) \\
&= \sum_{lmno} \left(B_{no,lm} \frac{\partial \kappa_{no}^*}{\partial \kappa_{pq}^P} \frac{\partial \kappa_{lm}^*}{\partial \kappa_{rs}^Q} + B_{no,lm}^* \frac{\partial \kappa_{no}}{\partial \kappa_{pq}^P} \frac{\partial \kappa_{lm}}{\partial \kappa_{rs}^Q} \right. \\
&\quad \left. + A_{no,lm} \frac{\partial \kappa_{no}^*}{\partial \kappa_{pq}^P} \frac{\partial \kappa_{lm}}{\partial \kappa_{rs}^Q} + A_{no,lm}^* \frac{\partial \kappa_{no}}{\partial \kappa_{pq}^P} \frac{\partial \kappa_{lm}^*}{\partial \kappa_{rs}^Q} \right).
\end{aligned}
\tag{5.72}
$$

Partial differentiation of Eqs. 5.70 and 5.71 with respect to κ_{pq}^P and κ_{pq}^Q leads to the following expression for the matrix elements of $\mathbf{M}^{PQ}$:

$$
\begin{aligned}
\mathbf{M}_{pq,rs}^{PQ} &= B_{\overline{pq},\overline{rs}} (-1)^{1-\tau_{\overline{r}}-\tau_{\overline{s}}} (-1)^{1-\tau_{\overline{p}}-\tau_{\overline{q}}} + B_{pq,rs}^* \\
&\quad - A_{pq,\overline{rs}}^* (-1)^{1-\tau_{\overline{r}}-\tau_{\overline{s}}} + A_{\overline{pq},rs} (-1)^{1-\tau_{\overline{p}}-\tau_{\overline{q}}} \\
&= -(-1)^{2-\tau_{\overline{p}}-\tau_{\overline{q}}-\tau_{\overline{r}}-\tau_{\overline{s}}} B_{\overline{pq},\overline{rs}} + B_{pq,rs}^* \\
&\quad - (-1)^{1-\tau_{\overline{r}}-\tau_{\overline{s}}} A_{pq,\overline{rs}}^* + (-1)^{1-\tau_{\overline{p}}-\tau_{\overline{q}}} A_{\overline{pq},rs}.
\end{aligned}
\tag{5.73}
$$

Using the expressions for $\mathbf{A}$ and $\mathbf{B}$ given in Eqs. 5.35 and 5.36, respectively, the relationship between $B_{\overline{pq},\overline{rs}}$ and $B_{pq,rs}^*$ as well as that between $A_{\overline{pq},rs}$ and $A_{pq,\overline{rs}}^*$ can be investigated:

$$
\begin{aligned}
A_{\overline{pq},rs} &= -(n_{\overline{p}} + n_r - 2n_{\overline{q}}) \delta_{\overline{q}s} F_{\overline{p}r} - (n_{\overline{q}} + n_s - 2n_r) \delta_{\overline{p}r} F_{s\overline{q}} \\
&\quad + (n_{\overline{p}} - n_{\overline{q}})(n_r - n_s) \left(2\Lambda_{\overline{pq}sr}^\eta + W_{\overline{pq}sr}^{\mathrm{XC}} \right)
\end{aligned}
\tag{5.74}
$$

$$
\begin{aligned}
B_{\overline{pq},\overline{rs}} &= (n_{\overline{p}} + n_{\overline{s}} - 2n_{\overline{q}}) \delta_{\overline{q}\overline{r}} F_{\overline{p}\overline{s}} + (n_{\overline{q}} + n_{\overline{r}} - 2n_{\overline{s}}) \delta_{\overline{p}\overline{s}} F_{\overline{r}\overline{q}} \\
&\quad + (n_{\overline{p}} - n_{\overline{q}})(n_{\overline{r}} - n_{\overline{s}}) \left(2\Lambda_{\overline{pqrs}}^\eta + W_{\overline{pqrs}}^{\mathrm{XC}} \right).
\end{aligned}
\tag{5.75}
$$

The Fock matrix itself has to be time–reversal symmetric, as its eigenvalues are related to the electronic energy, i.e. $F_{\overline{pq}} = (-1)^{\tau_p + \tau_q - 1} F_{pq}^*$. For the two-electron integrals one finds:

$$
\begin{aligned}
\Lambda_{\overline{pqrs}}^\eta &= \int \mathrm{d}^3 r_1 \mathrm{d}^3 r_2 \left[\Omega_{\overline{pq}}(\vec{r}_1) \frac{1}{r_{12}} \Omega_{\overline{rs}}(\vec{r}_2) - \eta \Omega_{\overline{ps}}(\vec{r}_1) \frac{1}{r_{12}} \Omega_{\overline{rq}}(\vec{r}_2) \right] \\
&= (-1)^{\tau_p + \tau_q + \tau_r + \tau_s - 2} \Lambda_{pqrs}^{\eta*},
\end{aligned}
\tag{5.76}
$$

since the matrix elements of the density operator defined in Eq. 5.22 fulfill the time-reversibility condition $\Omega_{\overline{pq}} = (-1)^{\tau_p + \tau_q - 1} \Omega_{pq}^*$ in order for the density to be symmetric under time–reversal. The functional contribution W_{pqrs}^{XC} is also time–reversal symmetric

since it is symmetric in the local spin density matrices $\mathbf{\Omega}^\uparrow$ and $\mathbf{\Omega}^\downarrow$ which are related by time–reversal as follows:

$$\Omega^\uparrow_{\overline{pq}} = \frac{1}{2}\left(\Omega_{\overline{pq}} + \Sigma^{\mathrm{p0}}_{\overline{pq}}\right) = (-1)^{\tau_p+\tau_q-1}\frac{1}{2}\left(\Omega^*_{pq} - \vec{e}_{\vec{m}_0}\cdot\vec{\Sigma}^*_{pq}\right) = (-1)^{\tau_p+\tau_q-1}\,\Omega^{\downarrow*}_{pq} \qquad (5.77)$$

$$\Omega^\downarrow_{\overline{pq}} = \frac{1}{2}\left(\Omega_{\overline{pq}} - \Sigma^{\mathrm{p0}}_{\overline{pq}}\right) = (-1)^{\tau_p+\tau_q-1}\frac{1}{2}\left(\Omega^*_{pq} + \vec{e}_{\vec{m}_0}\cdot\vec{\Sigma}^*_{pq}\right) = (-1)^{\tau_p+\tau_q-1}\,\Omega^{\uparrow*}_{pq}, \qquad (5.78)$$

where the time–reversal antisymmetry relation

$$\vec{\Sigma}_{\overline{pq}} = -\,(-1)^{\tau_p+\tau_q-1}\,\vec{\Sigma}_{pq} \qquad (5.79)$$

of the magnetization has been used. The exchange of the local spin densities under time–reversal corresponds to the exchange of alpha and beta spin orbitals in nonrelativistic theory. For $W^{\mathrm{XC}}_{\overline{pqrs}}$ this yields:

$$\begin{aligned}
W^{\mathrm{XC}}_{\overline{pqrs}} &= \int \mathrm{d}^3r\left(\frac{\delta^2\varepsilon^{\mathrm{XC}}}{\delta\rho^2_\uparrow}\Omega^\uparrow_{\overline{pq}}\Omega^\uparrow_{\overline{rs}} + \frac{\delta^2\varepsilon^{\mathrm{XC}}}{\delta\rho^2_\downarrow}\Omega^\downarrow_{\overline{pq}}\Omega^\downarrow_{\overline{rs}} + \frac{\delta^2\varepsilon^{\mathrm{XC}}}{\delta\rho_\uparrow\delta\rho_\downarrow}\left[\Omega^\uparrow_{\overline{pq}}\Omega^\downarrow_{\overline{rs}} + \Omega^\downarrow_{\overline{pq}}\Omega^\uparrow_{\overline{rs}}\right]\right) \\
&= \int \mathrm{d}^3r\left(\frac{\delta^2\varepsilon^{\mathrm{XC}}}{\delta\rho^2_\uparrow}(-1)^{\tau_p+\tau_q+\tau_r+\tau_s-2}\,\Omega^{\uparrow*}_{pq}\Omega^{\uparrow*}_{rs} + \frac{\delta^2\varepsilon^{\mathrm{XC}}}{\delta\rho^2_\downarrow}(-1)^{\tau_p+\tau_q+\tau_r+\tau_s-2}\,\Omega^{\downarrow*}_{pq}\Omega^{\downarrow*}_{rs}\right. \\
&\quad \left.+\frac{\delta^2\varepsilon^{\mathrm{XC}}}{\delta\rho_\uparrow\delta\rho_\downarrow}(-1)^{\tau_p+\tau_q+\tau_r+\tau_s-2}\left[\Omega^{\downarrow*}_{pq}\Omega^{\uparrow*}_{rs} + \Omega^{\uparrow*}_{pq}\Omega^{\downarrow*}_{rs}\right]\right) \\
&= (-1)^{\tau_p+\tau_q+\tau_r+\tau_s-2}\,W^{\mathrm{XC}*}_{pqrs}, \qquad (5.80)
\end{aligned}$$

for real valued the local spin densities $\rho_\uparrow$ and $\rho_\downarrow$ and exchange–correlation functional $\varepsilon^{\mathrm{XC}}$.

As the Kronecker delta fulfills $\delta_{\overline{pq}} = \delta_{pq}$, $\delta_{\overline{p}q} = \delta_{p\overline{q}} = 0$ and is real-valued, it can also be expressed as a time reversal symmetric matrix element $\delta_{\overline{pq}} = (-1)^{\tau_p+\tau_q-1}\delta^*_{pq}$. For the Kramer's conjugated matrix elements of $\mathbf{A}$ and $\mathbf{B}$ one thus arrives at the expression:

$$\begin{aligned}
A_{\overline{pq},rs} &= -\left(n_{\overline{p}} + n_r - 2n_{\overline{q}}\right)\delta_{q\overline{s}}\,(-1)^{\tau_p+\tau_q\tau_{\overline{r}}+\tau_{\overline{s}}-2}\,F^*_{\overline{p}\overline{r}} - \left(n_{\overline{q}} + n_s - 2n_r\right)\delta_{p\overline{r}}\,(-1)^{\tau_p\tau_q+\tau_{\overline{r}}+\tau_{\overline{s}}-2}\,F^*_{\overline{s}q} \\
&\quad + \left(n_{\overline{p}} - n_{\overline{q}}\right)\left(n_r - n_s\right)(-1)^{\tau_p+\tau_q+\tau_{\overline{r}}+\tau_{\overline{s}}-2}\left(2\Lambda^{\eta*}_{pq\overline{s}\overline{r}} + W^{\mathrm{XC}*}_{pq\overline{s}\overline{r}}\right) \qquad (5.81)
\end{aligned}$$

$$\begin{aligned}
B_{\overline{pq},\overline{rs}} &= \left(n_{\overline{p}} + n_{\overline{s}} - 2n_{\overline{q}}\right)\delta_{qr}\,(-1)^{\tau_p+\tau_q+\tau_r+\tau_s-2}\,F^*_{ps} + \left(n_{\overline{q}} + n_{\overline{r}} - 2n_{\overline{s}}\right)\delta_{ps}\,(-1)^{\tau_p+\tau_q+\tau_r+\tau_s-2}\,F^*_{rq} \\
&\quad + \left(n_{\overline{p}} - n_{\overline{q}}\right)\left(n_{\overline{r}} - n_{\overline{s}}\right)(-1)^{\tau_p+\tau_q+\tau_r+\tau_s-2}\left(2\Lambda^{\eta*}_{pqrs} + W^{\mathrm{XC}*}_{pqrs}\right). \qquad (5.82)
\end{aligned}$$

In case of a Kramer's paired closed shell system, $n_{\overline{p}} = n_p$ for all occupation numbers, and these expressions are reduced to:

$$A_{\overline{pq},rs} = (-1)^{\tau_p+\tau_q+\tau_{\overline{r}}+\tau_{\overline{s}}-2}\,A^*_{pq,\overline{rs}} \qquad (5.83)$$

$$B_{\overline{pq},\overline{rs}} = (-1)^{\tau_p+\tau_q+\tau_r+\tau_s-2}\,B^*_{pq,rs}. \qquad (5.84)$$

It follows that $\mathbf{M}^{PQ}$ of Eq. 5.73 has to vanish:

$$
\begin{aligned}
\mathbf{M}^{PQ}_{pq,rs} &= -\,(-1)^{2-\tau_{\overline{p}}-\tau_{\overline{q}}-\tau_{\overline{r}}-\tau_{\overline{s}}} B_{\overline{pq},\overline{rs}} + B^*_{pq,rs} - (-1)^{1-\tau_{\overline{r}}-\tau_{\overline{s}}} A^*_{pq,\overline{rs}} + (-1)^{1-\tau_{\overline{p}}-\tau_{\overline{q}}} A_{\overline{pq},rs} \\
&= -\,(-1)^{2(\tau_p+\tau_q+\tau_r+\tau_s)} B^*_{pq,rs} + B^*_{pq,rs} - (-1)^{1-\tau_{\overline{r}}-\tau_{\overline{s}}} A^*_{pq,\overline{rs}} + (-1)^{2(\tau_p+\tau_q)+\tau_{\overline{r}}+\tau_{\overline{s}}-1} A^*_{pq,\overline{rs}} \\
&= -B^*_{pq,rs} + B^*_{pq,rs} - (-1)^{-(\tau_{\overline{r}}+\tau_{\overline{s}}-1)} A^*_{pq,\overline{rs}} + (-1)^{(\tau_{\overline{r}}+\tau_{\overline{s}}-1)} A^*_{pq,\overline{rs}} \\
&= 0.
\end{aligned} \tag{5.85}
$$

For a Kramer's paired closed-shell system the response vector thus has the same symmetry with respect to time–reversal as the property gradient with the structure:[218]

$$
\vec{Y}^{\mathrm{T}} = \left(\vec{y}, \vec{z}, -t\vec{z}^{*}, t\vec{y}^{*}, h\vec{y}^{*}, h\vec{z}^{*}, -th\vec{z}, th\vec{y} \right), \tag{5.86}
$$

where the elements of $\vec{y}$ correspond to $X_{P\tau Q\tau}$ and the elements of $\vec{z}$ correspond to $X_{P\tau Q\overline{\tau}}$ for $P > Q$. The computational effort can thus be reduced by a factor of four.

5.4 PV potential

The parity violating potential V_{PV}, i.e. the shift in electronic energy induced in a molecule at a given structure by the parity violating weak interaction is defined to first order in G_{F} as the first derivative of the energy with respect to the PV perturbation parameter λ^{PV} (see for example reference [77] for a detailed discussion of different computational approaches):

$$
V_{\mathrm{PV}} = \left. \frac{\mathrm{d}E}{\mathrm{d}\lambda^{\mathrm{PV}}} \right|_{\underline{T}=\underline{0}}. \tag{5.87}
$$

In accordance with Eq. 5.28 this is equal to the partial derivative of the energy with respect to λ^{PV}, which in the ZORA framework is given by:

$$
V_{\mathrm{PV}} = \left. \frac{\partial E}{\partial \lambda^{\mathrm{PV}}} \right|_{\underline{T}=\underline{0}} = \sum_{pq} \left\langle \phi_p \left| \left\{ \vec{\sigma} \cdot \vec{p}, \frac{\tilde{\omega}}{c} \frac{G_{\mathrm{F}}}{2\sqrt{2}} \sum_{A=1}^{N_{\mathrm{nuc}}} Q_{\mathrm{W}}(A)\, \varrho_A(\vec{r}) \right\} \right| \phi_q \right\rangle N_{pq}. \tag{5.88}
$$

Above, the expression for the total energy of Eq. 5.27 has been used, where for vanishing perturbations, $\tilde{D}_{pq}(\kappa)$ corresponds to the occupation number matrix $\mathbf{N}$ with elements given in Eq. A.4 making the above summation one over occupied orbitals only as derived in references [58, 59]:

$$
V_{\mathrm{PV}} = \sum_{i=1}^{N_{\mathrm{occ}}} \left\langle \phi_i \left| \left\{ \vec{\sigma} \cdot \vec{p}, \frac{\tilde{\omega}}{c} \frac{G_{\mathrm{F}}}{2\sqrt{2}} \sum_{A=1}^{N_{\mathrm{nuc}}} Q_{\mathrm{W}}(A)\, \varrho_A(\vec{r}) \right\} \right| \phi_i \right\rangle. \tag{5.89}
$$

The contribution of the nuclear spin dependent part of the parity violating operator 4.3 to the PV potential is much smaller and appears only at higher orders.

5.5 PV NMR shielding tensor for closed shell systems

The parity conserving NMR shielding tensor is related to the second total derivative of the energy with respect to the external magnetic field and the nuclear magnetic moment of the nucleus in question. In order to unambiguously define the PV contribution to this molecular property, it is indicated to relate the lowest order contribution to the PV NMR shielding tensor of a nucleus Q to the third derivative of the total electronic energy E with respect to the external magnetic field $\vec{B}$, the magnetic moment of the nucleus $\vec{\mu}_Q$ and the PV perturbation parameter λ^{PV}, evaluated at zero external field, magnetic moments $\vec{\mu}_A$ (for $A = 1 \ldots N_{\mathrm{nuc}}$) and λ^{PV}:

$$\sigma_{kt}^{\mathrm{PV}}(Q) := \left. \frac{d^3 E}{dB_k d\mu_{Qt} d\lambda^{\mathrm{PV}}} \right|_{\underline{T=\underline{0}}} . \tag{5.90}$$

Here, the components $\sigma_{kt}^{\mathrm{PV}}(Q)$ of the shielding tensor are indexed by the Cartesian components k and t of the magnetic field $\vec{B}$ and nuclear magnetic moment $\vec{\mu}_Q$ of the nucleus under study, respectively. According to Eq. 5.30, the PV shielding tensor is thus given by:

$$\sigma_{kt}^{\mathrm{PV}}(Q) = \left(\frac{\partial^3 E}{\partial B_k \partial \mu_{Qt} \partial \lambda^{\mathrm{PV}}} \right) + \sum_{pq} \left[\left(\frac{\partial^3 E}{\partial B_k \partial \mu_{Qt} \partial \kappa_{pq}} \right) \left(\frac{\partial \kappa_{pq}}{\partial \lambda^{\mathrm{PV}}} \right) + \left(\frac{\partial^3 E}{\partial B_k \partial \kappa_{pq} \partial \lambda^{\mathrm{PV}}} \right) \left(\frac{\partial \kappa_{pq}}{\partial \mu_{Qt}} \right) \right.$$
$$+ \left. \left(\frac{\partial^3 E}{\partial \kappa_{pq} \partial \mu_{Qt} \partial \lambda^{\mathrm{PV}}} \right) \left(\frac{\partial \kappa_{pq}}{\partial B_k} \right) \right] + \sum_{pq,rs} \left[\left(\frac{\partial^3 E}{\partial B_k \partial \kappa_{rs} \partial \kappa_{pq}} \right) \left(\frac{\partial \kappa_{rs}}{\partial \mu_{Qt}} \right) \left(\frac{\partial \kappa_{pq}}{\partial \lambda^{\mathrm{PV}}} \right) \right.$$
$$+ \left. \left(\frac{\partial^3 E}{\partial \kappa_{rs} \partial \mu_{Qt} \partial \kappa_{pq}} \right) \left(\frac{\partial \kappa_{rs}}{\partial B_k} \right) \left(\frac{\partial \kappa_{pq}}{\partial \lambda^{\mathrm{PV}}} \right) + \left(\frac{\partial^3 E}{\partial \kappa_{rs} \partial \kappa_{pq} \partial \lambda^{\mathrm{PV}}} \right) \left(\frac{\partial \kappa_{rs}}{\partial B_k} \right) \left(\frac{\partial \kappa_{pq}}{\partial \mu_{Qt}} \right) \right]$$
$$+ \sum_{pq,rs,tu} \left(\frac{\partial^3 E}{\partial \kappa_{tu} \partial \kappa_{rs} \partial \kappa_{pq}} \right) \left(\frac{\partial \kappa_{tu}}{\partial B_k} \right) \left(\frac{\partial \kappa_{rs}}{\partial \mu_{Qt}} \right) \left(\frac{\partial \kappa_{pq}}{\partial \lambda^{\mathrm{PV}}} \right) . \tag{5.91}$$

Traditionally, σ as a symbol is used for both the NMR shielding tensor and the Pauli spin matrices. Here, $\vec{\sigma}$ and $\sigma_{x/y/z}$ refer to the spin matrices whereas all other σ-symbols are related to the shielding tensor. Furthermore, at this point only closed shell molecular systems are considered, which is essentially no restriction by virtue of the experimentally targeted resolution.

Eq. 5.91 is generally valid for variational electronic structure methods, independently of the treatment of electron correlation or relativistic effects. If constrained parameters $\vec{C}$ (e.g. LCAO MO coefficients) are used, the variational condition $\partial \widetilde{E} / \partial C_m = 0$ has

to be expressed in terms of an energy functional $\widetilde{E}$ which accounts for restrictions of the variational parameters. In this case, the expression for $\sigma_{kt}^{\mathrm{PV}}(Q)$ can contain some additional terms reflecting these restrictions, as discussed, for example, in Ref. [236].

The first term on the right hand side of Eq. 5.91 gives rise to an expectation value contribution of the mixed third partial derivative of $\hat{h}^{\mathrm{zora}}$ with respect to B_k, μ_{Qt} and λ^{pv} and possibly also to terms involving partial derivatives of the basis functions, if these depend directly on any of the perturbations. In four-component theory with perturbation independent basis sets, the expectation value term, corresponding to the diamagnetic part of the shielding tensor in the present formulation, does not arise at this point. The remaining terms on the right-hand side of Eq. 5.91 arise from linear and quadratic response type expressions which, for variational wavefunctions, can be evaluated by solving linear response equations only, in accordance with Wigner's (2n+1) rule.

In order to compare results to those of most previous studies of PV NMR parameters (e.g. Refs. [53, 68, 156–158]) the focus here will be exclusively on the nuclear spin-dependent part $\hat{f}_{\mathrm{PV}}^{(2)}$ of the PV operator of Eq. 4.3. Since $\hat{f}_{\mathrm{PV}}^{(2)}$ is bilinear in $\vec{\mu}_Q$ and λ^{PV} only those terms in Eq. 5.91 which contain mixed derivatives with respect to both $\vec{\mu}_Q$ and λ^{PV} can give a nonzero contribution to the shielding tensor. In this case, most of the terms on the right hand side of Eq. 5.91 vanish, resulting the following expression:

$$\sigma_{kt}^{\mathrm{PV}}(Q) = \left(\frac{\partial^3 E}{\partial B_k \partial \mu_{Qt} \partial \lambda^{\mathrm{PV}}} \right)$$
$$+ \sum_{pq} \left(\frac{\partial^3 E}{\partial \mu_{Qt} \partial \lambda^{\mathrm{PV}} \partial \kappa_{pq}} \right) \left(\frac{\partial \kappa_{pq}}{\partial B_k} \right), \tag{5.92}$$

where the kinetic energy and perturbation contribution to E are now related to

$$\hat{h}^{\mathrm{zora},(2)} = \vec{\sigma} \cdot \vec{p} \tilde{\omega} \vec{\sigma} \cdot \vec{p} + e \left\{ \vec{\sigma} \cdot \vec{p}, \tilde{\omega} \vec{\sigma} \cdot \vec{A} \right\}$$
$$+ \left\{ \vec{\sigma} \cdot \vec{p}, \frac{\tilde{\omega}}{c} \hat{f}_{\mathrm{PV}}^{(2)} \right\} + e \left\{ \vec{\sigma} \cdot \vec{A}, \frac{\tilde{\omega}}{c} \hat{f}_{\mathrm{PV}}^{(2)} \right\}$$
$$+ e^2 \left\{ \vec{\sigma} \cdot \vec{A}, \tilde{\omega} \vec{\sigma} \cdot \vec{A} \right\}. \tag{5.93}$$

The nuclear spin–independent term $\hat{f}_{\mathrm{PV}}^{(1)}$ of Eq. 4.3 is, for heavy nuclei, usually expected [6] to give a contribution three orders of magnitude smaller than that of the nuclear spin–dependent term. Other estimates for PV effects in Pb atoms seem to indicate, however, that under certain conditions the impact of the nuclear spin–independent term is comparable to that of the nuclear spin–dependent one [240]. The need for more research is clearly indicated, making an extension of the present approach to include

effects of the nuclear spin–independent PV operator in the calculation of NMR shielding tensors an interesting prospect.

5.5.1   Coupled vs. uncoupled DFT approach

According to Eq. 5.31 the response of the parameters κ_{pq} to the perturbation B_k can be calculated using the relation:

$$0 = \left(\frac{\partial^2 E}{\partial B_k \partial \kappa_{pq}} \right) + \sum_{rs} \left(\frac{\partial^2 E}{\partial \kappa_{pq} \partial \kappa_{rs}} \right) \left(\frac{\partial \kappa_{rs}}{\partial B_k} \right). \tag{5.94}$$

In general, these equations are coupled and an iterative method can be applied in order to solve them. Within a pure (non–hybrid) DFT closed–shell framework, however, and using functionals that depend on the density alone, as opposed to the non–collinear density functionals introduced earlier, which depend on local spin densities, Eqs. 5.94 can be decoupled through the exploitation of time–reversal symmetry.[230, 241]

Magnetic perturbations correspond to Hermitian, time–reversal antisymmetric operators and according to the discussion in Section 5.3 both the property gradient and the response vector inherit the same symmetries in a closed shell system.

Recasting Eq. 5.94 in matrix form analogously to Eq. 5.33, the equation involving the upper block of the property gradient $\vec{G}$

$$\vec{G} = \begin{pmatrix} \frac{\partial^2 E}{\partial B_k \partial \kappa_{pq}} \\ \frac{\partial^2 E}{\partial B_k \partial \kappa_{pq}^*} \end{pmatrix} \tag{5.95}$$

with $p > q$ and $r > s$ is given by:

$$\begin{aligned} G_{pq} &= -\sum_{rs} \left(A_{pq,rs} X_{rs} + h B_{pq,rs} X_{rs}^* \right) \\ &= F_{pq}^{(1)} + Z_{pq}, \end{aligned} \tag{5.96}$$

with the modified Fock matrix:

$$F_{pq}^{(1)} = 2 \sum_{r} \left[(n_p + n_r - 2n_q) F_{pr} X_{rq} + (n_q + n_r - 2n_p) X_{pr} F_{rq} \right], \tag{5.97}$$

where the relation $X_{rs}^* = -h X_{sr}$ has been used. In the case of canonical zero order orbitals, the unperturbed Fock matrix is diagonal and Eq. 5.97 reduces to:

$$F_{pq}^{(1)} = \begin{cases} 4 \left(\epsilon_i - \epsilon_a \right) X_{ai} & \text{for } p = a \text{ (unoccupied) and } q = i \text{ (occupied)} \\ 0 & \text{else,} \end{cases} \tag{5.98}$$

so that only the modified two–electron contribution Z_{pq} can constitute a coupling of Eqs. 5.94. In cases where this contribution vanishes, the response equations become uncoupled and elements of the solution vector $\vec{Y}$ are related to the corresponding elements of the property gradient divided by orbital energy differences.

The modified two-electron contribution is given by:

$$Z_{pq} = 2 \sum_{rs} (n_p - n_q)(n_r - n_s) \left[2\Lambda^{\eta}_{pq,sr} + W^{\mathrm{XC}}_{pq,sr} \right] X_{rs}, \tag{5.99}$$

where the Coulomb and exchange integrals take the following form:

$$\sum_{rs} (n_r - n_s) \Lambda^{\eta}_{pq,sr} X_{rs} = \sum_{rs} (n_r - n_s) \left(\int \mathrm{d}^3 r_1 \mathrm{d}^3 r_2 \Omega_{pq}(\vec{r}_1) \frac{1}{r_{12}} \Omega_{sr}(\vec{r}_2) \right.$$
$$\left. -\eta \int \mathrm{d}^3 r_1 \mathrm{d}^3 r_2 \Omega_{ps}(\vec{r}_1) \frac{1}{r_{12}} \Omega_{rq}(\vec{r}_2) \right) X_{rs}. \tag{5.100}$$

Utilizing the expansion of $\tilde{D}_{pq}$ given by Eq. A.3, it is evident, that the sum over rs in the Coulomb integral is equal to the first order change $\rho^{(1)}_k$ in the density ρ given by Eq. 5.20:

$$\rho^{(1)}_k = \frac{\mathrm{d}\rho}{\mathrm{d}B_k}\bigg|_{\underline{T=0}} = \sum_{pq} \left(\frac{\partial \rho}{\partial \kappa_{pq}} \right) \left(\frac{\partial \kappa_{pq}}{\partial B_k} \right) = \sum_{pq,rs} \Omega_{sr} \left\langle 0 \left| \left[\hat{a}^{\dagger}_p \hat{a}_q, \hat{a}^{\dagger}_s \hat{a}_r \right] \right| 0 \right\rangle X_{pq}$$
$$= \sum_{rs} (n_r - n_s) \Omega_{sr} X_{rs}. \tag{5.101}$$

For a time–reversal antisymmetric perturbation such as the external magnetic field however, this contribution has no real component in a closed shell system and must therefore vanish:

$$\sum_{rs} (n_r - n_s) \Omega_{sr} X_{rs} = \frac{1}{2} \sum_{rs} \left\{ (n_r - n_s) \Omega_{sr} X_{rs} + (n_r - n_s) \Omega_{\overline{sr}} X_{\overline{rs}} \right\}$$
$$= \frac{1}{2} \sum_{rs} (n_r - n_s) \left\{ \Omega_{sr} X_{rs} - (-1)^{2(\tau_s + \tau_r - 1)} \Omega^*_{sr} X^*_{rs} \right\}$$
$$= \sum_{rs} (n_r - n_s) \operatorname{Im} \left[\Omega_{sr} X_{rs} \right], \tag{5.102}$$

so that only the two–electron exchange integrals contribute to Z_{pq} in such systems. For integrals involving the exchange–correlation functional a similar restriction can be made in case of spin density–independent functionals.

The DFT contribution to Z_{pq} is proportional to:

$$\sum_{rs} (n_r - n_s) W_{pq,sr}^{\mathrm{XC}} X_{rs} = \sum_{rs} (n_r - n_s) \int \mathrm{d}^3 r \left(\frac{\delta^2 \varepsilon^{\mathrm{XC}}}{\delta \rho_\uparrow^2} \Omega_{pq}^\uparrow \Omega_{sr}^\uparrow + \frac{\delta^2 \varepsilon^{\mathrm{XC}}}{\delta \rho_\downarrow^2} \Omega_{pq}^\downarrow \Omega_{sr}^\downarrow \right.$$
$$\left. + \frac{\delta^2 \varepsilon^{\mathrm{XC}}}{\delta \rho_\uparrow \delta \rho_\downarrow} \left[\Omega_{pq}^\uparrow \Omega_{sr}^\downarrow + \Omega_{pq}^\downarrow \Omega_{sr}^\uparrow \right] \right) \Bigg|_{\rho_{\uparrow/\downarrow} = \rho_{\uparrow 0 / \downarrow 0}} X_{rs} \qquad (5.103)$$

and, for a closed shell system with vanishing initial magnetization, becomes (see appendix A for details)

$$\sum_{rs} (n_r - n_s) W_{pq,sr}^{\mathrm{XC}} X_{rs} = \frac{1}{4} \sum_{rs} (n_r - n_s) \int \mathrm{d}^3 r \left(\left[\frac{\delta^2 \varepsilon^{\mathrm{XC}}}{\delta \rho_\uparrow^2} + \frac{\delta^2 \varepsilon^{\mathrm{XC}}}{\delta \rho_\downarrow^2} \right] \Bigg|_{\rho_{\uparrow/\downarrow} = \rho_0} \left[\Omega_{pq} \Omega_{sr} + \vec{\Sigma}_{pq} \cdot \vec{\Sigma}_{sr} \right] \right.$$
$$\left. + 2 \frac{\delta^2 \varepsilon^{\mathrm{XC}}}{\delta \rho_\uparrow \delta \rho_\downarrow} \Bigg|_{\rho_{\uparrow/\downarrow} = \rho_0} \left[\Omega_{pq} \Omega_{sr} - \vec{\Sigma}_{pq} \cdot \vec{\Sigma}_{sr} \right] \right) X_{rs}. \qquad (5.104)$$

The products of local spin densities with the solution vector involve first order perturbed density which vanishes for magnetic perturbations in closed–shell systems and the first order perturbed magnetization (Eq. 5.21)

$$\vec{m}_{(k)}^{(1)} = \frac{\mathrm{d}\vec{m}}{\mathrm{d}B_k} \Bigg|_{\underline{T}=\underline{0}} = \sum_{pq} \left(\frac{\partial \vec{m}}{\partial \kappa_{pq}} \right) \left(\frac{\partial \kappa_{pq}}{\partial B_k} \right) = \sum_{pq,rs} \vec{\Sigma}_{sr} \left\langle 0 \left| \left[\hat{a}_p^\dagger \hat{a}_q, \hat{a}_s^\dagger \hat{a}_r \right] \right| 0 \right\rangle X_{pq}$$
$$= \sum_{rs} (n_r - n_s) \vec{\Sigma}_{sr} X_{rs}, \qquad (5.105)$$

which can give a non-vanishing contribution to Z_{pq}. For closed shell systems this takes the form:

$$\frac{1}{4} \int \mathrm{d}^3 r \left[\frac{\delta^2 \varepsilon^{\mathrm{XC}}}{\delta \rho_\uparrow^2} + \frac{\delta^2 \varepsilon^{\mathrm{XC}}}{\delta \rho_\downarrow^2} - 2 \frac{\delta^2 \varepsilon^{\mathrm{XC}}}{\delta \rho_\uparrow \delta \rho_\downarrow} \right] \Bigg|_{\rho_{\uparrow/\downarrow} = \rho_0} \vec{\Sigma}_{pq} \cdot \vec{m}_{(k)}^{(1)}. \qquad (5.106)$$

In cases where spin-density independent density functionals are used, there can thus be no modified two–electron contribution from the functional to Z_{pq}, and unless a fraction of Fock exchange is used in the calculations, $Z_{pq} = 0$ and Eq. 5.96 for $p > q$ and canonical zero order orbitals is reduced to:

$$G_{pq} = 4 \left(\epsilon_q - \epsilon_p \right) W_{pq}, \qquad (5.107)$$

with

$$W_{pq} = \begin{cases} X_{ai} & \text{for } p = a \text{ (unoccupied) and } q = i \text{ (occupied)} \\ 0 & \text{else.} \end{cases} \qquad (5.108)$$

In this case, Eqs. 5.94 become uncoupled and the first order response of the parameters of the wavefunction to an external magnetic field is given by:

$$
\begin{aligned}
\left(\frac{\partial \kappa_{pq}}{\partial B_k}\right) &= \frac{1}{4}\left(\frac{\partial^2 E}{\partial B_k \partial \kappa_{pq}}\right)(\epsilon_q - \epsilon_p)^{-1} \\
&= \begin{cases} \frac{1}{4}\left\langle a \left| \left(\frac{\partial \hat{h}^{\text{zora},(2)}}{\partial B_k}\right) \right| i \right\rangle (\epsilon_i - \epsilon_a)^{-1} & \text{for } p = a \text{ (unoccupied) and } q = i \text{ (occupied)} \\ 0 & \text{else,} \end{cases}
\end{aligned}
\tag{5.109}
$$

leading to a sum–over–states type expression (uncoupled DFT) for the second term on the right hand side of Eq. 5.92:

$$
\begin{aligned}
\sigma_{kt}^{\text{PV}}(Q) &= \sum_{i=1}^{N_{\text{occ}}} \left\langle i \left| \left(\frac{\partial^3 \hat{h}^{\text{zora},(2)}}{\partial B_k \partial \mu_{Qt} \partial \lambda^{\text{PV}}}\right) \right| i \right\rangle \\
&\quad + 2\text{Re}\left[\sum_{i=1}^{N_{\text{occ}}} \sum_{a=N_{\text{occ}}+1}^{M} \left\langle i \left| \left(\frac{\partial^2 \hat{h}^{\text{zora},(2)}}{\partial \mu_{Qt} \partial \lambda^{\text{PV}}}\right) \right| a \right\rangle \right. \\
&\quad \times \left. \left\langle a \left| \left(\frac{\partial \hat{h}^{\text{zora},(2)}}{\partial B_k}\right) \right| i \right\rangle (\epsilon_i - \epsilon_a)^{-1}\right].
\end{aligned}
\tag{5.110}
$$

So far, it has been assumed that the basis functions are independent of the perturbations, and no attempt was made to alleviate the lack of gauge origin independence in finite basis set expansions by employing e.g. Gauge Including Atomic Orbitals (GIAO) or the Individual Gauge for Localized Orbitals (IGLO) method (see also Ref. [242]). In this exploratory work such corrections were not included and a common gauge origin, localized at the nucleus of interest, was selected instead.

It should be noted, that generally, for a relativistic DFT approach in the presence of a magnetic field one would require that the exchange–correlation functional depends on the current density $\vec{j}$ as well as the density ρ or localized spin densities $\rho_\uparrow$ and $\rho_\downarrow$.[243, 244] Such a functional would contribute another non-vanishing term to the modified two-electron integrals Z_{pq} of Eq. 5.96 and necessitate the use of a coupled–perturbed Kohn–Sham approach to the solution of Eqs. 5.94.

As has been shown in the context of Eq. 5.100, the use of hybrid functionals also leads to a coupling of Eqs. 5.94, suggesting that spin polarization is enhanced by the introduction of the exchange integrals.[245, 246] For the nonrelativistic case, however, it has been demonstrated in reference [247] that the use of hybrid DFT eigenvalues and orbitals (calculated with a fraction of exact exchange reoptimized for the calculation of NMR parameters) in the uncoupled DFT expression for the shielding tensor corresponding to Eq. 5.110 can improve upon the accuracy in calculating this property when compared to

coupled DFT results obtained with the original hybrid functionals. The exact exchange contribution to Z_{pq} also leads to convergence problems in 4-component relativistic DFT calculations and has been neglected there on occasion.[230]

In the course of this thesis the uncoupled DFT approach (Eq. 5.110) to the calculation of PV NMR shielding tensors was implemented in a modified version of the TURBOMOLE program.[64, 65] In accordance with Refs. [230, 247] the method has also been used in connection with hybrid functionals for predicting PV NMR shieldings in some transition metal compounds. The results are presented in Chapter 7.

5.5.2 Perturbing operators

In order to evaluate Eq. 5.110, derivatives of the Hamiltonian with respect to the nuclear magnetic moments, the PV parameter and the magnetic field have to be calculated, which will be illustrated in this section.

In the upcoming Eqs. 5.111 to 5.124 the following notation is employed: The superscripts refer to the partial derivation status, i.e. 100 refers to a gradient with respect to the magnetic field $\vec{B}$, 010 to a gradient with respect to the nuclear magnetic moment $\vec{\mu}_Q$ and 001 to a partial derivative with respect to λ^{PV}. 110 refers to the mixed second derivative with first derivatives with respect to $\vec{B}$ and $\vec{\mu}_Q$, 011 to the mixed second derivative with first derivatives with respect to $\vec{\mu}_Q$ and λ^{PV} and so forth. The subscripts p, d and so refer to paramagnetic, diamagnetic and spin–orbit contributions in the way they are commonly used for parity conserving NMR parameters and subscripts after a comma such as $,k$ or $,kt$ refer to Cartesian components. The notation is kept similar to that of Ref. [62].

Derivatives of the ZORA Hamiltonian with respect to the nuclear magnetic moments, evaluated at $\vec{\mu}_A = \vec{0}$ for $A = 1, \ldots, N_{\mathrm{nuc}}$, are

$$\left(\frac{\partial \hat{h}^{\mathrm{zora},(2)}}{\partial \mu_{Qt}} \right) \Bigg|_{\vec{\mu}_A = \vec{0}} = h_{\mathrm{p},t}^{(010)} + h_{\mathrm{so},t}^{(010)}$$
$$+ \sum_{k=1}^{3} B_k \left(h_{\mathrm{d},kt}^{(110)} + \lambda^{\mathrm{PV}} h_{\mathrm{d},kt}^{(111)} \right)$$
$$+ \lambda^{\mathrm{PV}} \left(h_{\mathrm{p},t}^{(011)} + h_{\mathrm{so},t}^{(011)} \right), \tag{5.111}$$

where the parity conserving contributions for a point like distribution of the nucleus'
magnetic moment are given by:[62]

$$h_{\text{p},t}^{(010)} = \frac{e\mu_0}{4\pi} \left\{ \frac{\tilde{\omega}}{r_Q^3}, (\vec{r}_Q \times \vec{p})_t \right\} \tag{5.112}$$

$$h_{\text{so},t}^{(010)} = \mathrm{i}\frac{e\mu_0}{4\pi} \left(\sigma_t \left[\vec{p} \cdot \vec{r}_Q \frac{\tilde{\omega}}{r_Q^3} - \frac{\tilde{\omega}}{r_Q^3} \vec{r}_Q \cdot \vec{p} \right] \right. \tag{5.113}$$

$$\left. -\vec{\sigma} \cdot \left[p_t, \vec{r}_Q \frac{\tilde{\omega}}{r_Q^3} \right] \right) \tag{5.114}$$

$$h_{\text{d},kt}^{(110)} = \frac{e^2\mu_0}{8\pi} \frac{\tilde{\omega}}{r_Q^3} \left(\vec{r}_Q \cdot \vec{r}\,\delta_{kt} - r_{Qk}r_t \right). \tag{5.115}$$

In order to calculate the PV contributions, it is useful to decompose the corresponding
part of the ZORA Hamiltonian into electron spin–dependent and –independent contri-
butions using the Dirac identity, Eq. 4.30. Under this scheme, the contributions to the
ZORA operator which involves $\hat{f}_{\text{PV}}^{(2)}$ can be recast as

$$\hat{h}_{\text{PV}}^{\text{zora},(2)} = \left\{ \vec{\sigma} \cdot \vec{\pi}, \frac{\tilde{\omega}}{c} \hat{f}_{\text{PV}}^{(2)} \right\}$$

$$= \lambda^{\text{PV}} \frac{G_F}{2\sqrt{2}} \sum_{A=1}^{N_{\text{nuc}}} \frac{\kappa_A}{\hbar\gamma_A} \left\{ \vec{\sigma} \cdot \vec{\pi}, \frac{\tilde{\omega}}{c} \rho_A \vec{\sigma} \cdot \vec{\mu}_A \right\}$$

$$= \frac{\lambda^{\text{PV}}}{c} \frac{G_F}{2\sqrt{2}} \sum_{A=1}^{N_{\text{nuc}}} \frac{\kappa_A}{\hbar\gamma_A} \left[\{\vec{\pi} \cdot \vec{\mu}_A, \tilde{\omega}\rho_A\} \right.$$

$$+ \mathrm{i}\vec{\sigma} \left(\vec{\pi}\tilde{\omega}\rho_A \times \vec{\mu}_A \right) + \mathrm{i}\vec{\sigma} \cdot \left(\rho_A \vec{\mu}_A \times \tilde{\omega}\vec{\pi} \right) \right]$$

$$= \frac{\lambda^{\text{PV}}}{c} \frac{G_F}{2\sqrt{2}} \sum_{A=1}^{N_{\text{nuc}}} \frac{\kappa_A}{\hbar\gamma_A} \left(\vec{\mu}_A \cdot \{\vec{\pi}, \tilde{\omega}\rho_A\} \right.$$

$$\left. -\mathrm{i} \left(\vec{\sigma} \times \vec{\mu}_A \right) \cdot [\vec{\pi}, \tilde{\omega}\rho_A] \right). \tag{5.116}$$

With ε_{ktl} being the completely antisymmetric tensor, the remaining operators $h_{\text{p},t}^{(011)}$,
$h_{\text{so},t}^{(011)}$ and $h_{\text{d},kt}^{(111)}$ are thus given by:

$$h_{\text{p},t}^{(011)} = \frac{G_F}{2\sqrt{2}} \frac{\kappa_Q}{c\hbar\gamma_Q} \{p_t, \tilde{\omega}\rho_Q\} \tag{5.117}$$

$$h_{\text{so},t}^{(011)} = \mathrm{i}\frac{G_F}{2\sqrt{2}} \frac{\kappa_Q}{c\hbar\gamma_Q} [(\vec{\sigma} \times \vec{p})_t, \tilde{\omega}\rho_Q] \tag{5.118}$$

$$h_{\text{d},kt}^{(111)} = -\frac{G_F}{2\sqrt{2}} \frac{e\kappa_Q}{c\hbar\gamma_Q} \tilde{\omega}\rho_Q \sum_{l=1}^{3} \varepsilon_{ktl}r_l. \tag{5.119}$$

The partial derivative of the ZORA Hamiltonian with respect to the nuclear mag-
netic moments and the PV perturbation parameter λ^{PV}, evaluated at $\vec{\mu}_A = \vec{0}$ for

$A = 1, \ldots, N_{\mathrm{nuc}}$ and $\lambda^{\mathrm{PV}} = 0$ is given by:

$$
\left(\frac{\partial^2 \hat{h}^{\mathrm{zora},(2)}}{\partial \mu_{Qt} \partial \lambda^{\mathrm{PV}}} \right) \Bigg|_{\vec{\mu}_A = \vec{0}, \lambda^{\mathrm{PV}} = 0} = h_{\mathrm{p},t}^{(011)} + h_{\mathrm{so},t}^{(011)}
$$

$$
+ \sum_{k=1}^{3} B_k h_{\mathrm{d},kt}^{(111)} , \tag{5.120}
$$

and the partial derivative of the ZORA Hamiltonian with respect to the nuclear magnetic moments, λ^{PV} and magnetic field is:

$$
\left(\frac{\partial^3 \hat{h}^{\mathrm{zora},(2)}}{\partial B_k \partial \mu_{Qt} \partial \lambda^{\mathrm{PV}}} \right) \Bigg|_{\underline{T}=\underline{0}} = h_{\mathrm{d},kt}^{(111)} . \tag{5.121}
$$

Derivatives of the ZORA Hamiltonian with respect to the magnetic field, calculated for $\vec{B} = \vec{0}$, are given by:

$$
\left(\frac{\partial \hat{h}^{\mathrm{zora},(2)}}{\partial B_k} \right) \Bigg|_{\vec{B}=\vec{0}} = h_{\mathrm{p},k}^{(100)} + h_{\mathrm{so},k}^{(100)}
$$

$$
+ \sum_{A=1}^{N_{\mathrm{nuc}}} \sum_{t=1}^{3} \mu_{A_t} \left(h_{\mathrm{d},kt}^{(110)} + \lambda^{\mathrm{PV}} h_{\mathrm{d},kt}^{(111)} \right) , \tag{5.122}
$$

with the additional operators:[62]

$$
h_{\mathrm{p},k}^{(100)} = \frac{e}{2} \left\{ \tilde{\omega}, (\vec{r} \times \vec{p})_k \right\} \tag{5.123}
$$

$$
h_{\mathrm{so},k}^{(100)} = \mathrm{i} \frac{e}{2} \left(\sigma_k \left[\vec{p} \cdot \vec{r} \tilde{\omega} - \tilde{\omega} \vec{r} \cdot \vec{p} \right] - \vec{\sigma} \cdot \left[p_k, \vec{r} \tilde{\omega} \right] \right) . \tag{5.124}
$$

5.5.3   Shielding tensor and frequency splitting

Inserting Eqs. 5.121, 5.120 and 5.122 into Eq. 5.110 yields

$$
\sigma_{kt}^{\mathrm{PV}} (Q) = \sigma_{\mathrm{d},kt}^{\mathrm{PV}} (Q) + \sigma_{\mathrm{p},kt}^{\mathrm{PV}} (Q) + \sigma_{\mathrm{so},kt}^{\mathrm{PV}} (Q) , \tag{5.125}
$$

with the individual contributions given by

$$\sigma_{\mathrm{d},kt}^{\mathrm{PV}}(Q) = \sum_{i=1}^{N_{\mathrm{occ}}} \left\langle i|h_{\mathrm{d},kt}^{(111)}|i\right\rangle \tag{5.126}$$

$$\sigma_{\mathrm{p},kt}^{\mathrm{PV}}(Q) = 2\mathrm{Re}\left[\sum_{i=1}^{N_{\mathrm{occ}}}\sum_{a=N_{\mathrm{occ}}+1}^{M}\left(\frac{\left\langle i|h_{\mathrm{p},k}^{(100)}|a\right\rangle\left\langle a|h_{\mathrm{p},t}^{(011)}|i\right\rangle}{\epsilon_i - \epsilon_a}\right.\right.$$
$$\left.\left. + \frac{\left\langle i|h_{\mathrm{p},k}^{(100)}|a\right\rangle\left\langle a|h_{\mathrm{so},t}^{(011)}|i\right\rangle}{\epsilon_i - \epsilon_a}\right)\right] \tag{5.127}$$

$$\sigma_{\mathrm{so},kt}^{\mathrm{PV}}(Q) = 2\mathrm{Re}\left[\sum_{i=1}^{N_{\mathrm{occ}}}\sum_{a=N_{\mathrm{occ}}+1}^{M}\left(\frac{\left\langle i|h_{\mathrm{so},k}^{(100)}|a\right\rangle\left\langle a|h_{\mathrm{p},t}^{(011)}|i\right\rangle}{\epsilon_i - \epsilon_a}\right.\right.$$
$$\left.\left. + \frac{\left\langle i|h_{\mathrm{so},k}^{(100)}|a\right\rangle\left\langle a|h_{\mathrm{so},t}^{(011)}|i\right\rangle}{\epsilon_i - \epsilon_a}\right)\right] \tag{5.128}$$

Subscripts d, p and so have been used to refer to diamagnetic, paramagnetic and spin–orbit coupling contributions, respectively. The choice made in the collection of terms for the paramagnetic and spin–orbit coupling contributions to σ^{PV} was determined by the requirement that the individual terms combined to $\sigma_{\mathrm{p}}^{\mathrm{PV}}$ and $\sigma_{\mathrm{so}}^{\mathrm{PV}}$ display similar scaling behavior with respect to nuclear charge, while the parity conserving terms retain their conventional meaning.[62]

In Chapter 6, NMR frequency splittings $\Delta\nu^{\mathrm{PV}}$ between left– and right–handed enantiomers inside a constant magnetic field of strength B are reported. $\Delta\nu^{\mathrm{PV}}$ is given by:

$$\Delta\nu^{\mathrm{PV}}(Q) = B\gamma_Q\sigma^{\mathrm{PV}}(Q)/\pi,$$

with the isotropic shielding constant $\sigma^{\mathrm{PV}} = \frac{1}{3}\mathrm{Tr}\left[\sigma^{\mathrm{PV}}\right]$, to which the traceless diamagnetic PV shielding tensor $\sigma_{\mathrm{d},kt}^{\mathrm{PV}}(Q)$ of Eq. 5.126 does not contribute.

5.5.4 Calculation of the integrals

Integrals are calculated in the atomic orbital (AO) basis with matrices being subsequently transformed to the molecular orbital (MO) basis. Matrix elements are evaluated

as follows:

$$
\begin{aligned}
\left\langle i|h_{\mathrm{p},k}^{(100)}|a\right\rangle &= \sum_{\mu\nu} c_{\mu i}^{\dagger} c_{\nu a} \left\langle \chi_\mu |h_{\mathrm{p},k}^{(100)}|\chi_\nu\right\rangle \\
&= \sum_{\mu\nu} c_{\mu i}^{\dagger} c_{\nu a} \int \mathrm{d}^3 r\, \chi_\mu^* \left\{ (\vec{r}\times\vec{p})_k \,,\, \frac{e\tilde{\omega}}{2} \right\} \chi_\nu \\
&= \frac{\hbar}{\mathrm{i}} \sum_{\mu\nu}\sum_{lm} c_{\mu i}^{\dagger} c_{\nu a} \varepsilon_{klm} \left(\int \mathrm{d}^3 r\, \chi_\mu^* r_l \nabla_m \frac{e\tilde{\omega}}{2}\chi_\nu \right. \\
&\qquad \left. + \int \mathrm{d}^3 r\, \chi_\mu^* \frac{e\tilde{\omega}}{2} r_l \nabla_m \chi_\nu \right) \\
&= -\frac{\hbar}{\mathrm{i}} \sum_{\mu\nu}\sum_{lm} c_{\mu i}^{\dagger} c_{\nu a} \varepsilon_{klm} \left(\int \mathrm{d}^3 r\, \chi_\nu \frac{e\tilde{\omega}}{2} \nabla_m r_l \chi_\mu^* \right. \\
&\qquad \left. - \int \mathrm{d}^3 r\, \chi_\mu^* \frac{e\tilde{\omega}}{2} r_l \nabla_m \chi_\nu \right) \\
&= -\frac{\hbar}{\mathrm{i}} \sum_{\mu\nu}\sum_{lm} c_{\mu i}^{\dagger} c_{\nu a} \varepsilon_{klm} \left(\int \mathrm{d}^3 r\, \chi_\nu \frac{e\tilde{\omega}}{2} r_l \nabla_m \chi_\mu^* \right. \\
&\qquad \left. - \int \mathrm{d}^3 r\, \chi_\mu^* \frac{e\tilde{\omega}}{2} r_l \nabla_m \chi_\nu \right),
\end{aligned}
\tag{5.129}
$$

Using the fact that the AO basis consists of real (Gaussian) functions, Eq. 5.129 can be recast as:

$$
\begin{aligned}
\left\langle i|h_{\mathrm{p},k}^{(100)}|a\right\rangle &= \frac{e}{2} \sum_{\mu\nu} c_{\mu i}^{\dagger} c_{\nu a} \left(\langle \chi_\mu | \tilde{\omega}\, (\vec{r}\times\vec{p})_k |\chi_\nu \rangle \right. \\
&\qquad \left. - \langle \chi_\nu | \tilde{\omega}\, (\vec{r}\times\vec{p})_k |\chi_\mu \rangle \right).
\end{aligned}
\tag{5.130}
$$

Similarly, the remaining operators are calculated as:

$$
\begin{aligned}
\left\langle i|h_{\mathrm{so},k}^{(100)}|a\right\rangle &= \frac{e\hbar}{2} \sum_{\mu\nu} \left(c_{\mu i}^{\dagger} \vec{\sigma} c_{\nu a} \cdot (\langle \chi_\mu | \tilde{\omega}\vec{r}\nabla_k|\chi_\nu\rangle \right. \\
&\qquad + \langle \chi_\nu | \tilde{\omega}\vec{r}\nabla_k|\chi_\mu\rangle) - c_{\mu i}^{\dagger} \sigma_k c_{\nu a} \left(\left\langle \chi_\mu | \tilde{\omega}\vec{r}\cdot\vec{\nabla}|\chi_\nu \right\rangle \right. \\
&\qquad \left.\left. + \left\langle \chi_\nu | \tilde{\omega}\vec{r}\cdot\vec{\nabla}|\chi_\mu \right\rangle \right) \right),
\end{aligned}
\tag{5.131}
$$

$$
\begin{aligned}
\left\langle i|h_{\mathrm{p},t}^{(011)}|a\right\rangle &= \frac{G_{\mathrm{F}}}{2\sqrt{2}} \frac{\kappa_Q}{c\hbar\gamma_Q} \sum_{\mu\nu} c_{\mu i}^{\dagger} c_{\nu a} \left(\langle \chi_\mu | \tilde{\omega}\rho_Q p_t|\chi_\nu\rangle \right. \\
&\qquad \left. - \langle \chi_\nu | \tilde{\omega}\rho_Q p_t|\chi_\mu\rangle \right),
\end{aligned}
\tag{5.132}
$$

$$
\begin{aligned}
\left\langle i|h_{\mathrm{so},t}^{(011)}|a\right\rangle &= \frac{-\mathrm{i}G_{\mathrm{F}}}{2\sqrt{2}} \frac{\kappa_Q}{c\hbar\gamma_Q} \sum_{\mu\nu}\sum_{lm} \varepsilon_{tlm} c_{\mu i}^{\dagger} \sigma_l c_{\nu a} \\
&\qquad \times (\langle \chi_\mu | \tilde{\omega}\rho_Q p_m|\chi_\nu\rangle + \langle \chi_\nu | \tilde{\omega}\rho_Q p_m|\chi_\mu\rangle),
\end{aligned}
\tag{5.133}
$$

$$
\left\langle i|h_{\mathrm{d},kt}^{(111)}|a\right\rangle = -\frac{G_{\mathrm{F}}}{2\sqrt{2}} \frac{e\kappa_Q}{c\hbar\gamma_Q} \sum_{\mu\nu}\sum_{l} c_{\mu i}^{\dagger} c_{\nu a} \varepsilon_{ktl} \langle \chi_\mu | \tilde{\omega}\rho_Q r_l|\chi_\nu\rangle .
\tag{5.134}
$$

Calculation of operator matrix elements in the AO basis is performed fully numerically for PV operators. For integrals involving operators $h_{\mathrm{p},k}^{(100)}$ and $h_{\mathrm{so},k}^{(100)}$, $\tilde{\omega}$ of Eq. 4.18 is separated into a nonrelativistic part and a relativistic correction:

$$\tilde{\omega} = \frac{1}{2m_{\mathrm{e}}} \left(1 + \frac{\widetilde{V}}{2m_{\mathrm{e}}c^2 - \widetilde{\widetilde{V}}} \right). \tag{5.135}$$

The nonrelativistic contribution to the integrals is evaluated analytically and added to the numerically computed relativistic part.

5.6 Summary and conclusions

In this chapter, the calculation of molecular properties within the ZORA approach was discussed. Starting from a definition of such properties in terms of energy derivatives, a second quantization expression for the ZORA total energy was construed in Section 5.1 as a starting point for the calculation of derivatives. For properties of up to third order based on variational wavefunctions, linear response equations have to be solved (at the most), which were discussed in Section 5.3. Particular attention was paid to the possibility of exploiting symmetries of the Hamiltonian and perturbations in order to reduce the dimension of the problem, and it can be seen for example from Eq. 5.86 that a reduction by a factor four can be achieved in stationary closed–shell systems when Hermiticity and time–reversal symmetry of perturbing operators are exploited.

Time–reversal symmetry was also used in the derivation of an explicit expression for the PV NMR shielding tensor in Section 5.5. In the case of spin– and current–independent non–hybrid density functionals the coupled–perturbed Eqs. 5.94 become uncoupled because of the time–reversal–odd character of magnetic perturbations, leading to a simple sum–over–states expression for the shielding tensor, Eq. 5.110. This expression was implemented in the TURBOMOLE program package during the course of this thesis using the perturbing operators derived in Section 5.5.2, the matrix elements of which are computed as illustrated in Section 5.5.4.

The shielding tensor of Eqs. 5.110 or 5.125 forms the basis of calculations presented in Chapters. 6 and 7. For calculations of Chapter 7 it has been used also in connection with hybrid functionals, meaning that a coupling of the response equations introduced by Fock exchange has been neglected. This practice is occasionally used in nonrelativistic calculations, where the enhancement of spin polarization through the introduction of exact exchange is sometimes considered to be more of an artifact of the approach rather than a physical phenomenon.

The approach to the calculation of energy derivatives as it is discussed in the beginning of this chapter is rather general and can quite easily be extended to a variety of molecular properties. On the other hand, the expression for the PV NMR shielding tensor derived in Section 5.5 (Eq. 5.110) is highly specific and only valid for a limited class of density functionals. In this form, computational cost is minimal, but the choice of systems that can be treated is limited. The electronic structure of some of the transition metal complexes of Chapter 7, for example, can not be described well by non–hybrid density functionals, and in order to investigate them thoroughly, it will be necessary to implement the coupled–perturbed Eqs. 5.94 also. Another weakness of the approach is gauge dependence, stemming from the use of finite basis set expansions, which can be alleviated by employing a number of different methods, as mentioned in Section 5.5.1. The use of such methods would reduce the size of the basis set needed to achieve approximate gauge origin independence and they would therefore be particularly useful in calculations for some of the relatively large molecules of Chapter 7.

In the upcoming chapter, systematic effects of PV NMR frequencies such as scaling with nuclear charge and conformational dependence are studied for the series of dihydrogen dichalcogenides. These molecules are often used in order to compare different approaches to the calculation of PV properties and were also selected here for this purpose.

Chapter 6

Systematic effects in DFT parity violating NMR parameters

In this chapter, scaling with nuclear charge and conformational effects on DFT PV NMR parameters are investigated for the series of dihydrogen dichalcogenides (H_2X_2 with X=^{17}O, ^{33}S, ^{77}Se, ^{125}Te, ^{209}Po). In addition, basis set convergence and dependence on the density functional are discussed. It is shown that while early estimates [6] of the scaling with nuclear charge Z of different contributions to the PV NMR frequency splitting are essentially correct, conformational effects can be of similar importance. For the dihydrogen dichalcogenides, the typical $\sin(2\alpha)$–dependence of PV properties on the dihedral angle in these molecules could be reproduced for PV NMR frequency shifts.

This particular series of molecules was chosen because it or, in the case of nonrelativistic calculations, at least the subseries of its three lightest members has often been studied theoretically with respect to PV properties (see for example Refs. [27, 58, 66, 68, 156, 248–251]). It is thus well suited as a trial set for new approaches to the calculation of such effects. The content of this chapter is based on results presented in Ref. [57] where it was used to appraise the newly developed computational approach presented there and in Chapter 5 of this thesis.

As has been discussed before [66, 68, 156] the molecules appear unsuited for an actual measurement of PV effects but calculations may still indicate the order of magnitude of PV NMR frequency splittings for nuclei of similar charge as the respective chalcogens. For certain conformations of H_2Po_2 a PV NMR frequency splitting of 10 mHz between the two mirror image structures inside a magnetic field of 11.7 T was predicted. This indicates that according to the estimates in Ref. [56] PV effects would in principle be observable in NMR spectra of chiral molecules containing row 6 elements.

6.1   Conformational dependence

In Table 6.1 parity violating NMR frequency splittings $\Delta\nu^{\mathrm{PV}}(X)$ calculated for C_2–
symmetric conformations of the dihydrogen dichalcogenides as a function of the dihedral
angle α are reported (Figure 6.1 shows the basic structure of a dihydrogen dichalcogenide
at a dihedral angle of $120°$). Calculations were performed using the ZORA DFT ap-
proach to molecular parity violation presented in Chapter 5. Computational details,
such as structural parameters and basis sets are given in Appendix B.2.1, parameters of
model densities used in the determination of the ZORA factor $\tilde{\omega}$ of Eq. B.1 are listed in
Appendix B.1. In addition to the total two–component ZORA values, contributions due
to the paramagnetic and spin–orbit coupling terms of Eqs. 5.127 and 5.128, respectively,
are also given. For comparison with Refs. [66, 251] nonrelativistic limits of the ZORA
NMR frequency splittings are reported.
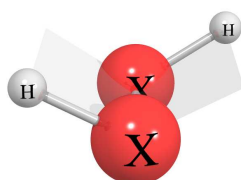
Figure 6.1: Illustration of the dihedral angle (the angle between the two planes indicated
in the figure) in C_2–symmetric dihydrogen dichalcogenides, i.e. X=O, S, Se, Te or Po.

For all compounds in this chapter the typical $\sin(2\alpha)$–like dependence on the dihedral
angle α is observed for the parity violating property, which vanishes for the achiral con-
formations with $\alpha = 0$ and $\alpha = 180$. This also holds true for the individual contributions
to the NMR frequency splittings. The H_2X_2 frequency splittings $\Delta\nu^{\mathrm{PV}}$ for X=^{33}S, ^{77}Se,
^{125}Te, ^{209}Po and individual contributions are plotted in Figure 6.2 as a function of the
dihedral angle α.

6.2   Significance of individual contributions

The paramagnetic and spin–orbit coupling contributions are generally of opposite sign
for all compounds studied herein. While the absolute value of the paramagnetic con-
tribution is larger than the nonrelativistic value, the spin–orbit contribution induces a
frequency shift in the opposite direction and can lead to a reduction of the absolute
value of the relativistic PV frequency splittings compared to the nonrelativistic values,
e.g. in H_2Se_2 and some conformations of H_2O_2. For H_2O_2 and H_2Se_2 the nonrelativistic
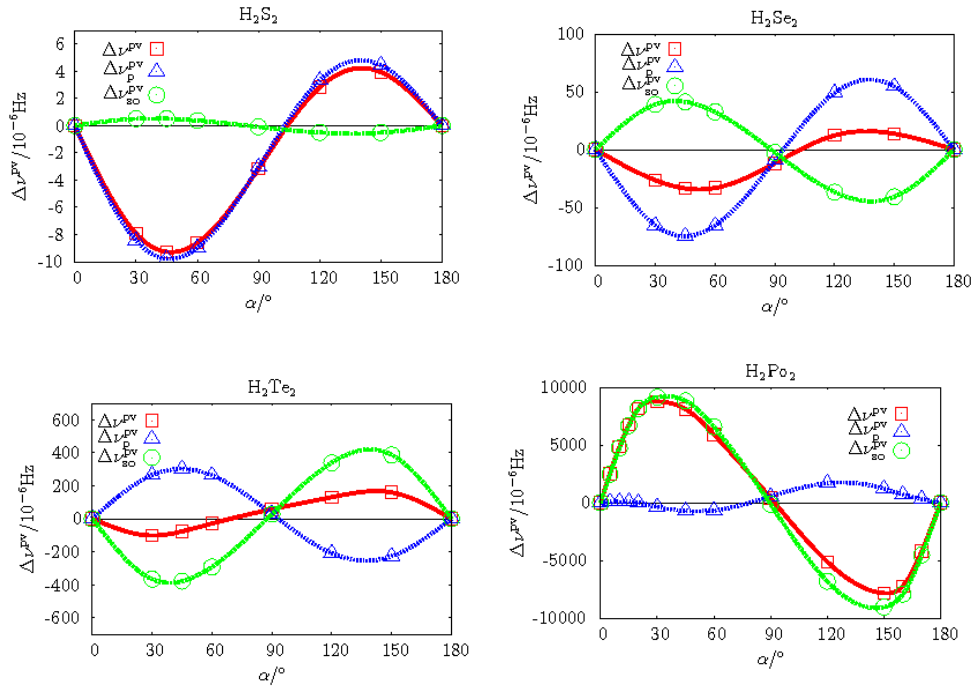
Figure 6.2: Dihedral angle dependence of the X=^{33}S, ^{77}Se, ^{125}Te, ^{209}Po PV NMR frequency splitting and its individual contributions in H_2X_2, calculated with the BLYP functional (containing Becke's gradient correction [252] and the Lee–Yang–Parr correlation contribution [253]). Basis sets are listed in Table B.7 except for H_2Po_2 where the basis set used was 1–25:2–26:12–25:15–22 in the nomenclature of Table B.7. The NMR frequencies were calculated for a magnetic flux density of $B = 11.7$ T. $\Delta\nu^{pv}$ denotes the full two–component ZORA NMR frequency splitting related to the isotropic part of the NMR shielding tensor of Eq. 5.125. $\Delta\nu_p^{pv}$ and $\Delta\nu_{so}^{pv}$ are related to the paramagnetic and spin–orbit coupling contributions to the isotropic part of the NMR shielding tensor (Eqs. 5.127 and 5.128, respectively).

absolute values are thus usually too high, whereas for H_2S_2 the absolute value of the nonrelativistic frequency shift is always smaller than the corresponding ZORA value.

For H_2O_2 and H_2S_2 the paramagnetic contribution to the frequency splitting is usually dominant and spin–orbit coupling effects lie between 1% and 6% except for H_2S_2 at dihedral angles 120° and 150° where spin–orbit coupling effects make up 18% and 13% of the total frequency splitting, respectively. In H_2Se_2 spin–orbit coupling already leads to a significant reduction of the magnitude of the frequency splittings and in H_2Te_2 the paramagnetic and spin–orbit coupling contributions almost cancel each other out. In H_2Po_2 the spin–orbit coupling contribution is dominant with respect to the paramagnetic one.

The results are consistent with previous nonrelativistic calculations of parity violating NMR parameters [66, 158] within the numerical errors of the computations. An additional difference between the nonrelativistic results for H_2O_2 presented here and those

Table 6.1: NMR frequency splitting between the $P-$ and $M-$conformations ($\Delta\nu = \nu^P - \nu^M$) of H_2X_2 for X=^{17}O, ^{33}S, ^{77}Se, ^{125}Te, ^{209}Po due to the isotropic parity violating NMR shielding constant; calculated with the BLYP functional as a function of the dihedral angle. The basis sets used for the heavy atoms are listed in Table B.7. The NMR frequencies were calculated for a magnetic flux density of $B = 11.7$ T and are given here in 10^{-6} Hz. $\Delta\nu^{\mathrm{PV}}$ is the full two–component ZORA NMR frequency splitting related to the isotropic part of the NMR shielding tensor of Eq. 5.125. $\Delta\nu_{\mathrm{p}}^{\mathrm{PV}}$ and $\Delta\nu_{\mathrm{so}}^{\mathrm{PV}}$ are related to the paramagnetic and spin–orbit coupling contributions to the isotropic part of the NMR shielding tensor (Eqs. 5.127 and 5.128, respectively). $\Delta\nu_{\mathrm{nr}}^{\mathrm{PV}}$ denotes the nonrelativistic limit of $\Delta\nu^{\mathrm{PV}}$. Results are given with three significant figures for $\Delta\nu^{\mathrm{PV}}$ and $\Delta\nu_{\mathrm{nr}}^{\mathrm{PV}}$, the individual contributions to $\Delta\nu^{\mathrm{PV}}$ were rounded to the same accuracy as $\Delta\nu^{\mathrm{PV}}$.

$\Delta\nu^{\mathrm{PV}}$ (X)	30°	45°	60°	90°	120°	150°
			H_2O_2			
$\Delta\nu^{\mathrm{PV}}$ (^{17}O)	0.826	0.906	0.711	−0.231	−1.10	−1.04
$\Delta\nu_{\mathrm{p}}^{\mathrm{PV}}$ (^{17}O)	0.868	0.954	0.751	−0.230	−1.14	−1.08
$\Delta\nu_{\mathrm{so}}^{\mathrm{PV}}$ (^{17}O)	−0.042	−0.048	−0.040	−0.002	0.04	0.04
$\Delta\nu_{\mathrm{nr}}^{\mathrm{PV}}$ (^{17}O)	0.850	0.935	0.740	−0.213	−1.10	−1.04
$\Delta\nu_{\mathrm{nr}}^{\mathrm{PVa)}}$ (^{17}O)	0.865	0.952	0.754	−0.216	−1.12	−1.06
$\Delta\nu_{\mathrm{nr}}^{\mathrm{PVb)}}$ (^{17}O)	0.8677	0.9568	0.7595	−0.2129	−1.121	−1.066
			H_2S_2			
$\Delta\nu^{\mathrm{PV}}$ (^{33}S)	−7.94	−9.28	−8.61	−3.15	2.82	3.93
$\Delta\nu_{\mathrm{p}}^{\mathrm{PV}}$ (^{33}S)	−8.44	−9.78	−8.99	−3.06	3.32	4.44
$\Delta\nu_{\mathrm{so}}^{\mathrm{PV}}$ (^{33}S)	0.50	0.51	0.37	−0.09	−0.51	−0.51
$\Delta\nu_{\mathrm{nr}}^{\mathrm{PV}}$ (^{33}S)	−7.61	−8.84	−8.15	−2.90	2.77	3.83
			H_2Se_2			
$\Delta\nu^{\mathrm{PV}}$ (^{77}Se)	−26.4	−33.6	−33.2	−11.9	12.3	13.7
$\Delta\nu_{\mathrm{p}}^{\mathrm{PV}}$ (^{77}Se)	−65.5	−74.9	−65.7	−9.4	49.0	54.6
$\Delta\nu_{\mathrm{so}}^{\mathrm{PV}}$ (^{77}Se)	39.1	41.3	32.6	−2.5	−36.7	−40.9
$\Delta\nu_{\mathrm{nr}}^{\mathrm{PV}}$ (^{77}Se)	−42.3	−48.7	−43.4	−8.96	27.3	31.9
			H_2Te_2			
$\Delta\nu^{\mathrm{PV}}$ (^{125}Te)	−102	−76.8	−29.1	57.5	130	160
$\Delta\nu_{\mathrm{p}}^{\mathrm{PV}}$ (^{125}Te)	265	302.0	262.8	29.4	−209	−228
$\Delta\nu_{\mathrm{so}}^{\mathrm{PV}}$ (^{125}Te)	−367	−378.8	−291.9	28.0	339	387
			H_2Po_2			
$\Delta\nu^{\mathrm{PV}}$ (^{209}Po)	8.77×10^3	8.11×10^3	5.90×10^3	0.395×10^3	$−5.13 \times 10^3$	$−7.84 \times 10^3$
$\Delta\nu_{\mathrm{p}}^{\mathrm{PV}}$ (^{209}Po)	$−0.37 \times 10^3$	$−0.72 \times 10^3$	$−0.67 \times 10^3$	0.539×10^3	1.70×10^3	1.21×10^3
$\Delta\nu_{\mathrm{so}}^{\mathrm{PV}}$ (^{209}Po)	9.14×10^3	8.83×10^3	6.57×10^3	$−0.144 \times 10^3$	$−6.82 \times 10^3$	$−9.05 \times 10^3$

[a)] Basis set (1–25:2–26:20–24) of Ref. [66] on ^{17}O
[b)] Ref. [66]

of Ref. [66] is introduced by the use of a Gaussian nuclear density distribution as opposed to a delta distribution. Presumably, however, this difference is smaller than the numerical uncertainty of the calculation for the light nucleus in question.

6.3 Comparison with DHFC study

In comparison with the recent four–component Dirac–Hartree–Fock scheme [68] the same general trends are observed: Opposite signs of paramagnetic and spin–orbit coupling contributions and an initially similar scaling behavior. However, in Ref. [68] a rather erratic dependence of the parity violating polonium shieldings on the dihedral angle in H_2Po_2 was reported as well as a dramatic increase in the spin–orbit coupling contribution from H_2Te_2 to H_2Po_2 for which no support is found here. These effects that differ from present results were most likely caused by an instability of the Kramer's restricted four–component Dirac–Hartree–Fock wavefunctions of Ref. [68] with respect to time reversal odd perturbations [69]. Conclusions drawn concerning the strong scaling behavior should therefore be revoked.

As the dihedral angle dependence of the PV frequency splitting in H_2Po_2 is somewhat between $\sin(2\alpha)$ and sawtooth, some additional ten points in Table 6.2 have been computed. Although point group symmetry is not exploited in these calculations, the condition that the PV frequency splitting has to vanish for dihedral angles $0°$ and $180°$ is met to 5 orders magnitude compared to the finite values obtained for the other dihedral angles. However, for small dihedral angles the paramagnetic contribution to the frequency splitting, which is relatively small in magnitude, behaves somewhat erratic, switching from a positive value at dihedral angle $20°$ to negative at $15°$ and back to a positive value close to zero at $0°$. This might be an indication for a more complicated electronic structure of H_2Po_2 compared to that of the lighter homologues and underlines the need to apply systematically improvable electronic structure methods for the accurate prediction of nuclear PV effects in H_2Po_2, in future.

6.4 Comparison of different density functionals

In Table 6.3, PV NMR frequency splittings obtained with the local density approximation (LDA) functional [254–256] are compared to those obtained with the gradient corrected functional BLYP for a dihedral angle of $\alpha = 45°$. According to the table, the BLYP functional consistently yields nonrelativistic and paramagnetic frequency splittings that are larger than the LDA values by 2% to 15%, except for H_2Po_2 where there

Table 6.2: NMR frequency splitting between the $P-$ and $M-$conformations ($\Delta\nu = \nu^P - \nu^M$) of H_2Po_2 due to the isotropic PV ^{209}Po NMR shielding constant; calculated with the BLYP functional for varying dihedral angles α. The basis set used on ^{209}Po is 1–25:2–26:12–25:15–22 in the nomenclature of Table B.7. NMR frequencies were calculated for a magnetic flux density of $B = 11.7$ T and are given here in 10^{-3} Hz. $\Delta\nu^{PV}$ is the full two–component ZORA NMR frequency splitting related to the isotropic part of the NMR shielding tensor of Eq. 5.125. $\Delta\nu_p^{PV}$ and $\Delta\nu_{so}^{PV}$ are related to the paramagnetic and spin–orbit coupling contributions to the isotropic part of the NMR shielding tensor (Eqs. 5.127 and 5.128, respectively). Results are given with three significant figures for $\Delta\nu^{PV}$, the individual contributions were rounded to the same accuracy. For dihedral angles of $0°$ and $180°$ $\Delta\nu^{PV}$ must be zero for symmetry reasons. Although point group symmetry was not used explicitly in the calculations, this condition is fulfilled numerically to five orders of magnitude compared to the finite values of $\Delta\nu^{PV}$ calculated for other dihedral angles.

$\alpha/°$	$\Delta\nu^{PV}$	$\Delta\nu_p^{PV}$	$\Delta\nu_{so}^{PV}$
0	-0.00_{001}	-0.00_{002}	0.00_{0001}
5	2.52	0.06	2.46
10	4.83	0.09	4.74
15	6.73	0.07	6.66
20	8.15	-0.00	8.16
30	9.50	-0.27	9.76
45	8.74	-0.63	9.36
60	6.34	-0.60	6.94
90	0.421	0.565	-0.144
120	-5.53	1.66	-7.19
140	-8.37	1.49	-9.86
150	-8.54	1.13	-9.67
160	-7.23	0.70	-7.93
170	-4.22	0.32	-4.53
180	0.00_{0003}	0.00_{0001}	0.00_{0001}

is an almost four–fold increase from LDA to BLYP for the paramagnetic shielding (this is analyzed in more detail below). The absolute values of the spin–orbit coupling contributions to the PV NMR frequency splittings obtained with the LDA functional are 4% to 10% bigger than the corresponding BLYP values for H_2O_2, H_2Se_2 and H_2Te_2, whereas they are approximately equal to the BLYP values for H_2S_2 and H_2Po_2.

For H_2Te_2 and H_2Po_2, PV NMR frequency splittings obtained with the local $X\alpha$ method [254, 257] are also listed. The $X\alpha$ values for the individual contributions to the frequency splittings in H_2Te_2 are 2% to 5% larger than those obtained with the LDA method and thus the deviation among the two local functionals is smaller than the deviation between

LDA/$X\alpha$ and the gradient corrected BLYP functional. For H_2Po_2 deviations between the local functionals are as big as the deviations between LDA and BLYP, for the spin–orbit coupling contribution even larger ($\approx 7\%$). Still, the parity violating NMR frequency splittings obtained with the $X\alpha$ method are bigger than those obtained with the LDA functional.

In Table 6.4 the dihedral angle dependences of the PV NMR frequency splittings obtained with the LDA and BLYP functionals for H_2Te_2 and H_2Po_2 are compared. For both compounds the absolute value of the LDA frequency splitting is larger than for the BLYP splittings (the only exception being H_2Te_2 at a dihedral angle of $90°$), which has been observed also for their parity violating energy differences [59]). Concerning individual contributions, the absolute value of the paramagnetic contribution is almost always bigger when computed with the BLYP functional, except for H_2Po_2 at $\alpha = 90°$, which is where the PV NMR frequency splitting changes sign. For H_2Te_2 the BLYP – LDA deviation in the paramagnetic contribution to the frequency splittings ranges from 10% to 15% for all dihedral angles except $90°$ and is therefore quite regular. The spin–orbit coupling contribution computed with the LDA functional is bigger by up to 5% when compared to the BLYP results for this compound. In contrast, for H_2Po_2 the deviations between the two functionals in the paramagnetic contributions are much larger, between 10% and 30% for the dihedral angles between $90°$ and $150°$ and increasing for smaller dihedral angles. For $\alpha = 30°$ the absolute value of the paramagnetic contribution to the frequency splitting from the LDA functional is almost seven times smaller than the corresponding BLYP value, with a change in sign. Contrarily, the differences between the spin–orbit coupling contributions computed with the BLYP and LDA functionals are quite small, always below 2%. For dihedral angles up to $60°$ and for $120°$ the absolute values of the BLYP results are bigger, while LDA gives a slightly larger value for a dihedral angle of $90°$ and the same as BLYP for $150°$. This particular sensitivity of the paramagnetic term in H_2Po_2 to a change of functional is another indication for a more complicated electronic structure of this molecular system.

Table 6.3: NMR frequency splitting between the $P-$ and $M-$conformations ($\Delta\nu = \nu^P - \nu^M$) of H_2X_2 for X=^{17}O, ^{33}S, ^{77}Se, ^{125}Te, ^{209}Po due to the isotropic parity violating NMR shielding constant, calculated with the BLYP and LDA functionals, and for H_2Te_2 and H_2Po_2 also with the $X\alpha$ functionals. The dihedral angle was $\alpha = 45°$, the basis sets used for ^{17}O, ^{33}S, ^{77}Se, and ^{125}Te are listed in Table B.7, the basis set used for ^{209}Po was 1–25:2–26:12–25:15–22 in the nomenclature of Table B.7. The NMR frequencies were calculated for a magnetic flux density of $B = 11.7$ T and are given here in 10^{-6} Hz. $\Delta\nu^{PV}$ is the full two–component ZORA NMR frequency splitting related to the isotropic part of the NMR shielding tensor of Eq. 5.125. $\Delta\nu_p^{PV}$ and $\Delta\nu_{so}^{PV}$ are related to the paramagnetic and spin–orbit coupling contributions to the isotropic part of the NMR shielding tensor (Eqs. 5.127 and 5.128, respectively) and $\Delta\nu_{nr}^{PV}$ denotes the nonrelativistic limit of $\Delta\nu^{PV}$, which was not computed (n. c.) with the LDA and $X\alpha$ functionals for H_2Te_2 and H_2Po_2. Results are given with three significant figures for $\Delta\nu^{PV}$ and $\Delta\nu_{nr}^{PV}$, the individual contributions to $\Delta\nu^{PV}$ were rounded to the same accuracy as $\Delta\nu^{PV}$.

Functional	$\Delta\nu^{PV}$	$\Delta\nu_p^{PV}$	$\Delta\nu_{so}^{PV}$	$\Delta\nu_{nr}^{PV}$
		H_2O_2		
BLYP	0.906	0.954	−0.048	0.935
LDA	0.881	0.930	−0.049	0.912
		H_2S_2		
BLYP	−9.28	−9.78	0.51	−8.84
LDA	−8.17	−8.68	0.51	−7.85
		H_2Se_2		
BLYP	−33.6	−74.9	41.3	−48.7
LDA	−25.2	−68.2	43.0	−44.4
		H_2Te_2		
BLYP	−76.8	302.0	−378.8	126
LDA	−127	267	−394	n. c.
$X\alpha$	−121	279	−400	n. c.
		H_2Po_2		
BLYP	8.74×10^3	-0.63×10^3	9.36×10^3	0.356×10^3
LDA	9.25×10^3	-0.16×10^3	9.41×10^3	n. c.
$X\alpha$	9.77×10^3	-0.29×10^3	10.10×10^3	n. c.

Table 6.4: NMR frequency splitting between the $P-$ and $M-$conformations ($\Delta\nu = \nu^P - \nu^M$) of $H_2\,^{125}Te_2$ and $H_2\,^{209}Po_2$ due to the isotropic PV NMR shielding constant, calculated with the BLYP and LDA functionals as a function of the dihedral angle. The basis sets used are listed in Table B.7. The NMR frequencies were calculated for a magnetic flux density of $B = 11.7$ T and are given here in 10^{-6} Hz. $\Delta\nu^{PV}$ is the full two–component ZORA NMR frequency splitting related to the isotropic part of the NMR shielding tensor of Eq. 5.125. $\Delta\nu_p^{PV}$ and $\Delta\nu_{so}^{PV}$ are related to the paramagnetic and spin–orbit coupling contributions to the isotropic part of the NMR shielding tensor (Eqs. 5.127 and 5.128, respectively). Results are given with three significant figures for $\Delta\nu^{PV}$, individual contributions were rounded to the same accuracy.

$\Delta\nu^{PV}(X)$	30°	45°	60°	90°	120°	150°
			H_2Te_2			
$\Delta\nu^{PV}\left(^{125}Te, BLYP\right)$	-102	-76.8	-29.1	57.5	130	160
$\Delta\nu^{PV}\left(^{125}Te, LDA\right)$	-149	-127	-69.3	55.9	167	206
$\Delta\nu_p^{PV}\left(^{125}Te, BLYP\right)$	265	302.0	262.8	29.4	-209	-228
$\Delta\nu_p^{PV}\left(^{125}Te, LDA\right)$	232	267	234.4	27.1	-186	-200
$\Delta\nu_{so}^{PV}\left(^{125}Te, BLYP\right)$	-367	-378.8	-291.9	28.0	339	387
$\Delta\nu_{so}^{PV}\left(^{125}Te, LDA\right)$	-382	-394	-303.7	28.8	353	406
			H_2Po_2			
$\Delta\nu^{PV}\left(^{209}Po, BLYP\right)$	8770	8110	5900	395	-5130	-7840
$\Delta\nu^{PV}\left(^{209}Po, LDA\right)$	9120	8510	6230	443	-5370	-8190
$\Delta\nu_p^{PV}\left(^{209}Po, BLYP\right)$	-370	-720	-670	539	1700	1210
$\Delta\nu_p^{PV}\left(^{209}Po, LDA\right)$	50	-270	-310	591	1440	860
$\Delta\nu_{so}^{PV}\left(^{209}Po, BLYP\right)$	9140	8830	6570	-144	-6820	-9050
$\Delta\nu_{so}^{PV}\left(^{209}Po, LDA\right)$	9070	8780	6540	-147	-6800	-9050

6.5   Basis set requirements

Table 6.5 lists PV NMR frequency splittings for all members of the dihydrogen dichalco-genide series at a dihedral angle of 45°, computed with the BLYP functional and different basis sets. For H_2O_2 a 2% decrease in the ZORA frequency splitting and the absolute values of the individual contributions is observed upon the addition of 5 polarizing f–functions to the even–tempered basis set. This supports previous findings within the nonrelativistic Hartree–Fock [66] and relativistic Dirac–Hartree–Fock [68] frameworks and underlines the importance of f–functions for reaching the basis set limit of this property in H_2O_2 when employing a common gauge origin. For H_2S_2, however, the same change in basis leads to an increase of 0.1% only, and the addition of further 6 d–functions increases the result by 0.5% more.

An addition of 5 f–functions to the even–tempered basis for H_2Se_2 leads to a 3% to 10% decrease of the absolute values of the individual contributions and to a 6% increase in the total PV NMR frequency splitting, due to a reduced cancellation of the paramagnetic and spin–orbit coupling contributions. The addition of further 2 f–functions does not change the result within the numerical accuracy. In Ref. [68] a large decrease of the property upon the addition of the 5 f–functions was reported because DHFC theory predicts the paramagnetic and spin–orbit coupling contributions to be of almost the same magnitude for H_2Se_2, whereas in the BLYP treatment the paramagnetic contribution is estimated to be larger in magnitude by a factor 2 compared to the spin–orbit coupling contribution. In Ref. [68], however, it was also observed that additional f– or d–functions have a much smaller effect in comparison.

In H_2Te_2 the addition of 7 f–functions leads to a decrease of the absolute value of the frequency splitting by almost 50% due to a strong cancellation of the paramagnetic and the spin–orbit coupling contributions. The change in the individual contributions is only around 5%, but while the positive paramagnetic contribution decreases, the absolute value of the negative spin–orbit coupling contribution decreases slightly stronger. This leads to a pronounced cancellation of the two contributions and causes the dramatic decrease in the total frequency splitting. It is evident, that the addition of f–functions to the even–tempered basis is of paramount importance in this case.

For H_2Po_2, it is observed that the addition of the 2 additional f–functions leads to a decrease of the absolute value of the frequency splitting by almost 10%, again confirming the findings of the DHFC study reported in Ref. [68].

Table 6.5: NMR frequency splitting between the $P-$ and $M-$conformations ($\Delta\nu = \nu^P - \nu^M$) of H_2X_2 for X=^{17}O, ^{33}S, ^{77}Se, ^{125}Te, ^{209}Po due to the isotropic PV NMR shielding constant, calculated with the BLYP functional and different basis sets as indicated in the nomenclature of Table B.7. The dihedral angle was $\alpha = 45°$. The NMR frequencies were calculated for a magnetic flux density of $B = 11.7$ T and are given here in 10^{-6} Hz. $\Delta\nu^{PV}$ is the full two–component ZORA NMR frequency splitting related to the isotropic part of the shielding tensor of Eq. 5.125. $\Delta\nu_p^{PV}$ and $\Delta\nu_{so}^{PV}$ are related to the paramagnetic and spin–orbit coupling contributions to the isotropic part of the shielding tensor (Eqs. 5.127 and 5.128, respectively) Results are given with three significant figures for $\Delta\nu^{PV}$, the individual contributions were rounded to the same accuracy.

Basis set	$\Delta\nu^{PV}$	$\Delta\nu_p^{PV}$	$\Delta\nu_{so}^{PV}$
	H_2O_2		
1–25:2–26:20–24	0.922	0.971	−0.049
1–25:2–26.20–24:20–24	0.906	0.954	−0.048
	H_2S_2		
1–25:2–26:20–24	−9.23	−9.77	0.54
1–25:2–26.20–24:20–24	−9.24	−9.75	0.51
1–25:2–26.15–25:20–24	−9.28	−9.78	0.51
	H_2Se_2		
1–25:2–26:15–25	−31.7	−77.4	45.7
1–25:2–26:15–25:20–24	−33.6	−74.9	41.3
1–25:2–26:15–25:19–25	−33.6	−74.9	41.3
	H_2Te_2		
1–25:2–26:15–25	−124	312	−437
1–25:2–26:15–25:19–25	−76.8	302.0	−378.8
	H_2Po_2		
1–25:2–26:12–25:15–22	8.74×10^3	-0.63×10^3	9.36×10^3
1–25:2–26:12–25:15–24	8.11×10^3	-0.72×10^3	8.83×10^3

6.6   Scaling with nuclear charge Z

Table 6.6 and Figure 6.3 illustrate the scaling behavior of the different contributions to the PV NMR frequency splittings with respect to the nuclear charge of the heavy nucleus. For the three heaviest nuclei in the series, the paramagnetic and spin–orbit contributions scale with approximately Z^3 and Z^5, respectively. For sulphur, the scaling is $Z^{3.6}$ for the paramagnetic and $Z^{3.4}$ for the spin–orbit coupling contribution. Early order–of–magnitude estimates of PV magnetic properties arrive at scaling laws of Z^2 for the paramagnetic and Z^4 for the spin–orbit contribution [6] but they did not include a possible relativistic enhancement explicitly.
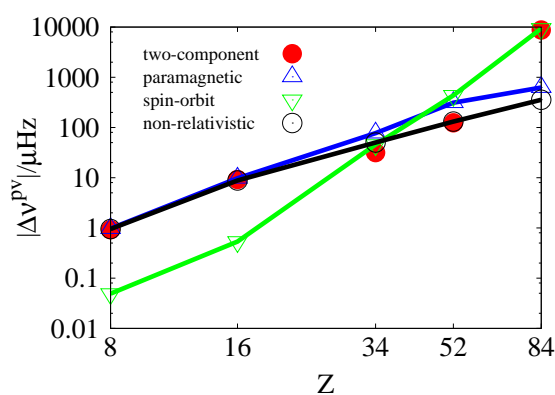
Figure 6.3: Scaling of PV NMR frequency splittings with nuclear charge for the series H_2X_2 at a dihedral angle of $45°$ and with $X=^{17}O$, ^{33}S, ^{77}Se, ^{125}Te, ^{209}Po.

Comparing the results presented in Table 6.6 to the scaling behavior observed within the DHFC scheme of Ref. [68], a similar scaling of the scalar–relativistic contribution $(|\Delta\nu_p^{PV} - \Delta\nu_{nr}^{PV}|)$ is obtained, on the DFT level, for all compounds under investigation except for H_2Po_2.

A perhaps remarkable point, however, is that in the DHFC as well as this ZORA study the scaling of the spin–orbit coupling contribution in H_2S_2 is lower than for the heavier dihydrogen dichalcogenides. The absolute value of the total ZORA PV NMR frequency splittings scale with $Z^{3.6}$ for H_2S_2, with $Z^{2.5}$ for H_2Se_2, with $Z^{2.4}$ for H_2Te_2 and with $Z^{3.9}$ for H_2Po_2, supporting the $Z^{3\pm1}$ scaling inferred in Ref. [156].

It should be noted, that all values of PV NMR frequency splittings reported herein are effective for a value of the nuclear state dependent parameter λ_A of Eq. 4.1 fixed to minus one. In order to make a prediction for the size of experimentally observable frequency splittings, results have to be scaled with the negative of the actual value of λ_A which, in the case of heavy nuclei, is estimated to be of the order of 1 to 10 [13, 91].

Table 6.6: Scaling with nuclear charge Z of the absolute values of different contributions to the NMR frequency splitting between the $P-$ and $M-$conformations ($\Delta\nu = \nu^P - \nu^M$) of H_2X_2 for X=^{17}O, ^{33}S, ^{77}Se, ^{125}Te, ^{209}Po due to the isotropic PV NMR shielding constant. NMR frequency splittings were calculated with the BLYP functional and the dihedral angle was $\alpha = 45°$. Basis sets used are listed in Table B.7. The NMR frequencies were calculated for a magnetic flux density of $B = 11.7$ T and are given here in 10^{-6} Hz. $\Delta\nu^{PV}$ is the full two–component ZORA NMR frequency splitting related to the isotropic part of the shielding tensor of Eq. 5.125. $\Delta\nu_p^{PV}$ and $\Delta\nu_{so}^{PV}$ are related to the paramagnetic and spin–orbit coupling contributions to the isotropic part of the shielding tensor (Eqs. 5.127 and 5.128, respectively) . $|\Delta\nu_{pc}^{PV}| = |\Delta\nu_p^{PV} - \Delta\nu_{nr}^{PV}|$ is the magnitude of the scalar–relativistic correction to the nonrelativistic frequency splittings. Results are given with three significant figures for $\Delta\nu^{PV}$ and $\Delta\nu_{nr}^{PV}$, the individual contributions to $\Delta\nu^{PV}$ were rounded to the same accuracy as $\Delta\nu^{PV}$. The exponents x of the scaling factors Z^x are given in parenthesis behind the various frequency contributions.

Z	$\Delta\nu^{PV}$		$\Delta\nu_p^{PV}$		$\Delta\nu_{so}^{PV}$		$\Delta\nu_{nr}^{PV}$		$|\Delta\nu_{pc}^{PV}|$	
8	0.906		0.954		−0.048		0.935		0.019	
16	−9.28	(3.6)	−9.78	(3.6)	0.51	(3.4)	−8.84	(3.2)	−0.94	(5.6)
34	−33.6	(2.5)	−74.9	(3.0)	41.3	(4.7)	−48.7	(2.7)	−26.1	(5.0)
52	−76.8	(2.4)	302.0	(3.1)	−378.8	(4.8)	126	(2.6)	176	(4.9)
84	8110	(3.9)	−716	(2.8)	8830	(5.2)	−352	(2.5)	−364	(4.1)

6.7   Quality assessment of the calculations

As for the quality of the calculations presented here, the following limitations have to be noted: In Ref. [66] it has been shown that density functional theory gives the correct order of magnitude for nonrelativistic PV NMR frequency splittings in H_2O_2, H_2S_2 and H_2Se_2 when compared to coupled–cluster singles and doubles (CCSD) values. It turned out to be unreliable, however, in producing the correct correlation contributions to these parity violating NMR properties. In Ref. [66] BLYP DFT calculations of PV NMR shielding tensors in H_2O_2, H_2S_2 and H_2Se_2 yield a correlation correction of about 20% with the wrong sign when compared to the CCSD values. In this nonrelativistic study, the magnitude of the PV NMR shielding tensor is always too large in the BLYP DFT calculations, for H_2Se_2 the BLYP shieldings were shown to be up to 50% bigger than the CCSD results. One can conclude that for this property DFT calculations are not necessarily preferable to Hartree–Fock calculations [66]. In the case of H_2Po_2, however, it should be kept in mind that the four–component, Kramer's–restricted DHFC results for $\Delta\nu^{PV}$ are unreliable, most likely due to an instability of the DHFC wavefunction.

The rather limited performance of DFT for this property has also been confirmed in Ref. [251] for the type of density functional used herein. The authors of Ref. [251] claim however, that hybrid DFT functionals can produce results which are in general much closer to the CCSD values than those obtained with pure density functionals or within a Hartree–Fock approach. While this apparently holds true for a limited range of structures, in general, the hybrid functionals employed in Ref. [251] also fail to give the correct sign for the correlation correction at dihedral angles below $90°$, which supports conclusions drawn in Ref. [66] with respect to the general performance of DFT for this property.

Within the DFT framework, accuracy is further limited by the necessity of numerical integration of atomic orbital matrix elements due to the ZORA factor $\tilde{\omega}$ (Eq. 4.18) and the use of the model potential $\widetilde{V}$ therein. This however is expected to cause minor deviations only. Additionally, the functionals employed do not depend on the current density or the spin density. If these restrictions are to be relaxed or if one intends to extend the range of methods to employ hybrid functionals which include some fraction of Hartree–Fock exchange, it will be necessary to implement linear response equations in their two–component form.

Furthermore, contributions arising from the nuclear spin independent parity violating Hamiltonian have been neglected. While these were estimated to be of minor importance [6], this is still to be confirmed in explicit numerical studies.

6.8   Conclusions

The method developed in Chapter 5.5 for the calculation of PV NMR frequency splittings has been tested for the chalcogen nuclei in C_2–symmetric dihydrogen dichalcogens, a series of molecules which is often used in the investigation of the systematics of PV effects [68, 153, 156, 159, 248–250]. Different contributions to the PV NMR shielding tensors have been calculated separately and were grouped into a paramagnetic and a spin–orbit contribution. It was found, that while the paramagnetic contribution to the parity violating frequency splittings has a scaling behavior of roughly Z^3, the spin–orbit contribution (of opposite sign) scales approximately with Z^5 for the three heaviest nuclei in the series and with Z^3 for sulphur. While relativistic effects can essentially be neglected for H_2O_2 and are within a 5% to 10% range for H_2S_2, they are already pronounced in H_2Se_2 and lead to a sign difference between the relativistic and nonrelativistic frequency splittings in H_2Te_2, when spin–orbit coupling effects become dominant. For H_2Po_2 scalar–relativistic effects are of the order of 5% compared to the spin–orbit coupling contribution.

An even more pronounced dependence of the spin–orbit coupling contribution on nuclear charge was claimed in Ref. [68] on the basis of four–component DHFC calculations. In contrast to [68], where a rather erratic dihedral angle dependence was reported for H_2Po_2, the typical $\sin(2\alpha)$–like behavior of σ^{PV} was found here for all dihydrogen dichalcogenides H_2X_2 as well as an overall Z^5 scaling of the spin–orbit coupling contribution. In total, the tentative scaling law $\sigma^{PV} \propto Z^{3\pm1}$ that was proposed in Ref. [156] is confirmed here for the H_2X_2 series. The unexpected scaling behavior reported in Ref. [68] for H_2Po_2 is most likely caused by an instability of the Kramer's restricted four–component DHFC wavefunction. Whereas such instabilities in H_2Po_2 are absent in the present DFT approach, the irregular dihedral angle dependence of the small paramagnetic contribution to $\Delta\nu^{PV}$ in H_2Po_2 may indicate the need for systematically improvable electronic structure methods in order to arrive at a sufficiently accurate estimate for this property in H_2Po_2.

Chapter 7

Towards an observation of PV NMR effects in chiral molecules

In this chapter the possibility of detecting molecular parity violation by means of NMR spectroscopy is addressed. The ZORA formalism for molecular parity violation introduced in Chapters 4 and 5 has been used extensively in the screening of possible experimental compounds containing heavy, NMR active nuclei, and some promising specimens are presented here. Thus, the main focus of this chapter is on the theoretical screening of candidate compounds, but experimental requirements and systematic effects relevant to the rational design of such compounds will also be discussed.

7.1   Motivation

The measurement of molecular parity violation through NMR spectroscopy seems particularly attractive, because the dominant contribution to these effects presumably stems from the nuclear spin–dependent part of the parity violating Hamiltonian, which only plays a minor role in other experimental schemes, involving for example the shifts in vibrational frequencies of chiral molecules discussed in Chapter 8. While effects of the nuclear spin–independent parity violating operator have been documented in several atomic systems (see the discussion in Chapter 2.1), a measurement of the effect of the nuclear spin–dependent PV operator and therefore the nuclear anapole moment has succeeded only once in cesium atoms.[39] An observation of PV effects in NMR spectroscopy would thus have direct consequences for the understanding of PV interactions inside the atomic nucleus.

From an experimental point of view the possibility of detecting these NMR shifts was addressed in an article by Robert and Barra [56]. The authors discussed the requirements for achieving a resolution of approximately 10 mHz in a high resolution ^{1}H 600 MHz NMR spectrometer and concluded that such a resolution was attainable with the commercially available technology and would allow for the detection of parity violating NMR frequency splittings larger than 6 mHz. The discussion in Chapter 6 supports the hypothesis that frequency splittings of this size can be found in some compounds containing heavy nuclei, which makes NMR spectroscopy a serious contestant for a first ever detection of parity violation in chiral molecules.

As a first step towards detecting molecular PV by means of NMR spectroscopy of chiral molecules, it is necessary to identify suitable candidate compounds, to synthesize them and then perform NMR measurements, the initial goal of which would probably be to set an upper bound for the tiny nuclear spin–dependent parity violating effect. Ultimately a parity violating difference in the resonance frequencies of two enantiomers might be detected, but since a measurement of this kind has apparently never been attempted before and the required experimental resolution is right at the limit of the currently possible, it will be a challenging task to understand all systematic effects and optimize the experimental technique. A successful measurement, however, could be the first measurement of parity violation in molecules and would have far reaching consequences for the understanding of molecular chirality and possibly also the weak interaction itself.

7.2   Experimental requirements[1]

In order to achieve the necessary resolution to be able to detect the PV frequency shifts in NMR spectra of chiral molecules, several requirements have to be met, which were discussed in Ref. [56]. The full width at half maximum of spectral lines is inversely proportional to the (transversal) spin–spin relaxation time T_2, and for a resolution of 10 mHz spin–spin relaxation times of more than 30 seconds have to be sought out. Different relaxation mechanisms contribute to T_2: dipolar coupling, quadrupolar, paramagnetic, scalar coupling[2], chemical shift anisotropy and spin–rotational. All of these mechanisms except for scalar coupling depend on the gyromagnetic ratios of the nuclei involved. Inhomogeneities of the applied magnetic field can lead to additional line broadening.

---

[1]Comments on this section by C. Thiele are gratefully acknowledged.

[2]The term "scalar coupling" is used here in accordance with tradition to refer to the indirect coupling of nuclear spins mediated by electrons between them. It can be considered misleading, however, in the sense that it does not refer to a scalar but a second order tensor quantity.

Of the different relaxation mechanisms, quadrupolar relaxation (the coupling of the nuclear quadrupole moment and electric field gradients) is often dominant for nuclei with spins $I > 1/2$, especially in an asymmetrical molecular environment.[258] Spin $1/2$ nuclei have a quadrupole moment of zero and usually relatively long relaxation times, so that compounds containing heavy, spin $1/2$ nuclei are preferred experimental candidates for a PV NMR experiment. Compounds with a molecular weight greater than 150 atomic mass units also have the added advantage that spin–rotational effects can be neglected.[56] Paramagnetic relaxation can lead to very short relaxation times in molecules with unpaired electron spins and is usually negligible in closed shell compounds. Open shell molecules are therefore excluded a priori from the search for an experimentally viable candidate.

For spin $1/2$ nuclei in heavy, closed shell compounds the remaining relaxation mechanisms are dipolar and scalar coupling and chemical shift anisotropy. Dipole–dipole interactions can have a significant impact on T_2. The dipole–dipole interaction, however, is proportional to the square of the gyromagnetic ratio of each nucleus divided by the internuclear distance to the power six. [259] It is therefore (because of the large gyromagnetic ratio of the proton) usually dominated by the interaction of adjacent protons with the nucleus under study. The corresponding relaxation rate can be reduced by a factor of approximately 36 through deuteration, easily leading to relaxation times longer than 30 seconds.[56] (The fact that ^{2}H is a quadrupolar nucleus poses no problem because of its extremely small quadrupole moment.) This leaves scalar coupling and chemical shift anisotropy. Scalar coupling corresponds to the interaction of two nuclei through a chemical bond. In conformationally and configurationally stable molecules (e.g. without exchangeable protons) scalar coupling of the nucleus under study to a speedily relaxing spin — usually of a quadrupole nucleus — is the dominant source of this line broadening mechanism. If the (spin–lattice) relaxation time T_1 of the other nucleus is too short, however, the induced field fluctuations are averaged out. The corresponding scalar relaxation is then inefficient, so that only quadrupole nuclei such as ^{14}N or ^{11}B with spin–lattice relaxation times greater than 10 ms need to be considered as contributing to scalar coupling relaxation.[258] The chemical shift anisotropy is difficult to assess for heavy nuclei and can be expected to constitute the limiting factor on the full width at half maximum of an otherwise optimized compound. [56]

Using standard NMR spectrometers, nuclei with a high gyromagnetic ratio γ offer better experimental sensitivity in a measurement. High relative sensitivity of the nuclei is also desirable. Compounds have to be configurationally stable and, in addition to this, resonance frequencies have to be insensitive to dilution of the sample.

Ideally, one thus looks for a configurationally stable, closed shell, possibly deuterated compound that is enantiomerically separable, displays small internal electric field gradients and contains heavy, spin 1/2 nuclei with large natural abundance, such as ^{119}Sn, ^{125}Te, possibly ^{199}Hg or ^{205}Tl and especially ^{195}Pt (^{205}Tl would seem to be the best choice here but due to the generally high toxicity of thallium compounds it is an impractical one). A compound containing more than one of these nuclei would offer an additional opportunity to eliminate systematic effects: if a similar line–splitting was detected for two NMR centers from different rows of the periodic table, it would most likely be caused by effects other than parity violation, e.g. formation of aggregates or dipolar couplings. Nuclei with low gyromagnetic ratio such as ^{183}W, ^{103}Rh or ^{187}Os can, in principle, also be used in connection with a low γ NMR probe. The nuclear properties of some isotopes of interest are listed in Table 7.1

Table 7.1: Physical properties of NMR active isotopes which seem to be particularly well suited for PV NMR measurements. Data was taken from "NMR Properties of Selected Isotopes" by W.E. Hull in the "Bruker Corporation Almanac 2009".

isotope	nuclear spin I	natural abundance (%)	gyromagnetic ratio (10^7 rad T^{-1} s^{-1})	relative sensitivity (^{1}H$\sim$ 1)
^{103}Rh	1/2	100	-0.84677	3.17×10^{-5}
^{119}Sn	1/2	8.59	-10.0317	5.27×10^{-2}
^{125}Te	1/2	7.07	-8.510843	3.22×10^{-2}
^{183}W	1/2	14.31	1.1282406	7.50×10^{-5}
^{187}Os	1/2	1.96	0.6192897	1.24×10^{-5}
^{195}Pt	1/2	33.832	5.8385	1.04×10^{-2}
^{199}Hg	1/2	16.87	4.845793	5.94×10^{-3}
^{205}Tl	1/2	70.48	15.692185	2.02×10^{-1}

As both the PV NMR frequency splittings and the chemical shift anisotropy scale with the applied magnetic field, the use of strong magnetic fields with flux densities of up to 23.4 T which are available in commercial NMR spectrometers has to be considered carefully and may not be advisable. With respect to anisotropies of the molecular motion caused by coupling to a strong magnetic field, estimates made in Ref. [56] indicate that the coupling of fields of magnetic flux densities of approximately 10 T to the molecular motion and the thus caused anisotropies would be small enough not to limit the experimental accuracy.

During a measurement it will be important to reduce all possible sources of anisotropies to a minimum. The temperature differences within the sample have to be regulated on

the level of milli–Kelvin in order to achieve a resolution of 10 mHz [56] and, since the property is linear in the magnetic flux density and typical resonance frequencies of the nuclei under consideration are of the order of 100 MHz, the applied field has to be homogeneous on a nano–Tesla scale, in order to obtain the desired 10 mHz resolution. Such a field homogeneity can be achieved through shimming. The diamagnetic susceptibility of the solvents used in the experiment also affects the homogeneity of the applied field over the sample, and it may eventually be necessary to use gas phase NMR in order to reach the desired accuracy. However, this would drastically restrict the choice in compounds for such an experiment.

At this point it is also important to remember, that the values of $\Delta\nu^{\mathrm{PV}}$ reported herein are effective in the sense that they will have to be scaled with the negative actual value of the parameter λ_A of the factor κ in Eq. 4.1. This parameter can be estimated by nuclear structure calculations and is predicted to take on values between 1 and 10 for heavy nuclei [13, 91]. It might therefore be possible to increase PV NMR frequency splittings by up to an order of magnitude through the use of high λ_A nuclei.

7.3   Systematic effects in a Pt model complex

As ^{195}Pt appears to be one of the more promising nuclei for detecting PV frequency splittings in NMR spectroscopy, some thought may be given to the design of a platinum complex optimized for the purpose of measuring PV effects in NMR spectroscopy. As a first step along this road, some systematic effects in the model complex platinum-palladium-1,1,2,2-tetraamine – $(NH_2)_2Pt$–$Pd(NH_2)_2$ [3] have been investigated. It should be noted here, that this complex is not intended to model any specific existing molecules, since diplatinum or platinum-palladium complexes usually contain bridging ligands between the two transition metal centers. Instead, this particular model complex was chosen because of its suitability for the investigation of conformational effects.

As with the dihydrogen dichalcogens in Chapter 6, conformational effects have a significant impact on the size of the PV frequency splittings between conformers of opposite chirality in this compound. In Table 7.2 ^{195}Pt PV frequency splittings in $(NH_2)_2Pt$–$Pd(NH_2)_2$ are listed as a function of the dihedral angle α. The frequency splittings were computed with the B-LYP functional using the ZORA DFT approach developed in Chapter 5 of this thesis. Apart from the total two-component ZORA values, the individual paramagnetic and spin–orbit coupling contributions related to the shielding tensors of Eqs.. 5.127 and 5.128, respectively, are also given. Figure 7.1 depicts the variation of α, the remaining geometrical parameters, which were kept constant, are listed in Table

---

[3]This model compound was kindly suggested by D. Avnir

B.8. Details of the optimization procedure used to obtain these parameters are given in Section B.2.2.

Table 7.2: ^{195}Pt NMR frequency splitting between conformations of $(NH_2)_2$Pt–Pd$(NH_2)_2$ due to the isotropic parity violating NMR shielding constant, calculated with the BLYP functional as a function of the dihedral angle. The basis sets used for the heavy atoms are listed in Table B.9. The NMR frequencies were calculated for a magnetic flux density of $B = 11.7$ T and are given here in 10^{-6} Hz. $\Delta\nu^{PV}$ is the full two-component ZORA NMR frequency splitting related to the isotropic part of the NMR shielding tensor of Eq. 5.125. $\Delta\nu_p^{PV}$ and $\Delta\nu_{so}^{PV}$ are related to the paramagnetic and spin–orbit coupling contributions to the isotropic part of the NMR shielding tensor (Eqs. 5.127 and 5.128, respectively). Results are given with three significant figures for $\Delta\nu^{PV}$, the individual contributions to $\Delta\nu^{PV}$ were rounded to the same accuracy as $\Delta\nu^{PV}$.

$\Delta\nu^{PV}$	30°	45°	60°	90°	120°	150°
$\Delta\nu^{PV}$ (^{195}Pt)	-8.87×10^2	-6.71×10^2	-3.79×10^2	0.0796×10^2	4.18×10^2	8.58×10^2
$\Delta\nu_p^{PV}$ (^{195}Pt)	-14.10×10^2	-14.30×10^2	-11.80×10^2	-0.0852×10^2	12.00×10^2	14.00×10^2
$\Delta\nu_{so}^{PV}$ (^{195}Pt)	5.19×10^2	7.56×10^2	8.01×10^2	0.1650×10^2	-7.81×10^2	-5.39×10^2
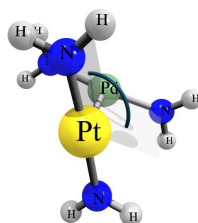
Figure 7.1: Illustration of the dihedral angle varied in $(NH_2)_2$Pt–Pd$(NH_2)_2$ in the investigation of conformational effects on the PV shift in the ^{195}Pt resonance frequency. Results are listen in Table 7.2 and displayed in Figure 7.2. Structural parameters are listed in Table B.8.

The $\sin(2\alpha)$-like dependence of the individual contributions to the frequency splittings on the dihedral angle is observed for this compound, as dictated by symmetry. The paramagnetic and spin–orbit coupling contributions are of opposite sign and similar in size when compared to the contributions in H_2Po_2 of Chapter 6, with the paramagnetic contribution usually being about twice as big as the spin–orbit coupling contribution. The angular dependence of the total frequency splitting shows a slight deviation from the $\sin(2\alpha)$-pattern, illustrated in Figure 7.2.

At the equilibrium geometry, where $\alpha = 0°$ and the other achiral conformations with $\alpha = 90°$ and $\alpha = 180°$, the PV NMR frequency splitting vanishes. For $\alpha \approx 45°$
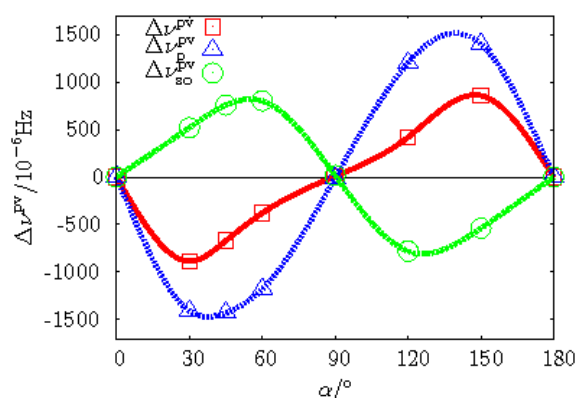
Figure 7.2: Dihedral angle dependence of the ^{195}Pt PV NMR frequency splitting and its individual contributions in $(NH_2)_2Pt–Pd(NH_2)_2$, calculated with the BLYP functional and the basis sets listed in Table B.9. The NMR frequencies were calculated for a magnetic flux density of $B = 11.7$ T. $\Delta\nu^{pv}$ denotes the full two-component ZORA NMR frequency splitting related to the isotropic part of the NMR shielding tensor of Eq. 5.125. $\Delta\nu_p^{pv}$ and $\Delta\nu_{so}^{pv}$ are related to the paramagnetic and spin–orbit coupling contributions to the isotropic part of the NMR shielding tensor (Eqs. 5.127 and 5.128, respectively).

and $\alpha \approx 135°$ it approaches it's maximum values of about 1 mHz. Synthetically, a manipulation of the dihedral angle could be possible by employing different ligands, so that the design of an axially chiral compound that conformationally maximizes the PV NMR frequency splitting of a ^{195}Pt nucleus on it's chiral axis is conceivable.

Table 7.3 lists the PV NMR frequency splittings for ^{195}Pt and ^{105}Pd in $(NH_2)_2Pt–Pd(NH_2)_2$ calculated for a dihedral angle $\alpha = 45°$. From ^{105}Pd to ^{195}Pt the frequency splitting increases as Z^x with a factor of $x \approx 5$, signifying an even more pronounced scaling than that observed for H_2Po_2 in the dihydrogen dichalcogenide series. As was discussed in Section 7.2, the existence of two NMR active centers from different rows of the periodic table in a chiral environment can be used in a PV NMR measurement, in order to assess systematic errors. Palladium however, is not an ideal choice for this purpose, as the only isotope is a spin 5/2 nucleus.

Table 7.4 lists the ^{195}Pt PV NMR frequency splittings for $(NH_2)_2Pt–Pd(NH_2)_2$ and $(NH_2)_2Pt–Pt(NH_2)_2$. Surprisingly, the frequency splitting predicted for the Pt–Pt compound is less than half as big as that predicted for $(NH_2)_2Pt–Pd(NH_2)_2$. While the negative spin–orbit coupling contributions to the frequency splittings are of comparable size in both compounds, the positive paramagnetic contribution is larger by a factor of 2 in $(NH_2)_2Pt–Pd(NH_2)_2$. It seems reasonable, that for PV effects on NMR observables of a heavy nucleus the mass of surrounding nuclei is of little importance, since the property depends on the overlap of the electronic wavefunction with this particular nucleus alone.

Table 7.3: ^{195}Pt and ^{105}Pd NMR frequency splitting between conformations of $(NH_2)_2Pt–Pd(NH_2)_2$ due to the isotropic parity violating NMR shielding constant, calculated with the BLYP functional at a dihedral angle of $\alpha = 45°$. The basis sets used for the heavy atoms are listed in Table B.9. The NMR frequencies were calculated for a magnetic flux density of $B = 11.7$ T and are given here in 10^{-6} Hz. $\Delta\nu^{PV}$ is the full two-component ZORA NMR frequency splitting related to the isotropic part of the NMR shielding tensor of Eq. 5.125. $\Delta\nu_p^{PV}$ and $\Delta\nu_{so}^{PV}$ are related to the paramagnetic and spin–orbit coupling contributions to the isotropic part of the NMR shielding tensor (Eqs. 5.127 and 5.128, respectively). Results are given with three significant figures for $\Delta\nu^{PV}$ and $\Delta\nu_{nr}^{PV}$, the individual contributions to $\Delta\nu^{PV}$ were rounded to the same accuracy as $\Delta\nu^{PV}$. The exponents x of the scaling factors Z^x are given in parenthesis behind the ^{195}Pt frequency contributions.

NMR center	$\Delta\nu^{PV}$	$\Delta\nu_p^{PV}$			$\Delta\nu_{so}^{PV}$	
^{105}Pd	53.8	127.8	-74.1			
^{195}Pt	-671	(4.8)	-1427	(4.5)	756	(4.4)

For a heavy nucleus, one can suspect, that the "degree of chirality" of the electronic wavefunction, which is potentially enhanced by a heteronuclear environment, is more important than the mass number of the surrounding nuclei. For a lighter nucleus under study, the addition of a heavy center to it's immediate surroundings, may have a more pronounced effect. [68]

7.4 Platinum candidate compounds

As a starting point for a collaboration with experimentalists, we have begun to screen compounds possibly suited for an NMR experiment for high values of $\Delta\nu^{PV}$. Results for three such compounds are listed in Table 7.5. The effect size in the platinum compounds is comparable to that in H_2Po_2 at equilibrium geometry. Exploitation of conformational effects could help maximize the PV frequency splittings for those compounds and they might reach a magnitude of about 10 mHz as for H_2Po_2 at a dihedral angle of roughly $45°$.

Table 7.4: ^{195}Pt frequency splitting between conformations of $(NH_2)_2Pt–Pd(NH_2)_2$ and $(NH_2)_2Pt–Pt(NH_2)_2$ due to the isotropic parity violating NMR shielding constant, calculated with the BLYP functional at a dihedral angle of $\alpha = 45°$. The basis sets used for the heavy atoms are listed in Table B.9. The NMR frequencies were calculated for a magnetic flux density of $B = 11.7$ T and are given here in 10^{-6} Hz. $\Delta\nu^{PV}$ is the full two-component ZORA NMR frequency splitting related to the isotropic part of the NMR shielding tensor of Eq. 5.125. $\Delta\nu_p^{PV}$ and $\Delta\nu_{so}^{PV}$ are related to the paramagnetic and spin–orbit coupling contributions to the isotropic part of the NMR shielding tensor (Eqs. 5.127 and 5.128, respectively). Results are given with three significant figures for $\Delta\nu^{PV}$, the individual contributions to $\Delta\nu^{PV}$ were rounded to the same accuracy as $\Delta\nu^{PV}$.

Compound	$\Delta\nu^{PV}$	$\Delta\nu_p^{PV}$	$\Delta\nu_{so}^{PV}$
Pt–Pd	670	1427	−756
Pt–Pt	−272	614	−887
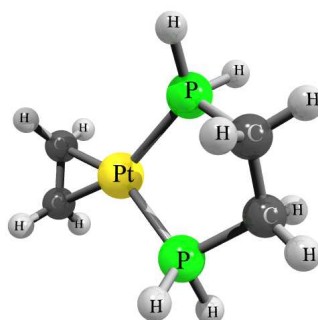
Figure 7.3: Platinum compound Pt–1: ethylene(ethylenediphosphine)platinum

Figure 7.3 depicts test compound Pt–1 (ethylene(ethylenediphosphine)platinum) [4]. Pt–1 seems attractive for a PV NMR experiment due to it's fairly simple structure, however, the molecule and especially the direct environment of the platinum nucleus is barely chiral, and accordingly the PV NMR frequency splitting for this compound is very small at -20 μHz. A strong conformational dependence of the size of the frequency splitting can be expected for this compound, since the chiral equilibrium structure can be converted to an achiral geometry by a twist of the ethylenediphosphine group. In addition, the presence of phosphorus which has only one isotope that is spin 1/2 and has a relatively large gyromagnetic ratio of 10.839×10^7 rad T^{-1} s^{-1} might increase dipolar relaxation which in turn increases the spectral line width.

---

[4]Kindly suggested by M. Bühl

Table 7.5: ^{195}Pt frequency splitting for three possible experimental candidate compounds due to the isotropic parity violating NMR shielding constant, calculated with the BLYP functional. The basis sets and structural parameters used for the heavy atoms are listed in Tables B.10 and B.11, respectively. The NMR frequencies were calculated for a magnetic flux density of $B = 11.7$ T and are given here in 10^{-6} Hz. $\Delta\nu^{\mathrm{PV}}$ is the full two-component ZORA NMR frequency splitting related to the isotropic part of the NMR shielding tensor of Eq. 5.125. $\Delta\nu_{\mathrm{p}}^{\mathrm{PV}}$ and $\Delta\nu_{\mathrm{so}}^{\mathrm{PV}}$ are related to the paramagnetic and spin–orbit coupling contributions to the isotropic part of the NMR shielding tensor (Eqs. 5.127 and 5.128, respectively). Results are given with three significant figures for $\Delta\nu^{\mathrm{PV}}$, the individual contributions to $\Delta\nu^{\mathrm{PV}}$ were rounded to the same accuracy as $\Delta\nu^{\mathrm{PV}}$.

Compound	$\Delta\nu^{\mathrm{PV}}$	$\Delta\nu_{\mathrm{p}}^{\mathrm{PV}}$	$\Delta\nu_{\mathrm{so}}^{\mathrm{PV}}$
Pt–1	19.6	-2.3	21.9
Pt–2	-16.6	59.8	-76.5
Pt–3	-410	-302	-108

Figure 7.4 shows the Pt$^{\mathrm{II}}$ complex Pt–2 (2,2′-bis(diphenylphosphanyl)biphenyl-platinumdichloride) [5]. As reported in Ref. [260] enantiopure Pt–2 can be synthesized and ^{1}H and ^{31}P NMR spectra of the compound have been recorded. Unfortunately, the predicted PV NMR frequency splitting is again rather small with a strong cancellation of the paramagnetic and the spin–orbit coupling contributions.
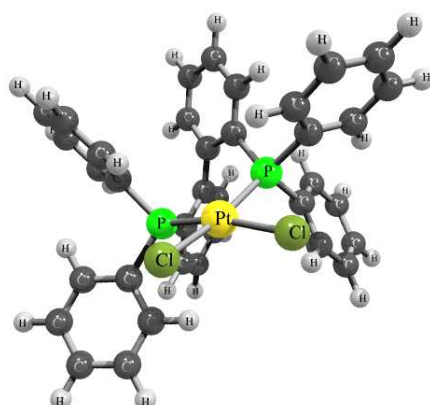
Figure 7.4: Platinum compound Pt–2: 2,2′-bis(diphenylphosphanyl)biphenyl-platinumdichloride

---

[5]Well recommended by P. Heretsch

The third platinum complex investigated in this study, Pt–3 (1,2-benzenediamine-2,2′-diamino-1,1′-binaphthaleneplatinum), is shown in Figure 7.5.[6] It is a 16 electron complex with four nitrogen atoms bound to the platinum center. The PV frequency at the equilibrium geometry is approximately equal to 400 μHz, one to two orders of magnitude below the envisaged optimal resolution of an experiment. This does not necessarily have to deter from an attempt at measuring the frequency splitting, however, since the immediate goal of such an experiment would be to set an upper bound for the nuclear spin–dependent PV interaction within a chiral molecule. Such an upper bound should be comparable to that set for the nuclear spin–independent PV interaction by means of vibrational spectroscopy [72], which was estimated to be about four orders of magnitude above the predicted size of the effect, see refs. [142–144].
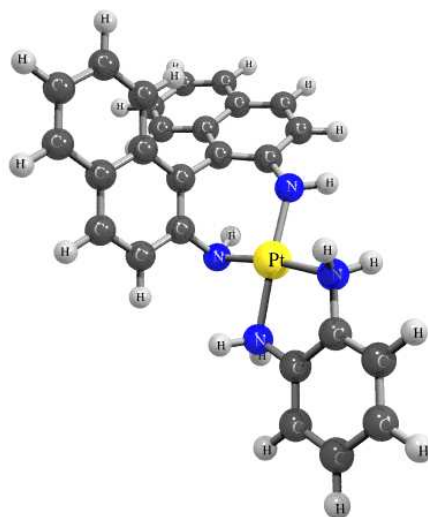
Figure 7.5: Platinum compound Pt–3: 1,2-benzenediamine-2,2′-diamino-1,1′-binaphthaleneplatinum

Consequently, Pt–3 might be suited for a first attempt at setting an upper bound PV NMR frequency shifts, and a chiral ligand similar to that of Pt–3, which could be used for this purpose, has been synthesized [7]. However, the results presented here are only preliminary and the compound might have high–spin states close in energy to the closed shell configuration. This would make the theoretical methods used here unreliable and could also lead to significant line broadening through paramagnetic relaxation. Another problem is the presence of nitrogen bonded to the platinum center, which would again limit the experimental resolution through strong scalar relaxation. Such effects will have to be thoroughly studied for the available ligand and modifications such as the replacing of nitrogen with oxygen will have to be considered. It will also be necessary to assess the

---

[6]The basic structure of this compound was obtained by P. Heretsch.

[7]P. Heretsch, private communication

effect of vibrational averaging on the property (which has been calculated for CHBrClF and was found to be as big as 15%, [261]), and solvent effects under realistic experimental conditions, before a reliable assessment of the suitability of the compound can be made.

7.5 Tellurium candidate compounds
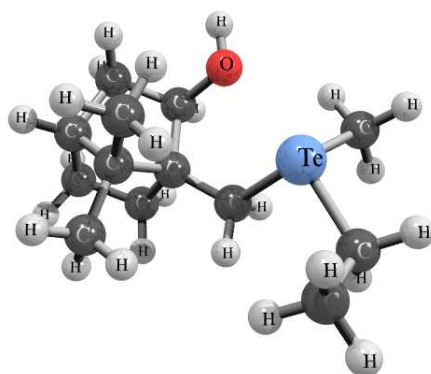
Figure 7.6:   Tellurium   compound   Te–1:   ethyl-(2-exo-hydroxy-10-bornyl)methyltelluronium cation

^{125}Te is a heavy, spin 1/2 nucleus with large gyromagnetic ratio and therefore equally well suited for PV NMR experiments as platinum. The large PV NMR frequency splittings predicted for some conformations of H_2Te_2 in Chapter 6 have been encouraging in screening PV NMR frequency splittings for the heavier homologues of three conformationally stable selenium compounds, in which selenium has been substituted by tellurium. [8] The compounds are depicted in Figures 7.6, 7.7 and 7.8. ^{125}Te PV NMR frequency splittings are listed in Table 7.6.

The values of the PV frequency splittings in the three compounds are of the same order as $\Delta\nu^{\text{PV}}$ of H_2Te_2 at equilibrium geometry, see Table 6.1. Taking a quick glance at these three compounds, one might expect, Te–3 and Te–2 to display a relatively large PV NMR frequency splittings with Te–1, where the immediate environment of the tellurium nucleus is achiral, bringing up the rear. Surprisingly, Te–1 displays the largest PV NMR frequency splitting of the three compounds, followed by Te–3 and Te–2. It is quite likely however, that this unexpected result is simply due to basis set effects, since according to Table B.12 Te–1 is the only one of the three compounds where large, even–tempered basis sets were used only on Te and not on some surrounding centers. This could result in an artificial polarization of the wavefunction in the region of Te and hence lead to an

---

[8]All three of these compounds were suggested by M. Bühl on the basis of nonrelativistic PV NMR calculations for H_2Se_2 and the predicted scaling behavior of the property in Ref. [156].

Table 7.6: ^{125}Te PV NMR frequency splitting for three possible experimental candidate compounds due to the isotropic PV NMR shielding constant, calculated with the BLYP functional. The basis sets and structural parameters used in the calculations are listed in Tables B.12 and B.13, respectively. The NMR frequencies were calculated for a magnetic flux density of $B = 11.7$ T and are given here in 10^{-6} Hz. $\Delta\nu^{\mathrm{PV}}$ is the full two-component ZORA NMR frequency splitting related to the isotropic part of the NMR shielding tensor of Eq. 5.125. $\Delta\nu_{\mathrm{p}}^{\mathrm{PV}}$ and $\Delta\nu_{\mathrm{so}}^{\mathrm{PV}}$ are related to the paramagnetic and spin–orbit coupling contributions to the isotropic part of the NMR shielding tensor (Eqs. 5.127 and 5.128, respectively). Results are given with three significant figures for $\Delta\nu^{\mathrm{PV}}$, the individual contributions to $\Delta\nu^{\mathrm{PV}}$ were rounded to the same accuracy as $\Delta\nu^{\mathrm{PV}}$.

Compound	$\Delta\nu^{\mathrm{PV}}$	$\Delta\nu_{\mathrm{p}}^{\mathrm{PV}}$	$\Delta\nu_{\mathrm{so}}^{\mathrm{PV}}$
Te–1	36.8	36.6	0.2
Te–2	-19.6	-19.7	0.2
Te–3	28.1	28.7	-0.6
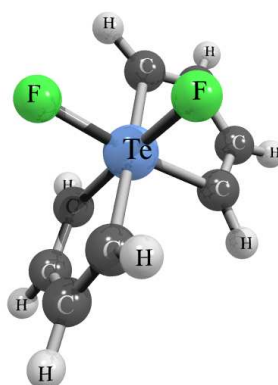
Figure 7.7: Tellurium compound Te–2: 5,5-difluoro-5λ^6-telluriumaspiro[4.4]nona-1,3,6,8-tetraene

increase in the PV NMR frequency splittings (as can be seen from Table 6.5 and the discussion in Section 6.5 an increase of the size of the basis set almost regularly decreases the calculated PV NMR frequencies).

It is conceivable, that the synthesis of any of these three compounds would not pose any significant difficulty, since the lighter homologues containing selenium are already available. Te–2 and Te–3 seem particularly interesting, since one might be able to influence the size of their PV NMR frequency splittings by atomic substitution or conformational changes. In the D$_2$-symmetric compound Te–3, for example, it would be interesting to

investigate the dependence of $\Delta\nu^{PV}$ on the dihedral angel between the spiro groups. If this dependence proved to be similar to that observed in the dihydrogen dichalcogens of Chapter 6 or the Pt model complex of Section 7.3, conformational changes could lead to an order of magnitude increase in the PV property for this compound. Such conformational changes are often quite easy to implement synthetically through the use of different ligands and one might thus be able to design a tellurium compound better suited for a PV NMR measurement.
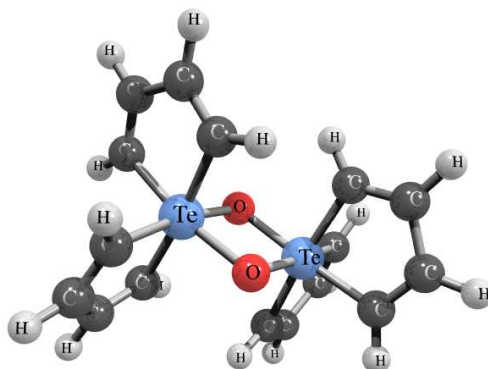
Figure 7.8: Tellurium compound Te–3: 6,16-dioxa-$5\lambda^6,7\lambda^6$-ditelluriumatrispiro[4.1.4^7.4^7.1^5.4^5]icosa-1,3,8,10,12,14,17,19-octaene

7.6 Effects of atomic substitution in tungsten model compounds

In order to facilitate the identification of a compound especially well suited for the investigation of PV NMR effects, it is important to assess the effect of different nuclei surrounding the nucleus under study. As has been mentioned in connection with the discussion of the platinum test compound in Section 7.3, the PV NMR frequency splittings of heavy NMR active centers are not very sensitive to the presence of other heavy nuclei in the surroundings. Other factors, such as perhaps the "degree of chirality" of the environment of the NMR nucleus could be more significant. These effects are further analyzed in this section.

PV NMR frequency splittings and energies for a series of chiral molecules of the general structure $NWXYZ$ with $X, Y, Z =$H,F,Cl,Br or I have been calculated and are listen in Table 7.7. [9] The compounds are derived by substitution from the recently synthesized NWH_3 and NWF_3 molecules, see Refs. [262] and [263], respectively, and a study of PV effects in the vibrational spectrum of NWHClI has already been published [150]. In

---

[9]The molecules were suggested by P. Schwerdtfeger, who also provided the optimized structures.
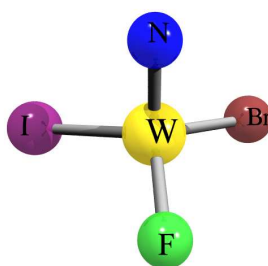
Figure 7.9: S enantiomer of NWFBrI

the group of molecules from **1** to **4** all three hydrogen atoms have been substituted by halogens, in the group from **5** to **10** only two hydrogen atoms have been substituted for. Basis sets and structural parameters of the compounds used in the calculations are listed in Tables B.14 and B.15, respectively. In addition, Figure 7.9 shows the structure of the S-enantiomer of NWFBrI.

In the first series of compounds, molecules **1** to **4**, the relative ordering of the absolute values of PV frequency splittings and energies is the same: **4 > 3 > 1 > 2**. The order of magnitude of the PV energies is comparable to V^{PV} in PbHBrClF reported in Ref. [143], but the ordering and sign of the PV energies are different from those reported for their chiral polyhalomethane (CHXYZ) [143, 149] and polyhalocubane [264] counterparts. The most significant effect seems to be an order of magnitude increase in V^{PV} and an even stronger increase in σ^{PV} upon substitution with fluorine. The large impact of fluorine substitution is most probably due to it's large electronegativity and, for PV energies, has been observed before [265].

For molecules **1** to **4**, the paramagnetic and spin–orbit coupling contributions to the frequency splitting, related to the contributions to the isotropic part of the NMR shielding tensor of Eqs. 5.127 and 5.128, respectively, are of opposite sign, with the negative spin–orbit coupling contribution being larger by an order of magnitude with respect to the paramagnetic one in compounds **1**, **3** and **4** and of roughly the same size in **3**. The total frequency splitting is thus negative for compounds **1**, **3** and **4** and positive for compound **2**, where the spin–orbit coupling paramagnetic contributions almost cancel each other out.

Regarding the PV frequency splittings, a comparison with ^{13}C NMR shielding tensors in CHBrClF and CHBrFI presented in Ref. [158] shows, that like the PV energy difference, the isotropic ^{183}W NMR shielding constants are of opposite sign in this series and the relative ordering of the resulting frequency splittings is also changed: In Ref. [158] the ^{13}C shieldings in CHBrClF and CHBrFI are similar in size with the ordering depending on the choice of density functional. In this study, the isotropic ^{183}W PV shielding

Table 7.7: ^{183}W PV NMR frequency splittings due to the isotropic parity violating NMR shielding constants) between the S- and R-enantiomers ($\Delta\nu = \nu^S - \nu^R$) and PV energies V^{PV} of the S-enantiomer of the series of compounds with structural formula NWXYZ, calculated with the BLYP functional. The basis sets and structural parameters used for the heavy atoms are listed in Tables B.14 and B.15, respectively. The NMR frequencies were calculated for a magnetic flux density of $B = 11.7$ T and are given here in 10^{-6} Hz. $\Delta\nu^{PV}$ is the full two-component ZORA NMR frequency splitting related to the isotropic part of the NMR shielding tensor of Eq. 5.125. $\Delta\nu_{\mathrm{p}}^{PV}$ and $\Delta\nu_{\mathrm{so}}^{PV}$ are related to the paramagnetic and spin–orbit coupling contributions to the isotropic part of the NMR shielding tensor (Eqs. 5.127 and 5.128, respectively). Results are given with three significant figures for $\Delta\nu^{PV}$, the individual contributions to $\Delta\nu^{PV}$ were rounded to the same accuracy as $\Delta\nu^{PV}$.

	Molecule	$\Delta\nu^{PV}$	$\Delta\nu_{\mathrm{p}}^{PV}$	$\Delta\nu_{\mathrm{so}}^{PV}$	V^{PV} / E_{h}
1	NWBrClF	-9.09	1.15	-10.24	-2.12×10^{-15}
2	NWBrClI	0.398	2.578	-2.179	-1.68×10^{-16}
3	NWBrFI	-16.7	4.8	-21.4	-3.62×10^{-15}
4	NWClFI	-25.9	3.6	-29.6	-5.62×10^{-15}
5	NWHBrCl	-94.1	-43.4	-50.8	6.34×10^{-15}
6	NWHBrF	-176	-74	-102	2.78×10^{-15}
7	NWHBrI	-196	-96	-101	1.02×10^{-14}
8	NWHClF	-88.4	-41.8	-46.6	-6.26×10^{-16}
9	NWHClI	-293	-139	-154	1.63×10^{-14} $^{a)}$
10	NWHFI	-363	-152	-210	7.91×10^{-15}

$^{a)}$ This value of V^{PV} is in good agreement with the DKS results of Ref. [150]

constant in NWBrFI is almost twice as big as that in NWBrClF. However, for the values of V^{PV} reported in Refs. [143, 149], the increase from CHBrClF to CHBrFI is even more pronounced than the one reported here for the ^{183}W shieldings in NWBrClF and NWBrFI.

In the second set of compounds, molecules **5** to **10**, the relative ordering of the absolute values of PV NMR frequency splittings is **10** > **9** > **7** > **6** > **5** > **8**, and not the same as that of the PV energies given by: **9** > **7** > **10** > **5** > **6** > **8**. For both properties, however, the three molecules containing iodine as one of the substituents display larger values than the other three.

The PV energies for molecules in the series are positive except for compound **8**, NWH-ClF, which also displays a somewhat smaller absolute value of V^{PV} than the other molecules in this series. It is possible, that the reason for the different sign of V^{PV}

is cancellation of contributions from different atoms to the property. Comparing the values of V^{PV} for NWHBrF and NWHBrCl presented here to those calculated for the corresponding compounds NHBrF and NHBrCl with nitrogen as chiral center in Ref. [266], the signs of V^{PV} for the S-enantiomers of the two sets of molecules are different, but the ordering of the two absolute values are the same. In both sets of molecules the chiral HBrCl-environment yields a larger PV energy shift than HBrF.

The paramagnetic and spin–orbit coupling contributions to the PV frequency splittings are of the same sign for molecules of the second set which enhances the increase in frequency splittings from molecules **1** through **4** to molecules **5** through **10**. The individual contributions themselves, however, are also bigger for the second series.

It may be considered surprising, that all of the predicted ^{183}W PV NMR frequency splittings for members of the second series of molecules, **5** to **10**, are significantly bigger than the values predicted for molecules **1** to **4**, because hydrogen is so much lighter than any of the other substituents. However, substituting any of the halogens in the first series by hydrogen almost always leads to at least an order of magnitude increase in the PV NMR frequency splittings. The only exception to this is the substitution of iodine by hydrogen in NWClFI, where there's an increase by a factor 4 "only". A possible reason for this trend is the larger asymmetry of the electronic environment of the tungsten nucleus, introduced by substituting atoms with greater mass differences or possibly differences in electronegativity.

The absolute values of V^{PV} in the second series are relatively similar to those in molecules **1** to **4** but also tend to be slightly bigger for similar substituents. There is a definite trend, that for a given two substituents X and Y, $\left|V^{PV}\left(NWXYZ\right)\right|$ decreases with increasing atomic mass of the third substituent Z. For example for $X, Y =$F,I: $\left|V^{PV}\left(NWHFI\right)\right| > \left|V^{PV}\left(NWClFI\right)\right| > \left|V^{PV}\left(NWBrFI\right)\right|$. This rule holds for all but the two lightest pairs of (X, Y), i.e. (F,Cl) and (F,Br). The same trend is also apparent for the PV frequency splittings, with the same exception of the two lightest pairs, (F,Cl) and (F,Br).

It is also possible to analyze the impact of atomic substitution with respect to the different electronegativities (χ) of the substituents, which is largest for fluorine and smallest for hydrogen: $\chi\left(F\right) > \chi\left(Cl\right) > \chi\left(Br\right) > \chi\left(I\right) > \chi\left(H\right)$ with $\chi\left(Cl\right) \gtrsim \chi\left(N\right) \gtrsim \chi\left(Br\right)$. As mentioned earlier, this could explain, why in the first series of molecules there is a pronounced increase in the absolute values of both V^{PV} and $\Delta\nu^{PV}$ upon fluorine substitution. It could also explain an increase in PV properties upon substitution of hydrogen for one of the three heavier halogens, but it is less clear, why there should be such a pronounced increase even when hydrogen is substituted for fluorine.

In general, the PV NMR frequency splittings are even more sensitive to atomic substitution than PV energies, with an increase of $\Delta\nu^{\mathrm{PV}}$ by three orders of magnitude from NWIBrCl to NWHFI! This sensitivity offers excellent prospects for the rational design of compounds suited for a PV NMR experiment, where it would seem prudent to surround a heavy, NMR active nucleus in the chiral center of a molecule with ligands providing a strongly heterogeneous electronic environment. To what extend this could be exploited for example in the platinum candidate complexes presented in Section 7.4, remains to be investigated.

7.7 Chiral organometallic clusters with tungsten as NMR active nucleus
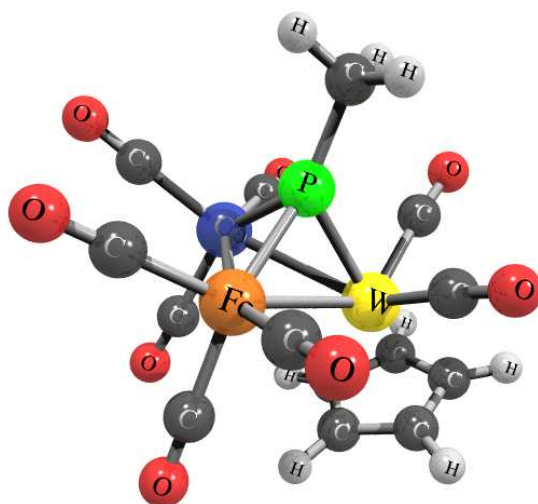
Figure 7.10: Tungsten compound W–1: trimetal cluster FeCoW(PMe)(CO)$_8$Cp

In order to explore the possibility of measuring PV NMR frequency splittings of nuclei with small gyromagnetic ratio (low–γ nuclei), calculations on organometallic complexes containing iron, rhodium and tungsten as possible NMR active centers have been performed using the ZORA approach to molecular parity violation presented in Chapters 4 and 5.[10] The small gyromagnetic ratios lead to lower sensitivity of standard NMR spectrometers, but an experiment would still be possible, with a different NMR sample head.

---

[10]For the molecules discussed in this chapter, J. L. Stuber provided some preliminary geometrical parameters that were used as the starting points of structure optimizations.
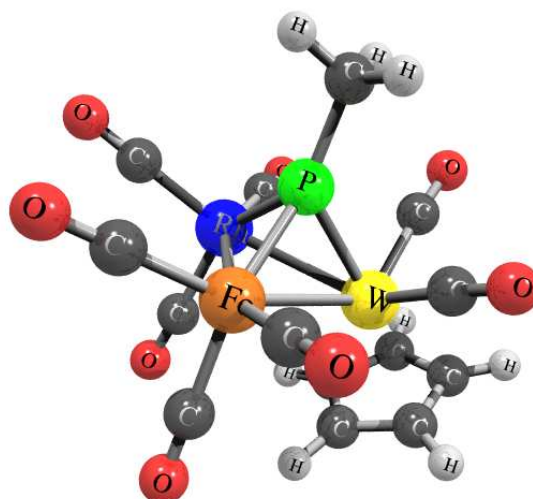
Figure 7.11: Tungsten compound W–2: trimetal cluster FeRhW(PMe)(CO)$_8$Cp

Figure 7.10 shows the transition metal compound FeCoW(PMe)(CO)$_8$Cp (denoted as W–1 for brevity), which has been synthesized and is enantiomerically separable [267]. Compounds W–2 and W–3 (FeRhW(PMe)(CO)$_8$Cp and RhOsW(PMe)(CO)$_8$Cp) shown in Figures 7.11 and 7.12, respectively, are derived from W–1 by substitution of cobalt by rhodium in W–2 and of cobalt by rhodium and iron by osmium in W–3. The substitutions were performed in order to investigate the effect of a heavier center in the neighborhood of tungsten. On the other hand, the existence of another NMR active nucleus from a different row of the periodic table than tungsten might be useful in the assessment of systematic effects, as discussed in Section 7.2. All three compounds also contain phosphorus which would lead to a slight broadening of spectral lines through dipolar coupling. Whether or not this could limit the attainable experimental resolution is unclear.

The fourth cluster, depicted in Figure 7.13, with three metal atoms and carbon in a tetrahedral arrangement, FeRhW(CPhMe)(CO)$_5$(Ph)$_3$, or W–4 for short, has been synthesized [268] but may not be easily enantiomerically separable. It does not contain phosphorus which would be advantageous for the experimentally achievable resolution, but rhodium would still cause dipolar couplings. A similar heteronuclear trimetal complex containing platinum, iron and tungsten [269] would most likely be more suited for a PV NMR experiment.

Table 7.8 lists PV potentials for the four clusters obtained within a ZORA HF framework. Considering the heavy nuclei involved, especially in W–3 with osmium and tungsten,
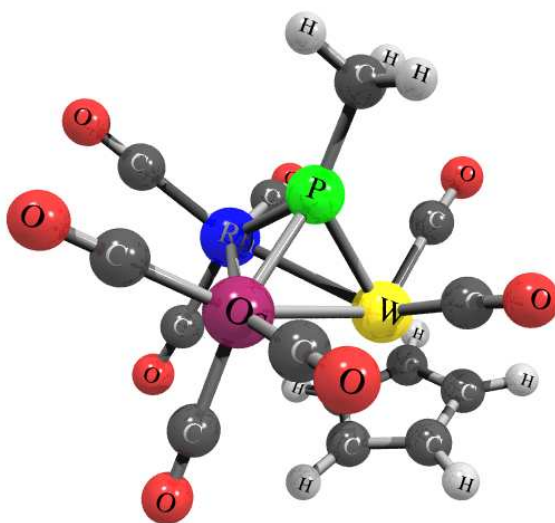
Figure 7.12: Tungsten compound W–3: trimetal cluster RhOsW(PMe)(CO)$_8$Cp
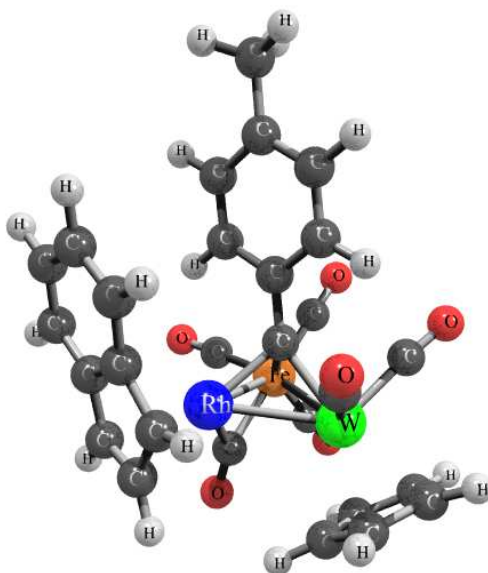
Figure 7.13: Tungsten compound W–4: trimetal cluster FeRhW(CPhMe)(CO)$_5$(Ph)$_3$

Table 7.8: PV potential for the tungsten complexes displayed in Figures 7.10, 7.11, 7.12 and 7.13. The values were calculated according to Eq. 5.89 within the ZORA HF approach. The basis sets used are listed in Table B.16.

Molecule	W–1	W–2	W–3	W–4
$V_{PV}/10^{-15}E_h$	-4.13	-0.564	-9.69	-10.3

the values for V_{PV} seem rather low. In H_2Po_2, even at equilibrium geometry where V_{PV} is comparatively small, the parity violating potential is bigger by an order of magnitude still than those found for W–3 and W–4 here [58, 250]. In W–1, W–2 and W–3 this may in part be due to the small double–zeta–type basis sets used on the lighter atoms, which do not offer the necessary flexibility to capture PV effects [250] (see Table B.16 for a list of all basis sets used in calculations of this section). However, for W–4 basis sets of triple–zeta quality including polarizing functions were used on the lighter atoms, which should be slightly more satisfactory, and it is unlikely that an order of magnitude increase in the result can be achieved by a manipulation of the basis set.

Substitution of different transition metals in the cluster has a pronounced effect. Upon the substitution of osmium for iron an order of magnitude increase in V_{PV} is observed from W–2 to W–3, which would seem to be in keeping with the strong scaling with nuclear charge of PV properties. Contrarily, there is an almost equally big increase in V_{PV} from W–2 to W–1, when cobalt is substituted for rhodium. This puzzling behavior can not be understood through scaling laws but might be due to electronic effects.

PV splittings of the ^{183}W NMR frequency in W–3 and W–4 are listed in Table 7.9 together with the PV potentials of these compounds. As with the platinum compounds of Section 7.4, the values for $\Delta\nu^{PV}$ are comparable to those obtained for H_2Po_2 at equilibrium geometry, and it is conceivable that through modification of substituents or conformational optimization measurable values can be reached. The effects of substituting different metals would be particularly interesting to investigate, since according to the discussion in Section 7.6 the PV NMR frequency splittings can be even more sensitive to such changes in their surroundings than PV potentials.

The calculations presented in Table 7.9 were performed using the hybrid, gradient corrected BHLYP functional (containing 50% of Becke's gradient correction [252] and 50%

Table 7.9: PV potential and ^{183}W NMR frequency splitting in the tungsten complexes W–3 and W–4, depicted in Figures 7.12 and 7.13, respectively. The parity violating NMR shielding tensor was calculated according to Eq. 5.125 with the wavefunction and orbital energies obtained from a BHLYP [270] calculation. Possible response contributions to the shielding tensor were thus neglected (see the discussion in Chapter 5.5). The basis sets used are listed in Table B.16. The NMR frequencies were calculated for a magnetic flux density of $B = 11.7$ T and are given here in 10^{-6} Hz. $\Delta\nu^{\mathrm{PV}}$ is the full two-component ZORA NMR frequency splitting related to the isotropic part of the NMR shielding tensor. $\Delta\nu_{\mathrm{p}}^{\mathrm{PV}}$ and $\Delta\nu_{\mathrm{so}}^{\mathrm{PV}}$ are related to the paramagnetic and spin–orbit coupling contributions to the isotropic part of the NMR shielding tensor (Eqs. 5.127 and 5.128, respectively).Results are given with three significant figures for $\Delta\nu^{\mathrm{PV}}$ and $\Delta\nu_{\mathrm{nr}}^{\mathrm{PV}}$, the individual contributions to $\Delta\nu^{\mathrm{PV}}$ were rounded to the same accuracy as $\Delta\nu^{\mathrm{PV}}$.

Molecule	$\Delta\nu^{\mathrm{PV}}$	$\Delta\nu_{\mathrm{p}}^{\mathrm{PV}}$	$\Delta\nu_{\mathrm{so}}^{\mathrm{PV}}$	$\mathrm{V}^{\mathrm{PV}} \,/\, 10^{-15}\mathrm{E_h}$
W–3	93.8	98.8	-5.0	-1.06
W–4	-73.9	-87.8	13.9	-5.88

exact Hartree-Fock exchange and the Lee-Yang-Parr correlation contribution [253]) with basis sets as listed in Table B.16. When hybrid functionals are used, Eq. 5.125 is no longer the exact expression for the PV NMR shielding tensor and the coupled–perturbed equations 5.31 have to be solved. Arguably, this suggests that the introduction of exact exchange integrals enhances spin–polarization,[245, 246] which at least in the spin–free nonrelativistic case can be considered as unphysical. The use of the uncoupled second order Eq. 5.125 has therefore been suggested also in connection with hybrid functionals, at least in nonrelativistic calculations [247] (this is also discussed in Chapter 5.5). Within a spin–dependent formalism the coupling terms should always be considered but since, at this point, a prediction of the order of magnitude of the PV NMR frequency splittings is fully sufficient, neglecting these terms probably does not cause any serious restrictions for the interpretability of the results, while it greatly increases the speed of the calculations.

The DFT values for V_{PV} presented in Table 7.9 are almost an order of magnitude smaller than their HF counter parts. A similarly strong dependence on the functional was found in Chapter 8 for a chiral thorium compound and in Ref. [149] for the series of chiral polyhalomethanes.

In summary, organometallic clusters such as the ones presented in this section are interesting candidates for a PV NMR experiment. Even though the calculated ^{183}W PV

NMR frequency splittings are not detectable at present, the clusters are very flexible with respect to the constituent metals and this flexibility presents a great opportunity to "design" a compound that presents larger PV NMR effects and has properties that help to achieve the best possible experimental resolution. In this respect, this class of organometallic compounds may prove to be superior to the platinum complexes discussed in Section 7.4, where flexibility lies more in the organic ligands than the NMR active centers of interest.

Of the two types of clusters discussed in this section, W–1 with W–2 and W–3 derived from it by substitution, and W–4, a compound of the type of W–1 seems a little more promising for a measurement of PV NMR frequency splittings. W–1 is readily enantiomerically separable, whereas it is not clear if this is easily possible with compounds of the type of W–4. However, phosphorus might have to be replaced in the tetrahedron in order to reach the necessary experimental resolution. In addition, the effect of vibrational averaging has not been considered at this point, which has been estimated to yield corrections of up to 40% even for low-lying vibrational states of fairly rigid molecules (see Ref. [261]) and therefore can not be ignored in the selection of a suitable candidate compound.

In the upcoming chapter, a different experimental approach, the detection of PV vibrational frequency shifts in infrared spectra of chiral molecules will be discussed. Unlike for NMR spectroscopy, an upper limit for PV frequency shifts has already been set for CHBrClF [72] and the experimental technique has since been improved. The molecule presented as a candidate for this class of experiments in the next chapter is particularly promising and seems to be the first existing molecule that displays PV vibrational frequency shifts within the experimental resolution.

Chapter 8

PV vibrational frequency shifts

The possibility of detecting molecular PV in vibrational spectra of chiral molecules is discussed, including the results of a previous attempted measurement [72]. The calculation of weak interaction induced vibrational splittings is reviewed and results for a newly synthesized chiral actinide compound [271] are presented. This molecule displays particularly large PV effects, that could be detected with the resolution obtained previously [72], but may not be ideally suited for experimental purposes due to a possibly large tunneling splitting.

8.1   Motivation

Computational tools are now sufficiently evolved to predict PV effects for a large variety of spectroscopic experiments and molecules but, despite numerous attempts, [22, 72, 78, 140, 141] the effect has yet to be observed. The reason for this is that for most experimentally suitable compounds the size of the effects is several orders of magnitude below the best possible resolution of the experiments. A good example for this is the very promising attempt to measure PV effects using infrared spectroscopy of bromochlorofluoromethane (CHBrClF) [72] discussed in Section 2.2.

PV splittings of molecular vibrational frequencies approximately scale with nuclear charge Z to the power five, and thus compounds containing heavy metal centers could be of greater experimental value than the originally used organic molecules. Calculations on molecules containing e.g. bismuth, rhenium, mercury and astatine have been reported, [146–149] but so far the relatively rare chiral actinide compounds have not been investigated with respect to PV properties.

The recent synthesis of the actinide methylidene complex $[H_2C = ThFCl]$ (chlorofluoromethylidenethorium), [271] the R–enantiomer of which is depicted in Figure 8.1, has prompted the quasirelativistic ZORA calculations of PV energy differences and vibrational frequency shifts reported here. The PV energy difference for this compound is of the order of 10^{-14} E_h, the relative PV frequency splitting of the Th–F stretching frequency between the enantiomers is about 10^{-12} and one of the largest ever to be reported for an existing molecule. It would be observable with an experiment of the kind reported in Ref. [72] and it seems that actinide chemistry offers some interesting prospects for molecular PV experiments.

8.2   Calculation of PV vibrational frequency splittings

8.2.1   Methodology

The approach pursued here in order to calculate PV vibrational frequency splittings has been described in detail in Ref. [149]. Only a brief synopsis will be given subsequently, in order to make this chapter comprehensive. For the task at hand it is necessary to determine the PV energy correction to the nth vibrational level, $E_{n,\text{PV}}$. To first order perturbation theory, this is given by:

$$E_{n,\text{PV}}^{(R/S)} \approx \left\langle \Psi_n^{(R/S)} \left| V_{\text{PV}} \right| \Psi_n^{(R/S)} \right\rangle. \tag{8.1}$$

$\left| \Psi_n^{(R/S)} \right\rangle$ is the nth vibrational wavefunction of the R– or S–enantiomer and can be determined by solving the parity–conserving rovibrational Schrödinger equation of the molecule. V_{PV} is the parity violating potential which, in this approach, is related to the ZORA expression 5.89 of Refs. [58, 59] derived in Section 5.4, which is evaluated at fixed nuclear coordinates. Because of the parity conserving rovibrational potential,

$$\left| \Psi_n^{(S)} \right\rangle = \hat{P} \left| \Psi_n^{(R)} \right\rangle \tag{8.2}$$

and the PV energy difference between the nth vibrational levels of two enantiomers is given by:

$$\Delta E_{n,\text{PV}} = E_{n,\text{PV}}^{(R)} - E_{n,\text{PV}}^{(S)} \approx 2 \left\langle \Psi_n^{(R)} \left| V_{\text{PV}} \right| \Psi_n^{(R)} \right\rangle. \tag{8.3}$$

In order to determine the vibrational wavefunction, the separable anharmonic adiabatic approximation of Ref. [272] was employed, in which $\left| \Psi_n^{(R/S)} \right\rangle$ is approximated to first

order as a product of one–dimensional anharmonic wavefunctions n_i computed for one–dimensional cuts through the potential energy hypersurface along the normal coordinates q_i:

$$|\Psi_n\rangle \approx |n_1, n_2, \ldots, n_{3N_{\mathrm{nuc}}-6}\rangle, \tag{8.4}$$

where $3N_{\mathrm{nuc}} - 6$ is the number of vibrational degrees of freedom of the molecule. If one assumes he PV potential to be similarly separable:

$$V_{\mathrm{PV}} \approx \sum_{i=1}^{3N_{\mathrm{nuc}}-6} V_{\mathrm{PV}}(q_i), \tag{8.5}$$

the first order PV energy shift for a vibrational mode i of an enantiomer is given by:

$$E_{n,\mathrm{PV}}^i \approx \langle n_i | V_{\mathrm{PV}}(q_i) | n_i \rangle, \tag{8.6}$$

and the PV frequency shift of a vibrational transition in a specific mode i is

$$h\nu_{\mathrm{PV}}^i \approx \left[\langle n_i' | V_{\mathrm{PV}}(q_i) | n_i' \rangle - \langle n_i | V_{\mathrm{PV}}(q_i) | n_i \rangle \right], \tag{8.7}$$

where n_i and n_i' are the initial and final states, respectively. The corresponding frequency splitting between the R– and S–enantiomers of a chiral molecule is given by:

$$\Delta\nu_{\mathrm{PV}}^i = \nu_{\mathrm{PV}}^{i(R)} - \nu_{\mathrm{PV}}^{i(S)} = 2\nu_{\mathrm{PV}}^{i(R)}. \tag{8.8}$$

8.2.2 Computational details

After optimization of the $[H_2C = ThFCl]$ geometry, gas-phase harmonic frequencies at the equilibrium structure were calculated using density functional theory (DFT) and a scalar–relativistic pseudopotential on thorium. Details are described in Appendix B and the results, which are in good agreement with those reported in Ref. [271], are listed in Table B.19. The Th–F stretching frequency is 534 cm^{-1}, which would be ideal for first overtone excitation by CO_2 laser radiation.

At equilibrium geometry a CASSCF calculation was performed in order to determine the extent to which the molecule can be described by a single determinantal wavefunction.[1] The thorium complex has a closed shell ground state, the multi reference character of which is small. This makes it accessible to a theoretical investigation using the two-component ZORA approach to molecular PV of Refs. [58, 59] discussed in Chapters 4 and 5.

---

[1] This was undertaken by T. Isaev.
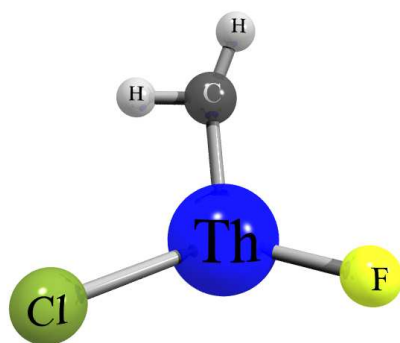
Figure 8.1: R–enantiomer of $[H_2C = ThFCl]$ (chlorofluoromethylidenethorium).
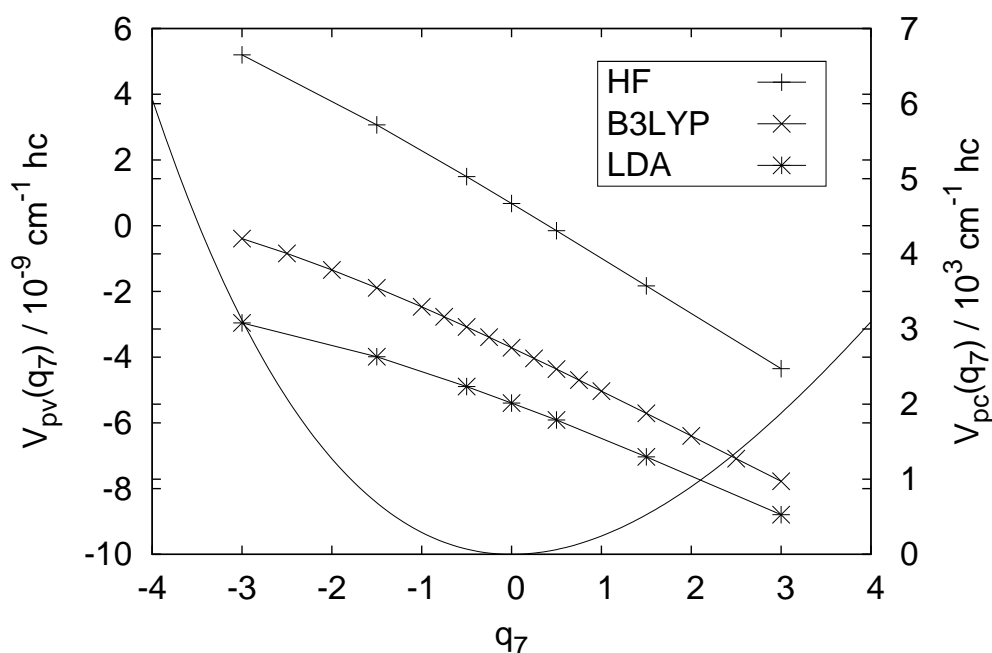
Figure 8.2: PV potentials (solid lines with symbols $+$, x and $*$; left ordinate) and parity conserving potential (solid line; right ordinate) as a function of the dimensionless reduced normal coordinate q_7 corresponding to the Th–F stretching normal mode of the R–enantiomer of $[H_2C = ThFCl]$.

The parity conserving electronic energy was calculated along the dimensionless reduced normal coordinate q_7, corresponding to the Th–F stretching mode (solid line in Fig. 8.2). This potential curve was then used to solve the parity conserving vibrational Schrödinger equation and determine the expectation values of q_7^x with $x = 1, \ldots, 5$.

V_{PV} was calculated for selected values of q_7 (solid lines with symbols in Fig. 8.2) according to Eq. 5.89 and a polynomial fit of the data was used to calculate the expectation values of $V_{PV} \approx \sum_{x=0}^{4} p_x^{(7)} q_7^x$ for the lowest vibrational levels of the Th–F stretching

mode. The expectation values of q_7^x for the two lowest vibrational levels and the coefficients $p_x^{(7)}$ are listed in Table B.20.

8.3 Results and discussion

The PV potential V_{PV} was calculated for the R–enantiomer of $[\mathrm{H_2C = ThFCl}]$ at equilibrium geometry, see Table 8.1. The value of V_{PV} depends quite strongly on the choice of density functional and has a different sign in Hartree–Fock and density functional theory. A previous ZORA study of PV potentials and frequency shifts in chiral polyhalomethanes already showed similar strong dependence of the properties on the method used.[149] The overall ordering from HF over B3LYP, BLYP to LDA has also been previously observed in calculations of PV potentials [149]. V_{PV} is found to be of the order of 10^{-14} $\mathrm{E_h}$ or 10^{-9} $\mathrm{cm^{-1}}$, comparable to some other compounds with similarly heavy centers. [147, 149]

Table 8.1: PV potential V_{PV} at the equilibrium geometry of the R–enantiomer of $[\mathrm{H_2C = ThFCl}]$. Calculations were performed using Hartree–Fock (HF) and density functional theory with different functionals (B3LYP, BLYP and LDA). Basis sets used are listed in Table B.21. Entries are given in 10^{-14} $\mathrm{E_h}$.

	HF	B3LYP	BLYP	LDA
V_{PV}	0.31	-1.69	-2.32	-2.46

PV frequency differences between the two enantiomers relative to the base frequencies $\nu_1 = 530.18$ $\mathrm{cm^{-1}}$ and $\nu_2 = 1057.20$ $\mathrm{cm^{-1}}$ of the rovibrational Schrödinger equation are listed in Table 8.2.

The listed values of $\Delta\nu_{\mathrm{PV}}/\nu \approx 10^{-12}$ are significantly bigger than those reported for other chiral compounds containing heavy metal centers [146–148, 273] and of the same order of magnitude as in the hypothetical CHAtFI molecule of Ref. [149]. The variation in the relative frequency splittings between different methods is much smaller than the one found for values of V_{PV}. This can possibly be ascribed to the small variation in the slope of the PV potential depicted in Figure 8.2, a phenomenon which has been observed also for the chiral polyhalomethanes studied in Refs. [149, 274].

Table 8.2: PV relative vibrational frequency splittings $\Delta\nu_{\mathrm{PV}}^{0-1}/\nu_1$ and $\Delta\nu_{\mathrm{PV}}^{0-2}/\nu_2$ between the Th–F stretching fundamental of the R– and S–enantiomers of $[\mathrm{H_2C = ThFCl}]$ for the 0–1 and 0–2 vibrational transitions, respectively. Calculation of the frequency differences was based on computations of V_{PV} using Hartree–Fock theory (HF) and different density functionals (B3LYP and LDA). Values are dimensionless and given in multiples of 10^{-12}. The negative sign indicates that for the R–enantiomer PV effects lead to a decrease of the vibrational frequency.

	HF	B3LYP	LDA
$\Delta\nu_{\mathrm{PV}}^{0-1}/\nu_1$	-0.885	-0.764	-0.696
$\Delta\nu_{\mathrm{PV}}^{0-2}/\nu_2$	-0.875	-0.756	-0.688

A reason for the big $\Delta\nu_{\mathrm{PV}}/\nu \approx 10^{-12}$ value in this compound is the favorable interplay of harmonic and anharmonic contributions. As is easily seen from Figure 8.2 both the first and second derivatives of the PV potential with respect to q_7 are negative around the equilibrium geometry. The anharmonicity of the parity conserving potential, on the other hand, ensures that the expectation values of q_7, q_7^2, q_7^3 and q_7^4 are all positive. Under these circumstances, the dominant contributions to $V_{\mathrm{PV}}(q_7)$ all enter with the same sign and there is no cancellation between harmonic and anharmonic contributions.

Unfortunately, the tunneling splitting for this compound is expected to be rather large. the barrier for interconversion from one enantiomer to the other was calculated to be $0.00326\ \mathrm{E_h}$ or $715\ \mathrm{cm}^{-1}$ at DFT level, a fairly small value, which indicates that chiral dynamics are determined by tunneling and not parity violation. It is possible, however, to "tune" tunneling effects by deuteration or substitution (see Ref. [152] for a summary), so that a compound derived from $[\mathrm{H_2C = ThFCl}]$ might still be suited for an experiment. A small barrier for stereomutation might also impair the quality of the approximation for the PV energy shift of a given vibrational level made in Eq. 8.1 (see e.g. Refs. [275] or [149]).

In summary, PV vibrational frequency splittings $\Delta\nu_{\mathrm{PV}}$ of the Th–F stretching mode for the newly synthesized chiral actinide compound $[\mathrm{H_2C = ThFCl}]$[271] have been calculated. The resulting relative frequency splitting $\Delta\nu_{\mathrm{PV}}/\nu$ of about 10^{-12} could in principle be observed in high–resolution laser spectroscopy which, it is hoped, can achieve a precision several orders of magnitude beyond this value of up to 10^{-16}.[145] It is also the biggest relative frequency splitting reported for an existing molecule, so far. It is conceivable, that the uranium homologue $[\mathrm{H_2C = UFCl}]$ of the thorium compound studied herein, which has also been synthesized,[271] would display even bigger PV effects, but

a theoretical analysis of the properties of this compound is much more demanding due to its more complicated ground state electronic structure.

Up to now, chiral actinide compounds had not been considered with respect to parity violation, as both theoreticians and experimentalists were focusing on main group elements and, more recently, some transition metal compounds. Even though the compound studied herein may not be suitable for a spectroscopic experiment due to the expected large tunneling splitting and other factors such as enantiomeric separability, the results presented here show that the rare chiral actinide compounds could be very valuable in attempts to measure molecular parity violation and the search for candidate molecules should be extended to include them.

Chapter 9

Summary and outlook

It was the goal of this work to add to the understanding of weak interaction–induced violation of mirror symmetry (parity) in chiral molecules. The intra–molecular (fundamental) weak interaction theoretically causes small differences in the electronic energies and spectroscopic properties of the two enantiomers (mirror image forms) of a chiral molecule. The induced effects are so small, however, that an experimental observation has not been accomplished so far.

In order to learn more about the effect and possibly assist in the planning of experiments, a theoretical approach to the calculation of parity violating (PV) nuclear magnetic resonance (NMR) shielding tensors of chiral molecules has been developed during the course of this thesis. The method includes relativistic effects on the level of the zeroth order regular approximation (ZORA) and effects of electron correlation through the use of density functional theory (DFT). It was the first approach to include both these aspects of electronic structure theory in the *ab initio* calculation of PV NMR properties and is based on the ZORA approach to molecular parity violation previously used to calculate PV energy differences between enantiomers.[58, 59]

The series of dihydrogen dichalcogenides (H_2X_2 with X=^{17}O, ^{33}S, ^{77}Se, ^{125}Te or ^{209}Po) was used to study the reliability of the ZORA approach and systematics of PV NMR frequency splittings between enantiomers.[57] Results obtained in the nonrelativistic limit of the ZORA approach reproduce those published in Ref. [66] and the observed scaling behavior of PV NMR frequency splittings with the charge Z of the nucleus under study (Z^3 scaling for the paramagnetic and Z^5 scaling for the spin–orbit coupling contributions) is in line with earlier order of magnitude estimates [6] when relativistic enhancement factors [67] are included. The usual $\sin(2\alpha)$–like conformational dependence of PV properties in these molecules on the dihedral angle α is observed for the isotropic

NMR shielding constant in all dihydrogen dichalcogenides. Due to discrepancies between these and four–component Diarc–Hartree–Fock–Coulomb (DHFC) calculations of PV NMR properties [68] an instability in the DHFC study of H_2Po_2 was discovered.[69]

The method was then used to start investigating different compounds possibly suited for a measurement aimed at detecting PV effects in NMR spectra of chiral molecules. The estimated experimental resolution is such that PV frequency splittings of ca 10 mHz could be detected,[56] but such a big effect has, so far, only been predicted for the hypothetical H_2Po_2 molecule at a specific conformation.[57] The estimate does however support an experimental preference for compounds containing heavy nuclei in conventional NMR spectroscopy, in connection with the above mentioned scaling behavior of up to Z^5. The possibility of performing relativistic calculations is therefore of particular importance in the investigation of experimentally suitable compounds.

^{195}Pt is one of the most interesting NMR active nuclei to study in this context, due to its large charge number Z and high gyromagnetic ratio. Three Pt complexes were considered as experimental candidates, of which one shows a particularly large PV NMR frequency splitting of approximately 400 μHz at equilibrium geometry and might be considered promising for a first attempt to measure these frequency splittings in chiral molecules.[70] For a platinum test complex, a similar dependence of the PV NMR frequency splittings on the dihedral angle as in the dihydrogen dichalcogens was observed, and this type of conformational dependence might well be exploited in order to design experimentally suited molecules.

Another nucleus that is of interest for the investigation of PV NMR effects is ^{183}W. For a set of tungsten model complexes $NWXYZ$ the effect of atomic substitution in the immediate neighborhood of ^{183}W in the chiral center of the molecule was investigated. Substitution seems to have an even more pronounced effect on the PV NMR frequency splittings than on PV energy differences between enantiomers, and a three order of magnitude difference between the highest and lowest ^{183}W PV NMR frequency splittings was found for the investigated series.[71] It seems that in the design of compounds optimized to present large PV NMR effects, the focus should be on surrounding the heavy nucleus under study with a very heterogeneous set of ligands, whereas the presence of further heavy nuclei might of lesser importance in comparison.

While the focus on NMR spectroscopy as a means to detect molecular parity violation has been increasing only recently, vibrational spectroscopy has long been considered a good choice for such a measurement.[51, 72] These two different experimental approaches are complementary in the sense that they do not measure the same effect. PV shifts in NMR frequencies are probably dominated by the nuclear spin–dependent PV interaction, whereas changes in the vibrational spectra would be interpreted as an effect of the

nuclear spin–independent PV interaction. During the course of this thesis PV effects in the vibrational spectrum of a recently synthesized chiral actinide compound have been calculated. The compound shows the largest vibrational splittings ever predicted for an existing molecule which could be detected with currently available experimental methods.[72, 73] A drawback is that the barrier for stereomutation in this compound is quite low so that chiral dynamics would likely be dominated by tunneling instead of parity violation.[74] This could possibly be changed, however, by means of isotopic substitution so that this or similar compounds should be considered in the planning of new experiments.

Future methodological work will include the extension of the approach presented here to a bigger variety of electronic structure methods, e.g. hybrid functionals within the DFT framework and Hartree–Fock theory, which will be helpful, in particular, when dealing with transition metal compounds. The inclusion of a method that alleviates dependence on the gauge origin of the magnetic field is also important, as it would drastically decrease computational expenditure. The approach will also be extended to include different molecular properties. For example, a recently presented experiment for the detection of nuclear spin–spin couplings at zero magnetic field [75] seems very interesting for a measurement of PV effects in these quantities and an extension of the ZORA approach to calculate them is pending.

From a phenomenological point of view, it is still unclear which factors determine whether or not a specific chiral compound displays large PV properties. Understanding this, however, would enable one to efficiently screen experimentally suitable molecules or help in the design of molecules optimized for experiment. Scaling of PV effects with nuclear charge is already utilized in the search for candidate compounds but there are certainly other important features. The studies presented here on the impact of conformational changes and atomic substitution on PV NMR frequency splittings indicate that the size of these splittings is correlated with the degree of asymmetry of the electronic environment of the nucleus under study. An understanding of chirality as an incremental property is clearly necessary when dealing with these phenomena. Another factor contributing to the size of PV effects could be the magnitude of spin–orbit coupling effects in the molecule. Understanding these different aspects and developing qualitative models to assess their impact on PV properties swiftly and without much computational effort is a direction or research that will greatly benefit this field.

Appendix A

Energy derivatives

A.1 Calculation of the electronic Hessian

In order to calculate the electronic Hessian introduced in equation 5.34, it is necessary to expand the total energy of the system, given by equation 5.27,

$$E\left(\kappa\right) = \sum_{pq} \left[z_{pq}^{\text{zora}} + l_{pq}^{\eta}\left(\kappa\right) + v_{pq}^{\text{xc}}\left(\kappa\right) + v_{pq}'(\vec{T})\right] \tilde{D}_{pq}\left(\kappa\right) + V_{NN}, \tag{A.1}$$

in terms of the parameters of the variational wavefunction.

The first step is to expand elements of the density matrix $\tilde{\mathbf{D}}$ with respect to the matrix elements κ_{pq} of the operator $\hat{\kappa}$ defined in equation 5.6:

$$\tilde{D}_{pq} = \left\langle 0 \left|\hat{a}_p^\dagger \hat{a}_q\right| 0 \right\rangle + \sum_{rs} \frac{\partial \tilde{D}_{pq}}{\partial \kappa_{rs}}\bigg|_{\kappa=\mathbf{0}} \kappa_{rs} + \frac{1}{2}\sum_{rs,tu} \frac{\partial^2 \tilde{D}_{ps}}{\partial \kappa_{tu}\partial \kappa_{rs}}\bigg|_{\kappa=\mathbf{0}} \kappa_{tu}\kappa_{rs} + \mathcal{O}\left(\kappa^3\right). \tag{A.2}$$

Using the Baker–Campbell–Hausdorff expansion of $\tilde{D}_{rs}$ given by equation 5.13, the derivatives of $\tilde{D}_{rs}$ with respect to the κ_{pq} are given by:

$$\frac{\partial \tilde{D}_{pq}}{\partial \kappa_{rs}} = \left\langle 0 \left|\left[\hat{a}_r^\dagger\hat{a}_s, \hat{a}_p^\dagger\hat{a}_q\right]\right| 0 \right\rangle + \frac{1}{2}\left(\left\langle 0 \left|\left[\hat{\kappa}, \left[\hat{a}_r^\dagger\hat{a}_s, \hat{a}_p^\dagger\hat{a}_q\right]\right]\right| 0 \right\rangle + \left\langle 0 \left|\left[\hat{a}_r^\dagger\hat{a}_s, \left[\hat{\kappa}, \hat{a}_p^\dagger\hat{a}_q\right]\right]\right| 0 \right\rangle\right) + \mathcal{O}\left(\kappa^2\right)$$

$$\frac{\partial^2 \tilde{D}_{pq}}{\partial \kappa_{tu}\partial \kappa_{rs}} = \frac{1}{2}\left(\left\langle 0 \left|\left[\hat{a}_t^\dagger\hat{a}_u, \left[\hat{a}_r^\dagger\hat{a}_s, \hat{a}_p^\dagger\hat{a}_q\right]\right]\right| 0 \right\rangle + \left\langle 0 \left|\left[\hat{a}_r^\dagger\hat{a}_s, \left[\hat{a}_t^\dagger\hat{a}_u, \hat{a}_p^\dagger\hat{a}_q\right]\right]\right| 0 \right\rangle\right) + \mathcal{O}\left(\kappa\right),$$

and consequently $\tilde{D}_{pq}$ takes the form (see e.g. Ref. [218]):

$$\tilde{D}_{pq} = N_{pq} + \sum_{rs} \left\langle 0 \left|\left[\hat{a}_r^\dagger\hat{a}_s, \hat{a}_p^\dagger\hat{a}_q\right]\right| 0 \right\rangle \kappa_{rs} + \frac{1}{2}\sum_{rs,tu} \left\langle 0 \left|\left[\hat{a}_r^\dagger\hat{a}_s, \left[\hat{a}_t^\dagger\hat{a}_u, \hat{a}_p^\dagger\hat{a}_q\right]\right]\right| 0 \right\rangle \kappa_{tu}\kappa_{rs} + \mathcal{O}\left(\kappa^3\right),$$

$$\tag{A.3}$$

where the occupation number matrix $\mathbf{N}$ with elements

$$N_{pq} = \left\langle 0 \left| \hat{a}_p^\dagger \hat{a}_q \right| 0 \right\rangle = \delta_{pq} n_p \qquad (A.4)$$

has been introduced. The n_p are equal to one if the orbital p is occupied in $|0\rangle$ and zero otherwise.

Using this expansion, the one–electron contributions to the Hessian and the two-electron contributions stemming from the operator $\hat{l}^\eta \left[\rho \right]$ can readily be calculated. The expansion of the two–electron Coulomb and exchange contributions to the energy in terms of κ is given by:

$$\sum_{pq} l_{pq}^\eta \left(\kappa \right) \tilde{D}_{pq} \left(\kappa \right) = \sum_{pqrs} \left[(\phi_p \phi_q | \phi_r \phi_s) - \eta \left(\phi_p \phi_s | \phi_r \phi_q \right) \right] \tilde{D}_{rs} \left(\kappa \right) \tilde{D}_{pq} \left(\kappa \right)$$

$$= \sum_{pqrs} \Lambda_{pqrs}^\eta \left[N_{rs} N_{pq} + \sum_{tu} \left(N_{rs} \left\langle 0 \left| \left[\hat{a}_t^\dagger \hat{a}_u, \hat{a}_p^\dagger \hat{a}_q \right] \right| 0 \right\rangle \right. \right.$$

$$\left. + N_{pq} \left\langle 0 \left| \left[\hat{a}_t^\dagger \hat{a}_u, \hat{a}_r^\dagger \hat{a}_s \right] \right| 0 \right\rangle \right) \kappa_{tu} + \sum_{tuvw} \left(\frac{1}{2} N_{rs} \left\langle 0 \left| \left[\hat{a}_t^\dagger \hat{a}_u, \left[\hat{a}_v^\dagger \hat{a}_w, \hat{a}_p^\dagger \hat{a}_q \right] \right] \right| 0 \right\rangle \right.$$

$$+ \frac{1}{2} N_{pq} \left\langle 0 \left| \left[\hat{a}_t^\dagger \hat{a}_u, \left[\hat{a}_v^\dagger \hat{a}_w, \hat{a}_r^\dagger \hat{a}_s \right] \right] \right| 0 \right\rangle$$

$$\left. \left. + \left\langle 0 \left| \left[\hat{a}_t^\dagger \hat{a}_u, \hat{a}_p^\dagger \hat{a}_q \right] \right| 0 \right\rangle \left\langle 0 \left| \left[\hat{a}_v^\dagger \hat{a}_w, \hat{a}_r^\dagger \hat{a}_s \right] \right| 0 \right\rangle \right) \kappa_{tu} \kappa_{vw} + \mathcal{O} \left(\kappa^3 \right) \right]$$

$$= \sum_{pqrs} \Lambda_{pqrs}^\eta \left[N_{rs} N_{pq} + 2 \sum_{tu} N_{rs} \left\langle 0 \left| \left[\hat{a}_t^\dagger \hat{a}_u, \hat{a}_p^\dagger \hat{a}_q \right] \right| 0 \right\rangle \kappa_{tu} \right.$$

$$+ \sum_{tuvw} \left(N_{rs} \left\langle 0 \left| \left[\hat{a}_t^\dagger \hat{a}_u, \left[\hat{a}_v^\dagger \hat{a}_w, \hat{a}_p^\dagger \hat{a}_q \right] \right] \right| 0 \right\rangle \right.$$

$$\left. \left. + \left\langle 0 \left| \left[\hat{a}_t^\dagger \hat{a}_u, \hat{a}_r^\dagger \hat{a}_s \right] \right| 0 \right\rangle \left\langle 0 \left| \left[\hat{a}_v^\dagger \hat{a}_w, \hat{a}_p^\dagger \hat{a}_q \right] \right| 0 \right\rangle \right) \kappa_{tu} \kappa_{vw} + \mathcal{O} \left(\kappa^3 \right) \right],$$

$$(A.5)$$

where the symmetry in pq and rs stemming from the expansion of $\tilde{D}_{pq}$ and $\tilde{D}_{rs}$ has been transferred to the two-electron matrix elements which satisfy the condition $\Lambda_{pqrs}^\eta = \Lambda_{rspq}^\eta$ using

$$\Lambda_{pqrs}^\eta = (\phi_p \phi_q | \phi_r \phi_s) - \eta \left(\phi_p \phi_s | \phi_r \phi_q \right). \qquad (A.6)$$

The contributions from the exchange–correlation potential have to be calculated with regard to the possible dependence of the functional on the local spin densities $\rho_\uparrow$ and $\rho_\downarrow$ defined in Eqs. 5.18 and 5.19, respectively (for a details of the non–collinear approach in the ZORA framework see Ref. [234]). The exchange–correlation energy defined in terms

of the exchange–correlation functional is given by:

$$E^{\mathrm{XC}} = \int \mathrm{d}^3 r \varepsilon^{\mathrm{XC}} \left[\rho_\uparrow, \rho_\downarrow\right]. \tag{A.7}$$

A possible dependence of the functionals on gradients of the local spin densities is neglected here for simplicity.

Expanding the energy density in terms of the matrix elements of the operator $\hat{\kappa}$ yields:

$$\varepsilon^{\mathrm{XC}}\left[\rho_\uparrow, \rho_\downarrow\right] = \varepsilon^{\mathrm{XC}}\left[\rho_{\uparrow 0}, \rho_{\downarrow 0}\right] + \sum_{pq} \left(\frac{\delta\varepsilon^{\mathrm{XC}}}{\delta\rho_\uparrow}\frac{\partial\rho_\uparrow}{\partial\kappa_{pq}} + \frac{\delta\varepsilon^{\mathrm{XC}}}{\delta\rho_\downarrow}\frac{\partial\rho_\downarrow}{\partial\kappa_{pq}}\right)\Bigg|_{\hat{\kappa}=0} \kappa_{pq}$$
$$+ \frac{1}{2}\sum_{pqrs}\left(\frac{\delta^2\varepsilon^{\mathrm{XC}}}{\delta\rho_\uparrow^2}\frac{\partial\rho_\uparrow}{\partial\kappa_{rs}}\frac{\partial\rho_\uparrow}{\partial\kappa_{pq}} + \frac{\delta^2\varepsilon^{\mathrm{XC}}}{\delta\rho_\downarrow^2}\frac{\partial\rho_\downarrow}{\partial\kappa_{rs}}\frac{\partial\rho_\downarrow}{\partial\kappa_{pq}} + \frac{\delta\varepsilon^{\mathrm{XC}}}{\delta\rho_\uparrow}\frac{\partial^2\rho_\uparrow}{\partial\kappa_{rs}\partial\kappa_{pq}}\right.$$
$$\left. + \frac{\delta\varepsilon^{\mathrm{XC}}}{\delta\rho_\downarrow}\frac{\partial^2\rho_\downarrow}{\partial\kappa_{rs}\partial\kappa_{pq}} + 2\frac{\delta^2\varepsilon^{\mathrm{XC}}}{\delta\rho_\uparrow\delta\rho_\downarrow}\frac{\partial\rho_\uparrow}{\partial\kappa_{rs}}\frac{\partial\rho_\downarrow}{\partial\kappa_{pq}}\right)\Bigg|_{\kappa=0}\kappa_{pq}\kappa_{rs} + \mathcal{O}\left(\kappa^3\right). \tag{A.8}$$

According to equations 5.18 and 5.19 the local spin densities are given by:[234]

$$\rho_\uparrow = \frac{1}{2}\left(\rho + s\right) \tag{A.9}$$

$$\rho_\downarrow = \frac{1}{2}\left(\rho - s\right), \tag{A.10}$$

In order to calculate the derivatives of the local spin densities with respect to the κ_{pq}, it is necessary to determine the corresponding derivatives of the absolute value of the magnetization $s = |\vec{m}|$ and the density ρ. A Taylor expansion of s around $\kappa = \mathbf{0}$ yields:

$$s = s_0 + \sum_{pq}\frac{\partial s}{\partial\kappa_{pq}}\Bigg|_{\kappa=\mathbf{0}}\kappa_{pq} + \frac{1}{2}\sum_{pqrs}\frac{\partial^2 s}{\partial\kappa_{pq}\partial\kappa_{rs}}\Bigg|_{\kappa=\mathbf{0}}\kappa_{pq}\kappa_{rs} + \mathcal{O}\left(\kappa^3\right) \tag{A.11}$$

with

$$\frac{\partial s}{\partial\kappa_{pq}}\Bigg|_{\kappa=\mathbf{0}} = \sum_{lm}\frac{\partial s}{\partial\tilde{D}_{lm}}\frac{\partial\tilde{D}_{lm}}{\partial\kappa_{pq}}\Bigg|_{\kappa=\mathbf{0}} \tag{A.12}$$

and

$$\frac{\partial^2 s}{\partial\kappa_{rs}\partial\kappa_{pq}}\Bigg|_{\kappa=\mathbf{0}} = \sum_{lm}\left(\frac{\partial s}{\partial\tilde{D}_{lm}}\frac{\partial^2\tilde{D}_{lm}}{\partial\kappa_{rs}\partial\kappa_{pq}} + \sum_{no}\frac{\partial^2 s}{\partial\tilde{D}_{no}\partial\tilde{D}_{lm}}\frac{\partial\tilde{D}_{no}}{\partial\kappa_{rs}}\frac{\partial\tilde{D}_{lm}}{\partial\kappa_{pq}}\right)\Bigg|_{\kappa=\mathbf{0}}. \tag{A.13}$$

From equation 5.21 and $s = |\vec{m}|$ one finds:

$$\frac{\partial s}{\partial\tilde{D}_{lm}} = \left(\nabla_{\vec{m}}s\right)\cdot\frac{\partial}{\partial\tilde{D}_{lm}}\vec{m} = \frac{\vec{m}}{|\vec{m}|}\cdot\vec{\Sigma}_{lm}\left(\vec{r}\right), \tag{A.14}$$

where $\nabla_{\vec{m}}$ denotes the gradient with respect to $\vec{m}$: $\nabla_{\vec{m}} = (\partial/\partial m_x, \partial/\partial m_y, \partial/\partial m_z)$. The second order contribution vanishes:

$$
\begin{aligned}
\frac{\partial^2 s}{\partial \tilde{D}_{no} \partial \tilde{D}_{lm}} &= \frac{\partial}{\partial \tilde{D}_{no}} \vec{\Sigma}_{lm} \left(\vec{r} \right) \cdot \frac{\vec{m}}{|\vec{m}|} \\
&= \vec{\Sigma}_{lm} \cdot \left\{ \left(\frac{\partial}{\partial \tilde{D}_{no}} \vec{m} \right) \frac{1}{|\vec{m}|} + \vec{m} \left(\frac{\partial}{\partial \tilde{D}_{no}} \frac{1}{|\vec{m}|} \right) \right\} \\
&= \frac{1}{|\vec{m}|} \vec{\Sigma}_{lm} \vec{\Sigma}_{no} + \vec{m} \left(2 \vec{\Sigma}_{no} \cdot \vec{m} \left(-\frac{1}{2} \frac{1}{|\vec{m}|^3} \right) \right) \cdot \vec{\Sigma}_{lm} \\
&= 0.
\end{aligned}
\tag{A.15}
$$

Using the expansion of $\tilde{\mathbf{D}}$ in terms of the κ_{pq}, equation A.3 and introducing the zero order magnetization $\vec{m}_0$ and magnetization direction $\vec{e}_{m_0}$:

$$
\vec{m}_0 = \sum_{pq} \vec{\Sigma}_{pq} \left(\vec{r} \right) \left\langle 0 \left| p^\dagger q \right| 0 \right\rangle
\tag{A.16}
$$

$$
\vec{e}_{m_0} = \frac{\vec{m}_0}{|\vec{m}_0|}
\tag{A.17}
$$

as well as the projection of the spin-dependent orbital overlap density $\vec{\Sigma}_{pq}$ defined in equation 5.25 on the zero order magnetization direction:

$$
\Sigma^{p0}_{pq} \left(\vec{r} \right) = \vec{\Sigma}_{lm} \left(\vec{r} \right) \cdot \vec{e}_{m_0},
\tag{A.18}
$$

s can be expressed as:

$$
s = s_0 + \sum_{pqlm} \Sigma^{p0}_{lm} \left\langle 0 \left| \left[\hat{a}_p^\dagger \hat{a}_q, \hat{a}_l^\dagger \hat{a}_m \right] \right| 0 \right\rangle \kappa_{pq} + \frac{1}{4} \sum_{pqrslm} \Sigma^{p0}_{lm} \left\langle 0 \left| \left[\hat{a}_r^\dagger \hat{a}_s, \left[\hat{a}_p^\dagger \hat{a}_q, \hat{a}_l^\dagger \hat{a}_m \right] \right] \right| 0 \right\rangle \kappa_{pq} \kappa_{rs} + \mathcal{O} \left(\kappa^3 \right).
\tag{A.19}
$$

In the same fashion, again using the expansion of $\tilde{\mathbf{D}}$ in terms of the κ_{pq}, equation A.3 and the expression for the density given in equation 5.20, ρ is given by (see also, for example, Refs [218, 230, 239]):

$$
\rho = \rho_0 + \sum_{pqrs} \Omega_{lm} \left\langle 0 \left| \left[\hat{a}_p^\dagger \hat{a}_q, \hat{a}_l^\dagger \hat{a}_m \right] \right| 0 \right\rangle \kappa_{pq} + \frac{1}{4} \sum_{pqrslm} \Omega_{lm} \left\langle 0 \left| \left[\hat{a}_r^\dagger \hat{a}_s, \left[\hat{a}_p^\dagger \hat{a}_q, \hat{a}_l^\dagger \hat{a}_m \right] \right] \right| 0 \right\rangle \kappa_{pq} \kappa_{rs} + \mathcal{O} \left(\kappa^3 \right),
\tag{A.20}
$$

where the orbital overlap density defined in equation 5.24 has been used.

With the results presented in equations A.20 and A.19 derivatives of the spin densities $\rho_\uparrow$ and $\rho_\downarrow$ with respect to the orbital rotation parameters are determined as follows:

$$\left.\frac{\partial \rho_\uparrow}{\partial \kappa_{pq}}\right|_{\kappa=\mathbf{0}} = \sum_{tu} \Omega_{tu}^\uparrow (\vec{r}) \left\langle 0 \left| \left[\hat{a}_p^\dagger \hat{a}_q, \hat{a}_t^\dagger \hat{a}_u \right] \right| 0 \right\rangle \tag{A.21}$$

$$\left.\frac{\partial \rho_\downarrow}{\partial \kappa_{pq}}\right|_{\kappa=\mathbf{0}} = \sum_{tu} \Omega_{tu}^\downarrow (\vec{r}) \left\langle 0 \left| \left[\hat{a}_p^\dagger \hat{a}_q, \hat{a}_t^\dagger \hat{a}_u \right] \right| 0 \right\rangle, \tag{A.22}$$

with the local spin density matrix elements $\Omega_{tu}^\uparrow$ and $\Omega_{tu}^\downarrow$

$$\Omega_{pq}^\uparrow = \frac{1}{2} \left(\Omega_{pq} + \Sigma_{pq}^{\mathrm{p0}} \right)$$

$$\Omega_{pq}^\downarrow = \frac{1}{2} \left(\Omega_{pq} - \Sigma_{pq}^{\mathrm{p0}} \right),$$

introduced in equations 5.41 and 5.42, respectively.

The second derivatives of the local spin densities with respect to the parameters of the wavefunction are given by:

$$\left.\frac{\partial^2 \rho_\uparrow}{\partial \kappa_{pq} \partial \kappa_{rs}}\right|_{\kappa=0} = \frac{1}{2} \sum_{tu} \Omega_{tu}^\uparrow (\vec{r}) \left(\left\langle 0 \left| \left[\hat{a}_r^\dagger \hat{a}_s, \left[\hat{a}_p^\dagger \hat{a}_q, \hat{a}_t^\dagger \hat{a}_u \right] \right] \right| 0 \right\rangle + \left\langle 0 \left| \left[\hat{a}_p^\dagger \hat{a}_q, \left[\hat{a}_r^\dagger \hat{a}_s, \hat{a}_t^\dagger \hat{a}_u \right] \right] \right| 0 \right\rangle \right) \tag{A.23}$$

$$\left.\frac{\partial^2 \rho_\downarrow}{\partial \kappa_{pq} \partial \kappa_{rs}}\right|_{\kappa=0} = \frac{1}{2} \sum_{tu} \Omega_{tu}^\downarrow (\vec{r}) \left(\left\langle 0 \left| \left[\hat{a}_r^\dagger \hat{a}_s, \left[\hat{a}_p^\dagger \hat{a}_q, \hat{a}_t^\dagger \hat{a}_u \right] \right] \right| 0 \right\rangle + \left\langle 0 \left| \left[\hat{a}_p^\dagger \hat{a}_q, \left[\hat{a}_r^\dagger \hat{a}_s, \hat{a}_t^\dagger \hat{a}_u \right] \right] \right| 0 \right\rangle \right). \tag{A.24}$$

Inserting equations A.21 to A.24 into the expansion of the exchange–correlation energy in terms of the κ_{pq}, Eq. A.8, one arrives at:

$$\varepsilon^{\mathrm{XC}} [\rho_\uparrow, \rho_\downarrow] = \varepsilon^{\mathrm{XC}} [\rho_{\uparrow 0}, \rho_{\downarrow 0}] + \sum_{pq} \sum_{lm} \left(\frac{\delta \varepsilon^{\mathrm{XC}}}{\delta \rho_\uparrow} \Omega_{lm}^\uparrow + \frac{\delta \varepsilon^{\mathrm{XC}}}{\delta \rho_\downarrow} \Omega_{lm}^\downarrow \right) \Bigg|_{\rho_{\uparrow/\downarrow} = \rho_{\uparrow 0/\downarrow 0}} \left\langle 0 \left| \left[\hat{a}_p^\dagger \hat{a}_q, \hat{a}_l^\dagger \hat{a}_m \right] \right| 0 \right\rangle \kappa_{pq}$$

$$+ \frac{1}{2} \sum_{pqrs} \left[\sum_{lm} \left(\frac{\delta \varepsilon^{\mathrm{XC}}}{\delta \rho_\uparrow} \Omega_{lm}^\uparrow + \frac{\delta \varepsilon^{\mathrm{XC}}}{\delta \rho_\downarrow} \Omega_{lm}^\downarrow \right) \Bigg|_{\rho_{\uparrow/\downarrow} = \rho_{\uparrow 0/\downarrow 0}} \left\langle 0 \left| \left[\hat{a}_r^\dagger \hat{a}_s, \left[\hat{a}_p^\dagger \hat{a}_q, \hat{a}_l^\dagger \hat{a}_m \right] \right] \right| 0 \right\rangle \right.$$

$$+ \sum_{lmno} \left(\frac{\delta^2 \varepsilon^{\mathrm{XC}}}{\delta \rho_\uparrow^2} \Omega_{lm}^\uparrow \Omega_{no}^\uparrow + \frac{\delta^2 \varepsilon^{\mathrm{XC}}}{\delta \rho_\downarrow^2} \Omega_{lm}^\downarrow \Omega_{no}^\downarrow + \frac{\delta^2 \varepsilon^{\mathrm{XC}}}{\delta \rho_\uparrow \delta \rho_\downarrow} \left[\Omega_{lm}^\uparrow \Omega_{no}^\downarrow + \Omega_{no}^\uparrow \Omega_{lm}^\downarrow \right] \right) \Bigg|_{\rho_{\uparrow/\downarrow} = \rho_{\uparrow 0/\downarrow 0}}$$

$$\left. \times \left\langle 0 \left| \left[\hat{a}_p^\dagger \hat{a}_q, \hat{a}_l^\dagger \hat{a}_m \right] \right| 0 \right\rangle \left\langle 0 \left| \left[\hat{a}_r^\dagger \hat{a}_s, \hat{a}_n^\dagger \hat{a}_o \right] \right| 0 \right\rangle \right] \kappa_{pq} \kappa_{rs} + \mathcal{O} \left(\kappa^3 \right). \tag{A.25}$$

The matrix elements of the electronic Hessian can now be determined using equations A.3, A.5 and A.25 in connection with the expression for the total energy, equation 5.27:

$$
\begin{aligned}
\frac{\partial^2 E\left[\rho\left(\kappa\right)\right]}{\partial \kappa_{pq} \partial \kappa_{rs}}\bigg|_{\kappa=\mathbf{0}} &= \sum_{lm}\left[z_{lm}^{\text{zora}} + v'_{lm}(\vec{T})\right]\left(\left\langle 0\left|\left[\hat{a}_r^\dagger \hat{a}_s, \left[\hat{a}_p^\dagger \hat{a}_q, \hat{a}_l^\dagger \hat{a}_m\right]\right]\right|0\right\rangle + \left\langle 0\left|\left[\hat{a}_p^\dagger \hat{a}_q, \left[\hat{a}_r^\dagger \hat{a}_s, \hat{a}_l^\dagger \hat{a}_m\right]\right]\right|0\right\rangle\right) \\
&+ \sum_{lmno}\Lambda_{lmno}^\eta \left(N_{lm}\left\langle 0\left|\left[\hat{a}_p^\dagger \hat{a}_q, \left[\hat{a}_r^\dagger \hat{a}_s, \hat{a}_n^\dagger \hat{a}_o\right]\right]\right|0\right\rangle + N_{lm}\left\langle 0\left|\left[\hat{a}_r^\dagger \hat{a}_s, \left[\hat{a}_p^\dagger \hat{a}_q, \hat{a}_n^\dagger \hat{a}_o\right]\right]\right|0\right\rangle \right. \\
&+ 2\left\langle 0\left|\left[\hat{a}_p^\dagger \hat{a}_q, \hat{a}_l^\dagger \hat{a}_m\right]\right|0\right\rangle\left\langle 0\left|\left[\hat{a}_r^\dagger \hat{a}_s, \hat{a}_n^\dagger \hat{a}_o\right]\right|0\right\rangle\bigg) \\
&+ \sum_{lm}V_{lm}^{\text{XC}}\left(\left\langle 0\left|\left[\hat{a}_p^\dagger \hat{a}_q, \left[\hat{a}_r^\dagger \hat{a}_s, \hat{a}_l^\dagger \hat{a}_m\right]\right]\right|0\right\rangle + \left\langle 0\left|\left[\hat{a}_r^\dagger \hat{a}_s, \left[\hat{a}_p^\dagger \hat{a}_q, \hat{a}_l^\dagger \hat{a}_m\right]\right]\right|0\right\rangle\right) \\
&+ \sum_{lmno}W_{lm,no}^{\text{XC}}\left\langle 0\left|\left[\hat{a}_p^\dagger \hat{a}_q, \hat{a}_l^\dagger \hat{a}_m\right]\right|0\right\rangle\left\langle 0\left|\left[\hat{a}_r^\dagger \hat{a}_s, \hat{a}_n^\dagger \hat{a}_o\right]\right|0\right\rangle, \qquad \text{(A.26)}
\end{aligned}
$$

with

$$
V_{lm}^{\text{XC}} = \frac{1}{2}\int \mathrm{d}^3 r \left(\frac{\delta\varepsilon^{\text{XC}}}{\delta\rho_\uparrow}\Omega_{lm}^\uparrow + \frac{\delta\varepsilon^{\text{XC}}}{\delta\rho_\downarrow}\Omega_{lm}^\downarrow\right)\bigg|_{\rho_{\uparrow/\downarrow}=\rho_{\uparrow 0/\downarrow 0}} \qquad \text{(A.27)}
$$

$$
W_{lm,no}^{\text{XC}} = \int \mathrm{d}^3 r \left(\frac{\delta^2\varepsilon^{\text{XC}}}{\delta\rho_\uparrow^2}\Omega_{lm}^\uparrow\Omega_{no}^\uparrow + \frac{\delta^2\varepsilon^{\text{XC}}}{\delta\rho_\downarrow^2}\Omega_{lm}^\downarrow\Omega_{no}^\downarrow + \frac{\delta^2\varepsilon^{\text{XC}}}{\delta\rho_\uparrow\delta\rho_\downarrow}\left[\Omega_{lm}^\uparrow\Omega_{no}^\downarrow + \Omega_{lm}^\downarrow\Omega_{no}^\uparrow\right]\right)\bigg|_{\rho_{\uparrow/\downarrow}=\rho_{\uparrow 0/\downarrow 0}}
$$
$$\text{(A.28)}$$

With regard to the anti-Hermiticity of the orbital rotation operator $\hat{\kappa}$, which allows for the matrix κ to be recast in vector form (equation 5.32)

$$
\vec{a} = \begin{pmatrix} \vec{\kappa} \\ \vec{\kappa}^* \end{pmatrix},
$$

one arrives at the typical structure of the Hessian given in equation 5.34:

$$
\mathbf{M} = \begin{pmatrix} \mathbf{A} & \mathbf{B} \\ \mathbf{B}^* & \mathbf{A}^* \end{pmatrix}. \qquad \text{(A.29)}
$$

Taking into account that partial derivatives should be evaluated with all perturbation parameters set to zero, the blocks of the Hessian are given by:

$$
A_{pq,rs} = \frac{\partial^2 E\left[\rho\left(\kappa\right)\right]}{\partial\kappa_{pq}^* \partial\kappa_{rs}}\bigg|_{\kappa=\mathbf{0}, \vec{T}=\vec{0}} \qquad \text{(A.30)}
$$

$$
B_{pq,rs} = \frac{\partial^2 E\left[\rho\left(\kappa\right)\right]}{\partial\kappa_{pq}^* \partial\kappa_{rs}^*}\bigg|_{\kappa=\mathbf{0}, \vec{T}=\vec{0}}, \qquad \text{(A.31)}
$$

for $p > q$ and $r > s$. Evaluation of the appropriate commutators yields:

$$A_{pq,rs} = -\left(n_p + n_r - 2n_q\right)\delta_{qs}F_{pr} - \left(n_q + n_s - 2n_r\right)\delta_{pr}F_{sq}$$
$$+ \left(n_p - n_q\right)\left(n_r - n_s\right)\left(2\Lambda^{\eta}_{pqsr} + W^{\text{XC}}_{pqsr}\right) \tag{A.32}$$

$$B_{pq,rs} = \left(n_p + n_s - 2n_q\right)\delta_{qr}F_{ps} + \left(n_q + n_r - 2n_s\right)\delta_{ps}F_{rq}$$
$$+ \left(n_p - n_q\right)\left(n_r - n_s\right)\left(2\Lambda^{\eta}_{pqrs} + W^{\text{XC}}_{pqrs}\right), \tag{A.33}$$

with the Fock matrix elements F_{pq} given by

$$F_{pq} = z^{\text{zora}}_{pq} + \sum_{i=1}^{N^{\text{occ}}} \Lambda^{\eta}_{iipq} + V^{\text{XC}}_{pq}. \tag{A.34}$$

For a closed shell system, the initial magnetization is equal to zero and in this limit $\vec{e}^{\,\text{T}}_{m_0} \to (0,0,0)$. One obtains:

$$\lim_{\vec{m}_0 \to \vec{0}} V^{\text{XC}}_{pq} = \frac{1}{4}\int \text{d}^3r \left.\left(\frac{\delta\varepsilon^{\text{XC}}}{\delta\rho_{\uparrow}} + \frac{\delta\varepsilon^{\text{XC}}}{\delta\rho_{\downarrow}}\right)\right|_{\rho_{\uparrow/\downarrow}=\rho_0} \Omega_{pq} \tag{A.35}$$

$$\lim_{\vec{m}_0 \to \vec{0}} W^{\text{XC}}_{lm,no} = \frac{1}{4}\int \text{d}^3r \left(\left.\left[\frac{\delta^2\varepsilon^{\text{XC}}}{\delta\rho^2_{\uparrow}} + \frac{\delta^2\varepsilon^{\text{XC}}}{\delta\rho^2_{\downarrow}}\right]\right|_{\rho_{\uparrow/\downarrow}=\rho_0}\left[\Omega_{lm}\Omega_{no} + \vec{\Sigma}_{lm}\cdot\vec{\Sigma}_{no}\right]\right.$$
$$\left.+2\left.\frac{\delta^2\varepsilon^{\text{XC}}}{\delta\rho_{\uparrow}\delta\rho_{\downarrow}}\right|_{\rho_{\uparrow/\downarrow}=\rho_0}\left[\Omega_{lm}\Omega_{no} - \vec{\Sigma}_{lm}\cdot\vec{\Sigma}_{no}\right]\right) \tag{A.36}$$

If non–redundant parameters are used, $\hat{\kappa}$ takes the form:

$$\hat{\kappa} = \sum_{ai}\left(\kappa_{ai}\hat{a}^{\dagger}_a\hat{a}_i - \kappa^*_{ai}\hat{a}^{\dagger}_i\hat{a}_a\right), \tag{A.37}$$

where the relation $\kappa_{ia} = -\kappa^*_{ai}$ has been used. In terms of the non-redundant parameters, the blocks of the stability matrix (equation 5.34) are given by

$$A_{ai,bj} = \left.\frac{\partial^2 E\left[\rho\left(\kappa\right)\right]}{\partial\kappa^*_{ai}\partial\kappa_{bj}}\right|_{\kappa=\mathbf{0}}$$
$$= 2\delta_{ij}F_{ab} - 2\delta_{ab}F_{ij} + 2\Lambda^{\eta}_{aijb} + W^{\text{XC}}_{ai,jb} \tag{A.38}$$

$$B_{ai,bj} = \left.\frac{\partial^2 E\left[\rho\left(\kappa\right)\right]}{\partial\kappa^*_{ai}\partial\kappa^*_{bj}}\right|_{\kappa=\mathbf{0}}$$
$$= 2\Lambda^{\eta}_{aibj} + W^{\text{XC}}_{ai,bj}. \tag{A.39}$$

A.2 Property derivatives

The individual terms that appear in the expression of a third order property as partial derivatives of the electronic energy with respect to perturbation parameters and parameters of the wavefunction, equation 5.30, can be determined from the expansion of the electronic energy in terms of the κ_{pq} of the previous section and specifically from the expansion of $\tilde{D}$ given in equation A.3.

A partial derivative with respect to one or more perturbation parameters is equal to the expectation value of the corresponding operator:

$$
\begin{aligned}
\left.\frac{\partial^n E}{\partial T_{i_1}\ldots\partial T_{i_n}}\right|_{\kappa=\mathbf{0},\vec{T}=\vec{0}} &= \left.\frac{\partial^n}{\partial T_{i_1}\ldots\partial T_{i_n}}\sum_{pq} v'_{pq}(\vec{T})\tilde{D}_{pq}\left(\kappa\right)\right|_{\kappa=\mathbf{0},\vec{T}=\vec{0}} \\
&= \sum_{pq} N_{pq}\left\langle\phi_p\left|\left.\frac{\partial^n v'(\vec{T})}{\partial T_{i_1}\ldots\partial T_{i_n}}\right|_{\vec{T}=\vec{0}}\right|\phi_q\right\rangle \\
&= \sum_{i=1}^{N_{\text{occ}}}\left\langle\phi_i\left|\left.\frac{\partial^n v'(\vec{T})}{\partial T_{i_1}\ldots\partial T_{i_n}}\right|_{\vec{T}=\vec{0}}\right|\phi_i\right\rangle.
\end{aligned}
\tag{A.40}
$$

A property gradient, i. e. partial derivative of the energy with respect to perturbation parameters and κ_{pq} yields a matrix element of the corresponding perturbing operator between occupied and unoccupied orbitals:

$$
\begin{aligned}
\left.\frac{\partial^{(n+1)} E}{\partial T_{i_1}\ldots\partial T_{i_n}\partial\kappa_{rs}}\right|_{\kappa=\mathbf{0},\vec{T}=\vec{0}} &= \left.\frac{\partial^n}{\partial T_{i_1}\ldots\partial T_{i_n}}\sum_{pq} v'_{pq}(\vec{T})\frac{\partial\tilde{D}_{pq}\left(\kappa\right)}{\partial\kappa_{rs}}\right|_{\kappa=\mathbf{0},\vec{T}=\vec{0}} \\
&= \sum_{pq}\left\langle\phi_p\left|\left.\frac{\partial^n v'(\vec{T})}{\partial T_{i_1}\ldots\partial T_{i_n}}\right|_{\vec{T}=\vec{0}}\right|\phi_q\right\rangle\left\langle 0\left|\left[\hat{a}_r^\dagger\hat{a}_s,\hat{a}_p^\dagger\hat{a}_q\right]\right|0\right\rangle \\
&= \sum_{pq}\left\langle\phi_p\left|\left.\frac{\partial^n v'(\vec{T})}{\partial T_{i_1}\ldots\partial T_{i_n}}\right|_{\vec{T}=\vec{0}}\right|\phi_q\right\rangle(N_{rq}\delta_{ps}-N_{ps}\delta_{qr}) \\
&= \begin{cases} -\left\langle\phi_i\left|\left.\frac{\partial^n v'(\vec{T})}{\partial T_{i_1}\ldots\partial T_{i_n}}\right|_{\vec{T}=\vec{0}}\right|\phi_a\right\rangle & \text{for}\quad \kappa_{rs}=\kappa_{ai} \\ -\left\langle\phi_a\left|\left.\frac{\partial^n v'(\vec{T})}{\partial T_{i_1}\ldots\partial T_{i_n}}\right|_{\vec{T}=\vec{0}}\right|\phi_i\right\rangle & \text{for}\quad \kappa_{rs}=\kappa_{ai}^* \\ 0 & \text{else} \end{cases}
\end{aligned}
\tag{A.41}
$$

where the convention that indices i, j, k signify orbitals occupied in $|0\rangle$ and indices a, b, c signify orbitals unoccupied in $|0\rangle$ was used.

A property Hessian, i. e. a partial derivative of the energy with respect to perturbation parameters and a second partial derivative with respect to κ_{rs} and κ_{tu} is given by:

$$
\left. \frac{\partial^{(n+2)} E}{\partial T_{i_1} \dots \partial T_{i_n} \partial \kappa_{rs} \partial \kappa_{tu}} \right|_{\kappa = \mathbf{0}, \vec{T} = \vec{0}} = \left. \frac{\partial^n}{\partial T_{i_1} \dots \partial T_{i_n}} \sum_{pq} v'_{pq}(\vec{T}) \frac{\partial^2 \tilde{D}_{pq}(\kappa)}{\partial \kappa_{rs} \partial \kappa_{tu}} \right|_{\kappa = \mathbf{0}, \vec{T} = \vec{0}}
$$

$$
= \sum_{pq} \left\langle \phi_p \left| \left. \frac{\partial^n v'(\vec{T})}{\partial T_{i_1} \dots \partial T_{i_n}} \right|_{\vec{T} = \vec{0}} \right| \phi_q \right\rangle
$$

$$
\times \left(\left\langle 0 \left| \left[\hat{a}_r^\dagger \hat{a}_s, \left[\hat{a}_t^\dagger \hat{a}_u, \hat{a}_p^\dagger \hat{a}_q \right] \right] \right| 0 \right\rangle + \left\langle 0 \left| \left[\hat{a}_t^\dagger \hat{a}_u, \left[\hat{a}_s^\dagger \hat{a}_r, \hat{a}_p^\dagger \hat{a}_q \right] \right] \right| 0 \right\rangle \right)
$$

$$
= \sum_{pq} \left\langle \phi_p \left| \left. \frac{\partial^n v'(\vec{T})}{\partial T_{i_1} \dots \partial T_{i_n}} \right|_{\vec{T} = \vec{0}} \right| \phi_q \right\rangle \left(N_{ps} \delta_{qt} \delta_{ru} + N_{pu} \delta_{qr} \delta_{st} \right.
$$

$$
\left. + N_{rq} \delta_{pu} \delta_{st} - 2 N_{ru} \delta_{ps} \delta_{qt} + N_{tq} \delta_{ps} \delta_{ru} - 2 N_{ts} \delta_{pu} \delta_{qr} \right).
$$

$$
(A.42)
$$

If non-redundant parameters are used, there is only one possible type of contribution to the property Hessian for $\kappa_{rs} = \kappa_{ai}$ and $\kappa_{tu} = \kappa_{bj}^*$ or vice versa, which is give by:

$$
\left. \frac{\partial^{(n+2)} E}{\partial T_{i_1} \dots \partial T_{i_n} \partial \kappa_{ai} \partial \kappa_{bj}^*} \right|_{\kappa = \mathbf{0}, \vec{T} = \vec{0}} = -2 \left(\delta_{ab} \left\langle \phi_i \left| \left. \frac{\partial^n v'(\vec{T})}{\partial T_{i_1} \dots \partial T_{i_n}} \right|_{\vec{T} = \vec{0}} \right| \phi_j \right\rangle \right.
$$

$$
\left. + \delta_{ij} \left\langle \phi_a \left| \left. \frac{\partial^n v'(\vec{T})}{\partial T_{i_1} \dots \partial T_{i_n}} \right|_{\vec{T} = \vec{0}} \right| \phi_b \right\rangle \right).
$$

$$
(A.43)
$$

Appendix B

Computational details

B.1 Model potential and nucleon density distribution

The model potential $\widetilde{V}$ used in the calculation of the ZORA factor $\tilde{\omega}$

$$\tilde{\omega} = \frac{1}{2m_{\mathrm{e}} - \widetilde{V}/c^2} \, , \tag{B.1}$$

is described in detail in Ref. [63]. The model potentials are calculated using the local density approximation exchange–correlation functional and superpositions of atomic model densities $\tilde{\rho}_A^{\mathrm{mod}}$. The model densities are expanded in terms of Gaussian functions:

$$\tilde{\rho}_A^{\mathrm{mod}}(r) = \pi^{-3/2} \sum_i c_{iA}^{\mathrm{mod}} \left[\alpha_{iA}^{\mathrm{mod}} \right]^{3/2} \exp\left(-\alpha_{iA}^{\mathrm{mod}} r^2 \right) \, , \tag{B.2}$$

as described in Ref. [58]. The parameters c_{iA}^{mod} are determined by fitting the $\tilde{\rho}_A^{\mathrm{mod}}$ to densities obtained from two–component atomic calculations with saturated basis sets. The exponents $\alpha_{iA}^{\mathrm{mod}}$ and coefficients c_{iA}^{mod} used in this work were determined by Christoph can Wüllen [63] and are given in Tables B.1 to B.6.

For the dihydrogen dichalcogenides used in the discussion of systematic PV NMR effects in Chapter 6, the model density used to construct $\widetilde{V}$ with additional damping was employed with the parameters given in Ref. [58]. For all other calculations reported herein, the model density was constructed using the parameters given in ref. [63].

Table B.1: Model density exponents $\alpha_{iA}^{\mathrm{mod}}$ and coefficients c_{iA}^{mod} used in the two–component calculations presented in Chapter 8. The nucleus is indicated above the parameters.

$\alpha_{iA}^{\mathrm{mod}}/a_0^{-2}$	c_{iA}^{mod}	$\alpha_{iA}^{\mathrm{mod}}/a_0^{-2}$	c_{iA}^{mod}
H		Th	
17.388049797	.0059257005	83896807.952106	.0000570529
3.615672064	.0701929046	46692386.789276	$-.0000664309$
1.131622661	.2942023101	19169059.318442	.0002480183
.414384954	.4675289539	11968789.539612	$-.0001345978$
.164265903	.1621501309	5688176.1027877	.0005499063
C		2834449.3178572	.0003739335
2070.774305545	.0010923571	1644832.6024157	.0015087906
461.404488918	.0131848517	909458.8153952	.0027493814
152.608754693	.0825787292	464281.03125142	.0081417843
59.791280065	.3185641540	248352.60615456	.0136817269
25.876222409	.7140266003	149576.25246546	.0275892856
11.859459978	.7316712413	85174.574838620	.0590099528
5.087813417	.0606645033	49202.073781541	.1170546114
2.969226350	$-.2268722274$	27493.580700688	.2472450779
1.211297436	1.0008540944	15030.556161857	.4300475342
.598767703	1.9692870936	8410.968619254	.5356776128
.280515660	1.1619425008	4843.681048090	.3840935699
.119495557	.1730061016	3054.923586192	$-.1045493011$
F		1670.944171566	$-.3008747515$
4419.253086854	.0013029633	1012.011833568	1.6869348217
960.909783424	.0162869683	605.922481254	5.0537219679
314.157764313	.1013887891	410.077981464	1.7453853218
123.001778863	.3765722564	219.887937228	-8.2229796608
53.566098852	.7705042247	124.515730511	5.8842801134
24.780284877	.6341543993	87.803713385	24.7011314683
11.568626848	$-.1642026549$	41.139436339	-24.3001747805
5.544792664	.1508323748	32.526889072	$-.6419166663$
2.695204902	2.1674479967	19.067170274	36.2663243029
1.278526970	3.0381335655	12.793096318	16.2132378373
.581993664	1.6487215029	8.380764409	-16.2218711074
.249186416	.2588576140	4.863746796	8.1963643933
Cl		3.363052789	18.1315275276
19287.804681839	.0010713781	2.018679611	2.5190268777
4020.200134141	.0137467966	1.342480482	-2.6410462345
1303.675237194	.0855561608	.968695434	7.0179632336
515.518210978	.3237621562	.641546622	4.9548459088
228.924324710	.7073948633	.449522356	2.6630844994
110.227592116	.6592431646	.292396731	.3499259933
45.560289938	$-.1879459248$	.201663081	1.6093477583
19.446917686	.6508221368	.124717599	2.1802290961
12.060796874	3.4101257134	.086881421	1.2131213705
6.680633765	3.9496006910	.053004463	.2191327999
2.000865011	-1.8777781585		
1.248998860	2.2026653269		
.627555462	4.3155618935		
.315937949	2.4154191526		
.152254250	.3307546495		

The Gaussian nuclear model [276] has been used with exponent coefficients

$$\alpha_{\mathrm{nuc}} = \frac{3}{2 r_{\mathrm{nuc}}\left(A\right)^2} \tag{B.3}$$

and

$$r_{\mathrm{nuc}}\left(A\right) = \left(0.836 A^{1/3} + 0.570\right) \mathrm{fm}, \tag{B.4}$$

A being the atomic mass number of the isotope with charge Z. For terms arising due to the vector potential $\vec{A}_\mu$, however, a point-like distribution of the nucleus' magnetic moment has been assumed.

Dense integration grids with up to 2000 radial points and high angular resolution were employed throughout for the numerical integration of the matrix elements and tight convergence criteria were used in the self-consistent field (SCF) calculation. Total energies were converged to up to $10^{-10} E_\mathrm{h}$ (Hartree) and the spin-orbit contributions to as much as $10^{-12} E_\mathrm{h}$. Contributions to the shielding tensor were computed in several subsequent SCF cycles to monitor convergence of this property. All calculations reported herein were performed with a modified version of the TURBOMOLE program [64, 65].

Table B.2: Model density exponents $\alpha_{iA}^{\mathrm{mod}}$ and coefficients c_{iA}^{mod} used in the calculations presented in Chapter 6. The nucleus is indicated above the parameters.

$\alpha_{iA}^{\mathrm{mod}}/a_0^{-2}$	c_{iA}^{mod}	$\alpha_{iA}^{\mathrm{mod}}/a_0^{-2}$	c_{iA}^{mod}
H		Te	
28.845879	.0024655845	1007659.7689384	.0002349792
5.356381	.0437248014	186251.80546131	.0019049405
1.494003	.2601803687	70278.316038598	.0058096502
.525566	.4765715866	35165.829275675	.0150025433
.217351	.2170576589	21045.626542483	.0280977567
O		11106.654226728	.1164880911
3688.394324965	.0011428881	5207.655646623	.3410786748
812.362963229	.0139804306	2533.512667533	.6435987065
268.444935323	.0867726726	1314.752856603	.5793433431
105.552781644	.3324328649	549.250587012	−.2776279642
45.840394193	.7344995912	312.846127112	.1354872554
21.028322044	.7077404217	196.057624651	3.5083053203
9.443369240	−.0755647841	121.743092666	4.6813525917
4.391064326	−.0672594592	54.182036958	−5.4377012440
2.244256246	1.7137492060	23.139691492	13.6013963729
1.059738739	2.7484775308	16.330083572	11.3175581407
.481256015	1.5580649809	7.655796758	−11.4120989387
.204616067	.2459636566	4.368150849	6.4857924740
S		2.702055925	14.1748848680
17134.633612831	.0010386948	1.514383114	5.1059014545
3582.212014449	.0134112074	.859455650	−2.4997605671
1155.484964122	.0853779041	.705652849	3.8998835702
450.776502088	.3331706583	.348291369	4.1824352741
196.412379312	.7394232354	.184839114	2.4784291997
92.078632184	.6576492110	.093694630	.3242035072
39.862074307	−.3101469111	Po	
25.982869619	.2944205448	28113940.014968	.0000742005
11.114062519	3.5136377352	4423061.4080931	.0004541876
5.708611215	4.2155481383	1636247.0216539	.0009364594
1.500289775	−1.6611353634	736523.14604909	.0032597412
1.015711168	2.1071214141	322644.57789128	.0084378281
.519118299	3.4915480695	159847.92553975	.0218831805
.267309294	2.1792029096	73972.377188275	.0690708236
.128892394	.3397325520	33638.502459676	.1868197966
Se		15960.225974200	.4062014708
166495.19222403	.0004562386	7908.249815763	.6437089071
33941.889225287	.0044917379	3748.230784795	.8210890535
12654.097985883	.0177981349	3069.527293134	−.4877251561
5832.507277050	.0670049332	1235.469244626	−.2779721024
2622.383522625	.2431553589	743.556945517	2.6826450229
1215.556430860	.5824203820	440.003716529	5.5674966509
602.732654944	.6977535816	176.592687563	−11.0739192321
388.719812638	.0984356504	160.538806875	4.3117151774
181.549549317	−.2525345702	79.513915271	24.9015837332
78.616566613	2.8133287570	41.830031568	37.5620742019
45.623320731	5.1463010138	37.934806760	−54.4338769203
15.661096902	−4.7525580324	14.994707372	29.6374357057
11.366302889	3.5906843202	10.376245244	14.6804299166
5.947262269	10.3865329453	6.505737121	−6.1379774023
3.383928344	7.0058849770	2.819603104	13.3480273340
1.783602949	.5526932574	1.788707590	4.5256358151
.677748473	2.4644333067	1.489340252	5.5802024161
.398358041	3.0942365754	.669591392	7.0133228575
.218554064	1.9520421941	.552209166	−5.7792921903
.109621895	.2874392383	.443244344	5.2630054138
		.289807753	2.4939052751
		.165524683	2.1802080360
		.082328797	.2811397987

Table B.3: Model density exponents $\alpha_{iA}^{\mathrm{mod}}$ and coefficients c_{iA}^{mod} used in the calculations presented in Sections 7.3 and 7.4. The nucleus is indicated above the parameters.

$\alpha_{iA}^{\mathrm{mod}}/a_0^{-2}$	c_{iA}^{mod}	$\alpha_{iA}^{\mathrm{mod}}/a_0^{-2}$	c_{iA}^{mod}
H		Pd	
17.388049797	.0059257005	702296.19882351	.0001981866
3.615672064	.0701929046	151554.76816541	.0011326052
1.131622661	.2942023101	72616.874050867	.0027188943
.414384954	.4675289539	34324.046031809	.0100610815
.164265903	.1621501309	17918.388130150	.0294914680
C		8414.422036699	.1193849964
2070.774305545	.0010923571	3837.258374850	.3551411479
461.404488918	.0131848517	1839.243490437	.6783029547
152.608754693	.0825787292	923.919466360	.6051222478
59.791280065	.3185641540	579.227287936	−.1539571137
25.876222409	.7140266003	376.630647592	−.1791025471
11.859459978	.7316712413	155.857622151	2.9911424643
5.087813417	.0606645033	94.556703723	5.1120737653
2.969226350	−.2268722274	38.436844505	−4.7396679882
1.211297436	1.0008540944	17.331112574	10.0749840695
.598767703	1.9692870936	11.566580939	12.5289714565
.280515660	1.1619425008	7.309307850	1.2163166402
.119495557	.1730061016	5.350717740	−6.4785879027
N		2.125120436	9.2349112932
2839.921379763	.0011175762	1.166020806	7.7753202854
618.085379667	.0140189506	.719310264	1.2894987553
203.548555559	.0869741625	.525524473	3.3080609948
80.217241952	.3290737587	.277948643	1.4257427988
35.004169720	.7222876616	.184119264	.6227936594
16.156759212	.7150884236	.094382193	.1699457865
6.619125279	−.0082841519	Pt	
3.954209277	−.1544708871	14763034.080453	.0000912551
1.706120974	1.3249369253	2021829.5557736	.0009652199
.823391404	2.3625194432	1451528.3166052	−.0002610608
.378803473	1.3884076006	584197.60730695	.0033952060
.161126155	.2183305368	262905.24981129	.0047810470
P		145564.10868473	.0171580798
14833.367817263	.0010458947	64087.184410285	.0573251041
3102.577362815	.0135733950	30623.245282781	.1282860091
1008.024030644	.0844070930	18229.473384465	.1544795611
401.360454916	.3141827131	11577.173214960	.3361278175
180.725464163	.6768814087	6414.742780312	.5800581672
88.334258066	.6788452250	3447.856535864	.5208589493
25.351716976	−.2297988406	2089.869019584	−.1403388257
13.224393519	1.4121004548	1036.694838336	−.3466517735
7.271730809	3.8319123794	631.420927415	2.4518008850
4.023024434	2.8977816499	369.962820490	5.7786893959
1.462598101	−.8394265596	146.578362637	−7.2949236270
.745218762	1.0545126610	71.315778815	17.4611237983
.432427955	2.8191428480	44.440340775	26.8858623098
.220187745	1.9673404297	35.986699101	−25.7060939592
.104069538	.3174992479	20.920160819	−13.1864732372
Cl		13.764270197	23.0354668399
19287.804681839	.0010713781	8.636964551	20.8834274009
4020.200134141	.0137467966	5.311004857	−.7360467960
1303.675237194	.0855561608	2.445061095	6.3418559565
515.518210978	.3237621562	1.556237535	9.0209459893
228.924324710	.7073948633	1.090973776	−3.3102466656
110.227592116	.6592431646	.925493382	8.1492849094
45.560289938	−.1879459248	.430932141	4.1216164417
19.446917686	.6508221368	.257056596	.2911359451
12.060796874	3.4101257134	.206218885	2.1656721229
6.680633765	3.9496006910	.102720881	.3306275343
2.000865011	−1.8777781585		
1.248998860	2.2026653269		
.627555462	4.3155618935		
.315937949	2.4154191526		
.152254250	.3307546495		

Table B.4: Model density exponents $\alpha_{iA}^{\mathrm{mod}}$ and coefficients c_{iA}^{mod} used in the calculations presented in Section 7.5. The nucleus is indicated above the parameters.

$\alpha_{iA}^{\mathrm{mod}}/a_0^{-2}$	c_{iA}^{mod}	$\alpha_{iA}^{\mathrm{mod}}/a_0^{-2}$	c_{iA}^{mod}
H		F	
17.388049797	.0059257005	4419.253086854	.0013029633
3.615672064	.0701929046	960.909783424	.0162869683
1.131622661	.2942023101	314.157764313	.1013887891
.414384954	.4675289539	123.001778863	.3765722564
.164265903	.1621501309	53.566098852	.7705042247
C		24.780284877	.6341543993
2070.774305545	.0010923571	11.568626848	$-.1642026549$
461.404488918	.0131848517	5.544792664	.1508323748
152.608754693	.0825787292	2.695204902	2.1674479967
59.791280065	.3185641540	1.278526970	3.0381335655
25.876222409	.7140266003	.581993664	1.6487215029
11.859459978	.7316712413	.249186416	.2588576140
5.087813417	.0606645033	Te	
2.969226350	$-.2268722274$	1007659.7689384	.0002349792
1.211297436	1.0008540944	186251.80546131	.0019049405
.598767703	1.9692870936	70278.316038598	.0058096502
.280515660	1.1619425008	35165.829275675	.0150025433
.119495557	.1730061016	21045.626542483	.0280977567
O		11106.654226728	.1164880911
3688.394324965	.0011428881	5207.655646623	.3410786748
812.362963229	.0139804306	2533.512667533	.6435987065
268.444935323	.0867726726	1314.752856603	.5793433431
105.552781644	.3324328649	549.250587012	$-.2776279642$
45.840394193	.7344995912	312.846127112	.1354872554
21.028322044	.7077404217	196.057624651	3.5083053203
9.443369240	$-.0755647841$	121.743092666	4.6813525917
4.391064326	$-.0672594592$	54.182036958	-5.4377012440
2.244256246	1.7137492060	23.139691492	13.6013963729
1.059738739	2.7484775308	16.330083572	11.3175581407
.481256015	1.5580649809	7.655796758	-11.4120989387
.204616067	.2459636566	4.368150849	6.4857924740
		2.702055925	14.1748848680
		1.514383114	5.1059014545
		.859455650	-2.4997605671
		.705652849	3.8998835702
		.348291369	4.1824352741
		.184839114	2.4784291997
		.093694630	.3242035072

Table B.5: Model density exponents $\alpha_{iA}^{\mathrm{mod}}$ and coefficients c_{iA}^{mod} used in the calculations presented in Section 7.6. The nucleus is indicated above the parameters.

$\alpha_{iA}^{\mathrm{mod}}/a_0^{-2}$	c_{iA}^{mod}	$\alpha_{iA}^{\mathrm{mod}}/a_0^{-2}$	c_{iA}^{mod}
H		**I**	
17.388049797	.0059257005	1152328.4026025	.0002152463
3.615672064	.0701929046	206153.01514185	.0018612039
1.131622661	.2942023101	74394.431161075	.0059463239
.414384954	.4675289539	35063.961002930	.0214513402
.164265903	.1621501309	14998.727194114	.0902900967
N		6572.126604388	.2833471666
2839.921379763	.0011175762	3082.118621454	.6049251012
618.085379667	.0140189506	1534.279537615	.6815519257
203.548555559	.0869741625	683.890382230	−.0206572962
80.217241952	.3290737587	441.876370298	−.3600658248
35.004169720	.7222876616	239.923702849	2.3747495110
16.156759212	.7150884236	141.699905325	5.6982349309
6.619125279	−.0082841519	48.582203508	−10.8354852030
3.954209277	−.1544708871	39.418201864	8.1871902725
1.706120974	1.3249369253	20.877154399	20.1678059591
.823391404	2.3625194432	13.564718336	2.9912604509
.378803473	1.3884076006	8.362039353	−11.8718401976
.161126155	.2183305368	3.942023464	11.8556340146
F		2.444980732	12.0605433627
4419.253086854	.0013029633	1.163326507	1.5512300749
960.909783424	.0162869683	.714651751	−2.5012549377
314.157764313	.1013887891	.586886446	5.5839864204
123.001778863	.3765722564	.333011606	3.7995937450
53.566098852	.7705042247	.200561695	2.3010127693
24.780284877	.6341543993	.106851364	.3284735436
11.568626848	−.1642026549	**W**	
5.544792664	.1508323748	11585824.214850	.0000784505
2.695204902	2.1674479967	2123734.7851771	.0003299157
1.278526970	3.0381335655	1099260.9109748	.0007072339
.581993664	1.6487215029	345404.80056492	.0084236329
.249186416	.2588576140	296212.78820684	−.0046806840
Cl		139089.59345049	.0172500050
19287.804681839	.0010713781	56845.797759264	.0520897715
4020.200134141	.0137467966	27329.083000879	.1186956514
1303.675237194	.0855561608	15185.664705262	.2097463445
515.518210978	.3237621562	8922.336221816	.3657980299
228.924324710	.7073948633	5239.582642854	.5148762018
110.227592116	.6592431646	3103.659707190	.4522704240
45.560289938	−.1879459248	1127.857916110	−.3513929025
19.446917686	.6508221368	700.780713365	.4241237129
12.060796874	3.4101257134	481.091424359	2.6961487875
6.680633765	3.9496006910	309.978252634	5.1534766337
2.000865011	−1.8777781585	129.656202108	−7.0465602824
1.248998860	2.2026653269	63.641088094	11.7505817536
.627555462	4.3155618935	48.850063210	14.4286155458
.315937949	2.4154191526	37.072653636	3.3165782786
.152254250	.3307546495	23.994196940	−17.9174356552
Br		10.095438385	23.5287906695
182464.36304025	.0004367396	6.367067396	12.5953915461
40843.980479792	.0032730734	3.344651980	−.9189543667
16297.184129947	.0135304741	2.375947375	6.1388547736
6717.723584933	.0673806117	1.423123163	8.7680643103
2808.709419944	.2545751550	.804332201	4.7518798769
1261.531647450	.6177770422	.731211092	−1.2852591081
604.565906839	.7404132330	.422747187	1.8590135738
276.374189024	−.0498473994	.237694953	2.5040316968
146.581616615	−.3930437919	.138183408	1.6744100881
89.243376413	2.7124752668	.074030149	.1940560906
49.964040905	5.4261428194		
17.539290386	−3.7611828044		
9.874183490	4.3778614712		
5.842686566	10.8836811610		
3.382342236	5.4262886413		
1.653923883	−1.0507343871		
1.074325744	1.7315214134		
.553362063	4.6803521179		
.279120303	2.9138897944		
.135308392	.4052093686		

Table B.6: Model density exponents $\alpha_{iA}^{\mathrm{mod}}$ and coefficients c_{iA}^{mod} used in the calculations presented in Section 7.7. The nucleus is indicated above the parameters.

$\alpha_{iA}^{\mathrm{mod}}/a_0^{-2}$	c_{iA}^{mod}	$\alpha_{iA}^{\mathrm{mod}}/a_0^{-2}$	c_{iA}^{mod}	$\alpha_{iA}^{\mathrm{mod}}/a_0^{-2}$	c_{iA}^{mod}
H		**Co**		**W**	
17.388049797	.0059257005	84850.644302962	.0005017983	11585824.214850	.0000784505
3.615672064	.0701929046	18785.315983227	.0044879669	2123734.7851771	.0003299157
1.131622661	.2942023101	7727.055495616	.0155681851	1099260.9109748	.0007072339
.414384954	.4675289539	3541.415370782	.0688610191	345404.80056492	.0084236329
.164265903	.1621501309	1551.161919410	.2558646846	296212.78820684	−.0046806840
C		713.914206488	.6056944550	139089.59345049	.0172500050
2070.774305545	.0010923571	352.416428920	.6962353615	56845.797759264	.0520897715
461.404488918	.0131848517	235.763637345	.0750857795	27329.083000879	.1186956514
152.608754693	.0825787292	115.825107174	−.1915945882	15185.664705262	.2097463445
59.791280065	.3185641540	44.009415722	3.1887256957	8922.336221816	.3657980299
25.876222409	.7140266003	24.730352786	4.9660959713	5239.582642854	.5148762018
11.859459978	.7316712413	10.014102410	−2.0232935024	3103.659707190	.4522704240
5.087813417	.0606645033	7.387108651	−.7082736407	1127.857916110	−.3513929025
2.969226350	−.2268722274	3.950699303	5.9319972074	700.780713365	.4241237129
1.211297436	1.0008540944	2.193037558	7.2558473696	481.091424359	2.6961487875
.598767703	1.9692870936	1.110033646	3.1328508733	309.978252634	5.1534766337
.280515660	1.1619425008	.527511739	1.1019959282	129.656202108	−7.0465602824
.119495557	.1730061016	.313510370	1.1713630400	63.641088094	11.7505817536
O		.163466710	1.2413936366	48.850063210	14.4286155458
3688.394324965	.0011428881	.080588694	.2105927591	37.072653636	3.3165782786
812.362963229	.0139804306	**Rh**		23.994196940	−17.9174356552
268.444935323	.0867726726	609499.15681031	.0002246835	10.095438385	23.5287906695
105.552781644	.3324328649	117128.70655624	.0018779621	6.367067396	12.5953915461
45.840394193	.7344995912	69710.081187214	.0007595515	3.344651980	−.9189543667
21.028322044	.7077404217	35994.969999958	.0102660654	2.375947375	6.1388547736
9.443369240	−.0755647841	16563.594527117	.0329629577	1.423123163	8.7680643103
4.391064326	−.0672594592	7845.027362356	.1175810045	.804332201	4.7518798769
2.244256246	1.7137492060	3672.115844828	.3436653656	.731211092	−1.2852591081
1.059738739	2.7484775308	1778.726858060	.6698863313	.422747187	1.8590135738
.481256015	1.5580649809	856.397736879	.8797908910	.237694953	2.5040316968
.204616067	.2459636566	718.078658182	−.3805913737	.138183408	1.6744100881
P		346.491033311	−.2361176775	.074030149	.1940560906
14833.367817263	.0010458947	152.228463721	2.7293264077	**Os**	
3102.577362815	.0135733950	91.916084301	5.2957734606	13925990.892532	.0000777378
1008.024030644	.0844070930	34.791151948	−5.0983192197	2233736.0806409	.0004809661
401.360454916	.3141827131	18.934727788	5.8123935862	1139638.5957507	.0004863367
180.725464163	.6768814087	12.160994570	15.3290086340	499938.77125021	.0027219474
88.334258066	.6788452250	7.035733246	3.7638622658	273378.79674556	−.0040434663
25.351716976	−.2297988406	4.928426101	−7.3971651222	129934.32216190	.0192631586
13.224393519	1.4121004548	2.403875383	5.0981748462	57622.772292166	.0514309102
7.271730809	3.8319123794	1.511892476	8.0522239252	33717.566438985	.0652450945
4.023024434	2.8977816499	.868186791	4.6560996110	19721.163020095	.2049358779
1.462598101	−.8394265596	.492464028	2.2243977313	9958.710160198	.4530905847
.745218762	1.0545126610	.284163198	1.7822566166	5139.119636541	.6364082395
.432427955	2.8191428480	.147401372	1.1447893768	2712.895441887	.4271625935
.220187745	1.9673404297	.072232732	.1668721191	1756.390377134	−.2750768910
.104069538	.3174992479			741.117057146	−1.3904868946
Fe				635.052187318	3.3553374180
85924.813288067	.0004067162			351.455214059	5.8903038779
19167.040797889	.0038355261			128.324956698	−10.0139940686
6886.832643182	.0204633824			95.201710325	6.5604304923
2819.379215784	.0922632688			56.102566189	23.8632197172
1232.061259708	.3115693120			35.671345225	1.7706379088
573.732379901	.6723700719			25.317621653	−18.5359690054
278.709530058	.6987861818			11.464753689	20.9482687272
167.920639583	−.1466387442			7.723359878	15.9008981785
88.329370886	−.1313974456			5.119400186	1.0194362229
40.433397015	3.1721822411			2.142964416	8.0444713992
22.598918165	4.9860777611			1.277043454	7.3955725779
8.834764890	−2.0629051888			1.052624482	.1839984062
6.772332653	−.5980563576			.689288520	3.8019806716
3.600284126	5.4655269229			.356702239	2.9409187373
2.028999611	6.8673133073			.246237789	.5774321327
1.049146139	3.0410525179			.172030832	1.8218303415
.479896747	1.2964273008			.088051712	.2754431372
.247555390	1.2413140523				
.134833257	.9422196070				
.068545637	.1271895666				

B.2 Basis sets and structural parameters of PV NMR calculations

B.2.1 H_2X_2

In Chapter 6 of this thesis the parity violating NMR frequency splittings for the heavy nuclei X of the series H_2X_2 with X=^{17}O, ^{33}S, ^{77}Se, ^{125}Te, ^{209}Po are reported for various dihedral angles α of the C_2-symmetric P-conformations. The remaining structural parameters were kept constant for comparison with the previous one- and four-component studies [66, 68, 156]. The gauge-origin was fixed at the nucleus under investigation. Large, even-tempered basis sets [68, 250] with varying numbers of basis functions were used on the chalcogens and the aug-cc-pVDZ basis set [277, 278] in uncontracted form on the hydrogen atoms. Details of the structural parameters and basis sets are listed in Table B.7 (see Refs. [58, 59, 68, 156, 250]).

Table B.7: Structural parameters and basis sets used for the computation of isotropic parity violating shielding constants of X in H_2X_2 (with X=chalcogen). The aug-cc-pVDZ basis set of Ref. [277, 278] was employed in uncontracted form for hydrogen. Exponent coefficients α_i^{orb} of the uncontracted spherical Gaussian basis sets for all other atoms were taken from an even tempered list generated according to $\alpha_i^{\mathrm{orb}} = \gamma \beta^{N-i}$ with $i = 1, 2, \ldots, N$ and $N = 26$. $\alpha_{26}^{\mathrm{orb}} = \gamma = (2/100)\ a_0^{-2}$ and $\alpha_1^{\mathrm{orb}} = 500000000\ a_0^{-2}$ were chosen as the smallest and largest exponent of this list, respectively. The intermediate exponents were used with at least nine significant figures. For example, 1-25:2-26:20-24:20-24 implies that the exponents from this list ranging from $i = 1$ to $i = 25$ were employed for the s-Gaussians, exponents $i = 2$ to $i = 26$ for the p-Gaussians and $i = 20$ to $i = 24$ for the d- and f-Gaussians. See also Refs. [68].

H_2X_2	r_{XX}/pm	r_{XH}/pm	τ_{XXH}/$^\circ$	Basis set for X
$^1H_2{}^{17}O_2$	149.0	97.0	100	1-25:2-26:20-24:20-24
$^1H_2{}^{33}S_2$	205.5	135.2	92	1-25:2-26:15-25:20-24
$^1H_2{}^{77}Se_2$	248.0	145.0	92	1-25:2-26:15-25:20-24
$^1H_2{}^{125}Te_2$	284.0	164.0	92	1-25:2-26:15-25:19-25
$^1H_2{}^{209}Po_2$	291.0	174.0	92	1-25:2-26:12-25:15-24

B.2.2 $(NH_2)_2$Pt-X$(NH_2)_2$

For the model compounds $(NH_2)_2$Pt-Pd$(NH_2)_2$ and $(NH_2)_2$Pt-Pt$(NH_2)_2$ used for the
discussion of systematic effects in Chapter 7.3 the structural parameters listed in Table B.8 were used. The equilibrium geometry was optimized at the DFT level using
the PBE0 functional and aug-cc-pVDZ basis sets on the light atoms H and N [277] as
well as the 28 and 60 core electron ECPs ecp-28-mwb and ecp-60-mwb of Ref. [279] on
Pd and Pt, respectively, in connection with the ecp-28-mwb-SVP and ecp-60-mwb-SVP
basis sets optimized for these ECPs and available with version 5.7 of the TURBOMOLE
program package [64, 65]. At equilibrium geometry the dihedral angles D(N2,Pd,Pt,N1)
and D(N2,Pt2,Pt1,N1) are equal to zero.

Table B.8: Structural parameters used in the calculation of PV NMR shielding tensors
of $(NH_2)_2$Pt-Pd$(NH_2)_2$ and $(NH_2)_2$Pt-Pt$(NH_2)_2$. The dihedral angle α was varied in
the investigation of conformational effects. The parameters correspond to the optimized
equilibrium geometry where $\alpha \approx 0°$ for $(NH_2)_2$Pt-Pd$(NH_2)_2$ and $(NH_2)_2$Pt-Pt$(NH_2)_2$.

R(X,Y)	R/Å	A(X,Y,Z)	A/°	D(W,X,Y,Z)	D/°
		$(NH_2)_2$Pt-Pd$(NH_2)_2$			
D(N2,Pd,Pt,N1)					
R(Pt,N1)	1.906201				
R(Pd,Pt)	2.450065	A(Pd,Pt,N1)	94.058411		
R(N2,Pd)	1.933273	A(N2,Pd,Pt)	97.044289	D(N2,Pd,Pt,N1)	α
R(N3,Pt)	1.906586	A(N3,Pt,Pd)	93.575439	D(N3,Pt,Pd,N2)	$\alpha - 180°$
R(N4,Pd)	1.933787	A(N4,Pd,Pt)	96.554871	D(N4,Pd,Pt,N1)	$\alpha - 180°$
R(H1,N4)	1.016095	A(H1,N4,Pd)	123.044205	D(H1,N4,Pd,Pt)	76.769127
R(H2,N4)	1.016153	A(H2,N4,Pd)	122.980049	D(H2,N4,Pd,Pt)	-75.487396
R(H3,N2)	1.016157	A(H3,N2,Pd)	122.830994	D(H3,N2,Pd,Pt)	-75.019859
R(H4,N2)	1.016240	A(H4,N2,Pd)	122.739235	D(H4,N2,Pd,Pt)	75.445679
R(H5,N1)	1.014682	A(H5,N1,Pt)	124.498550	D(H5,N1,Pt,N3)	-90.453079
R(H6,N1)	1.014673	A(H6,N1,Pt)	124.186394	D(H6,N1,Pt,N3)	90.589539
R(H7,N3)	1.014760	A(H7,N3,Pt)	124.450005	D(H7,N3,Pt,N1)	91.007088
R(H8,N3)	1.014795	A(H8,N3,Pt)	124.314590	D(H8,N3,Pt,N1)	-89.206085
		$(NH_2)_2$Pt-Pt$(NH_2)_2$			
R(Pt1,N1)	1.922493				
R(Pt2,Pt1)	2.428611	A(Pd,Pt,N1)	97.999123		
R(N2,Pt2)	1.922170	A(N2,Pt2,Pt1)	97.984528	D(N2,Pt2,Pt1,N1)	α
R(N3,Pt1)	1.923017	A(N3,Pt1,Pt2)	96.819794	D(N3,Pt1,Pt2,N2)	$\alpha - 180°$
R(N4,Pt2)	1.923203	A(N4,Pt2,Pt1)	96.852142	D(N4,Pt2,Pt1,N1)	$\alpha - 180°$
R(H1,N4)	1.014001	A(H1,N4,Pt2)	124.131943	D(H1,N4,Pt2,Pt1)	86.679520
R(H2,N4)	1.013998	A(H2,N4,Pt2)	123.984093	D(H2,N4,Pt2,Pt1)	-86.324883
R(H3,N2)	1.014357	A(H3,N2,Pt2)	123.961823	D(H3,N2,Pt2,Pt1)	-84.374176
R(H4,N2)	1.014246	A(H4,N2,Pt2)	123.835793	D(H4,N2,Pt2,Pt1)	84.627411
R(H5,N1)	1.013972	A(H5,N1,Pt1)	123.986862	D(H5,N1,Pt1,N3)	-94.615852
R(H6,N1)	1.014184	A(H6,N1,Pt1)	123.826248	D(H6,N1,Pt1,N3)	94.748726
R(H7,N3)	1.014056	A(H7,N3,Pt1)	123.992752	D(H7,N3,Pt1,N1)	93.586624
R(H8,N3)	1.014189	A(H8,N3,Pt1)	124.081070	D(H8,N3,Pt1,N1)	-93.604294

The basis sets used in the calculation of the PV NMR shielding tensors are listen in Table B.9.

Table B.9: Basis sets used for the computation of isotropic PV shielding constants of Pd and Pt in $(NH_2)_2Pt$-$Pd(NH_2)_2$ and $(NH_2)_2Pt$-$Pt(NH_2)_2$. The SV basis set of the TURBOMOLE program package [64, 65] was employed on hydrogen. Exponent coefficients α_i^{orb} of the uncontracted spherical Gaussian basis sets for all other atoms were taken from an even tempered list generated according to the prescription described in the caption of Table B.7.

X	Basis set for X	X	Basis set for X	X	Basis set for X
N	1-25:2-26:20-24:21-22	Pd	1-25:2-26:15-25:18-24	Pt	1-25:2-26:12-25:15-24

B.2.3 Platinum candidate compounds

The basis sets used in the PV NMR calculations on the three platinum candidate compounds introduced in Chapter 7.4 are listed in Table B.10. Structures are given as Cartesian nuclear coordinates in Table B.11. The equilibrium geometries of Pt–2 and Pt–3 were optimized at the B-P86 density functional and cc-pVDZ basis set on the light atoms (see Ref. [277] for H, C and N and Ref. [280] for P and Cl) and the 60 core electron ECP and corresponding basis set of Ref. [279] on platinum. For the optimization of the equilibrium structure of Pt–1 the B-3LYP density functional and default SV(P) basis sets available with version 5.7 of the TURBOMOLE program package [64, 65] were employed. On platinum, the 60 core electron ECP of Ref. [279] was used.

B.2.4 Tellurium candidate compounds

The basis sets used in the PV NMR calculations on the three selenium/tellurium candidate compounds introduced in Chapter 7.5 are listed in Table B.12. Structures are given as Cartesian nuclear coordinates in Table B.13. The equilibrium geometries of Te–2 and Te–3 were optimized at the B3-LYP density functional level [253, 281] with DZP basis sets on the light atoms C, O, F, H [282] and the 46 core electron default ECP and corresponding SVP basis set of the TURBOMOLE program [64, 65] on tellurium.

Table B.10: Basis sets used for the computation of isotropic parity violating shielding constants of ^{195}Pt in the candidate compounds Pt–1, Pt–2 and Pt–3 introduced in Chapter 7.4. In Pt–2 and Pt–3 the DZP basis set of the TURBOMOLE program package [64, 65] was employed on carbon and hydrogen. In the aug-cc-pVDZ basis set of Ref. [277, 278] was employed in contracted form on carbon and uncontracted on hydrogen. Exponent coefficients α_i^{orb} of the uncontracted spherical Gaussian basis sets for all other atoms were taken from an even tempered list generated according to the prescription described in the caption of Table B.7.

compound	X	Basis set for X	X	Basis set for X	X	Basis set for X
Pt–1	Pt	1-25:2-26:12-25:15-22	P	1-25:2-26:20-24		
Pt–2	Pt	1-25:2-26:12-25:15-24	P	1-25:2-26:15-25:20-24	Cl	1-25:2-26:15-25:20-24
Pt–3	Pt	1-25:2-26:12-25:15-24	N	1-25:2-26:15-25:20-24		

The structure of Te–1 was obtained through a B3-LYP optimization with def-SV(P) basis sets [283] of the TURBOMOLE program package on C, O, H and Te in connection with the default ECP of the program on tellurium.

B.2.5   NWXYZ

The basis sets used in the calculation of the PV NMR shielding tensors for the NWXYZ series of molecules discussed in Chapter 7.6 are listed in Table B.14. The Cartesian nuclear coordinates of the equilibrium geometries are listed in Table B.15. The structural parameters were obtained through a B3LYP-optimization using aug-cc-pVTZ basis sets in connection with MDF-ECPs on W, Br and I in the group of P. Schwerdtfeger.

B.2.6   Tungsten candidate compounds

Basis sets used in the calculation of the PV potential and NMR shielding tensors for the transition metal compounds discussed in Chapter 7.7 are listed in Table B.16. The

Cartesian nuclear coordinates of the equilibrium geometries of W–1, W–2 and W–3 are listed in Table B.17, those of W–4 in Table B.18.

The structure of W–2 was optimized at the BP86 [252, 284] DFT level using TURBOMOLE's default TZVP basis sets [285] and corresponding ECPs on tungsten and rhodium, default single–valence basis sets of the TURBOMOLE program package [64, 65] and corresponding core potentials on rhodium and tungsten were used in the geometry optimization of W–4 (see Fig. 7.13). For W–2 and W–3 geometry optimizations were performed by J. Stuber.

Table B.11: Cartesian nuclear coordinates in Ångstrøm used in the calculation of PV NMR shielding tensors of the possible experimental candidate platinum complexes in Chapter 7.4. The left half of the table gives the structure of test compound Pt–2, 2,2′-bis(diphenylphosphanyl)biphenylplatinumdichloride, the right half of the table corresponds to test compounds Pt–1 and Pt–3.

Nucleus	x	y	z	Nucleus	x	y	z
C	2.047775	−5.555618	1.457115		Pt–1		
C	0.928681	−5.675792	0.618463	H	0.005976	1.260989	−3.730125
C	0.282702	−4.527199	0.129933	H	−0.005975	−1.260996	−3.730122
C	0.751066	−3.248120	0.488369	H	1.407455	0.606083	−2.904461
C	1.868367	−3.129738	1.344310	H	−1.407454	−0.606089	−2.904461
C	2.516781	−4.279899	1.816627	H	1.270731	−2.249292	−1.604433
P	−0.032554	−1.704055	−0.187297	H	−0.786020	−2.739100	−1.422171
Pt	−0.000118	0.000212	1.339669	H	0.786017	2.739099	−1.422178
Cl	0.476752	1.590155	3.058479	H	−1.270732	2.249288	−1.604439
C	0.999231	−1.364782	−1.712012	H	−0.929475	1.227036	2.762878
C	0.639027	−0.391645	−2.687879	H	0.889852	1.256318	2.762913
C	1.496210	−0.195119	−3.795901	H	0.929475	−1.227042	2.762871
C	2.692148	−0.909430	−3.945299	H	−0.889851	−1.256324	2.762905
C	3.048047	−1.859279	−2.979172	Pt	0.000000	0.000000	0.487168
C	2.203993	−2.083920	−1.881673	P	−0.054255	1.619936	−1.274709
C	−0.638457	0.391134	−2.688323	P	0.054255	−1.619937	−1.274705
C	−0.999106	1.364427	−1.712783	C	0.320562	0.696644	−2.853396
C	−2.203926	2.083217	−1.882912	C	−0.320561	−0.696649	−2.853394
C	−3.048055	1.857865	−2.980031	C	−0.011133	0.701688	2.531409
C	−2.691797	0.908183	−3.946007	C	0.011133	−0.701693	2.531404
C	−1.495486	0.194275	−3.796416		Pt–3		
P	0.032276	1.703900	−0.187759	C	1.770296	1.301902	3.518506
C	−0.751413	3.247948	0.487579	C	1.885163	0.328822	2.475148
C	−0.282125	4.526693	0.129589	C	3.217708	−0.040439	2.046256
C	−0.927834	5.675899	0.617978	C	4.349785	0.534239	2.696235
C	−2.046599	5.555886	1.457052	C	4.198774	1.463819	3.715600
C	−2.516217	4.280018	1.816705	C	2.893050	1.857174	4.117212
C	−1.868879	3.129628	1.343046	C	0.735570	−0.253018	1.827359
C	1.690079	2.256868	−0.792939	C	0.928567	−1.112011	0.725563
C	2.785606	2.132608	0.088169	C	2.253912	−1.477164	0.328406
C	4.050377	2.602630	−0.300238	C	3.365978	−0.967348	0.972056
C	4.230827	3.191172	−1.563749	N	−0.163938	−1.626444	−0.035003
C	3.140945	3.314383	−2.442236	Pt	−0.486836	−0.099590	−1.360589
C	1.871702	2.849886	−2.060309	N	−1.305077	1.078084	0.071111
C	−1.690334	−2.256926	−0.792676	C	−1.555264	0.768521	1.400132
C	−2.785694	−2.133130	0.088680	C	−2.802625	1.232349	1.957134
C	−4.050526	−2.602630	−0.299667	C	−3.184216	0.967259	3.253605
C	−4.231333	−3.191093	−1.562969	C	−2.358031	0.177586	4.109411
C	−3.141511	−3.314445	−2.441860	C	−1.084100	−0.276078	3.597731
C	−1.871897	−2.850153	−2.060028	C	−0.653955	0.079118	2.265580
Cl	−0.476683	−1.588981	3.059574	C	−0.290464	−1.097938	4.462418
H	1.209718	0.554253	−4.548191	C	−0.716021	−1.429488	5.742986
H	3.339839	−0.721632	−4.813780	C	−1.958746	−0.957677	6.244067
H	3.979516	−2.436072	−3.073833	C	−2.761695	−0.168836	5.429949
H	2.485906	−2.843962	−1.142227	H	−3.472911	1.809567	1.297830
H	−1.209604	−0.554994	−4.549156	H	−4.148970	1.338862	3.633644
H	−3.339025	0.719124	−4.814784	H	−3.735307	0.198426	5.791925
H	−3.979579	2.434580	−3.075475	H	−2.282451	−1.221517	7.261625
H	−2.486439	2.843729	−1.143969	H	−0.080348	−2.069638	6.373856
H	−1.020301	−2.948498	−2.749922	H	0.670856	−1.480698	4.093592
H	−3.278532	−3.773413	−3.432214	H	2.361043	−2.208697	−0.488823
H	−5.225029	−3.554744	−1.864759	H	4.378628	−1.270967	0.666913
H	−4.899712	−2.505786	0.392188	H	5.354467	0.229526	2.362532
H	1.020283	2.948438	−2.750395	H	5.082022	1.900598	4.205154
H	3.277759	3.774025	−3.432418	H	2.768733	2.608267	4.911729
H	5.224189	3.554745	−1.865940	H	0.767066	1.614924	3.836399
H	4.899837	2.506820	0.391953	H	−0.992527	−1.610906	0.590557
H	−2.631660	−1.680764	1.080461	H	−2.129143	1.565390	−0.304503
H	2.631132	1.680367	1.079801	N	0.306344	−1.266890	−2.939761
H	−2.214526	2.133662	1.654831	N	−0.613476	1.373198	−2.951226
H	−3.380289	4.176197	2.488960	C	−0.194464	0.775426	−4.221689
H	−2.548498	6.456366	1.840838	C	−0.246843	1.492016	−5.430060
H	−0.545972	6.669591	0.342614	C	0.157023	0.883299	−6.628209
H	0.597797	4.633518	−0.519908	C	0.619322	−0.443788	−6.621017
H	2.213187	−2.133387	1.656556	C	0.675861	−1.160756	−5.416347
H	3.381350	−4.175868	2.488087	C	0.270367	−0.554877	−4.215400
H	2.549191	−6.456069	1.841351	H	−0.609299	2.531136	−5.428541
H	0.546832	−6.669795	0.342543	H	0.110528	1.448284	−7.569984
H	−0.596779	−4.634198	−0.519786	H	0.935857	−0.924486	−7.557371
				H	1.034812	−2.201001	−5.403580
				H	1.274813	−1.540642	−2.698890
				H	−0.232292	−2.148331	−2.986935
				H	−1.552460	1.791493	−3.057996
				H	0.017348	2.153389	−2.699976

Table B.12: Basis sets used for the computation of isotropic parity violating shielding constants of the ^{125}Te nucleus in the candidate compounds Te–1, Te–2 and Te–3 introduced in Chapter 7.5. On the H and C the aug-cc-pVDZ basis set of Ref. [277, 278] was employed in contracted form throughout and on O in Te–1. Exponent coefficients α_i^{orb} of the uncontracted spherical Gaussian basis sets on Te, F and O in Te–3 were taken from an even tempered list generated according to the prescription described in the caption of Table B.7.

compound	X	Basis set for X	X	Basis set for X
Te–1	Te	1-25:2-26:15-25:19-25		
Te–2	Te	1-25:2-26:15-25:19-25	F	1-25:2-26:20-24:20-24
Te–3	Te	1-25:2-26:15-25:19-25	O	1-25:2-26:20-24:20-24

Table B.13: Cartesian nuclear coordinates in Ångstrøm used in the calculation of PV NMR shielding tensors of the possible experimental candidate tellurium complexes in Chapter 7.5.

Nucleus	x	y	z	Nucleus	x	y	z
		Te–1				Te–2	
C	−1.526401	0.892315	−0.554030	H	1.989327	0.661136	−1.805356
C	−0.866748	−0.037731	0.546452	H	1.007940	3.009792	−2.176041
C	−1.243599	−1.474582	0.090029	H	−1.003265	3.688894	−0.817366
C	−2.622824	−1.274987	−0.601238	H	−1.949735	1.992098	0.893277
C	−2.926304	0.223605	−0.369269	H	1.949738	−1.992144	0.893273
C	−3.207268	0.401566	1.139454	H	1.003255	−3.688989	−0.817424
C	−1.796408	0.226617	1.777425	H	−1.007994	−3.009844	−2.176085
C	0.592152	0.165623	0.925937	H	−1.989322	−0.661126	−1.805324
Te	2.103199	−0.463617	−0.520839	Te	0.000005	−0.000010	0.221682
C	3.663907	0.799269	0.317695	F	−1.182187	−0.650338	1.664988
C	3.596002	2.241738	−0.181299	F	1.182208	0.650321	1.664965
O	−0.215305	−1.992360	−0.766574	C	−1.095215	1.841951	0.235693
C	−0.973478	0.763529	−1.988456	C	−1.129092	−1.075760	−1.279633
C	−1.498965	2.394677	−0.210046	C	1.095212	−1.841998	0.235685
C	2.760076	−2.229288	0.494935	C	1.129078	1.075787	−1.279602
H	0.817668	1.231051	1.097710	C	−0.580043	2.693320	−0.654524
H	0.860481	−0.393297	1.839264	C	−0.603632	−2.292105	−1.456440
H	−1.316809	−2.144066	0.966071	C	0.580034	−2.693281	−0.654557
H	−2.548828	−1.514255	−1.674536	C	0.603834	2.292086	−1.456472
H	−3.401880	−1.926912	−0.173142			Te–3	
H	−3.720478	0.615943	−1.023781	C	1.842418	1.156236	0.231572
H	−3.929666	−0.344208	1.509603	Te	−0.325635	1.096116	0.067370
H	−3.632538	1.392561	1.362913	O	−0.339123	−0.465418	−1.258838
H	−1.746888	−0.610795	2.493778	Te	−0.468097	−2.074022	0.006738
H	−1.477638	1.128679	2.324413	C	−0.268778	−3.583033	1.560735
H	−0.003132	1.286267	−2.090427	C	1.014210	−3.907660	1.745210
H	−0.831125	−0.271672	−2.327573	C	2.056070	−3.247570	0.919421
H	−1.663260	1.259824	−2.694598	C	1.691681	−2.323373	0.026413
H	−0.467364	2.793587	−0.253711	C	2.357881	2.051167	−0.615599
H	−2.083841	2.958174	−0.958568	C	1.451076	2.799591	−1.521640
H	−1.908762	2.646764	0.779383	C	0.134202	2.583993	−1.452755
H	3.023349	−1.978491	1.534819	C	−0.666486	2.534312	1.662427
H	1.925983	−2.944504	0.455143	C	−1.961693	2.852909	1.743565
H	3.636037	−2.627751	−0.041712	C	−2.922549	2.236884	0.794442
H	3.564034	0.727650	1.414541	C	−2.478525	1.348805	−0.099240
H	4.610696	0.310593	0.029831	O	−0.449699	−0.512344	1.332116
H	2.647438	2.738873	0.091874	C	−0.806218	−3.492196	−1.607943
H	3.718605	2.309610	−1.276802	C	−2.113972	−3.695708	−1.792722
H	4.411612	2.828165	0.278750	C	−3.089815	−2.983649	−0.930093
H	−0.512261	−2.817750	−1.189223	C	−2.641836	−2.128745	−0.006669
				H	2.390427	0.551706	0.953867
				H	−3.066413	0.835896	−0.859989
				H	2.345414	−1.773182	−0.649706
				H	−3.241527	−1.554185	0.698631
				H	0.130597	2.914586	2.301588
				H	−0.629073	3.070064	−2.060885
				H	−1.120504	−3.996035	2.101481
				H	0.002612	−3.952302	−2.175947
				H	3.431042	2.261301	−0.670753
				H	−3.973786	2.536486	0.857125
				H	3.099224	−3.544872	1.068778
				H	−4.155238	−3.187205	−1.079337
				H	1.893369	3.517252	−2.219810
				H	−2.346171	3.561134	2.484325
				H	1.331474	−4.652646	2.481778
				H	−2.499280	−4.377503	−2.557498

Table B.14: Basis sets used for the computation of isotropic parity violating shielding constants of ^{183}W in the NWXYZ compounds discussed in Chapter 7.6. On hydrogen, the aug-cc-pVDZ basis set of Ref. [277, 278] was employed in uncontracted form. For all other centers, exponent coefficients α_i^{orb} of the uncontracted spherical Gaussian basis sets for all other atoms were taken from an even tempered list generated according to the prescription described in the caption of Table B.7.

X	Basis set for X	X	Basis set for X	X	Basis set for X
N	1-25:2-26:20-24:22-23	Br	1-25:2-26:15-25:20-24	Cl	1-25:2-26:15-25:22-23
W	1-25:2-26:12-15:15-25	F	1-25:2-26:15-25:22-23	I	1-25:2-26:15-25:20-24

Table B.15: Cartesian nuclear coordinates in Ångstrøm used in the calculation of PV NMR shielding tensors of the NWXYZ compounds in Chapter 7.6.

Nucleus	x	y	z	Nucleus	x	y	z
		NWHFCl				NWHBrI	
N	−0.003204	−0.001027	1.620052	N	−0.002640	0.078825	1.672434
W	0.049028	−0.126663	−0.030939	W	0.050159	−0.057873	0.023424
H	−0.764547	1.333700	−0.389752	H	−0.763915	1.396007	−0.344018
F	−0.992098	−1.591769	−0.494737	Br	−1.330278	−1.934577	−0.606222
Cl	2.223615	0.057691	−0.645825	I	2.559469	0.189549	−0.686818
		NWHFBr				NWFClBr	
N	−0.027528	−0.001276	1.630013	N	−0.029648	−0.054315	1.611439
W	0.018412	−0.129708	−0.020848	W	−0.007278	−0.038273	−0.044073
H	−0.786605	1.334848	−0.381558	F	1.786305	−0.043772	−0.516759
F	−1.022611	−1.595484	−0.485152	Cl	−1.097138	1.855673	−0.653529
Br	2.331127	0.063552	−0.683656	Br	−1.165034	−2.047382	−0.720477
		NWHFI				NWFClI	
N	−0.057762	−0.001702	1.642115	N	−0.217417	−0.007679	1.619325
W	−0.026537	−0.132774	−0.008820	W	−0.221862	0.001747	−0.036596
H	−0.821467	1.337375	−0.369364	F	−1.102838	1.558722	−0.529268
F	−1.066213	−1.601123	−0.471220	Cl	−1.285290	−1.901919	−0.664598
I	2.484773	0.070155	−0.733910	I	2.314613	0.021061	−0.712262
		NWHClBr				NWFBrI	
N	0.013428	0.060732	1.653958	N	−0.204436	0.012605	1.627174
W	0.073973	−0.073582	0.004629	W	−0.205288	0.027993	−0.028670
H	−0.744860	1.378596	−0.360843	F	−1.090281	1.583103	−0.521557
Cl	−1.213940	−1.842233	−0.587926	Br	−1.345314	−1.994798	−0.698644
Br	2.384193	0.148419	−0.651019	I	2.332525	0.043028	−0.701703
		NWHClI				NWClBrI	
N	−0.016099	0.059489	1.664586	N	−0.165333	−0.058160	1.646894
W	0.029389	−0.079343	0.015303	W	−0.165930	−0.039643	−0.008496
H	−0.775920	1.380286	−0.350286	Cl	−1.246675	1.861968	−0.609637
Cl	−1.262364	−1.848193	−0.571885	Br	−1.307079	−2.059794	−0.679102
I	2.537789	0.159693	−0.698919	I	2.372223	−0.032439	−0.673058

Table B.16: Basis sets used for the computation of the parity violating potential and isotropic parity violating shielding constants of ^{183}W in the transition metal compounds discussed in Chapter 7.7. On the lighter atoms, the DZP basis set of Ref. [282] was employed in compounds W–1, W–2 and W–3. In W–4, the TZVP basis set of Ref. [285] was used on C, O and Fe, and the TZP basis set of Ref. [283] on H. For all other centers, exponent coefficients α_i^{orb} of the uncontracted spherical Gaussian basis sets for all other atoms were taken from an even tempered list generated according to the prescription described in the caption of Table B.7.

X	Basis set for X	X	Basis set for X	X	Basis set for X
Rh	1-25:2-26:15-25	Os	1-25:2-26:12-25:15-22	W	1-25:2-26:12-25:15-22

Table B.17: Cartesian nuclear coordinates in Ångstrøm used in the calculation of PV potentials and ^{183}W NMR shielding tensors of the chiral organometallic complexes W–1, W–2 and W–3 (Figures 7.10,7.11 and 7.12, respectively) discussed in Chapter 7.7.

Nucleus	x	y	z	Nucleus	x	y	z
		W–1				W–3	
W	0.009540	−0.114751	−0.100989	W	0.011606	−0.053419	−0.047328
C	−1.025812	1.358799	0.742254	C	−1.410462	1.166763	0.665353
O	−1.642115	2.183375	1.296128	O	−2.241453	1.836727	1.154492
C	−0.164704	−1.469782	1.831133	C	−0.093783	−1.302605	1.948378
C	0.774993	−2.126855	0.962851	C	1.102331	−1.733490	1.261779
C	0.066846	−2.580220	−0.190732	C	0.707077	−2.417465	0.062769
C	−1.306114	−2.211978	−0.047049	C	−0.727855	−2.407860	−0.013436
C	−1.449335	−1.519698	1.191763	C	−1.223529	−1.714222	1.143951
H	1.824905	−2.290893	1.168319	H	2.129419	−1.598915	1.614850
H	0.489077	−3.133259	−1.017606	H	1.381223	−2.894567	−0.651367
H	−2.103853	−2.450350	−0.735237	H	−1.331830	−2.892664	−0.781662
H	−2.375557	−1.133940	1.598122	H	−2.278037	−1.565462	1.396522
H	0.043848	−1.065883	2.812995	H	−0.137978	−0.806130	2.922014
C	1.643571	0.753455	0.666141	C	1.343129	1.203534	0.756536
O	2.585728	1.189126	1.193680	O	2.119149	1.885993	1.317608
Co	1.568237	0.334239	−2.568238	Rh	1.543357	0.184457	−2.681236
Fe	−1.148663	0.150741	−2.814960	Os	−1.384922	0.131770	−2.803814
C	−1.125506	−1.602421	−3.267032	C	−1.646406	−1.775596	−3.140986
O	−1.117281	−2.723295	−3.569126	O	−1.796091	−2.919357	−3.347614
P	−0.016302	1.662529	−1.800567	P	−0.010178	1.721100	−1.796069
C	2.949704	1.437149	−2.273319	C	3.272330	0.619589	−1.856178
O	3.850366	2.151375	−2.142071	O	4.316513	0.858398	−1.403775
C	2.232166	−1.309815	−2.255318	C	1.650634	−1.738359	−3.057282
O	2.770963	−2.328848	−2.123009	O	1.744300	−2.866826	−3.332299
C	1.467262	0.343700	−4.354550	C	1.759267	0.964035	−4.455858
O	1.527841	0.349891	−5.510317	O	1.916922	1.420058	−5.513343
C	−2.779826	0.258665	−2.131761	C	−3.159022	0.508660	−2.188872
O	−3.850929	0.330450	−1.686432	O	−4.235715	0.748318	−1.793986
C	−1.566502	0.940626	−4.367681	C	−1.674363	0.802068	−4.592523
O	−1.888714	1.459497	−5.352699	O	−1.856743	1.212073	−5.672981
C	0.014874	3.503038	−1.592736	C	0.116508	3.569903	−1.582317
H	0.877384	3.799517	−0.987192	H	1.010219	3.821382	−0.979828
H	−0.907937	3.831331	−1.102898	H	−0.797265	3.939764	−1.077601
H	0.085689	3.964476	−2.583126	H	0.195494	4.032337	−2.585159
		W–2					
W	0.171578	0.012893	1.348184				
C	−0.733647	1.567646	2.193780				
O	−1.247885	2.451329	2.755821				
C	0.535454	−0.985729	3.432220				
C	1.294864	−1.743506	2.476595				
C	0.374944	−2.410298	1.610826				
C	−0.949421	−2.068664	2.014828				
C	−0.853413	−1.180673	3.127075				
H	2.376475	−1.834896	2.449762				
H	0.634334	−3.095392	0.811723				
H	−1.867541	−2.450529	1.583855				
H	−1.690569	−0.763111	3.678889				
H	0.935156	−0.414351	4.264170				
C	1.845654	1.066887	1.573200				
O	2.833112	1.643860	1.797533				
Rh	1.028073	−0.113361	−1.535665				
Fe	−1.657621	−0.000672	−0.906438				
C	−1.877104	−1.773742	−1.013321				
O	−2.064342	−2.918345	−1.106304				
P	−0.231859	1.547968	−0.526608				
C	2.872816	0.483379	−1.399436				
O	3.973844	0.828289	−1.398342				
C	1.217111	−2.057593	−1.561207				
O	1.378454	−3.198634	−1.649990				
C	0.677236	0.274424	−3.397405				
O	0.497550	0.492341	−4.515557				
C	−3.040550	0.383427	0.113197				
O	−3.958457	0.633803	0.782315				
C	−2.408247	0.528665	−2.426903				
O	−2.940013	0.884458	−3.396036				
C	−0.070717	3.387139	−0.601297				
H	0.941230	3.687947	−0.302327				
H	−0.809810	3.845331	0.069159				
H	−0.264566	3.710730	−1.632011				

Table B.18: Cartesian nuclear coordinates in Ångstrøm used in the calculation of PV potential and ^{183} NMR shielding tensors of the chiral organometallic complex W–4 (Figure 7.13) discussed in Chapter 7.7.

Nucleus	x	y	z	Nucleus	x	y	z
C	−3.064400	−1.444432	−1.109286	O	−3.034401	−0.210291	3.317696
C	−3.621846	−0.727469	−0.004276	C	−0.859371	−1.872839	1.169530
C	−3.941535	0.597740	−0.449249	O	−1.504291	−2.842855	1.414916
C	−3.594739	0.699051	−1.845962	C	−0.163157	1.645202	2.458265
C	−3.044728	−0.572797	−2.244738	O	0.020245	2.705953	2.892826
W	−1.565883	0.447639	−0.664932	C	−1.616584	2.399441	−0.250504
Fe	−0.471276	−0.014124	1.872614	O	−1.724809	3.541542	−0.037351
C	0.674845	−0.712474	3.033123	C	−0.535384	0.852921	−2.316851
O	1.412074	−1.185509	3.800659	O	−0.021102	1.050079	−3.348184
Rh	0.503617	−1.364564	−0.125650	H	−4.419252	1.380670	0.154717
C	0.384629	0.649222	0.169724	H	−3.804249	−1.136996	0.995611
C	1.568873	1.520145	0.048475	H	−2.720948	−2.485702	−1.082878
C	1.615155	2.660485	−0.794930	H	−2.709120	−0.839156	−3.255976
C	2.748908	3.482682	−0.851925	H	0.740744	2.921168	−1.408812
C	3.894437	3.215092	−0.073919	H	2.737113	4.365018	−1.514962
C	3.862061	2.071707	0.755128	H	4.741902	1.821924	1.372904
C	2.733743	1.247613	0.817789	H	2.741364	0.366948	1.479094
C	5.097702	4.129325	−0.099194	H	6.049397	3.557932	−0.028628
C	2.688715	−2.634475	−0.340528	H	5.129767	4.741061	−1.026410
C	3.873010	−2.543097	0.427979	H	5.081959	4.837627	0.762295
C	4.890460	−1.688930	−0.010695	H	1.293719	−4.175055	0.597374
C	4.737369	−0.903031	−1.184239	H	0.842057	−1.760653	−3.061028
C	3.569128	−0.960531	−1.950512	H	3.456192	−0.343220	−2.855797
C	2.536122	−1.837579	−1.543818	H	5.558625	−0.238286	−1.497456
C	1.226152	−2.147643	−2.107723	H	5.828993	−1.621725	0.563909
C	0.652040	−3.225329	−1.343109	H	3.994357	−3.146553	1.341920
C	1.473590	−3.430468	−0.189983	H	−0.269567	−3.772097	−1.584431
C	−2.035846	−0.145783	2.721175	H	−3.778263	1.560387	−2.501033

Table B.19: Calculated structural parameters and harmonic vibrational frequencies of the R–enantiomer of $[H_2C = ThFCl]$ in the ground electronic state.

R(X,Y)	R/Å	A(X,Y,Z)	A/°	D(W,X,Y,Z)	D/°	Mode	ν/cm^{-1}
R(C,Th)	2.1254	A(Th,C,H1)	95.5603	D(H1,C,Th,F)	−153.3592	Th-F str	534.1
R(C,H1)	1.1207	A(Th,C,H2)	153.1387	D(H1,C,Th,Cl)	−30.4058	CH_2 wag	634.7
R(C,H2)	1.0943	A(H1,C,H2)	109.7566	D(H2,C,Th,F)	7.3526	C=Th str	673.0
R(Th,F)	2.1053	A(C,Th,F)	108.597	D(H2,C,Th,Cl)	130.306		
R(Th,Cl)	2.614	A(C,Th,Cl)	104.9954				
		A(F,Th,Cl)	114.5498				

B.3   Details of $[H_2C = ThFCl]$ vibrational frequency calculations

In Chapter 8 PV vibrational frequency splittings for the newly synthesized chiral actinide compound $[H_2C = ThFCl]$ were reported. Structures optimizations and harmonic force field calculations for this compound were performed with the Gaussian 03 program package, [286] using the 78 core–electron, scalar–relativistic Stuttgart pseudopotential together with an energy–optimized valence basis set with a (12s11p10d8f)/[8s7p6d4f] contraction on thorium. [287] For period 1–3 atoms (H, C, F and Cl) we employed the correlation consistent polarized triple–zeta basis set (cc-pVTZ), [277, 278, 280]. All of these calculations were performed at the density functional theory level using the PW91PW91 exchange–correlation functional.[288] Results are listed in Table B.19.

Along the reduced normal coordinate q_7 corresponding to the Th–F stretching mode, around 300 single–point calculations of the parity conserving electronic energy at fixed nuclear configurations from $q_7 = -7$ to $q_7 = 7$ were performed using the Gaussian 03 program package [286] at the same level of theory and using the same basis sets and pseudopotential on thorium as during the geometry optimization.

$V_{PV}(q_7)$ was calculated using Hartree–Fock and density functional theory at 17 points from $q_7 = -3$ to $q_7 = 3$ with the finest spacing near the equilibrium geometry. At the DFT level the local density approximation (LDA) [254–256] and the hybrid functional B3LYP[256, 270, 281, 289], containing Becke's generalized gradient approximation functional[252] and 20% exact exchange for the exchange–contribution and the Lee–Yang–Parr correlation function [253] were used. On all centers except hydrogen, large, even-tempered basis sets [68, 250] with varying numbers of basis functions were used in the two–component calculations. On hydrogen the aug-cc-pVDZ basis set [277, 278] in uncontracted form was employed. Details of the basis sets are listed in Table B.21 (see Refs. [58, 59, 68, 156, 250] for details of the nomenclature).

Table B.20: Expectation values of q_7^x (dimensionless) for the first two vibrational levels of $[H_2C = ThFCl]$ and $V_{PV}(q_7)$ fit parameters $p_x^{(7)}$ (10^{-12}cm^{-1}) for different functionals.

x	$\langle n_7^1 | q_7^x | n_7^1 \rangle$	$\langle n_7^2 | q_7^x | n_7^2 \rangle$	$\langle n_7^3 | q_7^x | n_7^3 \rangle$	$p_x^{(7)}$ HF	$p_x^{(7)}$ B3LYP	$p_x^{(7)}$ LDA
0	1.0	1.0	1.0	676.3	-3712.3	-5390.4
1	0.06624056769	0.1949127725	0.3204610176	-1646.2	-1288.2	-1027.9
2	0.5071472894	1.548712147	2.628853237	-24.63	-38.30	-54.06
3	0.1217271612	0.7820095616	2.100120497	6.044	6.393	6.139
4	0.7788313096	4.091412728	11.15614900	-0.3775	-0.3438	

Table B.21: Basis sets used for the computation of parity violating potentials in conformers of $[H_2C = ThFCl]$. Exponent coefficients α_i^{orb} of the uncontracted spherical Gaussian basis sets for all other atoms were taken from an even tempered list generated according to $\alpha_i^{\mathrm{orb}} = \gamma \beta^{N-i}$ with $i = 1, 2, \ldots, N$ and $N = 26$. $\alpha_{26}^{\mathrm{orb}} = \gamma = (2/100)\ a_0^{-2}$ and $\alpha_1^{\mathrm{orb}} = 500000000\ a_0^{-2}$ were chosen as the smallest and largest exponent of this list, respectively. The intermediate exponents were used with at least nine significant figures. For example, 1-25:2-26:20-24:20-24 implies that the exponents from this list ranging from $i = 1$ to $i = 25$ were employed for the s-Gaussians, exponents $i = 2$ to $i = 26$ for the p-Gaussians and $i = 20$ to $i = 24$ for the d- and f-Gaussians.

X	Basis set for X	X	Basis set for X
C	1-25:2-26:20-24	Cl	1-25:2-26:20-24
F	1-25:2-26:20-24	Th	1-25:2-26:6-25:12-26

Bibliography

[1] Y. Yamagata. A hypothesis for the asymmetric appearance of biomolecules on earth. *J. Theor. Biol.*, 11:495–498, 1966.

[2] D.W. Rein. Some remarks on parity violating effects of intramolecular interactions. *J. Mol. Evol.*, 4:15–22, 1974.

[3] V.S. Letokhov. On difference of energy levels of left and right molecules due to weak interactions. *Phys. Lett. A*, 53:275–276, 1975.

[4] R.A. Hegstrom, D.W. Rein, and P.G.H. Sandars. Calculation of the parity non-conserving energy difference between mirror-image molecules. *J. Chem. Phys.*, 73:2329–2341, 1980.

[5] I.B. Khriplovich. On the energy difference of optical isomers due to parity non-conservation. *Sov. Phys. JETP*, 52:177–183, 1980.

[6] V.G. Gorshkov, M.G. Kozlov, and L.N. Labzowsky. *P*-odd effects in polyatomic molecules. *Sov. Phys. JETP*, 55:1042–1048, 1982.

[7] S.F. Mason and G.E. Tranter. The parity-violating energy difference between enantiomeric molecules. *Chem. Phys. Lett.*, 94:34–37, 1983.

[8] M. Quack. On the measurement of the parity violating energy difference between enantiomers. *Chem. Phys. Lett.*, 132:147–153, 1986.

[9] I. B. Zel'dovich. Electromagnetic interaction with parity violation. *J. Exptl. Theoret. Phys. (U.S.S.R)*, 33:1531–1533, 1957.

[10] B.Ya. Zel'dovich. Parity nonconservation in the first order in the weak-interaction constant in electron scattering and other effects. *Sov. Phys. JETP*, 9:682–683, 1959.

[11] L.C. Bradley and N.S. Wall. The absence of circular dichroism in $^{16}O_2$ and a resultant upper limit for parity nonconservation. *Il Nuovo Cimento*, 25:48–54, 1962.

[12] P. G. H. Sandars. Measurability of the proton electric dipole moment. *Phys. Rev. Lett.*, 19:1396–1398, 1967.

[13] V.V. Flambaum and I.B. Khriplovich. Nuclear anapole moments. *Phys. Lett. B*, 146:367–369, 1984.

[14] V.V. Flambaum and I.B. Khriplovich. On the enhancement of parity nonconserving effects in diatomic molecules. *Phys. Lett. A*, 110:121–125, 1985.

[15] M.G. Kozlov, V.I. Fomichev, Y.Y. Dmitriev, L.N. Labzowsky, and A.V. Titov. Calculations of the P- and T-odd spin-rotational Hamiltonian of the PbF molecule. *J. Phys. B*, 20:4939–4948, 1987.

[16] D. DeMille, S. B. Cahn, D. Murphree, D. A. Rahmlow, and M. G. Kozlov. Using molecules to measure nuclear spin-dependent parity violation. *Phys. Rev. Lett.*, 100(2):023003, 2008.

[17] A. Czarnecki and W. J. Marciano. Particle physics Electrons are not ambidextrous. *Nature*, 435:437–438, 2005.

[18] S. G. Porsev, K. Beloy, and A. Derevianko. Precision determination of electroweak coupling from atomic parity violation and implications for particle physics. *Phys. Rev. Lett.*, 102(18):181601, 2009.

[19] Z. Han and W. Skiba. Effective theory analysis of precision electroweak data. *Phys. Rev. D*, 71:075009, 2005.

[20] A. Derevianko and S. G. Porsev. Theoretical overview of atomic parity violation. *Eur. Phys. J. A*, 32:517–523, 2007.

[21] J.L. Rosner. Role of present and future atomic parity violation experiments in precision electroweak tests. *Phys. Rev. D*, 65(7):073026, 2002.

[22] O.N. Kompanets, A.R. Kukudzhanov, V.S. Letokhov, and L.L. Gervits. Narrow resonances of saturated absorption of the asymmetrical molecule CHFClBr and the possibility of weak current detection in molecular physics. *Opt. Commun.*, 19: 414–416, 1976.

[23] B.Ya. Zel'dovich, D.B. Saakyan, and I.I. Sobel'man. Energy difference between right-hand and left-hand molecules, due to parity nonconservation in weak interactions of electrons with nuclei. *JETP Lett.*, 25:94–97, 1977.

[24] R.A. Harris and L. Stodolski. Quantum beats in optical activity and weak interactions. *Phys. Lett. B*, 78:313–317, 1978.

[25] D.W. Rein, R.A. Hegstrom, and P.G.H. Sandars. Parity non-conserving energy differences between mirror image molecules. *Phys. Lett.*, 71A:499–502, 1979.

[26] R.A. Harris and L. Stodolski. The effect of the parity violating electron-nucleus interaction on the spin-spin coupling Hamiltonian of chiral molecules. *J. Chem. Phys.*, 73:3862–3863, 1980.

[27] S.F. Mason and G.E. Tranter. The parity-violating energy difference between enantiomeric molecules. *Mol. Phys.*, 53:1091–1111, 1984.

[28] G.E. Tranter. The parity violating energy differences between the enantiomers of α-amino acids. *Chem. Phys. Lett.*, 120:93–96, 1985.

[29] G.E. Tranter. Parity-violating energy differences of chiral minerals and the origin of biomolecular homochirality. *Nature (London)*, 318:172–173, 1985.

[30] M. Cattani and J.M.F. Bassalo. Weak interactions and the tunneling racemization. *Chirality*, 10:519–521, 1998.

[31] R.A. Hegstrom. Parity nonconservation and the origin of biological chirality: Theoretical calculations. *Origins Life Evol. B*, 14:405–411, 1984.

[32] S.F. Mason and G.E. Tranter. The electroweak origin of biomolecular handedness. *Proc. Roy. Soc. Lond. A*, 397:45–65, 1985.

[33] W. A. Bonner. Parity violation and the evolution of biomolecular homochirality. *Chirality*, 12:114–126, 2000.

[34] M. Quack. How important is parity violation for molecular and biomolecular chirality? *Angew. Chem. Int. Ed.*, 41:4618–4630, 2002.

[35] R. Wesendrup, J. K. Laerdahl, R. Compton, and P. Schwerdtfeger. Biomolecular homochirality and electroweak interactions. I. The Yamagata hypothesis. *J. Chem. Phys.*, 107:6668–6673, 2003.

[36] J. Crassous, C. Chardonnet, T. Saue, and P. Schwerdtfeger. Recent experimental and theoretical developments towards the observation of parity violation (PV) effects in molecules by spectroscopy. *Org. Biomol. Chem.*, 3:2218–2224, 2005.

[37] I.B. Khriplovich. *Parity Nonconservation in Atomic Phenomena*. Gordon and Breach Science Publ., Philadelphia, 1991.

[38] M.G. Kozlov and L.N. Labzowsky. Parity violation effects in diatomics. *J. Phys. B*, 28:1933–1961, 1995.

[39] C. S. Wood, S. C. Bennett, D. Cho, B. P. Masterson, J. L. Roberts, C. E. Tanner, and C. E. Wieman. Measurement of parity nonconservation and an anapole moment in cesium. *Science*, 21:1759 – 1763, 1997.

[40] S.C. Bennett and C.E. Wieman. Measurement of the 6s → 7s transition polarizability in atomic cesium and an improved test of the standard model. *Phys. Rev. Lett.*, 82(12):2484–2487, 1999.

[41] M. J. D. Macpherson, K. P. Zetie, R. B. Warrington, D. N. Stacey, and J. P. Hoare. Precise measurement of parity nonconserving optical rotation at 876 nm in atomic bismuth. *Phys. Rev. Lett.*, 67:2784–2787, 1991.

[42] D. M. Meekhof, P. Vetter, P. K. Majumder, S. K. Lamoreaux, and E. N. Fortson. High-precision measurement of parity nonconserving optical rotation in atomic lead. *Phys. Rev. Lett.*, 71:3442–3445, 1993.

[43] P. A. Vetter, D. M. Meekhof, P. K. Majumder, S. K. Lamoreaux, and E. N. Fortson. Precise test of electroweak theory from a new measurement of parity nonconservation in atomic thallium. *Phys. Rev. Lett.*, 74:2658–2661, 1995.

[44] N. H. Edwards, S. J. Phipp, P. E. G. Baird, and S. Nakayama. Precise measurement of parity nonconserving optical rotation in atomic thallium. *Phys. Rev. Lett.*, 74: 2654–2657, 1995.

[45] K. Tsigutkin, D. Dounas-Frazer, A. Family, J. E. Stalnaker, V. V. Yashchuk, and D. Budker. Observation of a large atomic parity violation effect in ytterbium. *Phys. Rev. Lett.*, 103(7):071601, 2009.

[46] L.N. Labzowsky. Λ–doubling and parity–nonconservation effects in spectra of diatomic molecules. *Sov. Phys. JETP*, 48:434–439, 1978.

[47] O.P. Sushkov and V.V. Flambaum. Parity breaking effects in diatomic molecules. *Sov. Phys. JETP*, 48:608–611, 1978.

[48] A. V. Titov, N. S. Mosyagin, A. N. Petrov, T. A. Isaev, and D. P. DeMille. P,T–parity violation effects in polar heavy–atom molecules. In P. Schwerdtfeger, editor, *Recent Advances in the Theory of Chemical and Physical Systems*, pages 253–283, Netherlands, 2006. Springer.

[49] Malaya K. Nayak and B. P. Das. Relativistic configuration-interaction study of the nuclear-spin-dependent parity-nonconserving electron-nucleus interaction constant WA in BaF. *Phys. Rev. A*, 79(6):060502, 2009.

[50] R. Berger. Molecular parity violation in electronically excited states. *Phys. Chem. Chem. Phys.*, 5:12–17, 2003.

[51] M. Quack. Structure and dynamics of chiral molecules. *Angew. Chem. Int. Ed.*, 28:571–586, 1989.

[52] A. Amann. Chirality: A superselection rule generated by the molecular environment. *J. Math. Chem.*, 6:1–15, 1991.

[53] A.L. Barra, J.B. Robert, and L. Wiesenfeld. Parity non-conservation and NMR observables. Calculation of Tl resonance frequency differences in enantiomers. *Phys. Lett. A*, 115:443–447, 1986.

[54] A.L. Barra, J.B. Robert, and L. Wiesenfeld. Possible observation of parity non-conservation by high–resolution NMR. *Europhys. Lett.*, 5:217–222, 1988.

[55] A.L. Barra and J.B. Robert. Parity non-conservation and NMR parameters. *Mol. Phys.*, 88:875–886, 1996.

[56] J.B. Robert and A.L. Barra. NMR and parity nonconservation. Experimental requirements to observe a difference between enantiomer signals. *Chirality*, 13: 699–702, 2001.

[57] S. Nahrwold and R. Berger. Zeroth order regular approximation approach to parity violating nuclear magnetic resonance shielding tensors. *J. Chem. Phys.*, 130:214101–214114, 2009.

[58] R. Berger, N. Langermann, and C. van Wüllen. Zeroth order regular approximation approach to molecular parity violation. *Phys. Rev. A*, 71:042105, 2005.

[59] R. Berger and C. van Wüllen. Density functional calculations of molecular parity violating effects within the zeroth order regular approximation. *J. Chem. Phys.*, 122:134316, 2005.

[60] Ch. Chang, M. Pelissier, and Ph. Durand. Regular two-component Pauli-like effective Hamiltonians in Dirac theory. *Phys. Scr.*, 34:394–404, 1986.

[61] E. van Lenthe, E.-J. Baerends, and J.G. Snijders. Relativistic regular two-component Hamiltonians. *J. Chem. Phys.*, 99:4597, 1993.

[62] S.K. Wolff, T. Ziegler, E. van Lenthe, and E.J. Baerends. Density functional calculations of nuclear magnetic shieldings using the zeroth-order regular approximation (ZORA) for relativistic effects: ZORA nuclear magnetic resonance. *J. Chem. Phys.*, 110:7689, 1999.

[63] C. van Wüllen. Molecular density functional calculations in the regular relativistic approximation: Method, application to coinage metal diatomics, hydrides, fluorides and chlorides, and comparison with first-order relativistic calculations. *J. Chem. Phys.*, 109:392–399, 1998.

[64] R. Ahlrichs, M. Bär, M. Häser, H. Horn, and C. Kölmel. Electronic structure calculations on workstation computers: The program system turbomole. *Chem. Phys. Lett.*, 162:165–169, 1989.

[65] M. Häser and R. Ahlrichs. Improvements on the direct SCF method. *J. Comput. Chem.*, 10:104–111, 1989.

[66] G. Laubender and R. Berger. Electroweak quantum chemistry for nuclear magnetic resonance shielding constants: Impact of electron correlation. *Phys.Rev.A*, 74: 032105, 2006.

[67] M.A. Bouchiat and C. Bouchiat. I. Parity violation induced by weak neutral currents in atomic physics. *J. Phys. (Paris)*, 35:899–927, 1974.

[68] R. Bast, P. Schwerdtfeger, and Trond Saue. Parity nonconservation contribution to the nuclear magnetic resonance shielding constants of chiral molecules: A four-component relativistic study. *J. Chem. Phys.*, 125:064504, 2006.

[69] T. Saue. Private communication.

[70] S. Nahrwold, P. Heretsch, A. Giannis, and R. Berger. Parity violating effects in the ^{195}Pt NMR spectra of chiral platinum complexes. (in preparation), .

[71] S. Nahrwold, P. Schwerdtfeger, and R. Berger. Nuclear spin–dependent parity violation in tetrahedral tungsten complexes. (to be submitted), .

[72] C. Daussy, T. Marrel, A. Amy-Klein, C.T. Nguyen, C.J. Bordé, and C. Chardonnet. Limit on the parity nonconserving energy difference between the enantiomers of a chiral molecule by laser spectroscopy. *Phys. Rev. Lett.*, 83:1554–1557, 1999.

[73] M. Ziskind, C. Daussy, T. Marrel, and C. Chardonnet. Improved sensitivity in the search for a parity-violating energy difference in the vibrational spectrum of the enantiomers of CHFClBr. *Eur. Phys. J. D*, 20:219–225, 2002.

[74] S. Nahrwold, S. Brück, T. Isaev, and R. Berger. Measurable parity violating effect in chiral actinide complex. (submission pending), .

[75] M. P. Ledbetter, C. W. Crawford, A. Pines, D. E. Wemmer, S. Knappe, J. Kitching, and D. Budker. Optical detection of NMR J-spectra at zero magnetic field. *J. Magn. Reson.*, 199:25–29, 2009.

[76] I.B. Zel'dovich. Electromagnetic interaction with parity violation. *Sov. Phys. JETP*, 6(6):1184–1186, 1958.

[77] R. Berger. Parity-violation effects in molecules. In P. Schwerdtfeger, editor, *Relativistic Electronic Structure Theory, Part: 2, Applications*, pages 188–288, Netherlands, 2004. Elsevier.

[78] E. Arimondo, P. Glorieux, and T. Oka. Observation of inverted infrared lamb dips in separated optical isomers. *Opt. Commun.*, 23:369–372, 1977.

[79] R. Berger and M. Quack. Electroweak quantum chemistry of alanine: Parity violation in gas and condensed phases. *ChemPhysChem*, 1:57–60, 2000.

[80] L.N. Labzowsky. Λ–doubling and parity–nonconservation effects in spectra of diatomic molecules. *J. Exptl. Theoret. Phys. (U.S.S.R)*, 75:856, 1978.

[81] T. D. Lee and C. N. Yang. Question of parity conservation in weak interactions. *Phys. Rev.*, 104:254–258, 1956.

[82] H. Weyl. Elektron und Gravitation. I. *Z. Phys. A*, 56:330–352, 1929.

[83] W. Pauli. Die allgemeinen Prinzipien der Wellenmechanik. In H. Geiger and K. Scheel, editors, *Handbuch der Physik, Vol. 24*, page 233, Berlin, 1933. Springer Verlag.

[84] T. D. Lee and C. N. Yang. Parity nonconservation and a two-component theory of the neutrino. *Phys. Rev.*, 105:1671–1675, 1957.

[85] L. Landau. On the conservation laws for weak interactions. *Nuclear Physics*, 3: 127 – 131, 1957.

[86] A. Salam. On parity conservation and neutrino mass. *Il Nuovo Cimento (1955-1965)*, 5:299–301, 1957.

[87] R. Streater. Hermann Weyl, mathematician. http://www.mth.kcl.ac.uk/~streater/Weyl.html.

[88] C. S. Wu, E. Ambler, R. W. Hayward, D. D. Hoppes, and R. P. Hudson. Experimental test of parity conservation in beta decay. *Phys. Rev.*, 105:1413–1415, 1957.

[89] L. S. Rodberg and V. F. Weisskopf. Fall of Parity. *Science*, 125:627–633, 1957.

[90] December 27, 1956: Fall of parity conservation. *APS News*, 10(11), 2001.

[91] V.V. Flambaum and I.B. Khriplovich. *P*-odd nuclear forces — a source of parity violation in atoms. *Sov. Phys. JETP*, 52:835–839, 1980.

[92] W.C. Haxton and C.E. Wieman. Atomic parity nonconservation and nuclear anapole moments. *Ann. Rev. Nucl. Part. Sci.*, 51:261–293, 2001.

[93] M.A. Bouchiat and C. Bouchiat. An atomic linear stark shift violating p but not t arising from the electroweak nuclear anapole moment. *Eur. Phys. J. D*, 15:5–18, 2001.

[94] S.A. Bludman. On the universal Fermi interaction. *Il Nuovo Cimento*, 9:433–445, 1958.

[95] S. L. Glashow. Partial-symmetries of weak interactions. *Nucl. Phys.*, 22:579–588, 1961.

[96] A. Salam. Weak and electromagnetic interactions. In N. Svartholm, editor, *Proceedings of the Eighth Nobel Symposium*, pages 367–377, Stockholm, 1968. Amkvist and Wiksell.

[97] S. Weinberg. A model of leptons. *Phys. Rev. Lett.*, 19:1264–1266, 1967.

[98] Carl E. Carlson, Vahagn Nazaryan, and Keith Griffioen. Proton structure corrections to electronic and muonic hydrogen hyperfine splitting. *Phys. Rev. A*, 78(2): 022517, 2008.

[99] C.C. Bouchiat and M.A. Bouchiat. Parity violation induced by weak neutral currents in atomic physics. Part II. *J. Phys. (Paris)*, 36:493–509, 1975.

[100] F.J. Hasert, H. Faissner, W. Krenz, J. Von Krogh, D. Lanske, J. Morfin, K. Schultze, H. Weerts, G.H. Bertrand-Coremans, J. Lemonne, J. Sacton, W. Van Doninck, P. Vilain, C. Baltay, D.C. Cundy, D. Haidt, M. Jaffre, P. Musset, A. Pullia, S. Natali, J.B.M. Pattison, D.H. Perkins, A. Rousset, W. Venus, H.W. Wachsmuth, V. Brisson, B. Degrange, M. Haguenauer, L. Kluberg, U. Nguyen-Khac, P. Petiau, E. Bellotti, S. Bonetti, D. Cavalli, C. Conta, E. Fiorini, M. Rollier, B. Aubert, L.M. Chounet, P. Heusse, A. Lagarrigue, A.M. Lutz, J.P. Vialle, F.W. Bullock, M.J. Esten, T. Jones, J. McKenzie, A.G. Michette, G. Myatt, J. Pinfold, and W.G. Scott. Search for elastic muon-neutrino electron scattering. *Physics Letters B*, 46:121 – 124, 1973.

[101] L. M. Barkov and M. S. Zolotorev. Observation of parity nonconservation in atomic transitions. *Soviet Journal of Experimental and Theoretical Physics Letters*, 27: 357, 1978.

[102] L. M. Barkov and M. S. Zolotorev. Search for parity nonconservation in atomic transitions. *Soviet Journal of Quantum Electronics*, 8:986–988, 1978.

[103] R. Conti, P. Bucksbaum, S. Chu, E. Commins, and L. Hunter. Preliminary observation of parity nonconservation in atomic thallium. *Phys. Rev. Lett.*, 42(6): 343–346, 1979.

[104] C.Y. Prescott, W.B. Atwood, R.L.A. Cottrell, H. DeStaebler, Edward L. Garwin, A. Gonidec, R.H. Miller, L.S. Rochester, T. Sato, D.J. Sherden, C.K. Sinclair, S. Stein, R.E. Taylor, J.E. Clendenin, V.W. Hughes, N. Sasao, K.P. Schüler, M.G. Borghini, K. Lübelsmeyer, and W. Jentschke. Parity non-conservation in inelastic electron scattering. *Phys. Lett. B*, 77:347 – 352, 1978.

[105] G. Arnison et al. Experimental observation of lepton pairs of invariant mass around 95-GeV/c**2 at the CERN SPS collider. *Phys. Lett.*, B126:398–410, 1983. doi: 10.1016/0370-2693(83)90188-0.

[106] M.A. Bouchiat, J. Guena, L. Pottier, and L. Hunter. Atomic parity violation measurements in the highly forbidden $6S_{1/2}$ - $7S_{1/2}$ caesium transition. - III. Data acquisition and processing. results and implications. *J. Phys.*, 47:1709–1730, 1986.

[107] S. L. Gilbert, M. C. Noecker, R. N. Watts, and C. E. Wieman. Measurement of parity nonconservation in atomic cesium. *Phys. Rev. Lett.*, 55(24):2680–2683, 1985.

[108] D. V. Neuffer and E.D. Commins. Calculation of parity-nonconserving effects in the $6P_{1/2}$-$7P_{1/2}$ forbidden M1 transition in thallium. *Phys. Rev. A*, 16(3):844–862, 1977.

[109] P.S. Drell and E.D. Commins. Parity nonconservation in atomic thallium. *Phys. Rev. Lett.*, 53(10):968–971, 1984.

[110] P.S. Drell and E.D. Commins. Parity nonconservation in atomic thallium. *Phys. Rev. A*, 32(4):2196–2210, 1985.

[111] L. M. Barkov and M. S. Zolotorev. Parity nonconservation in bismuth atoms and neutral weak-interaction currents. *Sov. Phys. JETP*, 52:360, 1980.

[112] G. N. Birich, Yu. V. Bogdanov, S. I. Kanorskij, I. I. Sobelman, V.N. Sorokin, I. I. Struk, and E. A. Yukov. Nonconservation of parity in atomic bismuth. *Sov. Phys. JETP*, 87:776, 1984.

[113] J. Guéna, M. Lintz, and M.-A. Bouchiat. Atomic Parity Violation: Principles, recent results, present motivations. *Modern Physics Letters A*, 20:375–389, 2005.

[114] J. S. M. Ginges and V. V. Flambaum. Violations of fundamental symmetries in atoms and tests of unification theories of elementary particles. *Physics Reports*, 397:63–154, 2004.

[115] J. Sapirstein. Parity violation. In P. Schwerdtfeger, editor, *Relativistic Electronic Structure Theory, Part: 1, Fundamentals*, pages 471–525, Netherlands, 2002. Elsevier.

[116] A. Derevianko. Reconciliation of the measurement of parity nonconservation in cs with the standard model. *Phys. Rev. Lett.*, 85:1618–1621, 2000.

[117] N. Fortson. Possibility of measuring parity nonconservation with a single trapped atomic ion. *Phys. Rev. Lett.*, 70:2383–2386, 1993.

[118] J. A. Sherman, T. W. Koerber, A. Markhotok, W. Nagourney, and E. N. Fortson. Precision measurement of light shifts in a single trapped Ba+ ion. *Phys. Rev. Lett.*, 94:243001, 2005.

[119] L. W. Wansbeek, B. K. Sahoo, R. G. E. Timmermans, K. Jungmann, B. P. Das, and D. Mukherjee. Atomic parity nonconservation in Ra+. *Phys. Rev. A*, 78(5): 050501, 2008.

[120] J. Guéna, D. Chauvat, Ph. Jacquier, E. Jahier, M. Lintz, S. Sanguinetti, A. Wasan, M. A. Bouchiat, A. V. Papoyan, and D. Sarkisyan. New manifestation of atomic parity violation in cesium: A chiral optical gain induced by linearly polarized $6S - 7S$ excitation. *Phys. Rev. Lett.*, 90(14):143001, 2003.

[121] M. Lintz, J.Guena, and M. A. Bouchiat. Pump-probe measurement of atomic parity violation in caesium with a precision of 2.6%. *Eur. Phys. J. A*, 32:525, 2007.

[122] M.G. Kozlov. Semiempirical calculations of P- and P,T-odd effects in diatomic molecules-radicals. *Sov. Phys. JETP*, 62:1114–1118, 1985.

[123] L. D. Carr, D. DeMille, R. V. Krems, and J. Ye. Cold and ultracold molecules: science, technology and applications. *New Journal of Physics*, 11:055049 (87pp), 2009.

[124] F. Vester, T. L.V. Ulbricht, and H. Krauch. Optische Aktivität und die Paritätsverletzung im β-Zerfall. *Naturwissenschaften*, 46:68–68, 1959.

[125] D.K. Kondepudi and G.W. Nelson. Weak neutral currents and the origin of biomolecular chirality. *Nature*, 314:438–441, 1985.

[126] R.A. Hegstrom. Parity violation and chiral symmetry breaking of a racemic mixture. *Biosystems*, 20:49, 1987.

[127] R. Berger, M. Quack, and G.S. Tschumper. Electroweak quantum chemistry for possible precursor molecules in the evolution of biomolecular homochirality. *Helv. Chim. Acta*, 83:1919–1950, 2000.

[128] M. Quack and J. Stohner. Molecular chirality and the fundamental symmetries of physics: Influence of parity violation on rovibrational frequencies and thermodynamic properties. *Chirality*, 13:745–753, 2001.

[129] S. Chandrasekhar. Molecular homochirality and the parity-violating energy difference. a critique with new proposals. *Chirality*, 20:84–95, 2008.

[130] D.K. Kondepudi and G.W. Nelson. Chiral symmetry-breaking in non-equilibrium systems. *Phys. Rev. Lett.*, 50:1023–1026, 1983.

[131] D.K. Kondepudi and G.W. Nelson. Chiral symmetry-breaking in nonequilibrium chemical systems — time scales for chiral selection. *Phys. Lett. A*, 106:203–206, 1984.

[132] A. Salam. The role of chirality in the origin of life. *J. Mol. Evol.*, 33:105–113, 1991.

[133] W.A. Bonner. Chiral amplification — the accumulation principle revisited. *Orig. Life Evol. B.*, 29:615–623, 1999.

[134] S.F. Mason. Extraterrestrial handedness revisited. *Origins Life Evol. B.*, 30: 435–437, 2000.

[135] A. Jorissen and C. Cerf. Asymmetric photoreactions as the origin of biomolecular homochirality: A critical review. *Origins Life Evol. B.*, 32:129–142, 2000.

[136] R.A. Hegstrom and D.K. Kondepudi. Influence of static magnetic fields on chirally autocatalytic radical-pair reactions. *Chem. Phys. Lett.*, 253:322–326, 1996.

[137] R.S. Cahn, C. Ingold, and V. Prelog. Specification of molecular chirality. *Angew. Chem. Int. Ed.*, 5:385, 1966.

[138] A. S. Wightman. Superselection rules; old and new. *Il Nuovo Cimento B*, 110: 751–769, 1995.

[139] A. Vardi. On the role of intermolecular interactions in establishing chiral stability. *J. Chem. Phys.*, 112:8743–8746, 2000.

[140] A.S. Lahamer, S.M. Mahurin, R.N. Compton, D. House, J.K. Laerdahl, M. Lein, and P. Schwerdtfeger. Search for a parity-violating energy difference between enantiomers of a chiral iron complex. *Phys. Rev. Lett.*, 85:4470–4473, 2000.

[141] A. Szabó-Nagy and L. Keszthelyi. Demonstration of the parity-violating energy difference between enantiomers. *Proc. Natl. Acad. Sci. U S A*, 96:4252–4255, 1999.

[142] M. Quack and J. Stohner. Influence of parity violating weak nuclear potentials on vibrational and rotational frequencies in chiral molecules. *Phys. Rev. Lett.*, 84: 3807–3810, 2000.

[143] J.K. Laerdahl, P. Schwerdtfeger, and H.M. Quiney. Theoretical analysis of parity-violating energy differences between the enantiomers of chiral molecules. *Phys. Rev. Lett*, 84:3811–3814, 2000.

[144] R.G. Viglione, R. Zanasi, P. Lazzeretti, and A. Ligabue. Theoretical determination of parity-violating vibrational frequency differences between the enantiomers of the CHFClBr molecule. *Phys. Rev. A*, 62:052516, 2000.

[145] C. Chardonnet, C. Daussy, O. Lopez, and A. Amy-Klein. Towards a first observation of molecular parity violation by laser spectroscopy. In G. Maroulis and T. Simos, editors, *Trends and Perspectives in Modern Computational Science*, pages 324–331, Leiden, 2006. Brill Academic Publisher.

[146] F. Faglioni and P. Lazzeretti. Parity violation effect on vibrational spectra. *Phys. Rev. A*, 67:032101, 2003.

[147] P. Schwerdtfeger, J. Gierlich, and T. Bollwein. Large parity-violation effects in heavy-metal-containing chiral compounds. *Angew. Chem. Int. Ed.*, 42:1293–1296, 2003.

[148] R. Bast and P. Schwerdtfeger. Parity-violation effects in the C-F stretching mode of heavy-atom methyl fluorides. *Phys. Rev. Lett.*, 91:023001, 2003.

[149] R. Berger and J. L. Stuber. Electroweak interactions in chiral molecules: two-component density functional theory study of vibrational frequency shifts in polyhalomethanes. *Mol. Phys.*, 105:41–49, 2007.

[150] D. Figgen, A. Koers, and P. Schwerdtfeger. NWHClI: A small and compact chiral molecule with large parity–violating effects in the vibrational spectrum. *Angew. Chem. Int. Ed.*, 49:2941–2943, 2010.

[151] M. Quack and J. Stohner. Combined multidimensional anharmonic and parity violating effects in cdbrclf. *J. Chem. Phys.*, 119:11228–11240, 2003.

[152] M. Quack, J. Stohner, and M. Willeke. High-resolution spectroscopic studies and theory of parity violation in chiral molecules. *Ann. Rev. Phys. Chme.*, 59:741–769, 2008.

[153] R. Berger and M. Quack. Multiconfiguration linear response approach to the calculation of parity violating potentials in polyatomic molecules. *J. Chem. Phys.*, 112(7):3148–3158, 2000.

[154] P. Schwerdtfeger and R. Bast. Large parity violation effects in the vibrational spectrum of organometallic compounds. *J. Am. Chem. Soc.*, 126:1652–1653, 2004.

[155] A.L. Barra, J.B. Robert, and L. Wiesenfeld. Possible observation of parity non-conservation by high-resolution NMR. *Europhys. Lett.*, 5:217–222, 1988.

[156] G. Laubender and R. Berger. *Ab initio* calculation of parity violating chemical shifts in nuclear magnetic resonance spectra of chiral molecules. *ChemPhysChem*, 4:395–399, 2003.

[157] A. Soncini, F. Faglioni, and P. Lazzeretti. Parity-violating contributions to nuclear magnetic shielding. *Phys. Rev. A*, 68:033402, 2003.

[158] V. Weijo, P. Manninen, and J. Vaara. Perturbational calculations of parity-violating effects in nuclear-magnetic-resonance parameters. *J. Chem. Phys.*, 123: 054501, 2005.

[159] R. Berger. Breit interaction contribution to parity violating potentials in chiral molecules containing light nuclei. *J. Chem. Phys.*, 129:154105, 2008.

[160] B. Swirles. The relativistic self-consistent field. *Proc. Roy. Soc. Lond. A*, 152: 625–649, 1935.

[161] H. Goldstein. *Klassische Mechanik*. Akademische Verlagsgesellschaft, Frankfurt, 1963.

[162] O. Klein. Quantentheorie und fünfdimensionale Relativitätstheorie. *Z. f. Phys. A*, 37:895, 1926.

[163] W. Gordon. Der Comptoneffekt nach der Schrödingerischen Theorie. *Z. Phys.*, 40:117, 1926.

[164] S. Weinberg. *The Quantum Theory of Fields: Volume I: Foundations*. Cambridge University Press, Cambridge, 1995.

[165] P.A.M. Dirac. The quantum theory of the electron. *Proc. Roy. Soc. Lond. A*, 117: 610–624, 1928.

[166] P.A.M. Dirac. *The Principles of Quantum Mechanics*. Oxford University Press, Oxford, 1982.

[167] P. A. M. Dirac. A theory of electrons and protons. *Proc. Roy. Soc. Lond. A*, 126: 360–365, 1930.

[168] H. Weyl. *Gruppentheorie und Quantenmechanik*. Hirzel, Leipzig, 2nd edition, 1931.

[169] P. A. M. Dirac. Quantised singularities in the electromagnetic field. *Proc. Roy. Soc. Lond. A*, 133:60–72, 1931.

[170] C. G. Darwin. The wave equations of the electron. *Proc. Roy. Soc. A*, 118:654–680, 1928.

[171] C. G. Darwin. On the magnetic moment of the electron. *Proc. Roy. Soc. A*, 120: 621–631, 1928.

[172] W. Gordon. Die Energieniveaus des Wasserstoffatoms nach der Diracschen Quantentheorie des Elektrons. *Z. Phys.*, 48:11, 1928.

[173] W. E. Lamb Jr. and R.C. Retherford. Fine structure of the hydrogen atom by a microwave method. *Phys. Rev.*, 72:241–243, 1947.

[174] J. P. Desclaux. Tour historique. In P. Schwerdtfeger, editor, *Relativistic Electronic Structure Theory, Part: 1, Fundamentals*, pages 1–22, Netherlands, 2002. Elsevier.

[175] G. E. Brown and D. G. Ravenhall. On the interaction of two electrons. *Proc. R. Soc.London Ser. A*, 208:552–559, 1951.

[176] W. Kutzelnigg. The relativistic many body problem in molecular theory. *Physica Scripta*, 36:416–431, 1987.

[177] I. P. Grant and H. M. Quiney. Application of relativistic theories and quantum electrodynamics to chemical problems. *Int. J. Quant. Chem.*, 80:283–297, 2000.

[178] W. Buchmueller. Variational approach to bound states in quantum electrodynamics. *Phys. Rev.*, 18:1784–1792, 1978.

[179] W. Buchmueller and K. Dietz. Multiparticle bound states in QED. *Z. Phys. C*, 5: 45–54, 1980.

[180] J. Sucher. Foundations of the relativistic theory of many-electron atoms. *Phys. Rev. A*, 22:348–362, 1980.

[181] M. H. Mittleman. Configuration-space hamiltonian for heavy atoms and correction to the Breit interaction. *Phys. Rev. A*, 5:2395–2401, 1972.

[182] M.H. Mittleman. Theory of relativistic effects on atoms: Configuration-space Hamiltonian. *Phys. Rev. A*, 24:1167–1175, 1981.

[183] L.N. Labzowsky, G.L. Klimchitskaya, and Y.Y. Dmitriev. *Relativistic Effects in Spectra of Atomic Systems*. IOP Publishing, Bristol, 1993.

[184] I. Lindgren. Relativistic many–body and QED calculations on atomic systems. *Int. J. Quant. Chem.*, 57:683–695, 1996.

[185] P. J. Mohr, G. Plunien, and G. Soff. Qed corrections in heavy atoms. *Phys. Rep.*, 293:227–369, 1998.

[186] C. Hainzl, M. Lewin, E. Séré, and J. P. Solovej. Minimization method for relativistic electrons in a mean-field approximation of quantum electrodynamics. *Phys. Rev. A*, 76(5):052104, 2007.

[187] L.N. Labzowsky and I. Goidenko. QED theory of atoms. In P. Schwerdtfeger, editor, *Relativistic Electronic Structure Theory, Part: 1, Fundamentals*, pages 403–470, Netherlands, 2002. Elsevier.

[188] I. P. Grant and H. M. Quiney. Relativistic self–consistent fields. In P. Schwerdtfeger, editor, *Relativistic Electronic Structure Theory, Part: 1, Fundamentals*, pages 107–202, Netherlands, 2002. Elsevier.

[189] S. S. Schweber. *An Introduction to Relativistic Quantum Field Theory*. Harper & Row, New York, 1966.

[190] M. E. Psekin and D. V. Schroeder. *An Introduction to Quantum Field Theory*. Perseus Books, Cambridge, Massachusetts, 1995.

[191] W. H. Furry. On bound states and scattering in positron theory. *Phys. Rev.*, 81 (1):115–124, 1951.

[192] M. Gell-Mann and F. Low. Bound states in quantum field theory. *Phys. Rev.*, 84: 350–354, 1951.

[193] J. Sucher. *S*-matrix formalism for level-shift calculations. *Phys. Rev.*, 107:1448–1449, 1957.

[194] J. A. Gaunt. The triplets of helium. *Proc. Roy. Soc. A*, 122:513–532, 1929.

[195] G. Breit. The effect of retardation on the interaction of two electrons. *Phys. Rev.*, 34:553–573, 1929.

[196] W. Kutzelnigg. Perturbation theory of relativistic effects. In P. Schwerdtfeger, editor, *Relativistic Electronic Structure Theory, Part: 1, Fundamentals*, pages 669–762, Netherlands, 2002. Elsevier.

[197] M. Dolg. Relativistic effective core potentials. In P. Schwerdtfeger, editor, *Relativistic Electronic Structure Theory, Part: 1, Fundamentals*, pages 793–862, Netherlands, 2002. Elsevier.

[198] J.L. Heully, I. Lindgren, E. Lindroth, S. Lundqvist, and A.M. Mårtensson-Pendrill. Diagonalisation of the Dirac Hamiltonian as a basis for a relativistic many-body procedure. *J. Phys. B*, 19:2799–2815, 1986.

[199] L. Visscher. Post dirac-fock-methods – electron correlation. In P. Schwerdtfeger, editor, *Relativistic Electronic Structure Theory, Part: 1, Fundamentals*, pages 291–332, Netherlands, 2002. Elsevier.

[200] Y. S. Lee and A.D. McLean. Relativistic effects on R_e and D_e in AgH and AuH from all–electron Dirac–Hartree–Fock calculations. *J. Phys. Chem.*, 76:735–736, 1982.

[201] R. E. Stanton and S. Havriliak. Kinetic balance: A partial solution to the problem of variational safety in Dirac calculations. *J. Chem. Phys.*, 81:1910–1918, 1984.

[202] P. J. C. Aerts and W. C. Nieuwpoort. On the optimization of Gaussian basis sets for Hartree-Fock-Dirac calculations. *Chem. Phys. Lett.*, 125:83–90, 1986.

[203] E. van Lenthe, E.-J. Baerends, and J.G. Snijders. Relativistic total energy using regular approximations. *J. Chem. Phys.*, 101:9783–9792, 1994.

[204] E. van Lenthe. *The ZORA Equation*. PhD thesis, Vrije Universiteit de Amsterdam, 1996.

[205] L.L. Foldy and S.A. Wouthuysen. On the dirac theory of spin 1/2 particle and its non-relativistic limit. *Phys. Rev.*, 78:29–36, 1950.

[206] A. Wolf, M. Reiher, and B.A. Hess. Two-component methods and the generalized Douglas-Kroll transformation. In P. Schwerdtfeger, editor, *Relativistic Electronic Structure Theory, Part: 1, Fundamentals*, pages 627–668, Netherlands, 2002. Elsevier.

[207] M. Douglas and M.N. Kroll. Quantum electrodynamical corrections to the fine structure of helium. *Ann. Phys.*, 82:89–155, 1974.

[208] B.A. Hess. Relativistic electronic-structure calculations employing a two-component no-pair formalism with external-field projection operators. *Phys. Rev. A*, 33:3742, 1986.

[209] W. Kutzelnigg. Perturbation theory of relativistic corrections. *Z. Phys. D*, 11: 15–28, 1989.

[210] D. Sundholm. Perturbation theory based on quasi-relativistic Hamiltonians. In P. Schwerdtfeger, editor, *Relativistic Electronic Structure Theory, Part: 1, Fundamentals*, pages 763–798, Netherlands, 2002. Elsevier.

[211] K.G. Dyall and E. van Lenthe. Relativistic regular approximations revisited: An infinite-order relativistic approximation. *J. Chem. Phys.*, 111:1366, 1999.

[212] W. Kutzelnigg and W. Liu. Quasirelativistic theory equivalent to fully relativistic theory. *J. Chem. Phys.*, 123:241102, 2005.

[213] W. Liu and D. Peng. Infinite-order quasirelativistic density functional method based on the exact matrix quasirelativistic theory. *J. Chem. Phys.*, 125:044102–+, 2006.

[214] M. Iliaš and T. Saue. An infinite-order two-component relativistic hamiltonian by a simple one-step transformation. *J. Chem. Phys.*, 126:064102, 2007.

[215] W. Liu and D. Peng. Exact two-component hamiltonians revisited. *J. Chem. Phys.*, 131:031104, 2009.

[216] W. Kutzelnigg. Relativistic one-electron Hamiltonians for electrons only and the variational treatment of the Dirac equation. *Chem. Phys.*, 225:203–222, 1997.

[217] E. van Lenthe, J.G. Snijders, and E.-J. Baerends. The zero-order regular approximation for relativistic effects: The effect of the spin-orbit coupling in closed shell molecules. *J. Chem. Phys.*, 105:6505, 1996.

[218] T. Saue. Post dirac-fock-methods – properties. In P. Schwerdtfeger, editor, *Relativistic Electronic Structure Theory, Part: 1, Fundamentals*, pages 333–402, Netherlands, 2002. Elsevier.

[219] A. Devarajan, A. Gaenko, and J. Autschbach. Two-component relativistic density functional method for computing nonsingular complex linear response of molecules based on the zeroth order regular approximation. *J. of Chem. Phys.*, 130:194102, 2009.

[220] K. Nakamura and Particle Data Group. Review of particle physics. *J. Phys. G*, 37:075021, 2010.

[221] W. Greiner and B. Müller. *Gauge theory of weak interactions.* Springer, Berlin, 3 edition, 2000.

[222] P. L. Anthony, R. G. Arnold, C. Arroyo, K. Bega, J. Biesiada, P. E. Bosted, G. Bower, J. Cahoon, R. Carr, G. D. Cates, J.-P. Chen, E. Chudakov, M. Cooke, P. Decowski, A. Deur, W. Emam, R. Erickson, T. Fieguth, C. Field, J. Gao, M. Gary, K. Gustafsson, R. S. Hicks, R. Holmes, E. W. Hughes, T. B. Humensky, G. M. Jones, L. J. Kaufman, L. Keller, Yu. G. Kolomensky, K. S. Kumar, P. LaViolette, D. Lhuillier, R. M. Lombard-Nelsen, Z. Marshall, P. Mastromarino, R. D. McKeown, R. Michaels, J. Niedziela, M. Olson, K. D. Paschke, G. A. Peterson, R. Pitthan, D. Relyea, S. E. Rock, O. Saxton, J. Singh, P. A. Souder, Z. M. Szalata, J. Turner, B. Tweedie, A. Vacheret, D. Walz, T. Weber, J. Weisend,

M. Woods, and I. Younus. Precision measurement of the weak mixing angle in møller scattering. *Phys. Rev. Lett.*, 95:081601, 2005.

[223] E. Engel and R. Dreizler. Relativistic density functional theory. In R. F. Nalewajski, editor, *Density Functional Theory II*, chapter 1, pages 1–80. Springer, Berlin, 1996.

[224] E. Engel. Relativistic density functional theory: Foundations and basic formalism. In P. Schwerdtfeger, editor, *Relativistic Electronic Structure Theory*, chapter 10, pages 523 – 621. Elsevier, Netherlands, 2002.

[225] H. Eschrig. *The fundamentals of density functional theory.* B. G. Teubner, Stuttgart, 1996.

[226] K.G. Dyall and K. Fægri. *Relativistic Quantum Chemistry.* Oxford University Press, Oxford, 2007.

[227] T. Isaev, S. Nahrwold, and R. Berger. Spin-dependent parity violating interaction in heavy-atom molecules: Two-component zeroth-order regular approximation approach. (submission pending).

[228] G. Schreckenbach, S.K. Wolff, and T. Ziegler. NMR shielding calculations across the periodic table: Diamagnetic uranium compounds. 1. Methods and issues. *J. Phys. Chem. A*, 104:8244–8255, 2000.

[229] T. Helgaker, P. Jørgensen, and J. Olsen. *Molecular Electronic–Structure Theory.* John Wiley & Sons Ltd, West Sussex, 2000.

[230] P. Salek, T. Helgaker, and T. Saue. Linear response at the 4-component density-functional level: application to the frequency-dependent dipole polarizability of Hg, AuH and PtH$_2$. *Chem. Phys.*, 311:187–201, 2005.

[231] D.J. Thouless. *The quantum mechanics of many-body systems; 1st ed.* Academic Press, New York, NY, 1961.

[232] J. L. Stuber. *Broken symmetry Hartree-Fock solutions and the many-electron correlation problem.* PhD thesis, University of Waterloo, 2002.

[233] J. L. Stuber and J. Paldus. Symmetry breaking in the independent particle model. In E. J. Brändas and E. S. Kryachko, editors, *Fundamental World of Quantum Chemistry: A Tribute Volume to the Memory of Per-Olov Löwdin*, pages 67–139, Dordrecht, 2003. Kluwer Academic Publishers.

[234] C. van Wüllen. Spin densities in two-component relativistic density functional calculations: Noncollinear versus collinear approach. *J. Comput. Chem.*, 23:779–785, 2002.

[235] P. Pulay. Analyical derivative methods in quantum chemistry. *Adv. Chem. Phys.*, 69:241–286, 1987.

[236] J. Gauss. Molecular properties. In J. Grotendorst, editor, *Modern Methods and Algorithms of Quantum Chemistry*, volume 3, pages 541–592, Jülich, 2000. John von Neumann Institute for Computing.

[237] R. P. Feynman. Forces in molecules. *Phys. Rev.*, 56:340–343, 1939.

[238] J. Olsen and P. Jørgensen. Linear and nonlinear response functions for an exact state and for an MCSCF state. *J. Chem. Phys.*, 82:3235–3264, 1985.

[239] T. Saue and H. J. Aa. Jensen. Linear response at the 4-component relativistic level: Application to the frequency-dependent dipole polarizabilities of the coinage metal dimers. *J. Chem. Phys.*, 118:522–536, 2003.

[240] V.V. Flambaum and O.B. Sushkov. Possibility of observing parity nonconservation by measuring the nuclear anapole moment using the nmr frequency shift in a laser beam. *Phys. Rev. A*, 47(2):R751–R754, 1993.

[241] Y. Xiao, W. Liu, L. Cheng, and D. Peng. Four-component relativistic theory for nuclear magnetic shielding constants: Critical assessments of different approaches. *J. Chem. Phys.*, 126:214101, 2007.

[242] C. van Wüllen. Density functional calculations of nuclear magnetic resonance chmical shifts. *J. Chem. Phys.*, 102:2806–2811, 1995.

[243] G. Vignale and M. Rasolt. Density-functional theory in strong magnetic fields. *Phys. Rev. Lett.*, 59:2360–2363, 1987.

[244] G. Vignale and M. Rasolt. Current- and spin-density-functional theory for inhomogeneous electronic systems in strong magnetic fields. *Phys. Rev. B*, 37:10685–10696, 1988.

[245] D.A. Braden and D.R. Tyler. Density funtional theory calculations on 19-electron organometallic complexes: The $Mn(CO)_5Cl^-$ anion. the difference between unpaired electron density and spin density due to spin polarization. *Organometallics*, 17:4060–4064, 1998.

[246] J.A. Pople, P.M.W. Gill, and N.C. Handy. Spin-unrestricted character of Kohn-Sham orbitals for open-shell systems. *Int. J. Quantum Chem.*, 56:303–305, 1995.

[247] P.J. Wilson, R.D. Amos, and N.C. Handy. Towards coupled-cluster accuracy in the prediction of nuclear magnetic shielding constants: a simple and efficient DFT approach. *Chem. Phys. Lett.*, 312:475–484, 1999.

[248] A. Bakasov, T.-K. Ha, and M. Quack. *Ab initio* calculation of molecular energies including parity violating interactions. In J. Chela-Flores and F. Raulin, editors, *Chemical Evolution: Physics of the Origin and Evolution of Life*, pages 287–296, Netherlands, 1996. Kluwer Academic Publisher.

[249] P. Lazzeretti and R. Zanasi. On the calculation of parity-violating energies in hydrogen peroxide and hydrogen disulphide molecules within the random-phase approximation. *Chem. Phys. Lett.*, 279:349–354, 1997.

[250] J.K. Laerdahl and P. Schwerdtfeger. Fully relativistic ab initio calculation of the energies of chiral molecules including parity-violating weak interactions. *Phys. Rev. A*, 60:4439–4453, 1999.

[251] V. Weijo, R. Bast, P. Manninen, T. Saue, and J. Vaara. Methodological aspects in the calculation of parity-violating effects in nuclear-magnetic-resonance parameters. *J. Chem. Phys.*, 126:074107, 2007.

[252] A.D. Becke. Density-functional exchange-energy approximation with correct asymptotic-behavior. *Phys. Rev. A*, 38:3098–3100, 1988.

[253] C. Lee, W. Yang, and R.G. Parr. Development of the Colle-Salvetti correlation-energy formula into a functional of the electron-density. *Phys. Rev. B*, 37:785–789, 1988.

[254] P.A.M. Dirac. Note on exchange phenomena in the Thomas atom. *Proc. Cambridge Phil. Soc.*, 26:376–385, 1930.

[255] W. Kohn and L.J. Sham. Self-consistent equations including exchange and correlation effects. *Phys. Rev.*, 140:A1133–A1138, 1965.

[256] S.H. Vosko, L. Wilk, and M. Nuisar. Accurate spin-dependent electron liquid correlation energies for local spin density calculations: A critical analysis. *Can. J. Phys.*, 58:1200–1211, 1980.

[257] J.C. Slater. A simplification of the Hartree-Fock method. *Phys. Rev.*, 81:385–390, 1951.

[258] V. I. Bakhmutov. *Practical NMR Relaxation for Chemists.* John Wiley & Sons Ltd, West Sussex, 2004.

[259] A. Abragam. *Principles of Nulear Magnetism.* Oxford University Press, Oxford, 1999.

[260] K. Mikami, H. Kakuno, and K. Aikawa. Enantiodiscrimination and enantiocontrol of neutral and cationic Pt[ii] complexes bearing the tropos biphep ligand: Application to asymmetric Lewis acid catalysis. *Angew. Chem. Int. Ed.*, 44:7257–7260, 2005.

[261] V. Weijo, M. B. Hansen, O. Christiansen, and P. Manninen. Vibrational effects in the parity-violating contributions to the isotropic nuclear magnetic resonance chemical shift. *Chem. Phys. Lett.*, 470(4-6):166 – 171, 2009.

[262] X. Wang and L. Andrews. Infrared spectra, structure, and bonding of the group 6 and ammonia $M:NH_3$, H_2N-MH, and NMH_3 reaction products in solid argon. *Organometallics*, 27(19):4885–4891, 2008.

[263] X. Wang, L. Andrews, R. Lindh, V. Veryazov, and B. O. Roos. A combined theoretical and experimental study of simple terminal group 6 nitride and phosphide NMX_3 and PMX_3 molecules. *J. Phys. Chem. A*, 112(35):8030–8037, 2008.

[264] A. A. Fokin, P. R. Schreiner, R. Berger, G. H. Robinson, P. Wei, and C. F. Campana. Pseudotetrahedral polyhalocubanes: Synthesis, structures, and parity violating energy differences. *J. Am. Chem. Soc.*, 128:5332–5333, 2006.

[265] M. Gottselig and M. Quack. Steps towards molecular parity violation in axially chiral molecules. I. Theory for allene and 1,3-difluoroallene. *J. Chem. Phys.*, 123: 084305, 2005.

[266] F. Faglioni and P. Lazzeretti. Understanding parity violation in molecular systems. *Phys. Rev. E*, 65:011904, 2001.

[267] H. Vahrenkamp. Framework chirality and optical activity of organometallic cluster compounds. *J. Organomet. Chem.*, 370:65–73, 1988.

[268] M. Green, J. C. Jeffery, S. J. Porter, H. Razay, and F. G. A. Stone. Chemistry of di- and tri-metal complexes with bridging carbene or carbyne ligands. Part 14. Triangulo-metal complexes containing tungsten with iron, cobalt, rhodium, or nickel and a capping tolylidyne ligand; crystal structure of the complex $[RhFeW(\mu_3\text{-}CC_6H_4Me\text{-}4)(\mu\text{-}CO)(CO)_5(\nu\text{-}C_5H_5)(\nu\text{-}C_9H_7)]$. *J. Chem. Soc. Dalton Trans.*, 12:2475–2483, 1982.

[269] M. J. Chetcuti, J. A. K. Howard, R. M. Mills, F. Gordon, A. Stone, and P. Woodward. Chemistry of di- and tri-metal complexes with bridging carbene or carbyne ligands. Part 13. Synthesis of platinumirontungsten trimetal compounds with μ_3-tolylidyne groups ; crystal structures of $[FePtW(\mu_3\text{-}CR)(CO)_5(PMePh_2)_2(\eta\text{-}C_5H_5)]$ and $[FePtW(\mu_3\text{-}CR)(Co)_6\text{-} (PEt_3)(\eta\text{-}C_5H_5)]$ (R = $C_6H_4Me\text{-}4$). *J. Chem. Soc. Dalton Trans.*, 9:1757–1764, 1982.

[270] A.D. Becke. A new mixing of Hartree-Fock and local density-functional theories. *J. Chem. Phys.*, 98:1372–1377, 1993.

[271] J. Li, H.-S. Hu, J. T. Lyon, and L. Andrews. Chirality, agostic interaction and pyramidality in actinide methylidene complexes. *Angew. Chem.*, 119:9203–9207, 2007.

[272] M. Quack and J. Stohner. How do parity violating weak nuclear interactions influence rovibrational frequencies in chiral molecules? *Z. Phys. Chem.*, 214: 675–703, 2000.

[273] V. Barone and R. G. Viglione. Harmonic and anharmonic contributions to parity-violating vibrational frequency difference between enantiomers of chiral molecules. *J. Chem. Phys*, 123:4304, 2005.

[274] P. Schwerdtfeger, T. Saue, J. N. P. van Stralen, and L. Visscher. Relativistic second-order many-body and density-functional theory for the parity-violation contribution to the C-F stretching mode in CHFClBr. *Phys. Rev. A*, 71:012103, 2005.

[275] R. Berger, M. Gottselig, M. Quack, and M. Willeke. Parity violation dominates the dynamics of chirality in dichlorodisulfane. *Angew. Chem. Int. Ed.*, 40:4195–4198, 2001.

[276] L. Visscher and K.G. Dyall. Dirac-Fock atomic electronic structure calculations using different nuclear charge distributions. *At. Data Nucl. Data Tables*, 67:207–224, 1997.

[277] T.H. Dunning, Jr. Gaussian basis sets for use in correlated molecular calculations. I. The atoms boron through neon and hydrogen. *J. Chem. Phys.*, 90:1007–1023, 1989.

[278] R.A. Kendall, T.H. Dunning, Jr., and R.J. Harrison. Electron affinities of the first-row atoms revisited. systematic basis sets and wave functions. *J. Chem. Phys.*, 96:6796–6806, 1992.

[279] D. Andrae, U. Haeussermann, M. Dolg, H. Stoll, and H. Preuss. Energy-adjusted *ab initio* pseudopotentials for the second and third row transition elements. *Theor. Chim. Acta*, 77:123–141, 1990.

[280] D.E. Woon and T.H. Dunning, Jr. Gaussian basis sets for use in correlated molecular calculations. III. The atoms aluminium through argon. *J. Chem. Phys.*, 98: 1358–1371, 1993.

[281] A.D. Becke. Density-functional thermochemistry. III. The role of exact exchange. *J. Chem. Phys.*, 98:5648–5652, 1993.

[282] T.H. Dunning, Jr. Gaussian basis functions for use in molecular calculations. 1. contraction of (9s5p) atomic basis sets for first-row atoms. *J. Chem. Phys.*, 53: 2823–2833, 1970.

[283] A. Schäfer, H. Horn, and R. Ahlrichs. Fully optimized contracted Gaussian basis sets for atoms Li to Kr. *J. Chem. Phys.*, 97:2571–2577, 1992.

[284] J. P. Perdew and W. Yue. Accurate and simple density functional for the electronic exchange energy: Generalized gradient approximation. *Phys. Rev. B*, 33:8800–8802, 1986.

[285] A. Schäfer, C. Huber, and R. Ahlrichs. Fully optimized contracted Gaussian basis sets of triple zeta valence quality for atoms Li to Kr. *J. Chem. Phys.*, 100:5829–5835, 1994.

[286] M. J. Frisch, G. W. Trucks, H. B. Schlegel, G. E. Scuseria, M. A. Robb, J. R. Cheeseman, J. A. Montgomery, Jr., T. Vreven, K. N. Kudin, J. C. Burant, J. M. Millam, S. S. Iyengar, J. Tomasi, V. Barone, B. Mennucci, M. Cossi, G. Scalmani, N. Rega, G. A. Petersson, H. Nakatsuji, M. Hada, M. Ehara, K. Toyota, R. Fukuda, J. Hasegawa, M. Ishida, T. Nakajima, Y. Honda, O. Kitaoand, H. Nakai, M. Klene, X. Li, J. E. Knox, H. P. Hratchian, J. B. Cross, V. Bakken, C. Adamo, J. Jaramillo, R. Gomperts, R. E. Stratmann, O. Yazyev, A. J. Austin, R. Cammi, C. Pomelli, J. W. Ochterski, P. Y. Ayala, K. Morokuma, G. A. Vothand P. Salvador, J. J. Dannenberg, V. G. Zakrzewski, S. Dapprich, A. D. Daniels, M. C. Strain, O. Farkas, D. K. Malick, A. D. Rabuck, K. Raghavachari, J. B. Foresman, J. V. Ortiz, Q. Cui, A. G. Baboul, S. Clifford, J. Cioslowski, B. B. Stefanov, G. Liu, A. Liashenko, P. Piskorz, I. Komaromi, R. L. Martin, D. J. Fox, T. Keith, M. A. Al-Laham, C. Y. Peng, A. Nanayakkara, M. Challacombe, P. M. W. Gill, B. Johnson, W. Chen, M. W. Wong, C. Gonzalez, and J. A. Pople. Gaussian 03, Revision C.02. Gaussian, Inc. , Wallingford, CT, 2004.

[287] W. Kuechle, M. Dolg, H. Stoll, and H. Preuss. Energy-adjusted pseudopotentials for the actinides. Parameter sets and test calculations for thorium and thorium monoxide. *J. Chem. Phys.*, 100:7535–7542, 1994.

[288] J.P. Perdew. *Electronic Structure of Solids*. Akademie Verlag, Berlin, 1991.

[289] P.J. Stephens, F.J. Devlin, C.F. Chabalowski, and M.J. Frisch. Ab initio calculation of vibrational absorption and circular dichroism spectra using density functional force fields. *J. Phys. Chem.*, 98:11623–11627, 1994.

Curriculum Vitae

EDUCATION

Ph.D. **Frankfurt Institute for Advanced Studies**

Frankfurt University, Germany

Physics

Thesis: ***Electroweak quantum chemistry: Parity violation in spectra of chiral molecules containing heavy atoms***

Advisors: Robert Berger (principal) and Dieter Schuch

Diplom **Heidelberg University**

Germany

Thesis: ***Development of a Detector for Bound Quantum States of Neutrons in the Earth's Gravitational Field***

Advisors: Hartmut Abele (principal) and Valery Nesvizhevsky

Examination Fields: *General Experimental and Theoretical Physics, Theoretical High Energy Physics and Field Theory, Mathematics*

CSYS   **Cademuir International School**
Moniaive, Scotland
Scottish Highers and Certificate of Sixth Year Studies, 1998
(University Entrance Qualification)

PUBLICATIONS

Peer–reviewed

S. Nahrwold and R. Berger, Zeroth Order Regular Approximation Approach to Parity Violating Nuclear Magnetic Resonance Shielding Tensors, Journal of Chemical Physics **130**, 214101–214114 (2009)

In Preparation

T. Isaev and S. Nahrwold and R. Berger, Spin–dependent Parity Violating Interaction in Heavy–atom Molecules: Two-component Zeroth Order Regular Approximation Approach

S. Nahrwold and S. Brück and T. Isaev and R. Berger, Measurable Parity Violating Effect in Chiral Actinide Complex

S. Nahrwold and P. Schwerdtfeger and R. Berger, Nuclear Spin–dependent Parity Violation in Tetrahedral Tungsten Complexes

S. Nahrwold and P. Heretsch and A. Giannis and R. Berger, Parity Violating Effects in the ^{195}Pt NMR Spectra of Chiral Platinum Complexes

PRESENTATIONS

Talks

"Parity violation in chiral molecules", Santa Fe Institute 2010, New Mexico, USA

"Quasi Relativistic Approach to Parity Violating NMR Parameters", VW Foundation Junior Research Group Colloquium 2007, Frankfurt Institute for Advanced Studies, Germany

"Spin and Structure Formation", Frankfurt Institute for Advanced Studies Graduate Student Retreat 2007, Riezlern, Austria

"Quasi Relativistic Density Functional Theory Approach to Parity Violating Shifts in NMR Spectra of Chiral Molecules", Workshop on Theoretical Chemistry in Mariapfarr 2006, University of Graz, Austria

"Neutron detectors with ultra-high spatial resolution for the measurement of bound states in the earth's gravitational field", Spring meeting of the German Physical Society 2005, Berlin, Germany

Posters

S. Nahrwold, P. Schwerdtfeger and R. Berger, "Quasi Relativistic Approach to Magnetic Molecular Properties Including Weak Interaction Effects", Symposium on Theoretical Chemistry 2009, Düsseldorf University, Germany

S. Nahrwold and R. Berger, "Nuclear Magnetic Resonance Shieldings: A Quasi-Relativistic Approach Including Weak Interaction Effects", Sanibel Symposium 2009, University of Florida, USA

S. Nahrwold, M. Bühl and R. Berger, "Parity Violating Nuclear Magnetic Resonance Parameters: Scaling Laws and Conformational Effects", Symposium on Theoretical Chemistry 2007, Saarbrücken University, Germany

S. Nahrwold and R. Berger, "Quasi-Relativistic DFT Approach to Parity Violating NMR Shielding Constants", Relativistic Effects in Heavy Elements 2007, University of Strasbourg, France

S. Nahrwold and R. Berger, "ZORA Approach to Electroweak Effects on NMR Shielding Constants", International Conference of Computational Methods in Sciences and Engineering 2006, University of Peloponnese, Greece.

S. Nahrwold and R. Berger, "Two-Component Quasi-Relativistic Density Functional Theory Approach to Parity-Violating Shifts in NMR Spectra of Chiral Molecules", Symposium on Theoretical Chemistry 2006, Humboldt University Berlin, Germany